

**Towards a Benign and Viable Rhodium Catalyzed
Hydroformylation of Higher Olefins: Economic and
Environmental Impact Analyses, Solvent Effects and
Membrane-based Catalyst Separation**

Jing Fang

Submitted to the graduate degree program in Chemical & Petroleum
Engineering and the Graduate Faculty of the University of Kansas School
of Engineering in partial fulfillment of the requirements for the degree of
Doctor of Philosophy

Committee Members:

Bala Subramaniam (Chair)

Darryl Fahey

Palghat A. Ramachandran

Aaron Scurto

Jon Tunge

Date of Defense: 04-10-2009

The Dissertation Committee for Jing Fang certifies
that this is the approval version of the following dissertation:

**Towards a Benign and Viable Rhodium Catalyzed
Hydroformylation of Higher Olefins: Economic and
Environmental Impact Analyses, Solvent Effects and
Membrane-based Catalyst Separation**

Committee Members:

Bala Subramaniam (Chair)

Darryl Fahey

Palghat A. Ramachandran

Aaron Scurto

Jon Tunge

Date approved: _____

Abstract

Researchers at the Center for Environmentally Beneficial Catalysis (CEBC) had previously reported a novel rhodium-based hydroformylation process concept based on the use of CO₂-expanded liquids (CXLs) to intensify rates and obtain higher linear/branched aldehydes selectivity at relatively mild temperatures (30-60 °C) and pressures (~4 MPa). This dissertation continues investigations aimed at addressing the fundamental and practical issues associated with this concept.

ReactIR studies of Rh/triphenylphosphine-catalyzed 1-octene hydroformylation, complemented by microkinetic and reactor modeling investigations revealed that the intrinsic kinetic rate constants are of similar magnitude with or without CO₂ addition to the reaction mixture. This implies that the enhanced reaction rate observed in CXL is due to the increased hydrogen solubility in that medium.

Environmental impact analysis revealed that the overall toxicity index for the CEBC process is approximately 40 times less than the Exxon process against which the CEBC process was benchmarked. Economic analysis of the CXL concept revealed that at an aldehyde production rate of 19,900 kg/(kg Rh·h), > 99.8% rhodium has to be recovered per pass for the CEBC process to be competitive with the Exxon process. Assuming a similar hydroformylation turnover frequency, rhodium recovery levels that exceed this criterion for economic viability were successfully demonstrated in a membrane-based nano/ultra-filtration reactor system using polymer supported phosphorus ligands, synthesized and provided by researchers from the Department of Chemistry. During continuous filtration of a toluene-based solution containing polymer-supported Rh complexes, the Rh and P concentrations in the permeate, quantified using ICP analysis, were on the order of a few tens of ppb. During continuous 1-octene hydroformylation studies in the membrane reactor at a syngas pressure of 0.6 MPa and 60 °C, the 1-octene conversion and product (mostly aldehydes) concentrations reached a steady state with the Rh concentrations in the permeate stream being lower than 120 ppb. However, the conversions and product concentrations during the continuous run are lower than those obtained in a batch ReactIR under identical operating conditions. This is attributed to syngas starvation in the membrane reactor that might be caused by inadequate mixing.

In complementary investigations, it was found that the dissolution of CO₂ in the organic phase (to create CO₂-expanded liquids) decreases the viscosities of the mixtures with increasing CO₂ pressure. This offers an opportunity to enhance mixing and also tune the membrane flux so as to increase the throughput of the membrane filter. The demonstrated technology concept, when fully optimized, should find applications in a variety of other applications in homogeneous catalysis, including hydrogenation and carbonylation of conventional and biomass-based substrates.

Acknowledgement

I would like to express my sincere gratitude to my advisor Dr. Bala Subramaniam, director of Center for Environmentally Beneficial Catalysis (CEBC), for his guidance, support and encouragement during my PhD program. His optimistic, enthusiastic, and meticulously hard-working attitude has been and will always be inspiring me during the course of my scientific life.

I would like to acknowledge my committee members, Professor Aaron Scurto, Professor Palghat A. Ramachandran, Professor Jon Tunge and Dr. Darryl Fahey for their precious time, suggestions and critical review. I would like to acknowledge Professor Raghunath V. Chaudhari, who was one of my committee members during comprehensive examination, for his instructions in kinetic modeling and experiment design.

I would like to express my special thanks to Dr. Ranjan Jana for synthesizing and providing ligands for membrane filtration testings, Dr. Debangshu Guha for his collaboration in kinetic modeling, Dr. Kirk Snavely for his constant assistance with the experiment setup modification and his time spent in enlightening conversations as well as dissertation revision.

I would like to gratefully acknowledge Ed Atchison, Fenghui Niu, Allan Walker and Scott Ramskill for their assistance with the experimental setup, instrumentation and automatic control software, Jim Busse for his timely help with the drawings and figures in the publications and this dissertation, and Deanna

Bieberly, Claudia Bode and Nancy Crisp for their assistance and arrangements with courses and meetings.

I would like to thank Dr. Ruihu Wang, Dr. Hu Cai and Dr. Anindhya Ghosh for their collaboration in catalyst design and screening during the early stage of this dissertation. I would like to thank Dr. Chicheng Ma, Dr. Tie Pan Shi and Dr. Andrew Danby for all their kind help and support in development of analytical methods and instrument training and maintenance.

I would like to sincerely acknowledge Kent Pennybaker, Tom Ruddy, Megan Aary, Peter Winter, Lauren Byers and Kean Wong for the most rewarding experiences of collaborations since 2004.

I would also like to thank members of Professor Bala Subramaniam's research group, Dr. Hong Jin, Dr. Sargar Sarshani, Dr. Bhuma Rajagopalan, Dr. Chad Jonson, Dr. Jack Ford, Dr. Shengwei Tang, Kening Gong, Shirley Xie, Madhav Ganta and Meng Li for their involvement in our friendly laboratory atmosphere.

I would like to thank my parents back in China for their unconditional love, enduring support and financial aid for my higher level education. Thanks to Xuhai's patience and faith throughout my PhD and Ashley's entry in my life.

I would like to acknowledge CEBC for providing the financial support under the National Science Foundation Engineering Research Centers Grant (EEC-0310689).

Table of Contents

Title Page	
Acceptance Page	I
Abstract	II
Acknowledgement	III
Table of Contents	V
List of Figures	XII
List of Tables	XVII
Chapter 1. Introduction	1
1.1 Industrial Challenges in Higher Olefin Hydroformylation.....	2
1.2 Homogeneous Hydroformylation in CO ₂ -Expanded Liquids (CXLs).....	4
1.3 Goals and Objectives of Current Work.....	7
1.4 References.....	12
Chapter 2. Economic and Environmental Impact Analyses of Catalytic Higher Olefin Hydroformylation in CO₂-Expanded Liquids (CXLs) Media	14
2.1 Background.....	15
2.2 Literature Review.....	17
2.3 Methodology.....	21
2.3.1 Simulation parameters and assumptions.....	22
2.3.2 Process simulation details.....	26
2.3.3 E-factor analysis.....	28

2.4 Economic Analysis	29
2.5 Environmental Impact Analysis.....	31
2.6 Results and Discussion	35
2.6.1 Economic analysis	36
2.6.2 Environmental impact analysis	38
2.7 Summary and Recommendations for Future Work	41
2.8 References.....	44
Chapter 3. Microkinetic Studies of Rhodium Catalyzed Hydroformylation of 1- Octene in Neat and CO₂-Expanded 1-Octene	47
3.1 Introduction and Background	48
3.2 Literature Review.....	49
3.3 Experimental Studies	52
3.3.1 Apparatus – ReactIR	52
3.3.2 Materials	54
3.3.3 Experimental procedure	54
3.3.4 Reproducibility	56
3.4 Modeling Studies	57
3.4.1 Kinetic Scheme	57
3.4.2 Reactor Model.....	59
3.5 Results and Discussion	61
3.6 Concluding Remarks and Future Work	72
3.7 References.....	73

Chapter 4. Batch Membrane Nano/Ultra-Filtration of Rhodium Complexes from Homogeneous Organic Solutions.....	77
4.1 Introduction and Background	78
4.2 Literature Review.....	80
4.2.1 Membrane filtration	82
4.2.1.1 Dendrimer supported catalysts.....	84
4.2.1.2 Soluble polymer supported catalysts	85
4.2.1.3 Unmodified or non-macromolecular ligand modified catalysts	87
4.2.2 Commercially available membranes and filtration setups.....	90
4.3 Experimental Apparatus.....	92
4.3.1 STARMEM [®] membrane.....	92
4.3.2 MET cell	93
4.3.3 Setup	94
4.4 Catalytic Systems and Analytical Methodology.....	95
4.4.1 Catalytic systems	95
4.4.2 Analytical techniques.....	97
4.4.2.1 The ICP configuration and specifications.....	98
4.4.2.2 Calibration.....	100
4.5 Experimental Procedure.....	101
4.5.1 Membrane preconditioning and equilibration.....	101
4.5.2 Flux measurements	102
4.5.3 Batch filtration experiment procedure	104

4.6 Results and Discussions	105
4.6.1 Triphenylphosphine (TPPine), BiPhePhos and PBB20 ligands	105
4.6.2 BiPhPhM and PBB10 ligands	109
4.7 Summary and Future Work.....	113
4.8 References.....	116
Chapter 5. Continuous Homogeneous Hydroformylation of 1-Octene in a Stirred Reactor Equipped with <i>in situ</i> Membrane Filtration	120
5.1 Introduction and Background	121
5.2 Literature Review.....	121
5.3 Experimental Procedure.....	128
5.3.1 Materials	128
5.3.2 Filtration apparatus	128
5.3.3 Continuous experiment procedure without reaction	129
5.3.4 Continuous experimental procedure with reaction	129
5.4 Results and Discussion	130
5.4.1 Continuous filtration runs without reaction	130
5.4.1.1 Polymer bound ligand (PBB10).....	130
5.4.2 Continuous filtration runs with reaction	134
5.4.2.1 Run with PBB10d under 0.6 MPa syngas.....	134
5.4.2.2 Batch runs in ReactIR	136
5.4.2.3 Rh and P concentrations in the permeate	139
5.5 Summary	141

5.6 References.....	143
Chapter 6. Viscosity Measurements of CO₂-Expanded Hydroformylation	
Systems.....	145
6.1 Introduction and Background	145
6.2 Literature Review.....	147
6.2.1 Viscosity	147
6.2.1.1 Viscosity measurement methods.....	147
6.2.1.2 Toluene viscosity with or without CO ₂	148
6.2.1.3 Viscosities of toluene and polymer mixture with or without CO ₂	149
6.2.2 Membrane flux and solute rejection prediction	151
6.2.3 Cloud point measurements.....	153
6.2.4 Volume expansion measuring techniques.....	154
6.3 Experimental Details.....	154
6.3.1 Chemicals.....	154
6.3.2 Apparatus	155
6.3.3 Expansion and cloud point measurement procedure	159
6.3.4 Viscosity measurement procedure	160
6.4 Results and Discussion	162
6.4.1 Volume expansion studies and cloud point data measurements.....	162
6.4.2 Viscosity measurements.....	164
6.5 Summary	167
6.6 References.....	169

Chapter 7. Conclusions and Recommendations.....	174
7.1 Conclusions.....	174
7.2 Recommendations.....	177
7.3 Reference	183
Appendix.....	184
Appendix I. Economic and Environmental Analysis.....	184
II.1 Tables	184
II.2 Aldehyde Production Rate Calculation	188
Appendix II. Experimental Kinetic Studies	189
II.1 Calibration of Pressure Transducer	189
II.2 ReactIR Purge Gas Generator Operation and Diagnosis	192
II.3 Purification and Storage of Solvents and Substrate	195
II.4 Gas Chromatography Methods for Analysis of Typical Hydroformylation Reaction Mixtures.....	198
II.5 ReactIR Peak Calibration	200
II. 6 Reproducibility of the Experiments	205
Appendix III. ICP-OES Elemental Analysis	207
III.1 ICP Method Optimization.....	207
III.1.1 Spectral interference and analytical lines	207
III.1.2 Power optimization	208
III.1.3 Nebulizer pressure and flowrate as well as gainage optimization	209
III.1.4 Uptake and rinse-out profiles.....	210

III.2 Calibration Procedure	210
III.2.1 Standards availability and chemical reagents	210
III.2.2 Excitation conditions	211
III.2.3 Operating procedure.....	213
III.2.4 Calibration curves	213
III.2.5 Shelf life of standards	214
III.3 Study Materials	215
Appendix IV. Mass Balance and Uncertainty Analysis.....	217
IV.1 Mass Balance and Uncertainty Analysis Calculation Formulae.....	217
IV.2 Example	219
Appendix V. Phosphorus Ligands	222

List of Figures

- Figure 1.1 Hydroformylation reaction scheme
- Figure 1.2 CEBC's systems approach for developing alternate hydroformylation technology
- Figure 2.1 Industrialized Exxon oxo process flow diagram adapted from US 5,237,104
- Figure 2.2 HYSYS flowsheet for the simulated conventional process
- Figure 2.3 HYSYS flowsheet for proposed CXL process
- Figure 2.4 Calculation structure of environmental analysis tool – EFRAT
- Figure 2.5 Comparison of total capital investment for the simulated conventional and CXL process
- Figure 2.6 Comparison of total production cost for the simulated conventional and CXL process
- Figure 2.7 Breakdown of composite environmental impact index by each category of emission sources
- Figure 2.8 Breakdown of environmental impact attributed to various environmental impact categories
- Figure 3.1 Ligand modified rhodium catalyzed hydroformylation mechanism
- Figure 3.2 Schematic of ReactIR apparatus
- Figure 3.3 Schematic of a two-phase semi-batch hydroformylation reactor
- Figure 3.4 Comparison of experimental and predicted normalized concentration profiles of 1-octene and nonanal in neat 1-octene hydroformylation

- at low conversion using preliminary kinetic scheme in Table 3.1
- Figure 3.5 Comparison of experimental and predicted dimensionless concentration profiles of 1-octene and nonanal in CO₂-expanded 1-octene hydroformylation at low conversion using preliminary kinetic scheme in Table 3.1
- Figure 3.6 Comparison of experimental and predicted normalized concentration profiles of 1-octene and nonanal in neat 1-octene hydroformylation at high conversion using modified kinetic scheme in Table 3.4
- Figure 3.7 Comparison of experimental and predicted normalized concentration profiles of 1-octene and nonanal in CO₂-expanded 1-octene hydroformylation at high conversion using modified kinetic scheme in Table 3.4
- Figure 4.1 The schematic of reaction coupled with membrane filtration
- Figure 4.2 Filtration and separation spectrum
- Figure 4.3 GE Sepa™ CF II Med/High foulant system from Osmonics (USA)
- Figure 4.4 Cross-flow filtration scheme
- Figure 4.5 Configuration of MET cell assembly
- Figure 4.6 Membrane filtration setup configuration
- Figure 4.7 Schematic of the ICP sample introduction
- Figure 4.8 The configuration of Jobin Yvon 2000 2 ICP
- Figure 4.9 Calibration curves for P
- Figure 4.10 Calibration curves for Rh

- Figure 4.11 A typical flux measurement protocol
- Figure 4.12 Permeate fluxes before, during and after filtration of catalytic solutions containing each ligand
- Figure 4.13 Rhodium concentrations in permeate and the Rh pass-through for batch filtrations of solutions containing various dissolved catalyst + ligands combinations
- Figure 4.14 Phosphorus concentrations and pass-through values in permeate for batch filtrations of solutions containing various dissolved catalyst + ligands combinations
- Figure 5.1 Schematic representation of a nano/ultra-filtration membrane unit
- Figure 5.2 Rh-EtDUPHOS (MW=723 Da)
- Figure 5.3 Ru-BINAP (MW=929 Da)
- Figure 5.4 Allylic substitution in a continuous membrane reactor with the catalyst based on dendritic ligand
- Figure 5.5 Residual concentration as function of the number of residence times
- Figure 5.6 dppf-based dendrimer
- Figure 5.7 Continuous hydrogenation using dppf (a) and dendrimeric ligand (b)
- Figure 5.8 Membrane flux, rhodium and phosphorous concentrations in permeate for the first continuous filtration run
- Figure 5.9 Membrane flux, rhodium and phosphorous concentrations in permeate for the second continuous filtration run
- Figure 5.10 Experimental results for continuous 1-octene hydroformylation with

in situ membrane

- Figure 5.11 Experimental results for continuous 1-octene hydroformylation with *in situ* membrane at different syngas pressures
- Figure 5.12 The nonanal absorbance vs time profile for batch reaction #11 in Table 5.1
- Figure 5.13 Rh and P concentrations in permeate for the two consecutive continuous 1-octene hydroformylation runs at different syngas pressures
- Figure 5.14 GPC analysis of polymer bound phosphorous ligand
- Figure 6.1 Relative solvent power and transport ability of different solvent types
- Figure 6.2 Experimental setup for volume expansion, cloud point pressure and viscosity measurements
- Figure 6.3 Configuration of the air bath including Jerguson viewcell, viscometer and micropump
- Figure 6.4 Cross section of SPL-440 viscometer sensor
- Figure 6.5 Schematic of the experiment setup
- Figure 6.6 Pure toluene viscosities in this work compared to the reported data in literature
- Figure 6.7 Expansion data for various systems at three temperatures
- Figure 6.8 Cloud point measurements of different (toluene + soluble polymer bound ligand + CO₂) mixtures at different temperatures

- Figure 6.9 Variation of viscosities with temperature for toluene + 0.7 wt% PBB10c mixtures at different CO₂ pressures
- Figure 6.10 Variation of viscosities of toluene + 0.7 wt% PBB10c mixtures with CO₂ pressures at different temperatures
- Figure 6.11 Variation of viscosities with temperature for toluene + 1.8 wt% PBB10c mixtures at different CO₂ pressures
- Figure 6.12 Variation of viscosities of toluene + 1.8 wt% PBB10c mixtures with CO₂ pressures at different temperatures
- Figure 6.13 Viscosities versus CO₂ pressures of toluene + 1.8 wt% PBB10c mixture at 60 °C

List of Tables

- Table 1.1 Operating conditions for industrial higher olefin hydroformylation processes
- Table 2.1 Simulation parameters for the simulated conventional process
- Table 2.2 Simulation parameters for CXL process
- Table 2.3 E-factors for both CXL and the simulated conventional processes
- Table 2.4 Weighting factors for each category of environmental impacts
- Table 2.5 Positive and negative credits assigned to each process by different operating conditions
- Table 3.1 Preliminary kinetic scheme for rhodium catalyzed hydroformylation reaction
- Table 3.2 Experimental conditions and model parameters for both neat 1-octene and CO₂-expanded 1-octene hydroformylation reactions at low conversions
- Table 3.3 Estimated kinetic constants using preliminary kinetic scheme in Table 3.1 for both neat and CO₂-expanded 1-octene hydroformylation at low conversion
- Table 3.4 Modified kinetic scheme for rhodium catalyzed hydroformylation reaction
- Table 3.5 Estimated kinetic constants using modified kinetic scheme in Table 3.4 at low conversion
- Table 3.6 Experimental conditions and model parameters for both neat 1-octene

and CO₂-expanded 1-octene hydroformylation reactions at high conversions

Table 3.7 Estimated kinetic constants for neat and CO₂-expanded 1-octene hydroformylation using modified kinetic scheme in Table 3.4 at high conversions

Table 3.8 Comparison of estimated kinetic constants for neat and CO₂-expanded 1-octene hydroformylation using modified kinetic scheme in Table 3.4 at high conversions

Table 4.1 Commercial dead-end membrane filters

Table 4.2 Phosphorus ligands and their molecular weights

Table 4.3 The Jobin Yvon 2000 2 ICP specifications

Table 4.4 Batch filtration results for TPPine ligand

Table 4.5 Batch filtration results for PBB20 ligand

Table 4.6 Batch filtration results for BiPhePhos ligand

Table 4.7 Catalyst and ligand compositions in the initial catalyst solutions in each run

Table 4.8 Membrane, permeate flux and nitrogen pressure used in each run

Table 5.1 Batch and continuous data comparisons

Chapter 1. Introduction

The chemical industry has long been recognized as one of the prominent industrial areas that are critical to both the world and the U.S. economy. As the world's largest producer, the American chemistry industry produces more than 70,000 different products and 21% of the world's chemical output. In 2007, the business of chemistry employed nearly 900,000 jobs directly and another 4.8 million indirectly in other industries, accounting for 4% of the total US workforce. It also contributes 10% U.S. merchandise exports, \$664 billion shipped value and \$481 billion final sales in 2007.¹ The chemistry sector provides indispensable goods that are essential to our high-quality modern life, such as man-made fibers and plastics, pharmaceuticals for life care, fertilizers and pesticides for agricultural produce and materials for cell phones and computers. However, it also faces challenges in reducing raw material production and/or consumption, energy usage, and waste generation. Technology vision 2020: The Chemical Industry² identifies the barriers and challenges faced by the chemical industry and defines goals of 30% reduction in material, water and energy usage as well as environmental burden by 2020. Major science and technology challenges in this area include the development of (a) new catalysts and reaction systems to prepare economical and environmentally safe processes with low life-cycle costs, and (b) new cost-effective technologies to create a broader variety of molecular architectures in alternative reaction media. Advances in chemistry and reaction engineering will lead to processes with better properties, such as increased selectivity, reduced by-product formation, less energy consumption

via process integration and intensification as well as sustainable operation with minimal environment footprints.

To address these great challenges, the Center for Environmentally Beneficial Catalysis (CEBC) has initiated novel alternative technologies to several existing megaton processes and the mission of CEBC is to develop proven technological processes enabling economically viable and environmentally sustainable conversions in bulk fuel or chemical productions. The representative approaches are: replacement of conventional organic solvents with environmentally friendly solvents such as carbon dioxide while improving the desired product yield or the process safety, substitution of corrosive liquid mineral acids with solid acids and efficient transformation of readily available raw materials, such as biomass, into more useful molecules and products through solvent engineering. Specifically, this dissertation addresses alternative process concept for such a megaton process – hydroformylation.

1.1 Industrial Challenges in Higher Olefin Hydroformylation

Hydroformylation of olefins, also known as oxo synthesis, was discovered by Otto Roelen of Ruhrchemie in 1938.³ Hydroformylation is one of the largest processes in the chemical industry and has a worldwide production capacity of over 15 billion pounds.^{3, 4} The hydroformylation reaction involves the catalytic conversion of olefins with synthesis gas ($\text{CO}:\text{H}_2 = 1:1$) to product aldehydes and is highly atomically efficient as all reactants are stoichiometrically consumed to form products. The reaction takes place with rhodium or cobalt catalysts, shown in Figure 1.1.

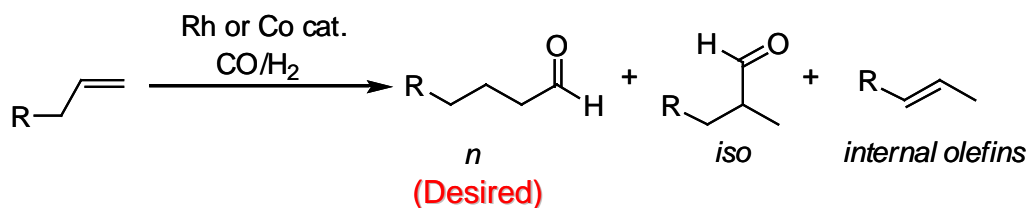


Figure 1.1 Hydroformylation reaction scheme

The hydroformylation reaction is exothermic. On average, the heat generated is 118 kJ per mole of product formed.³ The desired product is most often the linear aldehyde, which is used in the manufacturing of surfactants, detergents and plasticizers. It also has applications in asymmetric catalysis in the manufacturing of pharmaceutical and specialty chemicals. There are three different types of industrial hydroformylation processes practiced: two for lower olefins (C₄ or less) and the other for higher olefins (C₅-C₁₂), which is the focus of this dissertation.

In current industrial processes involving higher olefins, a cobalt (Co) catalyst is used even though it requires rather harsh temperatures (to ensure an acceptable rate of reaction) and pressures (to avoid decomposition of the cobalt carbonyl hydrides and maintain the catalyst stability). As shown in the Table 1.1, all industrial process temperatures are well above 100 °C and pressure is up to 300 bars.

Table 1.1 Operating conditions for industrial higher olefin hydroformylation processes

Process	BASF (Co)	Shell (Co/P)	Exxon (Co)
Substrate	1-octene	1-octene	1-octene
P, bar	300	80	300
T, °C	150	200	165
TOF, h ⁻¹	35	20	158
S _n , %	50	80	56

Further, the catalyst separation process is complex and tedious and requires the use of hazardous reagents such as acid or alkali (normally on the order of millions of pounds annually). Despite all these drawbacks, Co-based catalysts are still in use because Co is much cheaper than rhodium (Rh) which is known to be a better hydroformylation catalyst.⁵ Therefore, developing a process that requires milder temperatures and pressures, and also easier and efficient catalyst separation without the use of hazardous reagents is desirable. In the present work, we aim at developing a sustainable and environmentally benign process that can: a) deploy highly efficient Rh-based catalysts with higher selectivity and recoverability; b) minimize hazardous reagents usage for catalyst separation and recycle; c) be operated at milder conditions, i.e. tens of bars and lower than 100 °C.

1.2 Homogeneous Hydroformylation in CO₂-Expanded Liquids (CXLs)

A proposed approach by CEBC researchers^{6, 7} suggests that CO₂-expanded liquids (CXLs) can be used as reaction media, which helps address those challenges existing in the Co-based processes. A CXL is generated by partially replacing an

organic liquid solvent with compressible CO₂. The dissolution of CO₂ into organic phase can affect the properties of the organics, including its viscosity,⁸⁻¹⁰ diffusivity,^{11, 12} dielectric constants¹³ and its ability to solubilize permanent gaseous components.^{7, 14} These properties which are critical to reaction engineering can be tuned from neat organics to supercritical CO₂ by varying the operating pressure. For example, with the addition of CO₂, the increased diffusivities and decreased viscosities of CO₂-dissolved organic solvents are favorable for the gas-liquid biphasic reaction. The CXLs combine the advantages of both dense CO₂ and organic solvents.^{15, 16}

1-Octene has been chosen as a model substrate representing higher olefins and organometallic Rh as the homogeneous hydroformylation catalyst. Olefins, aldehydes and Rh complexes, the key components of hydroformylation reaction mixtures, are miscible with CO₂ at mild temperatures and pressures. Moreover, the solubility of gaseous reactant hydrogen can be enhanced as well. The batch experimental result shows that the CXL process gives acceptable turnover frequency ($\sim 300 \text{ h}^{-1}$) and aldehyde selectivity ($\sim 90\%$) at milder operating conditions (under tens of bars pressure 4-6 MPa and at temperature 60-90 °C). In addition, the selectivity towards desired linear aldehyde, represented by molar ratio of linear to branched aldehydes (n/i ratio), is greater than 10, four times higher than that in neat 1-octene.^{6, 7}

Yao *et al.*¹⁷ predicted vapor-liquid equilibrium for binary system, CO₂-expanded 1-octene, at 60°C using the Gibbs ensemble Monte Carlo molecular

simulation method. The volume expansions results simulated by this model give a close agreement with those calculated by Peng-Robinson equation of state (PR-EOS) since the binary mixing parameters used in PR-EOS were obtained from the vapor-liquid equilibrium data derived from this model. CO₂ mole fraction in liquid phase was found to increase linearly with increasing CO₂ pressure up to 5 MPa.

Guha *et al.*¹⁸ developed a reactor model combined with reaction kinetics, mass transfer rates and phase equilibrium to probe the mass transfer effects on the induction period in 1-octene hydroformylation in CXL. Both experimental and modeling results have shown that the stirring rate and introduction method of gaseous reactants have significant effects on both induction period and reaction rate. At high agitation speeds above 1000 rpm, the induction period leveled off at 12 min, indicating the elimination of mass transfer limitations. The non-zero induction period is the time required to convert catalyst precursor to active catalyst species.

CO₂ also has been applied as an inducing agent for separating homogeneous hydroformylation catalyst from product stream. Eckert *et al.*¹⁹ found that CO₂ addition induced phase splitting in an aqueous-organic homogeneous hydroformylation system and led to favorable catalyst and products separation. By introducing CO₂ into the post reaction mixture, the hydrophobic products aldehydes and unreacted substrate 1-octene partitioned, leaving the water-soluble ligands, TPPTS (tris(3-sulfophenyl)phosphine) and TPPMS ((3-sulfophenyl)-diphenylphosphine) quantitatively remained in the aqueous phase. The catalysts in aqueous phase were reused for up to three cycles and no loss in catalyst activity was

observed. It was also found that increasing CO₂ pressure favors the partitioning of both hydrophilic catalysts from organic phase and hydrophobic components from the aqueous phase.

Cole-Hamilton *et al.*²⁰ demonstrated a continuous flow homogeneous hydroformylation of 1-octene, in which ionic liquid modified rhodium is retained in the reactor with continuously supplied feed mixture including 1-octene, CO and H₂ dissolved in scCO₂. The products were carried away in the mobile scCO₂ phase and separated out downstream by releasing CO₂, while the catalyst is immobilized in the steady state mixture of substrate and products. The optimal performance was found in the case where [OMIM][TPPMS] ([OMIM]=[1-octyl-3-methyl imidazolium]⁺, [TPPMS] = [Ph₂P(3-C₆H₄SO₃)]⁻) was used as the ligand. Under a total pressure of 140 bar, the reaction reached steady state after 10 h, giving a turnover frequency of ca. 180 h⁻¹ in the optimized system and nearly 100 ppb Rh was detected in the recovered product compared to the steady Rh concentration of around 550 ppm in the reactor.

1.3 Goals and Objectives of Current Work

The goals of this dissertation are to investigate the kinetics of rhodium catalyzed higher olefin hydroformylation in CXL media and propose an economically practical and environmentally benign approach for recovery of expensive homogeneous rhodium catalyst based on economic and environmental assessments.

The specific objectives of the current work are therefore to:

- Exploit CO₂-expanded liquids as environmentally green solvents for hydroformylation of higher olefins and benchmark the catalyst systems^{6, 7, 21}
- Perform economic and environmental analyses for Rh-based CXL process benchmarked against the simulated conventional oxo process to identify research targets and drivers for economic viability and environmental benefits²²
- Design and synthesize highly soluble and recyclable polymer-bound rhodium complexes and screen catalysts by comparing the performance (activities and regioselectivities) in neat and CO₂-expanded 1-octene²³
- Develop a reactor model to investigate mass transfer and solvent effects on the kinetics of higher olefin hydroformylation in CXLs, guided by the experimental kinetic and phase equilibria studies
- Demonstrate continuous hydroformylation with *in situ* membrane filtration of rhodium catalyst complexes in collaboration with Professor Jon Tunge's group

The current work involves multidisciplinary collaborations contributed by three research groups in two universities (chemical engineers and chemists in University of Kansas and chemical engineers in Washington University in St. Louis). Figure 1.2 shows how CEBC's multiscale strategic research plan was employed to develop a bench-scale engineered system with industry input. Figure 1.2 also shows how the various activities are integrated across the research, education and industry partnership activities of the center. Industrial need and faculty expertise stimulated

the development of the testbed and its constituent research projects. These diverse projects were actively coordinated by the testbed leader and facilitated by CEBC's specialized research infrastructure.

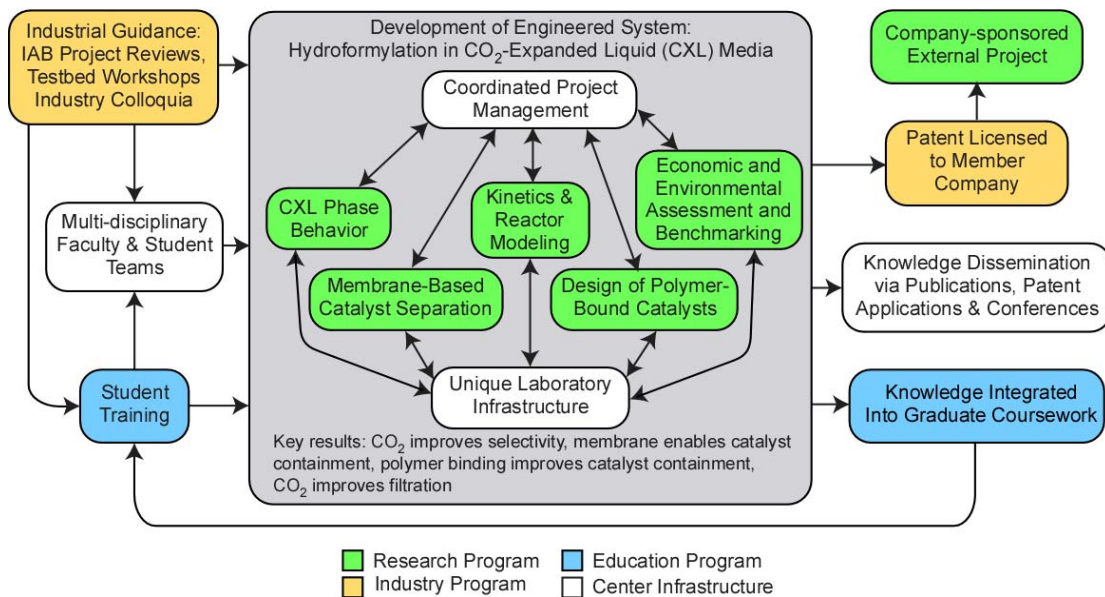


Figure 1.2 CEBC's systems approach for developing alternate hydroformylation technology

As presented in the Figure 1.2, to tackle the problems and overcome the barriers in engineering this alternative process, the hydroformylation testbed is divided into five subprojects, each of which deals with a well-defined topic and is accomplished by competent personnel. Professor Jon Tunge's group in Department of Chemistry at the University of Kansas primarily focuses on the chemistry aspect including catalyst design and synthesis, characterization, activity and selectivity testing. The potential and mature catalysts will undergo media testing in CXLs, such as phase equilibrium studies, solubility measurements (cloud point measurements),

viscosity measurements, catalyst separation and recovery by simple precipitation. Chemical engineers from Department of Chemical and Petroleum Engineering at the University of Kansas deal with a series of performance tests for the newly developed catalyst in bench-scale engineered systems. These activities include transport and kinetic studies, reactor scale up, solvent effects and retention tests of catalyst complexes through membrane filtration. In addition, computer-based programming and prediction, such as process simulation and kinetic modeling, are involved to identify the major research targets and gain profound insights.

This dissertation is composed of seven chapters. In addition to the introductory Chapter 1 and conclusion Chapter 7, the other five chapters emphasize the aforementioned objectives of the present work. In Chapter 2, a HYSYS-based process diagram was created for our novel CEBC process, named the CXL process, and benchmarked by a simulated conventional process extracted from Exxon patents. Total capital investments and total production costs for CXL and conventional processes were calculated and compared to recognize the major factors that have considerable influence on the economy of the processes. E-factor and environmental composite index were computed and compared to determine which emission source dominates each environmental impact category, providing guidance for process development and improvement and corresponding solution seeking.

Chapter 3 presents both experimental and modeling studies on the kinetics of rhodium/triphenylphosphine catalyzed hydroformylation in neat and CO₂-expanded 1-octene. The experiments were run in the kinetic regime without mass transfer

limitations at low and high 1-octene conversions. The concentrations versus time profiles were acquired using a high-pressure autoclave reactor equipped with an *in situ* infrared probe (ReactIR) built in the bottom. A Fortran-based program combining the reactor model with kinetic scheme was developed to obtain intrinsic kinetic constants for each elementary step by fitting the experimental data.

Chapter 4 implements the recovery of rhodium metal modified by various phosphorous ligands through batchwise or continuous membrane filtration under inert gas pressure. Triphenylphosphine served as the benchmark ligand and other lab-synthesized ligands including bulky bidentate ligands and soluble and bulky polymer bound bidentate ligands, were also examined. The rhodium metal and phosphorous ligand leaching in permeate were measured by elemental analysis technique. Chapter 5 demonstrates continuous membrane filtration integrated with *in-situ* hydroformylation reaction at elevated temperature under synthesis gas pressure using polymer bound rhodium, to test the rhodium leaching as well as catalyst complexes stability, activity and selectivity. In Chapter 6, volume expansions, cloud point pressures and the viscosities of the hydroformylation reaction mixtures are measured and the possibility of increasing membrane flux resulting from viscosity reduction by CO₂ addition is explored.

1.4 References

1. Industry statistics by American Chemistry Council. <http://www.americanchemistry.com>
2. Technology vision 2020: The US chemical industry. <http://www.chemicalvision2020.org>, **1996**.
3. Frohling, C. D.; Kohlpaintner, C. W.; Bohnen, H.-W., Carbon monoxide and synthesis gas chemistry - hydroformylation (Oxo synthesis, Roelen reaction). In *Applied homogeneous catalysis with organometallic compounds*, Cornils, B.; Herrmann, W. A., Eds. Wiley-VCH: Weinheim, **2002**; Vol. 1, pp 29-103.
4. Bahrmann, H.; Bach, H., Oxo synthesis. In *Ullmann's Encyclopedia of Industrial Chemistry*, 6th ed.; Wiley-VCH: Weinheim, Germany, **2003**; Vol. 24, p 553.
5. Cobalt with purity of 99.8% in North America (\$15/LB in March, **2009**) [<http://www.metalprices.com>] is over 800 times cheaper than rhodium (\$12,456/LB, averaged price from February to March, **2009**) [<http://www.kitco.com>].
6. Jin, H.; Subramaniam, B., Homogeneous catalytic hydroformylation of 1-octene in CO₂-expanded solvent media. *Chemical Engineering Science* **2004**, 59, (22-23), 4887-4893.
7. Jin, H.; Subramaniam, B.; Ghosh, A.; Tunge, J., Intensification of catalytic olefin hydroformylation in CO₂-expanded media. *AIChE Journal* **2006**, 52, (7), 2575-2581.
8. Sih, R.; Armenti, M.; Mammucari, R.; Dehghani, F.; Foster, N. R., Viscosity measurements on saturated gas-expanded liquid systems - ethanol and carbon dioxide. *The Journal of Supercritical Fluids* **2008**, 43, (3), 460-468.
9. Sih, R.; Dehghani, F.; Foster, N. R., Viscosity measurements on gas expanded liquid systems - methanol and carbon dioxide. *Journal of Supercritical Fluids* **2007**, 41, (1), 148-157.
10. Sih, R.; Foster, N. R., Viscosity measurements on saturated gas expanded liquid systems - acetone and carbon dioxide. *The Journal of Supercritical Fluids* **2008**, 47, (2), 233-239.
11. Dariva, C.; Coelho, L. A. F.; Oliveira, J. V., A kinetic approach for predicting diffusivities in dense fluid mixtures. *Fluid Phase Equilibria* **1999**, 160, 1045-1054.
12. Maxey, N. B., Transport and phase transfer catalysis in gas - expanded liquids. *Ph.D. Dissertation* **2006**.
13. Subramaniam, B.; Rajewski, R. A.; Snavely, K., Pharmaceutical processing with supercritical carbon dioxide. *Journal of Pharmaceutical Sciences* **1997**, 86, (8), 885-890.
14. Freitag, N. P.; Robinson, D. B., Equilibrium phase properties of the hydrogen methane carbon-dioxide, hydrogen carbon-dioxide n-pentane and hydrogen n-pentane systems. *Fluid Phase Equilibria* **1986**, 31, (2), 183-201.

15. Eckert, C. A.; Liotta, C. L.; Bush, D.; Brown, J. S.; Hallett, J. P., Sustainable reactions in tunable solvents. *Journal of Physical Chemistry B* **2004**, 108, (47), 18108-18118.
16. Jessop, P. G.; Subramaniam, B., Gas-expanded liquids. *Chemical Reviews* **2007**, 107, (6), 2666-2694.
17. Houndonougbo, Y.; Jin, H.; Rajagopalan, B.; Wong, K.; Kuczera, K.; Subramaniam, B.; Laird, B., Phase equilibria in carbon dioxide expanded solvents: experiments and molecular simulations. *Journal of Physical Chemistry B* **2006**, 110, (26), 13195-13202.
18. Guha, D.; Jin, H.; Dudukovic, M. P.; Ramachandran, P. A.; Subramaniam, B., Mass transfer effects during homogeneous 1-octene hydroformylation in CO₂-expanded solvent: modeling and experiments. *Chemical Engineering Science* **2007**, 62, (18-20), 4967-4975.
19. Hallett, J. P.; Ford, J. W.; Jones, R. S.; Pollet, P.; Thomas, C. A.; Liotta, C. L.; Eckert, C. A., Hydroformylation catalyst recycle with gas-expanded liquids. *Industrial & Engineering Chemistry Research* **2008**, 47, (8), 2585-2589.
20. Frisch, A. C.; Webb, P. B.; Zhao, G.; Muldoon, M. J.; Pogorzelec, P. J.; Cole-Hamilton, D. J., "Solventless" continuous flow homogeneous hydroformylation of 1-octene. *Dalton Transactions* **2007**, (47), 5531-5538.
21. Jin, H., Exploiting CO₂-expanded liquids as reaction media for catalytic hydroformylation of higher olefins. *Ph.D Dissertation* **2006**.
22. Fang, J.; Jin, H.; Ruddy, T.; Pennybaker, K.; Fahey, D.; Subramaniam, B., Economic and environmental impact analyses of catalytic olefin hydroformylation in CO₂-expanded liquid (CXL) media. *Industrial & Engineering Chemistry Research* **2007**, 46, (25), 8687-8692.
23. Wang, R.; Cai, F.; Jin, H.; Xie, Z.; Subramaniam, B.; Tunge, J. A., Hydroformylation in CO₂-expanded media. In *Gas-expanded liquids and near-critical media: green chemistry and engineering*, Hutchenson, K. W.; Scurto, A. M.; Subramaniam, B., Eds. ACS Symposium Series No. 1006 American Chemical Society: Washington, D.C., **2009**; pp 202-217.

Chapter 2. Economic and Environmental Impact Analyses of Catalytic Higher Olefin Hydroformylation in CO₂-Expanded Liquids (CXLs) Media

Recently, CEBC researchers reported a new hydroformylation process concept that uses CO₂-expanded liquids (CXLs) as reaction media.^{1, 2} The hydroformylation turnover frequencies (TOFs) were up to four-fold higher in CXLs relative to those in neat organic solvent. The enhanced rates were achieved at milder conditions (30-60 °C and 4-12 MPa) compared to industrial processes (140-200 °C and 5-30 MPa). Preliminary economic and environmental analyses of the CXL process are presented in this chapter and benchmarked against a simulated conventional hydroformylation process for which non-proprietary data were obtained mostly for the Exxon process. The simulation results indicate that the CXL process has clear potential to be economically viable and environmentally favorable subject to nearly quantitative recovery and recycle of the rhodium-based catalysts. For the simulated conventional process, acetic acid discharged during the catalyst recovery steps is the dominant source of adverse environmental impact. These analyses have provided guidance in catalyst design and in choosing materials and operating conditions that favor process economics while lessening the environmental footprint.

Section 2.1 introduces the background, objectives and the significance of this chapter and how it fits in the whole scenario of this dissertation. Section 2.2 reviews the limited literature concerning economic and environmental analyses of hydroformylation processes. Section 2.3 details the methodology and simulation parameters used in the economic and environmental analyses for both the CEBC and

simulated conventional processes. Sections 2.4 and 2.5 explain the cost estimation and environmental impact calculation procedures, respectively. The results of the simulations are discussed in Section 2.6. A brief summary in Section 2.7 concludes this chapter.

2.1 Background

Industrial hydroformylation of higher olefins employs cobalt-based catalysts that require rather harsh operating conditions (140-200 °C and 5-30 MPa).³ Large quantities of acid and alkaline solutions are involved in the catalyst recovery (demetallization) step for that portion of catalyst that cannot be directly recycled.⁴ Rhodium-based catalysts are more efficient than cobalt-based catalysts for higher olefin hydroformylation but are significantly more expensive. Hence rhodium-based technology must demonstrate near-quantitative catalyst recovery and durability in order to be economically viable.

Recently, investigations at the Center for Environmentally Beneficial Catalysis (CEBC) laboratories and elsewhere^{1, 2, 5-11} have demonstrated how a relatively new class of solvents, CO₂-expanded liquids (CXLs), is a promising alternative media for performing catalytic reactions. The improved transport properties of CXLs⁶ compared to neat organic solvents and the enhanced solubilities of permanent gases (*i.e.*, O₂,^{12,7} H₂^{13, 14}) in CXLs, which alleviate mass transfer limitations and increase the availability of gaseous reactants in the liquid phase, have been shown to intensify overall reaction rates in laboratory experiments. Other potential advantages of CXL usage include substantial replacement of volatile organic

solvents with non-toxic CO₂, and milder operating pressures (tens of bars) compared to reported supercritical CO₂-based process concepts, which typically require well in excess of 100 bars (10 MPa). In addition, the ability to easily tune CXL polarity by changing the CO₂ content provides an opportunity to separate and recycle polar homogeneous catalysts.⁷

In the CXL-based hydroformylation process concept demonstrated by CEBC,^{1, 2} part of the liquid substrate and solvent is replaced with dense CO₂ to generate a CO₂-expanded reaction medium. For Rh(acac)(CO)₂ catalysts modified with triphenyl phosphine (TPP) ligand, the turnover frequencies (TOFs) for higher olefin hydroformylation were up to four-fold higher in CXLs relative to those in neat organic solvent and neat CO₂. The turnover frequency (TOF) is defined as the number of moles of 1-octene reacted per mole catalyst per hour of batch run time. The enhanced rates were achieved at milder conditions (30-60 °C and <12 MPa) than those employed in industrial processes (140-200 °C and 5-30 MPa). The addition of CO₂ improved the chemo- and regio-selectivities resulting in enhanced yields of the desired product; the aldehydes selectivity exceeds 97% and the *n/i* ratios are as high as 17.5. In addition, CO₂ also showed potential as an anti-solvent for effectively recovering the rhodium-based catalysts post reaction.

When developing alternative technologies, it is extremely beneficial to perform early quantitative analyses to answer questions such as the following: (i) What are the important economic and environmental impact drivers in the conventional and alternative processes? (ii) Does the alternative technology concept

have a chance to be economically viable while providing superior environmental benefits? Answers to such questions will help establish quantitative performance benchmarks (such as catalyst recovery, reactor size, operating pressure and temperature, etc.) that must be met so that the alternative technology concept has a chance to be economically feasible. In this chapter, we report economic and environmental impact analyses of the CO₂-based hydroformylation technology based on a plant-scale process simulation. For comparison, we perform similar economic and environmental impact analyses for a simulated conventional process using data from the Exxon hydroformylation process. We employ this simulated conventional process as the industrial benchmark against which the CXL process economics and environmental impact are compared.

2.2 Literature Review

With the increasing environmental concerns and stricter regulations, it is imperative to design chemical processes with less pollution generation and maximized economic output. During the past two decades, economic and environmental assessments have been popularly employed to guide process design and integration, product development as well as waste minimization. Aiming at maximizing economic returns and minimizing environmental footprints, the term of ecoefficiency was invented and defined as economic index divided by environmental index, representing a single indicator incorporating two separate measures of performance.¹⁵ However, unlike the simplicity of the ecoefficiency definition, in the practical applications, the judicious decision-making not only involves complicated

flow diagram development and cost estimation but also requires systematic approach and appropriate metrics that allow quantitative assessment of environmental hazards.

Economic and environmental analyses have been widely applied to various research areas and turn out to be a profitable tool to identify the key operational parameters, facilitate deficiency elimination and guide subsequent improvements and optimizations. Recent case studies¹⁶⁻¹⁹ of industrial chemical processes provide relevant procedural guidance for our simulations including a process design for 1-octene hydroformylation by modified homogeneous rhodium catalyst immobilized on silica.²⁰

Motamedi and Senhorst²¹ illustrate the process design, economic and environmental analysis of a novel dyeing process using supercritical CO₂ as an alternative to water, which is commonly used as a medium to transport the dye to the textile fibers in the conventional process. For the economic aspects, the preliminary cost analysis indicates that there is an insignificant difference in the total costs between the conventional process and its alternatives, but a large difference in cost composition. Moreover, the environmentally related costs and the energy costs of the supercritical process are substantially lower than those of the conventional process and the identified major environmental impact contributor is the polluted water.

The life cycle assessment (LCA) technique has been identified as a powerful tool to calculate environmental impacts derived from products and system, and to calculate resource consumption.²² Kniel and Petrie²³ describe how to use LCA as a tool for process design, in a case study of a nitric acid plant to quantify and compare

the environmental burden and economic performance of three alternative processes including the original plant, selective catalyst reduction (SCR) and high pressure modified processes. Softwares HYSIMTM and the Excel-based software PEMS are used to provide mass and energy flow information and to perform inventory analysis and impact assessment, respectively. The high-pressure modification process is found to be superior to its counterparts from an environmental point of view. The results using the developed economic and environmental models are consistent with the intuitive judgments suggesting that the proposed methodology is suitable for problems where the relationships are perhaps not as straightforward.

Gasafi *et al.*²⁴ present an application of LCA in the early stage design of supercritical water gasification (SCWG) of bio-based feedstock and perform a dominance analysis to recognize the key issues in the process chain with regard to environmental impacts. Based on the proposed flow diagram for SCWG, four environmental impact categories (resource depletion, global warming potential, acidification and eutrophication) are inventoried and compared for each subsystem so that the dominant process steps, which impose the major environmental impacts, are identified. This analysis is more illustrative than determinative focusing on describing methodological approach in evaluating environmental impacts. No economic analyses and comparison between different possible processing routes were provided. Optional improvements for further development to reduce the environmental burden are also suggested.

Lim and Park²⁵ first attempt to analyze the environmental and economic performance of a water network system (WNS) and to identify principal contributors to environmental burdens and economic costs using LCA and life cycle costing (LCC). Compared to the conventional water system (CWS), WNS has lower environmental burdens and economic costs than the CWS and was therefore more eco-efficient. The consumptions of industrial and ionized water are principal contributors to the environmental and economic burdens. The third principal contributor to the environmental burdens is consumption of electricity, while that to the economic costs is piping cost. This work provides fundamental and valuable information being employed to obtain the simple and practical mathematical optimization models synthesizing the most environmentally friendly, economical, or sustainable WNSs.

Wen and Shonnard²⁶ evaluate the economic and environmental impacts of heat exchanger networks (HEN) for optimum minimum approach temperature and found that the optimum temperatures are not identical when using environmental index I_{PC} and annualized costs as objectives, respectively. The environmental impacts for HEN are significantly reduced compared to those with the no network, and the pre-manufacturing stages contribute dominantly to several environmental impact categories, such as total toxic release (TTR) and volatile organic compounds (VOC). In addition, the sensitivity analysis of the optimum temperature to several parameters is performed and among all the parameters studied the environmental annualization

factor and overall heat transfer coefficient are found to have the most significant impact on the variability of optimum temperature.

An early stage analysis is reported by Reek²⁰ concerning process design of 1-octene hydroformylation to nonanal by N-(3-trimethoxysilane-n-propyl)-4,5-bis(diphenylphosphino)-phenoxazine modified homogeneous rhodium catalyst immobilized on silica. The process with production capacity of 100 kton is simulated using Aspen Plus[®] assuming that the packed bed reactor is operated at temperature of 80 °C and pressure of 50 bars (5 MPa) at a catalyst concentration of 0.1 wt%. It also assumes that an Rh equilibrium concentration of 10 ppb is leached in the product stream and the corresponding Rh loss is 1 kilogram per year. However, detailed and systematic estimation about capital investment and operating costs or environmental impact analysis is lacking for this particular process.

The aforementioned studies are only a few examples out of numerous publications in regard to the applications of economic and environmental analyses. The purpose of this selection of the literature is to show how the combination of the economic and environmental analyses affects the decision-making and problem solving in any level or any scale of process design. This is a restricted review and is not intended to be exhaustive.

2.3 Methodology

Plant-scale data needed to prepare a process flow diagram for the simulated conventional process and for performing an economic analysis were obtained from

data available in the literature. Data for preparing a flow diagram of the CXL process and for performing an economic analysis were extrapolated from laboratory studies.

2.3.1 Simulation parameters and assumptions

The following common assumptions were made for both processes. The annual production capacity was set at 200 kton, which is in the range of a typical petrochemical process (10-500 kton/yr²⁷). The conventional process produced aldehydes and alcohols while the CXL process produced linear and branched aldehydes. Identical feeds (pure 1-octene and syngas with fixed CO/H₂ ratio) were employed. The costs of feedstock, products, utilities, and labor were also assumed to be identical for both processes.

The parameters for simulated conventional process were extracted for the most part from literature and patents assigned to Exxon Chemical Patents Inc. and Exxon Research & Engineering Co., pertaining to a higher olefin hydroformylation process, commonly known as the oxo process. In this process, a higher olefin mixture (C₅-C₁₂) feedstock is hydroformylated with the proper proportions of CO and H₂ by unmodified cobalt to produce C₆-C₁₃ aldehydes. Beside the predominant product aldehydes, other species, such as alcohols, paraffins, acetals and aldol condensation products, are also formed in the hydroformylation reaction. The cobalt catalyst can be initially supplied in the form of salt cobalt acetate Co(OAc)₂ or recycled from a precarbonylation stage in the form of a cobalt anion (Co⁻¹) or organically soluble form of Co⁺², such as cobalt naphthalate.⁴ Prior to sending the hydroformylation product to the next processing step, which is normally

hydrogenation where the aldehydes are converted to the corresponding alcohols, the cobalt catalyst must be removed. The volatile hydro cobalt carbonyl $\text{HCo}(\text{CO})_4$ stripped from the product stream is absorbed using olefin feed or higher olefin than the feed olefin itself and then is recycled back to the oxo reactor. The crude oxonation product mixture from the reactors then experiences the demetalling stage, contacting with a stream of dilute acetic acid and optionally chosen oxidant including oxygen and air (U.S. Patent 4,255,279²⁸). The crude product stream containing dissolved cobalt species is contacted with water and an organic acid and split into two immiscible phases, with the organic phase containing desired aldehyde product and the aqueous phase containing cobalt salt, $\text{Co}(\text{OAc})_2$. The organic phase then is sent to the downstream unit operations to be converted to the final product. The aqueous cobalt metal is subjected to high pressure sythesis gas (CO/H_2) in the presence of an organic solvent and is hydrogenated to oil-soluble active cobalt hydrocarbonyl $\text{HCo}(\text{CO})_4$.

Numerous patents were published spanning the last five decades, from the 1960s to the present, addressing the cobalt recovery issues and variations in modifications and improvements. For example, a cobalt flash process was disclosed in U.S. Patent 4,625,067²⁹, wherein the crude product stream is contacted with a stream of stripping gas to entrain the volatile cobalt compounds. In U.S. Patent 5,237,104³⁰, an olefin of a heavier weight than the feed olefin in the hydroformylation process is used as absorbent for recovering hydro cobalt carbonyl stripped from an oxonation reactor product. In U.S. Patent 5,410,090³¹, airless cobalt demetalling in

the cobalt flash combination catalyst cycle is disclosed. The simplified flow diagram of the Exxon patented oxo process is redrawn from U.S. Patent 5,237,104³⁰ and shown in Figure 2.1, to illustrate the typical features of different updated versions with various cobalt catalyst recovery strategies.

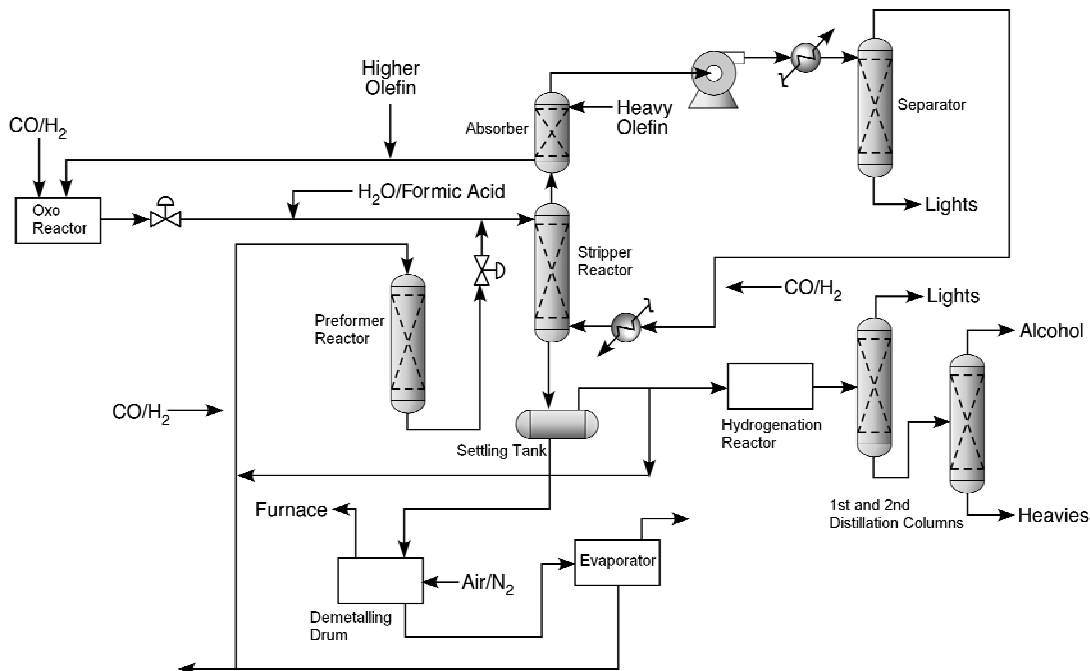


Figure 2.1 Industrialized Exxon oxo process flow diagram adapted from US 5,237,104

In the following context, we endeavored to extract the critical operating parameters in the Exxon oxo process from the exemplified data in the available patents, but were only able to reproduce certain parts of the process, such as reaction and product distillation.

Tables 2.1 and 2.2 summarize the simulation parameters that are unique to the conventional and CXL processes (catalyst, solvent, operating conditions and product

selectivity), respectively, along with the source references. The Peng-Robinson equation of state was chosen as the thermodynamic property method for the simulations since it can be applied to polar, non-electrolyte solutions at high pressures.³²

Table 2.1 Simulation parameters for the simulated conventional process

Reaction conditions ³³	Reactor: CSTR (three loop reactors in series) P = 30 MPa; T = 165 °C; X = 90%; n/i = 4 Syngas/olefin = 3.22:1; H ₂ /CO = 1.18:1 LHSV ³⁴ (Liquid Hourly Space Velocity) = 2.5 h ⁻¹
Catalyst	Co(OAc) ₂ ²⁸ ; [Cobalt] = 0.15 wt% (2856 ppmw) based on olefins ³³ Oxygen/Cobalt = 2:1 ³⁴ ; Organic acid/Cobalt = 2:1 ³⁴ Cobalt Recovery Rate ³⁵ : 98%
Product selectivity ^{33, 36}	Light Oxo Fraction (LOF): S(paraffin) = 2% Heavy Aldehydes & Alcohols (HA): S(aldehydes) = 70%; S(alcohols) = 10% Heavy Oxo Fraction (HOF): S(heavy ends) = 18%

Table 2.2 Simulation parameters for CXL process

Reaction conditions ²	Reactor: CSTR; LHSV (Liquid Hourly Space Velocity) = 5 h ⁻¹ P = 3.8 MPa; T = 60 °C; X = 90%; n/i = 9.6 Syngas/olefin = 3.22:1; H ₂ /CO = 1.18:1
Catalyst	Rh(acac)(CO) ₂ ; [Rh] = 0.028 wt% (280 ppmw) based on olefins Ligand: Triphenylphosphine (TPP); [TPP] = 5 wt% ²⁷ ; TPP Loss = 0.5%; Rhodium Recovery Rate ³⁷ : 99.8%

Solvents	Carbon dioxide = 10 vol% ²
Product Selectivity ²	Aldehydes: S(aldehydes) = 97.5% Isomers: S(isomers) = 1.5% Heavy ends: S(assumed to be acetal only) = 1%

2.3.2 Process simulation details

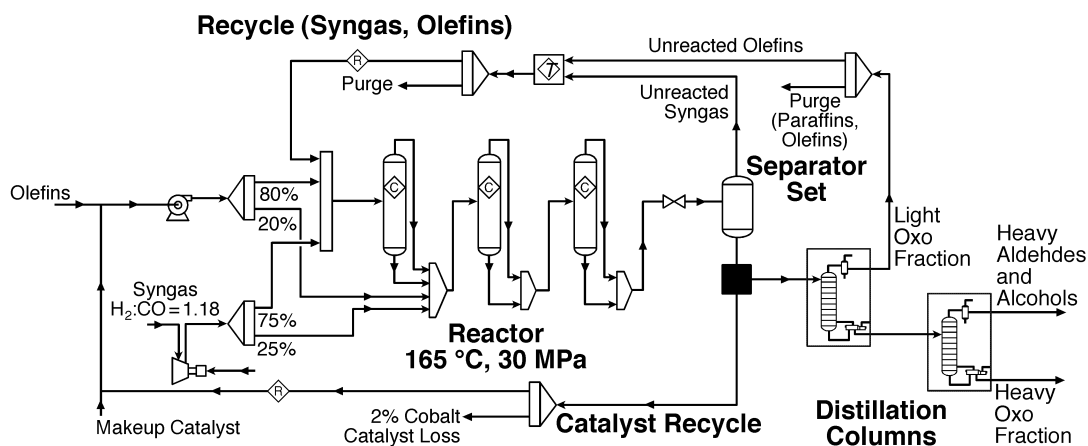


Figure 2.2 HYSYS flowsheet for the simulated conventional process

Detailed process simulations were performed with Aspen HYSYS[®] 2004.2³⁸ software from Aspen Technology, Inc. The flowsheets for the conventional and CXL processes are illustrated in Figures 2.2 and 2.3, respectively. For the conventional process, the olefinic feed along with catalyst and syngas are pressurized to 30 MPa and distributed between the first and the second loop reactors at ambient temperature. The hydroformylation reaction is exothermic and is sustained at 165 °C under steady operation. The cobalt-catalyzed hydroformylation occurs in the three loop reactors in-series. The loop reactor is modeled as a CSTR in the HYSYS simulator because of its high internal circulation rate.³⁹ The unreacted syngas and olefins are separated

downstream from the third reactor and recycled back to the reactors (details not shown in Figure 2.2 but included in the HYSYS sub-flowsheet indicated as “T” in the figure). The catalyst is separated from the crude product (n/i ratio of 4) and the nearly catalyst-free product stream is distilled in three stages: Light Oxo Fraction (LOF), Heavier Aldehydes and Alcohols (HA), and Heavy Oxo Fraction (HOF). The catalyst separation and recycle steps along with the product downstream hydrogenation and steam cracking steps are simulated only to the level of detail provided by the limited literature data. Hence, these steps are not shown in detail in Figure 2.2. However, even without consideration of these unit operations, valuable insights into the economic and environmental impact factors are gained, as discussed later.

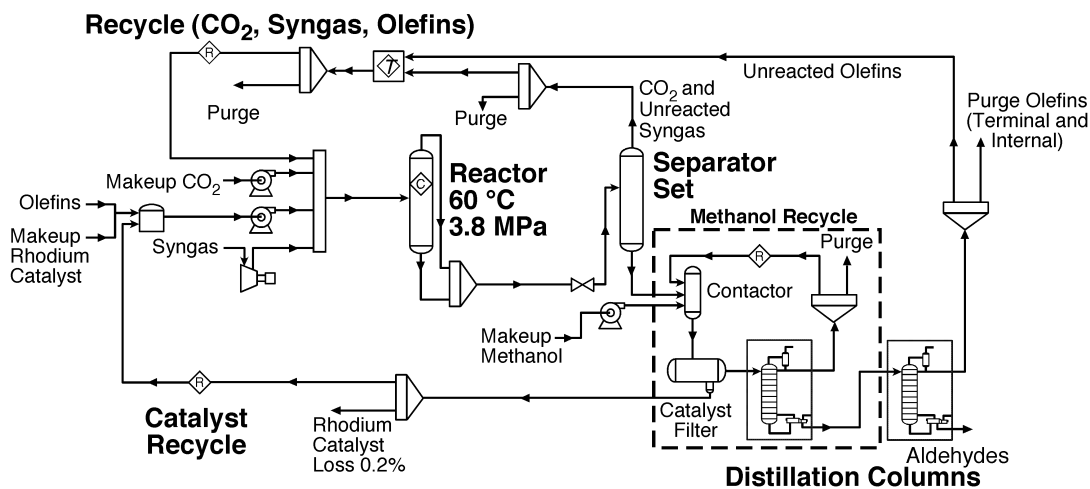


Figure 2.3 HYSYS flowsheet for proposed CXL process

For the CXL process, the olefin, syngas, and co-solvent (CO₂) are introduced at 60 °C and 38 MPa. Rhodium-catalyzed hydroformylation is performed in stirred tank

vessels. As shown in Figure 2.3, the unreacted syngas, olefin and the CO₂ are pressurized and recycled in sub-flowsheet “T”. The relatively non-polar crude product stream containing the rhodium catalyst complex is contacted with anti-solvent methanol, a highly polar solvent, to precipitate the catalyst. A catalyst recovery rate of 99.8%, which is 0.15% lower than the value reported for polymer bound bulky-phosphite modified rhodium catalyst,³⁷ is used in the simulation. The catalyst is separated by filtration, re-dissolved in the olefinic substrate and recycled. The methanol is distilled off from the product mixture and reused. The products are further purified through distillation that separates the unreacted olefins and the olefin isomers.

2.3.3 E-factor analysis

The environmental burden index, or the E-factor, is defined as kilograms of waste generated per kilogram of desired product in the process.⁴⁰ Waste is defined as everything but the desired products generated in the process. The E-factors for the simulated conventional and CXL processes are tabulated in Table 2.3 and calculated based on the process flowsheets shown in Figures 2.2 and 2.3.

Table 2.3 E-factors for both CXL and the simulated conventional processes

	E-factor	Waste
CXL process	0.34	purged reactants & solvents, by-products
the simulated conventional process	0.96	including HOF, without steam cracking
the simulated conventional process	0.66	including HOF, 12% improvement by steam cracking

In addition to the major byproducts, all purges along with unit-specific and fugitive emissions are treated as waste. Purges and byproducts go to incineration.

CO₂ emissions due to energy consumption are also categorized as waste. Based on these definitions, the estimated E-factor for the conventional process is 0.66, assuming that part of the Heavy Oxo Fraction (HOF) is reformed by the steam-cracking step. The E-factor is in the range reported for the bulk chemicals industry segment.⁴⁰ In contrast, the E-factor for the CXL process is 0.34 because of higher product selectivity. In other words, the CXL process generates half as much waste as the simulated conventional process. The potential environmental impacts of the waste generated in the two processes are discussed in a later section. A similar E-factor for a cobalt catalyzed process and a much lower E-factor for a rhodium-catalyzed process (Ruhrchemie/Rhône-Poulenc process) have been reported in the literature.⁴¹

2.4 Economic Analysis

The total capital investment (TCI) and total production cost (TPC) are calculated based on standard methods.⁴² The mass and energy balance calculations with HYSYS[®] provide the stream properties such as flow rate, composition and heat duty for process equipment sizing. Carbon steel is chosen as the material of construction because the reaction mixture including reactants, solvents and products is not corrosive. Costs are adjusted for inflation to 2006 dollars using the Marshall and Swift Equipment Cost Index.⁴³

Total production cost is the sum of two categories: general expenses and total operating costs. General expenses make up approximately 19% of TPC. Total operating costs include variable production costs (raw materials, catalyst, solvents,

utilities, labor, maintenance costs, and etc.), fixed charges, and plant overhead costs (research and development costs, distribution and marketing costs, administrative costs). Depreciation is ignored in the present analyses. The cost of raw materials, products, catalysts and solvents are taken from a variety of sources including Chemical Market Reporter.⁴⁴ Utilities costs are obtained from the Energy Information Administration, Department of Energy.⁴⁵

Excel spreadsheet is used for chemical components inventory and cost calculations. Aspen Icarus Process Evaluator also is available for economic estimation enabling front-end consideration of life cycle costs. The tabulated formats of Total Capital Investment and Total Production Cost calculations are given in Tables I.1 and I.2 in Appendix I. The chemicals and utilities involved and their prices inventory are provided in Table I.3 in Appendix I as well.

The aldehyde turnover frequency is 19,900 kg / (kg Rh · h) (See Appendix I.2 for details). With the assumption of a 99.8% Rh recovery rate (equivalent to 560 ppb in crude product stream when Rh concentration in the reactor is 280 ppmw), the yearly loss of Rh for a 200 kton production plant will be about 118 kg, accounting for 3.5 million dollars at an assumed Rh price of \$30,000/kg. At an aldehyde yield of 88% (equivalent to 0.9 kg aldehyde per kg the crude product), the make-up Rh cost per pound aldehyde is calculated as

$$\frac{1 \text{ kg crude product} \times 560 \text{ ppb Rh} \times 10^{-9} \text{ kg Rh/kg crude product} \times \$30000/\text{kg Rh}}{1 \text{ kg crude product} \times 0.90 \text{ kg aldehyde/kg crude product}}$$

$$= \frac{\$1.68 \times 10^{-2} \times 100 \text{ cents}/\$}{0.90 \text{ kg aldehyde} \times 2.2 \text{ lbs/kg}} = 0.85 \text{ cents/lb}$$

Assuming an aldehyde price of \$1/lb, the Rh loss alone is about 0.85% of the product value.

2.5 Environmental Impact Analysis

In addition to economic aspects, environmental impacts are also evaluated to gain insight into how the reaction route, operating conditions and separation together play their roles in sustainable design. The environmental analysis tool utilized for process evaluation is called EFRAT (Environmental Fate and Risk Assessment Tools) and resides within the SCENE⁴⁶ (Simultaneous Comparison of Environmental and Non-Environmental Process Criteria) software. Figure 2.4 illustrates the information flow inside the EFRAT database.

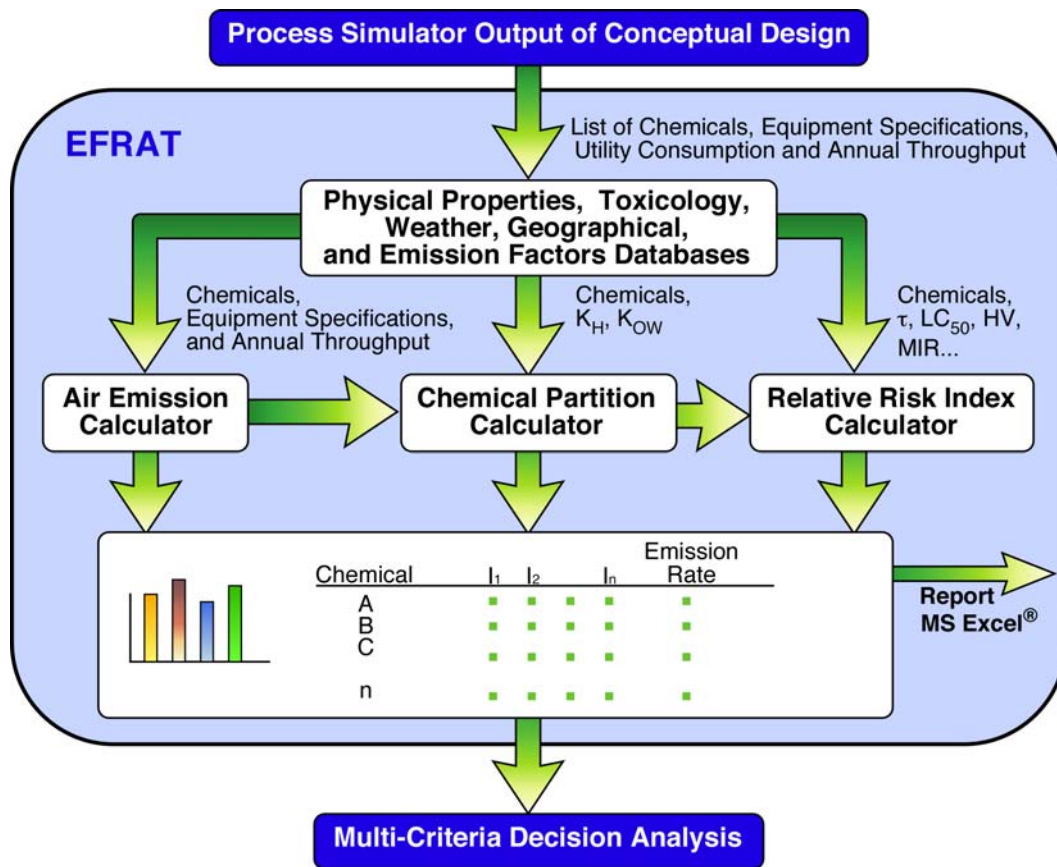


Figure 2.4 Calculation structure of environmental analysis tool – EFRAT

The process simulator HYSYS[®] provides the mass and energy balances, a list of chemicals, stream properties, unit operations and equipment sizes associated with the processes. The physical and thermodynamic properties for each chemical are retrieved from a database resident within HYSYS[®]. Three calculation routines make up the heart of EFRAT. The Air Emissions Calculator uses emission factors, correlations, and process simulator stream information to provide an estimate of the unit-specific and fugitive air emission rates for each chemical within the process. It is assumed that 99% of all waste organic compounds are incinerated to carbon dioxide

and only 1% of each is released to the environment.⁴⁷ The Chemical Partition Calculator uses a multimedia compartment model to estimate the equilibrium mole fraction of the emitted chemical into the air, water, soil, or sediment compartments of the environment. The Relative Risk Index Calculator generates nine environmental and health impact indices for the given process. These indices are relative to a benchmark compound and are based on the physical, chemical and toxic properties of each chemical.

The environmental impact categories include global warming (GW), ozone depletion (OD), smog formation (SF), acid rain (AR), non-carcinogenic toxicities associated with human inhalation (INH) and human ingestion (ING) routes, carcinogenic toxicities associated with human inhalation (CINH) and human ingestion (CING) routes, and fish toxicity (FT). First, a cumulative process index I_k for environmental impact category k is computed by Equation (1) based on the product of the total emission rate E_i (kg/yr) of each chemical from all process sources and the relative risk index $I_{i,k}^*$ of the chemical in the impact category k ;

$$I_k = \sum_{i=1}^n (I_{i,k}^* \cdot E_i) \quad (1)$$

The process index is then normalized with the published national index. The National Index \hat{I}_k for each impact category is the product of the annual national emission \hat{E}_k (kg/yr) of the chemical representing the impact category k and the

average relative risk index $\langle I^* \rangle_k$ attributed to the chemical in the national inventory.

It is expressed as follows:

$$\hat{I}_k = \hat{E}_k \cdot \langle I^* \rangle_k \quad (2)$$

Finally, a composite index (IPC) is estimated as the sum of normalized index

$I_k^N = \frac{I_k}{\hat{I}_k}$ times weighting factor W_k for each environmental impact category:

$$I_{PC} = \sum_k I_k^N \cdot W_k \quad (3)$$

The weighting factors (W_k) are generated for quantification of environmental effects that damage ecosystems or human health on a European scale in Life Cycle Assessment (LCA), based on the distance-to-target principle and the assumption that a 5% ecosystem impairment is equivalent to the death of one person per million per year. The weighting factors are given in Table 2.4. This information reveals that the reduction of each environmental effect must be of the order of the corresponding weighting factor to keep the ecosystem impairment below 5%.⁴⁸

After the process simulation is completed (meaning converged process and balanced mass and energy), using the commercial process simulator HYSYS in this case, the SCENE software is synchronized with HYSYS. The list of chemicals, unit operations, and stream information is automatically retrieved from a database resident in the software HYSYS and classified into certain categories in SCENE. The synchronization step can be repeated any time when the flowsheet is changed or updated.

Table 2.4 Weighting factors for each category of environmental impacts

Global Warming (GW)	2.5
Ozone Depletion (OD)	100
Smog Formation (SF)	2.5
Acid Rain (AR)	10
Noncarcinogenic (INH, ING)	5
Carcinogenic (CINH, CING)	5
Fish Toxicity (FT)	10
Source: Eco-Indicator 95 framework for life cycle assessment, Pre Consultants, http://www.pre.nl	

2.6 Results and Discussion

Based on the predicted economic and environmental impact trends, either positive or negative credit is assigned for the various performance criteria as summarized in Table 2.5.

Table 2.5 Positive and negative credits assigned to each process by different operating conditions

	The Simulated Conventional Process	CXL Process
Temperature	+	-
Pressure	-	+
Catalyst cost	+	-
Energy for solvent recycle	+	-
Linear selectivity	-	+
By-products	-	+
Catalyst recycle	-	+

“+”: Environmental or economic favorable;

“-”: Environmental or economic unfavorable.

The reduction of raw material (i.e. 1-octene) usage and the use of milder operating conditions (lower pressure) in the CXL process lessen the environmental

impact. Qualitatively, the attributes rated in Table 2.5 show that the CXL process has the potential to be economically and environmentally more favorable than the simulated conventional process.

2.6.1 Economic analysis

Figure 2.5 compares the various costs associated with the Total Capital Investment (TCI) for the simulated conventional and CXL processes:

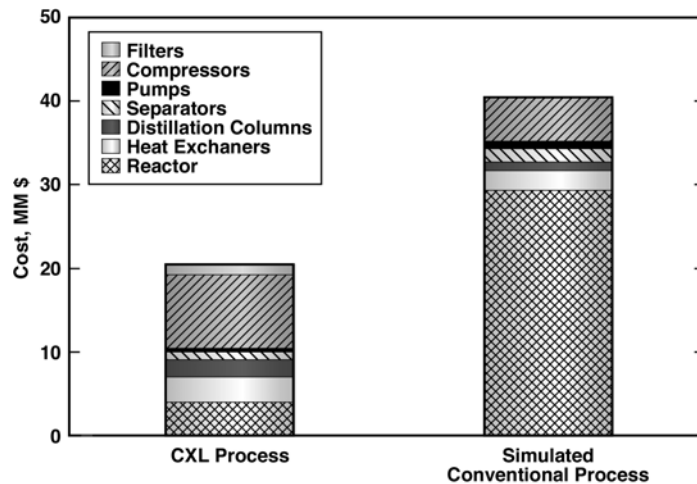


Figure 2.5 Comparison of total capital investment for the simulated conventional and CXL process

The estimated TCI for the conventional process is almost twice that of the CXL process, even though catalyst recovery costs were not considered in the conventional process. For the simulated conventional process, the combination of high operating pressure and relatively low-activity cobalt catalyst causes the reactor costs to account for approximately 75% of the TCI. For the CXL process, the higher compression and utilities costs are associated with CO₂ recycle. The filtration costs and higher distillation costs stem from the catalyst separation and methanol

separation. Table I.4 in Appendix I provides equipment purchased costs data for both processes.

Figure 2.6 compares the Total Production Costs (TPC) associated with the simulated conventional and CXL processes:

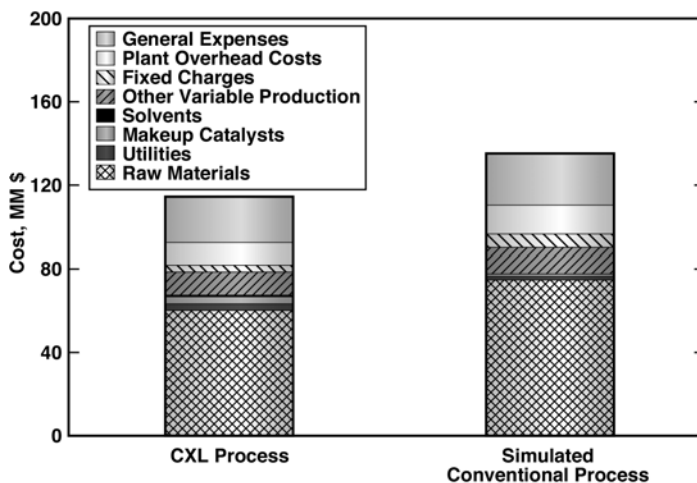


Figure 2.6 Comparison of total production cost for the simulated conventional and CXL process

The lower raw material costs in the CXL process results from the higher selectivity towards aldehydes. The cost of makeup catalyst in the CXL process is higher since the rhodium catalyst is roughly 1000 times more expensive than the cobalt catalyst. Higher utilities cost results from solvent CO₂ pressurization. The general expenses and plant overhead costs constitute a fixed percentage of the TPC in each process. Table I.5 in Appendix I provides material, labor and utilities costs for both processes.

The main economic drivers or hurdles in the CXL process are the recovery of Rh catalyst and CO₂ recycle. As inferred from Figure 2.6, the cost of the Rh catalyst is a key economic factor. If the Rh catalyst is recovered quantitatively and recycled,

then the CXL process economics compare favorably with the simulated conventional process. Sensitivity analysis shows that a decrease in the Rh catalyst recovery rate to 99% quadruples the catalyst costs and adversely affects the economics of the CXL process. Because of higher compression costs for CO₂ recycle, the utility costs are significantly higher in the CXL process. Hence, the process development should strive to further lower operating pressures and CO₂ usage. Clearly, the CXL process has the potential to be commercially viable if it meets or surpasses the performance targets used in the simulations.

2.6.2 Environmental impact analysis

The environmental impact analysis provides a comparison of the potential sources of environmental impact other than the desired product (the aldehydes). Even though the amounts of acid and alkali used in the simulated conventional process to recover the cobalt catalysts are not publicly available, it is possible to perform an approximate environmental impact analysis of the process. For the conventional process, acetic acid emitted from catalyst recovery units is categorized as fugitive emissions. Figure 2.7 shows the total IPC for the conventional and CXL processes along with the contributions of the various emission sources to the IPC. The potential IPC for the conventional process is about 40 times more than that of the CXL process, implying that the simulated CXL process is potentially environmentally friendlier than the simulated conventional process. Fugitive emissions in the conventional process are dominated by the acetic acid vapor emitted during catalyst recovery, contributing about 95% of the IPC. For the CXL process, the CO₂ solvent usage and

associated emissions do not increase the environmental burden since the CO₂ solvent is obtained from abundantly available existing sources where it is a by-product and much of it is recycled back into the process.

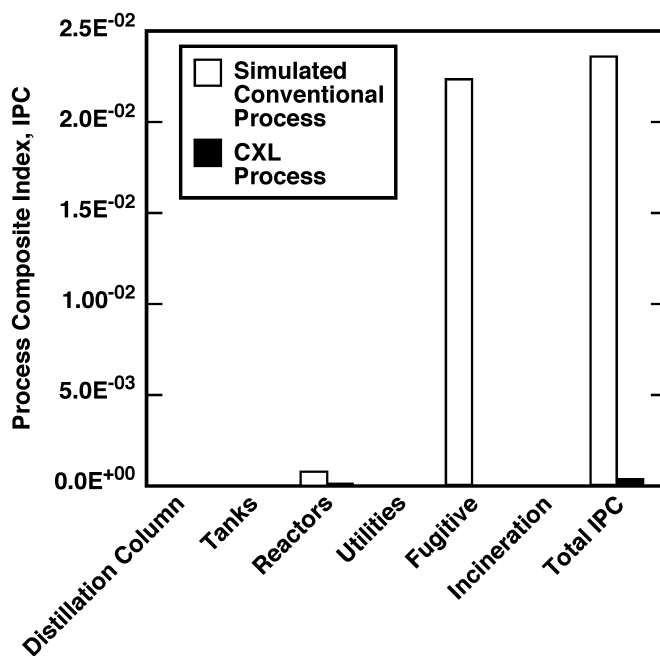


Figure 2.7 Breakdown of composite environmental impact index by each category of emission sources

Figure 2.8 shows the relative contributions of the nine environmental impact categories to the IPC. For the conventional process, fish toxicity (IFT) potential is dominated by acetic acid discharge and the non-carcinogenic inhalation toxicity (INH) is caused by CO emissions. For the CXL process (with a 40-fold lower IPC), the fish toxicity (IFT) potential is dominated by methanol discharge and the non-carcinogenic inhalation toxicity (INH) potential is caused by carbon monoxide. The higher percentages of global warming and acid rain effects in the CXL process are

due to higher utility consumption. These results provide research and process engineering guidance for reducing potential environmental impact in the two processes.

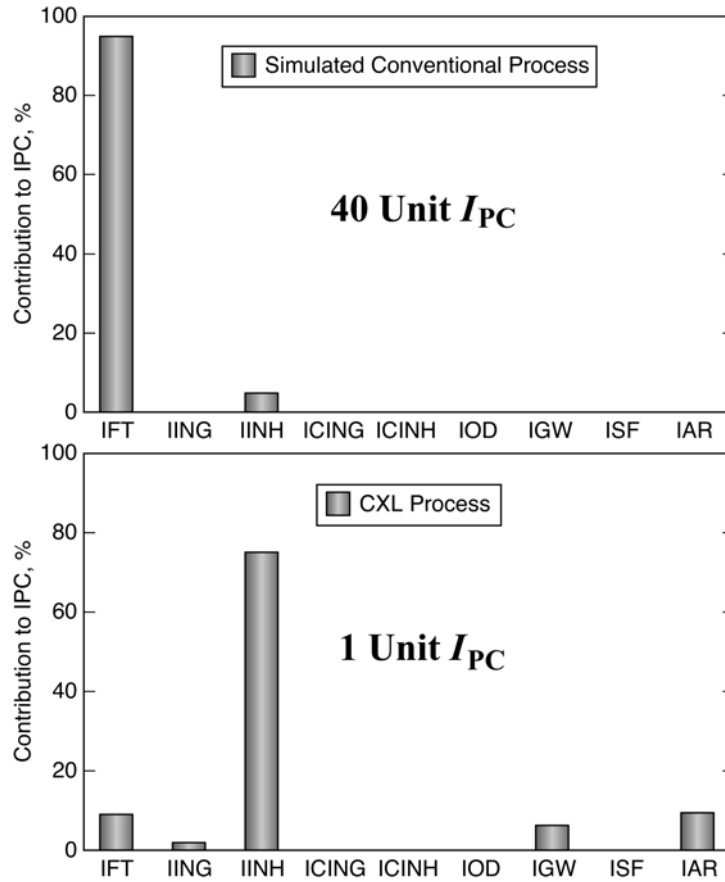


Figure 2.8 Breakdown of environmental impact attributed to various environmental impact categories

Table I.6 in Appendix I provides the annual controlled emission of each chemical from each process (all the values are in units of kg/yr) and Table I.7 in Appendix I provides chemical partitioning into environmental compartments (air, sediment, soil and water). Most of the emitted chemicals remain in the air compartment creating air pollution problems, and they can affect human health

through inhalation. The table indicates that less than 1% of all chemicals remain in the sediment compartment. About 78% of aldehyde partitions into air and the rest stays in soil and water. Over 95% of methanol resides in the soil and water compartments due to the strong affinity between these two chemicals and the media. Interestingly, almost all the acetic acid stays in the water compartment because of the low volatility and high hydrophilicity of the acid.

2.7 Summary and Recommendations for Future Work

The preliminary economic and environmental assessments of the simulated conventional and CXL processes illustrate that the CXL process has the potential to be both economically competitive with the simulated conventional process as well as environmentally friendlier. The CXL reactor costs are significantly lower than the conventional process, due to the attainment of higher TOF and comparable or better product selectivity at relatively mild operating conditions (60 °C and ~ 4MPa). For identical plant production capacities, the estimated capital cost is 50% lower and the production cost is 15% lower in CXL process compared to the conventional process. It is significant especially considering the fact that catalyst recovery costs were not included in the simulated conventional process but were included in the CXL process. The CXL process is also environmentally friendlier than the simulated conventional process, with overall toxicity index being approximately 40 times lower than the simulated conventional process. The acetic acid emissions during the catalyst recovery step are identified as the main environmental impact source for the simulated conventional process.

The economic viability of the CXL process is dependent on the ability to recover and recycle the Rh catalyst. At an aldehyde production rate of 19,900 kg/(kg Rh · h), more than 99.8% Rh has to be retained or recovered. Such a catalyst recycle target is not unreasonable, considering that near-total recovery (99.95%) of polymer-bound bulky-phosphite modified rhodium catalysts has been reported in the literature.³⁷ The development of active and easily recyclable forms of the less expensive Co-based catalysts provides an even better opportunity to make the CXL-based process more competitive.

The comparative results show that the CO₂-based process has the potential to be practically viable subject to the assumed performance benchmarks. It must be noted that these comparisons are based on the best plant data available to us in the patent and open literature. The analyses, especially those for CXLs, must be updated based on improved data becoming available in the following areas:

- Kinetics on soluble polymer bound catalysts, mass transport parameters and gas solubilities in CXLs
- The rhodium catalyst recovery from membrane filtration (Chapters 4 and 5), including the membrane costs and solvent usage
- Replace acetic acid in the Exxon process with formic acid, which is expected to have the same functionality and yet less severe environmental impacts when decomposed to water and CO₂

- Update the Exxon process, mainly for the cobalt catalyst recovery, according to the data from purchased SRI reports from SRI Consulting. However, this report is restricted from public exposure by bound agreement.

2.8 References

1. Jin, H.; Subramaniam, B., Homogeneous catalytic hydroformylation of 1-octene in CO₂-expanded solvent media. *Chemical Engineering Science* **2004**, 59, (22-23), 4887-4893.
2. Jin, H.; Subramaniam, B.; Ghosh, A.; Tunge, J., Intensification of catalytic olefin hydroformylation in CO₂-expanded media. *AIChE Journal* **2006**, 52, (7), 2575-2581.
3. Frohling, C. D.; Kohlpaintner, C. W.; Bohnen, H.-W., Carbon monoxide and synthesis gas chemistry - hydroformylation (Oxo synthesis, Roelen reaction). In *Applied homogeneous catalysis with organometallic compounds*, Cornils, B.; Herrmann, W. A., Eds. Wiley-VCH: Weinheim, **2002**; Vol. 1, p 29.
4. Garton, R. D.; Ritchie, J. T.; Caers, R. E. Oxo Process. PCT Intl. Appl., WO 2003/082789 A2, **2003**.
5. Lyon, C. J.; Sarsani, V. S. R.; Subramaniam, B., 1-butene plus isobutane reactions on solid acid catalysts in dense CO₂-based reaction media: experiments and modeling. *Industrial & Engineering Chemistry Research* **2004**, 43, (16), 4809-4814.
6. Subramaniam, B.; Busch, D. H., Use of dense-phase carbon dioxide in catalysis. In *CO₂ conversion and utilization*, Gaffney, A. M.; Song, C.; Fujimoto, K., Eds. American Chemical Society: Washington, DC: ACS Symposium, **2002**; p 364.
7. Wei, M.; Musie, G. T.; Busch, D. H.; Subramaniam, B., Autoxidation of 2,6-di-tert-butylphenol with cobalt Schiff base catalysts by oxygen in CO₂-expanded liquids. *Green Chemistry* **2004**, 6, (8), 387-393.
8. Beckman, E. J., Using CO₂ to produce chemical products sustainably. *Environmental Science & Technology* **2002**, 36, (17), 347a-353a.
9. DeSimone, J. M., Practical approaches to green solvents. *Science* **2002**, 297, (5582), 799-803.
10. Eckert, C. A.; Liotta, C. L.; Bush, D.; Brown, J. S.; Hallett, J. P., Sustainable reactions in tunable solvents. *Journal of Physical Chemistry B* **2004**, 108, (47), 18108-18118.
11. Jessop, P. G., Homogeneous catalysis and catalyst recovery using supercritical carbon dioxide and ionic liquids. *Journal of Synthetic Organic Chemistry Japan* **2003**, 61, (5), 484-488.
12. Hert, D. G.; Anderson, J. L.; Aki, S. N. V. K.; Brennecke, J. F., Enhancement of oxygen and methane solubility in 1-hexyl-3-methylimidazolium bis(trifluoromethylsulfonyl) imide using carbon dioxide. *Chemical Communications* **2005**, (20), 2603-2605.
13. Solinas, M.; Pfaltz, A.; Cozzi, P. G.; Leitner, W., Enantioselective hydrogenation of imines in ionic liquid/carbon dioxide media. *Journal of the American Chemical Society* **2004**, 126, (49), 16142-16147.
14. Bezanehtak, K.; Dehghani, F.; Foster, N. R., Vapor-liquid equilibrium for the carbon dioxide plus hydrogen plus methanol ternary system. *Journal of Chemical and Engineering Data* **2004**, 49, (3), 430-434.

15. Marteel, A. E.; Davies, J. A.; Olson, W. W.; Abraham, M. A., Green chemistry and engineering: drivers, metrics, and reduction to practice. *Annu. Rev. Environ. Resour.* **2003**, 28, 401.
16. Alexander, B.; Barton, G.; Petrie, J.; Romagnoli, J., Process synthesis and optimisation tools for environmental design: methodology and structure. *Computers & Chemical Engineering* **2000**, 24, (2-7), 1195-1200.
17. Clauson-Kaas, J.; Poulsen, T. S.; Neergaard-Jacobsen, B.; Guildal, T.; Thirsing, C., Economic and environmental optimization of phosphorus removal. *Water Science and Technology* **2004**, 50, (7), 243-248.
18. Dunn, J. B.; Savage, P. E., Economic and environmental assessment of high-temperature water as a medium for terephthalic acid synthesis. *Green Chemistry* **2003**, 5, (5), 649-655.
19. Rao, A. B.; Rubin, E. S., A technical, economic, and environmental assessment of amine-based CO₂ capture technology for power plant greenhouse gas control. *Environmental Science & Technology* **2002**, 36, (20), 4467-4475.
20. Reek, J. N. H.; van Leeuwen, P. W. N. M.; Van Der Ham, A. G. J.; De Haan, A. B., Immobilisation of tailor-made homogeneous catalysts. In *Catalyst separation, recovery and recycling: chemistry and process design*, Cole-Hamilton, D. J.; Tooze, R. P., Eds. Springer: Dordrecht, the Netherlands: **2006**; Vol. 30, p 65.
21. Motamedi, L.; Senhorst, H. A. J., Dyeing of textile using supercritical CO₂: process design, economic and environmental analysis. *The 1997 Jubilee research event: a two-day symposium held at the East Midlands Conference Centre, Nottingham* **1997**, 1, 129.
22. Fussler, C., Driving eco-innovation: a breakthrough discipline for innovation and sustainability. London; Washington DC: Pitman Publishing: **1996**.
23. G. E. Kniel, K. D. J. G. P., Life cycle assessment applied to process design: environmental and economic analysis and optimization of a nitric acid plant. *Environmental Progress* **1996**, 15, (4), 221-228.
24. Gasafi, E.; Meyer, L.; Schebek, L., Using life-cycle assessment in process design supercritical water gasification of organic feedstocks. *Journal of Industrial Ecology* **2004**, 7, 75.
25. Lim, S. R.; Park, J. M., Environmental and economic analysis of a water network system using LCA and LCC. *AIChE Journal* **2007**, 53, (12), 3253-3262.
26. Wen, Y.; Shonnard, D. R., Environmental and economic assessments of heat exchanger networks for optimum minimum approach temperature. *Computers & Chemical Engineering* **2003**, 27, (11), 1577-1590.
27. Arnoldy, P., Process aspects of rhodium-catalyzed hydroformylation. In *Rhodium catalyzed hydroformylation*, van Leeuwen, P. W. N. M.; Claver, C., Eds. Kluwer Academic Publishers: Dordrecht, the Netherlands, **2000**; Vol. 22, p 204.
28. Spohn, R. J.; Ellsworth, P. A.; Lyford, J. Dual demetalling of oxo products with catalyst recycle. US 4,255,279, **1981**.
29. Hanin, J. A. A. Hydroformylation catalyst removal. US 4,625,067, **1986**.
30. Summerlin, W. H. Cobalt catalyst recovery using heavy olefin absorbent. 5,237,104, **1993**.

31. Beadle, S. W.; Summerlin, W. H.; Van Driessche, E. T. A. Airless cobalt demetalling in the cobalt flash combination catalyst cycle. 5,410,090, **1995**.
32. Carlson, E. C., Don't gamble with physical properties for simulations. *Chem. Eng. Prog.* **1996**, 92
33. Hanin, J. A. A. Hydroformylation of olefins. US 4,658,068, **1987**.
34. Garton, R., In ExxonMobil Chemical Company, Baton Rouge, Louisiana, USA, **2005**.
35. De Munck, N. A.; Olijve, M. D.; Caers, R.; Vliet, A. V.; Hanin, J. A. A.; Driessche, E. V. Minimizing cobalt catalyst loss in the production of alcohols by hydroformylation of olefins. US 5,130,107, **1992**.
36. Ullmann, F., In *Ullmann's Encyclopedia of Industrial Chemistry*, 6th ed.; Weinheim: Wiley-VCH, Germany, **2003**; Vol. 24, p 553.
37. van Leeuwen, P. W. N. M.; Jongsma, T.; Challa, G., Polymer-bound bulky-phosphite modified rhodium hydroformylation catalysts. *Macromolecular Symposia* **1994**, 80, 241-256.
38. *HYSYS 2004.2.*; Hyprotech Ltd.: 2004.
39. Beckers, H. J.; De Rijke, J. M.; Garton, R. D. Hydroformylation process employing loop reactors. US 5,763,678, **1998**.
40. Sheldon, R. A., Atom efficiency and catalysis in organic synthesis. *Pure and Applied Chemistry* **2000**, 72, (7), 1233-1246.
41. Wiebus, E.; Cornils, B., Biphasic systems: water-organic. In *Catalyst separation, recovery and recycling: chemistry and process design*, Cole-Hamilton, D. J.; Tooze, R. P., Eds. Springer: Dordrecht, the Netherlands: **2006**; Vol. 30, p 133.
42. Peters, M. S.; Timmerhaus, K. D.; West, R. E., *Plant design and economics for chemical engineers*. 5th ed.; McGraw Hill: Boston: **2003**.
43. Economic indicators published in Chemical Engineering and located in back of issues. For 2006 Index, refer to Chem. Eng., **2006**, 113, 76.
44. Chemical Market Reporter <http://chemicalmarketreporter.com>.
45. Energy Information Administration (EIA), Department of Energy. <http://www.eia.doe.gov>.
46. Chen, H.; Shonnard, D. R., Green Engineering tutorial: environmentally-conscious design of chemical processes. Michigan Technological University.
47. Chen, H.; Shonnard, D. R., Systematic framework for environmentally conscious chemical process design: early and detailed design stages. *Industrial & Engineering Chemistry Research* **2004**, 43, (2), 535-552.
48. Goedkoop, M., The eco-indicator 95: weighting method for environmental effects that damage ecosystem or human health on a European scale. Netherlands Agency for Energy and the Environment (NOVEM) and National Institute of Public Health and Environmental Protection (RIVM): Amersfoort. **1995**.

Chapter 3. Microkinetic Studies of Rhodium Catalyzed Hydroformylation of 1-Octene in Neat and CO₂-Expanded 1-Octene

In this chapter, experimental studies of 1-octene hydroformylation in both neat and CO₂-expanded media were carried out with *in situ* ReactIR in semi-batch mode to investigate CO₂ effects on the kinetics of Rh/triphenylphosphine-catalyzed 1-octene hydroformylation in CO₂-expanded liquid (CXL) medium. A complementary reactor model incorporated with microkinetic and mass transfer proved to be an effective tool for prediction and the results show that CO₂ has no significant effect on the intrinsic kinetic rate constants implying that the enhanced reaction rate in CXL is due to the increased solubility of hydrogen in the CXL media relative to neat 1-octene.

Section 3.1 introduces the research objectives of the present work and its background. Section 3.2 reviews the literature related to kinetic studies of homogeneous hydroformylation systems including conventional organic solvents and supercritical CO₂ and also touches on the analytical techniques employed to obtain reaction rate. Section 3.3 deals with the experimental setup, materials, procedure as well as reproducibility check. The modeling work is extensively discussed in Section 3.4 including the derived kinetic scheme and reactor model development. Section 3.5 covers the modeling results and discussion. Section 3.6 summarizes this chapter and provides the guide for the future work.

3.1 Introduction and Background

As introduced in Chapters 1 and 2, homogeneous hydroformylation of higher olefins with Rh-based catalysts continues to attract attention.¹⁻⁴ The use of dense CO₂ to partially replace the excess substrate (1-octene) was shown to provide both reaction and environmental advantages.⁵⁻⁹ The ability to tune syngas solubility in CXLs was exploited to mitigate syngas starvation that typically occurs with highly active Rh-based catalysts.⁷ Excellent turnover numbers, chemoselectivity (towards the aldehydes) and regioselectivity (towards the linear aldehydes) were obtained with CXLs. The turnover numbers (TONs) for aldehyde formation were obtained at relatively low temperatures (30-60 °C) and mild pressures (~ 4 MPa), and are fourfold greater than those compared with neat organic solvents and scCO₂. Syngas mass transfer into the CXL phase and batch conversion data were modeled well using a batch reactor model that incorporated both reaction kinetics and phase equilibrium.¹⁰

To address the mass transfer and catalyst activation phenomena on the induction period observed by us and other researchers during batch hydroformylations, a reactor model that incorporated reaction kinetics and phase equilibrium was developed.¹⁰ The modeling results suggested that the induction period was caused by H₂ starvation in the liquid phase, which inhibits the formation of the hydrogenated rhodium complex, the active catalyst species. This hypothesis was verified by mass transfer studies, which revealed that increasing the impeller speed from 0 to 1200 rpm reduced the induction period by several fold. The mass transfer coefficients leveled off at impeller speeds above 1000 rpm, implying elimination of

mass transport limitations at this stirrer speed. At impeller speeds above 1000 rpm, the induction period leveled off at 12 min, which accounts for the time needed to convert the catalyst precursor to the active catalyst species.

This work is aimed at a better understanding the effects of CXL media on intrinsic hydroformylation kinetics. Transient conversion and product evolution profiles were obtained in a stirred reactor (equipped with an *in situ* ReactIR) at constant syngas pressure and temperature. The previously developed reactor model and microkinetic scheme were applied to fit the experimental data and extract kinetic parameters.¹⁰ The kinetic parameters are compared with those obtained from experiments performed with the neat solvent (i.e., without CO₂) under otherwise identical conditions. The results have provided a clearer understanding of CO₂ effects and provide a general framework for the rational design and analysis of CXL-based reactors.

3.2 Literature Review

Kinetic studies of homogeneous rhodium catalyzed hydroformylation in organic solvents or substrate have been investigated for a wide spectrum of substrate species including lower olefins (ethylene¹¹, propene¹² and 1-butene¹³), higher olefins (hexene¹⁴⁻¹⁷, 1-octene^{3, 18}, 1-dodecene¹⁹), substituted olefins (styrene^{20, 21}, vinyl esters²²) and C=C bond-containing polymers (monoterpenic polyenes²³, styrene-butadiene copolymers²⁴, high-molecular-weight cis-1,4-Polybutadiene²⁵), etc.

A commonly used method is to derive a rate equation based on the assumption of rate determining steps in a proposed kinetic scheme and then to fit the rate

equation to the experimental data by adjusting the unknown parameters. The rate equation usually is a power law rate expression as a function of the concentrations of H₂, CO, catalyst complexes and substrate. Various kinetic models have been proposed to fit the available experimental data and most of these models express the rate in the general form:

$$R = \frac{kC_{H_2}C_{CO}C_{cat}C_{substrate}}{(1 + K_1C_{CO})^m(1 + K_1C_L)^n(1 + K_2C_{substrate})^p} \quad L = \text{ligand}$$

These empirical models, however, do not provide a fundamental understanding of the effects of various parameters on reactor performance and scale-up. Furthermore, the effect of mass transfer on each elementary step (e.g. catalyst activation or product formation) is not considered in such models.

Evans *et al.*²⁶ proposed two kinetic schemes including dissociative pathway (as shown in Figure 3.1) and associative pathway (as shown in Section 3.4.1). These mechanisms were speculated based on the observations of intermediate species *via* high-tech instruments like IR and NMR while the reactions took place.

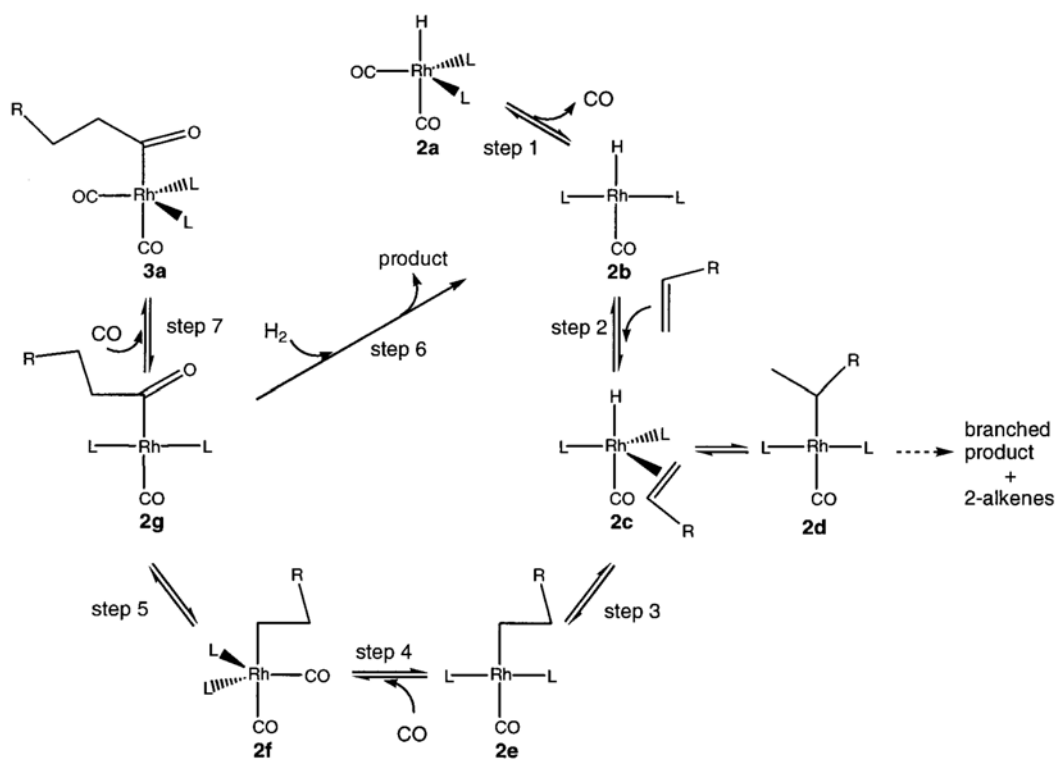


Figure 3.1 Ligand modified rhodium catalyzed hydroformylation mechanism²⁷

Several books²⁸ and reviews²⁹ discuss in detail the mechanism and kinetic studies of rhodium catalyzed homogeneous hydroformylation. Kinetic modeling in $scCO_2$ or in CXLs is relatively less studied compared to modeling in conventional solvents, and very few studies exist on hydroformylation in such media.³⁰⁻³⁴ Again, most of these studies use empirical rate forms, although the assumed rate expression might be different³² from those in conventional solvents. The helpful techniques employed to obtain concentration profiles include periodical sampling¹¹, pressure decline curve³⁵ and IR profiles.³⁶

3.3 Experimental Studies

3.3.1 Apparatus - ReactIR

Figure 3.2 provides the schematic of the ReactIR apparatus used for the *in situ* measurement of reactant concentrations during 1-octene hydroformylation in neat 1-octene and CO₂-expanded 1-octene.

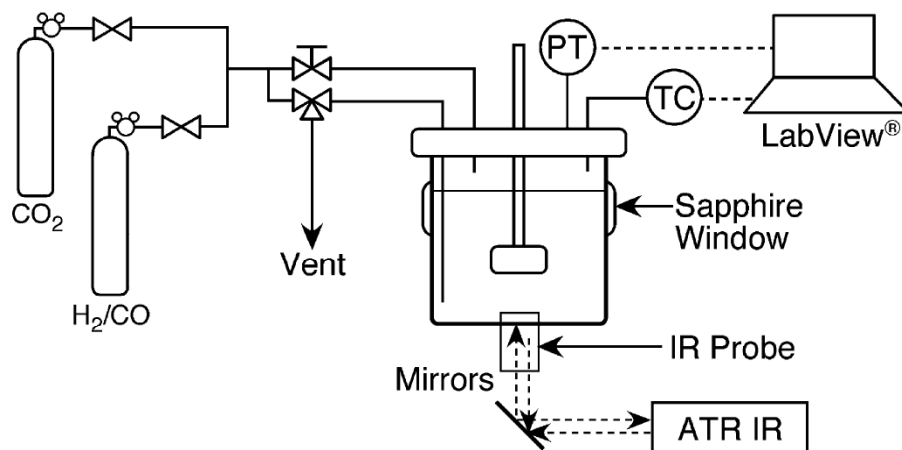


Figure 3.2 Schematic of ReactIR apparatus

The reactions were performed in a 50 cm³ high-pressure autoclave reactor (Model 4592 micro bench top reactor, Parr Instrument Company) equipped with a magnetically driven 4-blade impeller (stirrer speed ranges from 0 to 1700 rpm) for mixing. Two electric heating elements fitted around the external reactor wall provide the energy needed to maintain constant reactor temperature. The reactor temperature and the impeller rotating speed were controlled via a Parr 4843 controller and monitored via a LabView 8.6 data acquisition system. Independent pressure transducers, interfaced with the LabView system, continuously record the reactor and

syngas reservoir pressures. A dip tube extending to the bottom of reactor facilitates the introduction of CO₂ and the dispersion of the gaseous reactants (CO and H₂) and the collection of the product mixture following a batch reaction cycle. A cold trap was used to cool the hot product mixture such that non-condensable gaseous components could escape without entraining the liquid phase while collecting products. A safety rupture disc (not shown in Figure 3.2) exhausts the reactor contents to the building vent in case of unintended overpressure.

Syngas was introduced from an external gas reservoir, which was equipped with a pressure regulator and a pressure transducer. The pressure regulator, located at the exit of the reservoir, was used to regulate syngas flow into the reactor such that constant pressure is maintained in the reactor. The pressure transducer continuously monitors the syngas reservoir pressure, which decreases due to syngas consumption by the reaction. Appendix II.1 presents a stepwise procedure for calibration of pressure transducer and the plot of the response of the transducer in voltage against the actual pressure gives perfect linearity.

The reaction progress was monitored by ReactIR™ 4000 system (Mettler Toledo, Inc.) composed of an *in situ* attenuated total reflectance (ATR) IR probe equipped with a laser source and software. The SiComp IR probe (chemical resistant silicon film as the ATR element) is placed at the bottom and provides a wavelength range from 4000 ~ 650 cm⁻¹. The maximum working pressure of the probe is approximately 103 bars. The light path (K4 conduit) is purged by a flowing stream of dried air supplied by purge gas generator (Puregas, LLC) with impurities of less than

1 ppm CO₂ and moisture and particulate at concentration of less than 0.01 ppm. Appendix II.2 provides diagnostic guideline for ReactIR purge gas generator operation. The infrared spectra of different species in the liquid phase were collected by ReactIR™ 3 reaction analysis software and processed by ConcIRT for qualitative analysis and QuantIR for quantitative analysis.

3.3.2 Materials

Substrate 1-octene (purity > 97%) was procured from Alfa Aesar® (a Johnson Matthey company) was pretreated with sodium metal to remove water and peroxides, then distilled with CaH₂ under N₂ using a Schlenk line. The freeze-pump-thaw method was applied to remove the dissolved gas from the substrate 1-octene, which was then stored in a glove box under argon prior to use. The unmodified rhodium catalyst, Rh(acac)(CO)₂ (Rh-50) (purity, 99%) and ligand triphenylphosphine (PPh₃) (purity, 99%) were obtained from Alfa Aesar®. All catalysts and ligands were stored under argon before usage. Industrial grade liquid CO₂ (99.99% purity) was supplied by Linweld, Inc. in cylinders with dip tube. Research-grade syngas (99.99 % purity and H₂/CO molar ratio of 1:1) was provided by Airgas, Inc. Appendix II.3 provides detailed methods for purifications and storage of solvents and substrate used for oxygen and moisture free studies.

3.3.3 Experimental procedure

As preparation for a batch run, the IR probe was cleaned and dried for background spectra collection and the reactor was flushed at least three times with an

inert gas (nitrogen or carbon dioxide) to purge out oxygen and moisture. A background spectrum was acquired after the reactor was heated to the desired reaction temperature with stirring. The background spectrum and the reaction spectra were collected at the same temperature to avoid any baseline shift due to temperature change. A solution (preheated if needed) containing known amounts of catalyst precursor Rh-50 and ligand triphenylphosphine (TPPine) dissolved in 1-octene substrate was then transferred into the reactor via a syringe. Following this step, the reactor temperature was allowed to stabilize in a typical neat 1-octene hydroformylation run and then the acquisition of 3-dimensional (absorbance - wavelength - time) *in situ* reaction data was commenced. The experiments were performed at impeller speeds exceeding 1000 rpm to eliminate gas-liquid mass transport limitations.¹⁰

To maintain constant pressure and gas phase compositions, the reactor was operated in a semi-batch mode, wherein the syngas consumed during reaction was constantly replenished from the external reservoir. The species concentrations in the liquid phase were also monitored with sampling intervals on the order of seconds to hours. The raw 3-D IR data are then processed using ConcIRT software to extract the absorbance versus time profiles for each species, based on their characteristic peaks (identified with standards).

In a typical run in CO₂-expanded 1-octene, the catalytic solution is first syringed into the reactor followed by CO₂ addition to the desired partial pressure and temperature. Following attainment of stable pressure and temperature, the total

pressure is increased to the desired value with syngas addition and the IR data acquisition was commenced following a similar procedure as before with neat 1-octene. At the conclusion of the reaction cycle (determined by leveling off of the 1-octene conversion and product spectral signals), the product mixture was collected as explained before and analyzed using an offline GC (Varian 3800) to calculate conversion and selectivity. The absolute concentrations of substrate and products were calculated based on calibrating the 3-D IR peaks of the substrate and product with QuantIR software. Appendix II.5 offers procedural calibration of infrared absorbance with ReactIR. The typical liquid volume in the reactor is 20 cm³. At the CO₂ pressure of 3.2 MPa, the reaction system has a 10% volume expansion. Appendix II.4 contains the general gas chromatography methods for analysis of typical hydroformylation reaction mixtures.

3.3.4 Reproducibility

To ensure the reproducibility of hydroformylation of 1-octene using Rh(acac)(CO)₂ as a catalyst, three separate experiments in CO₂-expanded media were done under identical conditions. The agreement of the conversion, selectivity, and n/i ratio of the aldehydes for these three experiments were within 7% variation, confirming the repeatability of the results as given in Appendix II.6. During all the kinetic experiments, the aldehyde selectivity was observed to be in the range of 93-97%.

3.4 Modeling Studies

3.4.1 Kinetic Scheme

Previous reports on the kinetics of Rh-catalyzed homogeneous hydroformylation of different olefinic substrates in conventional solvents provide useful guidance.^{15, 18,}

²¹ The common approach in kinetic modeling is the development of an empirical rate expression assuming a rate-limiting step in the detailed kinetic scheme as proposed by Evans et al. (1968).²⁶ Kinetic modeling in *sc*CO₂ is relatively less studied compared to conventional solvents, and few studies exist on hydroformylations in such media.^{30, 32, 37} Most of these studies use empirical rate forms and do not provide insights into the effect of the elementary reactions on the overall kinetics, particularly when there are multiple steps of comparable rate in the reaction mechanism.

In this work, the associative kinetic schemes reported for hydroformylations in conventional solvents^{21, 26} are adopted assuming that the mechanism in CXL media is similar to those in organic solvents. The desired catalytic cycle starts only after the active catalyst species is formed by hydrogenation. This is followed by olefin coordination, CO insertion, formation of the aldehydes through hydrogenolysis and regeneration of active catalyst species that continues the catalytic cycle. Depending on the electronic and steric properties of the ligands used, different intermediates will result and different steps will control the reaction rate. The undesired side reactions include those that result in the formation of octane and olefin isomers as well as those that lead to catalyst deactivation. Table 3.1 shows the composite kinetic scheme for hydroformylation reaction. Three possible internal olefins (2-octene, 3-octene and 4-

octene) are typically represented as a single species, 2-octene. Also, the linear and branched aldehydes are usually lumped together and expressed as the total aldehydes yield.

Table 3.1 Preliminary kinetic scheme for rhodium catalyzed hydroformylation reaction

$2\text{Rh}(\text{CO})_2\text{L}_2 + \text{H}_2 \rightarrow 2\text{HRh}(\text{CO})_2\text{L}_2$	(R1)
$\text{HRh}(\text{CO})_2\text{L}_2 + \text{RCH} = \text{CH}_2 \Leftrightarrow \text{Rh}(\text{CO})_2\text{L}_2(\text{CH}_2\text{CH}_2\text{R})$	(R2)
$\text{Rh}(\text{CO})_2\text{L}_2(\text{CH}_2\text{CH}_2\text{R}) \Leftrightarrow \text{Rh}(\text{CO})\text{L}_2(\text{COCH}_2\text{CH}_2\text{R})$	(R3)
$\text{Rh}(\text{CO})\text{L}_2(\text{COCH}_2\text{CH}_2\text{R}) + \text{H}_2 \rightarrow \text{HRh}(\text{CO})\text{L}_2 + \text{RCH}_2\text{CH}_2\text{CHO}$	(R4)
$\text{HRh}(\text{CO})\text{L}_2 + \text{CO} \Leftrightarrow \text{HRh}(\text{CO})_2\text{L}_2$	(R5)
$\text{RCH} = \text{CH}_2 + \text{H}_2 \rightarrow \text{RCH}_2\text{CH}_3$	(R6)
$\text{Rh}(\text{CO})\text{L}_2(\text{COCH}_2\text{CH}_2\text{R}) + \text{CO} \Leftrightarrow \text{Rh}(\text{CO})_2\text{L}_2(\text{COCH}_2\text{CH}_2\text{R})$	(R7)
$\text{RCH} = \text{CH}_2 \rightarrow \text{R}'\text{CH} = \text{CH}(\text{CH}_3)$	(R8)

The microkinetic model summarizing the various elementary steps in the reaction mechanism is provided in Table 3.1. In step 1, rhodium catalyst precursor is hydrogenated to form an active catalyst species. Step 2 represents 1-octene coordination with the active catalyst species and is assumed to be the fastest step in this kinetic scheme. Steps 2-5 represent the propagation steps for aldehyde formation and catalyst regeneration. Steps 6 and 8 are undesired side reactions representing 1-octene hydrogenation and isomerization respectively. Step 7 is the catalyst deactivation step, suggesting that lower CO concentration suppresses formation of the inactive rhodium complex and favors aldehyde formation (Step 4). It should be noted that the formations of hydrogenation and isomerization byproducts are also involved in the catalytic cycle. However, in this preliminary work, only the overall reactions are given as shown in steps 6 and 8, due to the low selectivities towards these

byproducts and the inability of ReactIR to extract the concentration profiles for internal olefins at low concentrations.

The n-octane formed in the reaction cannot be detected by ReactIR. Gas chromatographic analysis of the end-of-run samples showed low levels (<1%) of the hydrogenation product in the product. The two significant IR peaks detected were 1729 cm^{-1} for C_9 aldehydes and 1640 cm^{-1} for C_8 olefins. From these peak intensities, transient concentration vs. time profiles were generated for these species and were utilized in extracting the kinetic parameters as explained in the following section.

3.4.2 Reactor Model

Figure 3.3 shows the schematic of a semi-batch two-phase hydroformylation reactor that was modeled. Consistent with the experimental procedure, syngas at a fixed composition was continuously fed in order to maintain a constant total pressure in the reactor. The model assumptions are as follows: (a) The liquid and gas phases are perfectly mixed such that there are no spatial gradients in these phases; (b) Gas-liquid mass transfer limitations are negligible at the stirrer speed used in the experiments. This implies that the liquid and vapor phases are always at equilibrium; (c) The catalyst species are non-volatile. Hence the reaction occurs only in the liquid phase; (d) The solubilities of CO and H_2 in the liquid phase are unaffected by product formation.

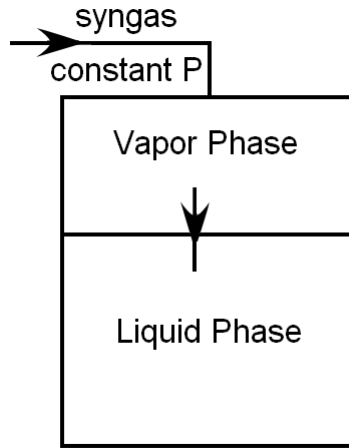


Figure 3.3 Schematic of a two-phase semi-batch hydroformylation reactor

Based on the foregoing assumptions, the model equations for the liquid phase are as follows:

For hydrogen and carbon monoxide:

$$\frac{dc_i}{dt} = k_L a (c_i^* - c_i) + \sum_{k=1}^{NR} \nu_{ki} r_k$$

where, c_i is the concentration of component i in the liquid phase, c_i^* is the saturation concentration of component i at the gas-liquid interface, t is the reaction time, $k_L a$ is the volumetric mass transfer coefficient, k is the number associated with the elementary step, NR is the total number of steps in the reaction network, ν_{ki} is the stoichiometric coefficient of component i in k th reaction step and r_k is the intrinsic reaction rate of the k th reaction step.

For the non-volatile reactant and product species, the mass balance equations are given by

$$\frac{dc_i}{dt} = \sum_{k=1}^{NR} \nu_{ki} r_k, \quad r_k = f(c_i)$$

where the reaction rate r_k is a function of the species concentrations.

The numerical method consists of an orthogonal distance regression parameter estimation program (ODRPACK) coupled with a stiff ordinary differential equation solver (LSODE) available from Netlib Libraries.³⁸ The absorbance values were converted to concentrations using calibration curves for the components involved.

The modeling inputs are as follows: 1) the concentration vs time data profiles for species including 1-octene and nonanals; 2) Mass transfer coefficient $k_L a$ obtained from experimental measurement; 3) The saturation concentrations c_i^* for CO and H₂ in the liquid phase obtained from solubility measurements. The outputs are a set of estimated kinetic parameters along with the 95% confidence interval range for each parameter as well as the concentration profiles estimated with the parameters.

3.5 Results and Discussion

Table 3.2 gives the experimental conditions and the kinetic parameters estimated for Rh-catalyzed hydroformylation in both neat 1-octene and CO₂-expanded 1-octene.

Table 3.2 Experimental conditions and model parameters for both neat 1-octene and CO₂-expanded 1-octene hydroformylation reactions at low conversions

Systems	Neat 1-octene	CO ₂ -expanded 1-octene
Experimental conditions		
Pressure, MPa	2.0	3.8*
Time, hrs	3.0	2.0
Impeller speed, rpm	1200	1000
1-octene/Rh	2038	2168
n/i ratio	2.5	10.2
X, %	50	35
S(al), %	37	94
Model parameters		
Conc., mol·m ⁻³		
Initial 1-octene	6400	5818
CO saturation	92	25
H ₂ saturation	56	49

X: Conversion; S (al): Selectivity towards aldehydes including linear and branched; T=60°C; P/Rh=207; CO/H₂=1:1 molar ratio;

* 3.2 MPa CO₂ plus 0.6 MPa CO/H₂

A detailed microkinetic scheme presented in Table 3.1 was used, where the reversible steps are assumed fast with large rate constants in both directions and are kept fixed. The kinetic constants for the catalyst hydrogenation (k_1), aldehyde formation (k_4) and isomerization (k_8) steps were estimated using the experimental data given in Table 3.2 for neat 1-octene and CO₂-expanded 1-octene hydroformylation at low 1-octene conversions. The estimated kinetic parameters, presented in Table 3.3, are found to predict the experimentally observed concentration profiles reasonably well. The comparison between experimental and predicted concentration profiles (1-octene and nonanal) obtained in neat and CO₂-expanded 1-octene are shown in Figures 3.4 and 3.5, respectively. Compared to

values in neat solvent, both the 1-octene conversion and aldehyde selectivity in CXL medium are enhanced, with the 1-octene conversion being almost twofold greater at the end of 2 hour run.

Table 3.3 Estimated kinetic constants using preliminary kinetic scheme in Table 3.1 for both neat and CO₂-expanded 1-octene hydroformylation at low conversion

Parameter	Unit	Value	95% confidence intervals
Neat 1-octene hydroformylation			
k1	(m ³ /mol-s)	5.63E-06	2.41E-06 to 8.85E-06
k4	(m ³ /mol-s)	4.04E-04	4.04E-04 to 4.04E-04
k8	(1/s)	1.52E-05	1.44E-05 to 1.61E-05
CO ₂ -expanded 1-octene hydroformylation			
k1	(m ³ /mol-s)	1.25E-04	1.25E-04 to 1.25E-04
k4	(m ³ /mol-s)	2.30E-03	2.21E-03 to 2.38E-03
k8	(1/s)	6.53E-06	4.77E-06 to 8.28E-06

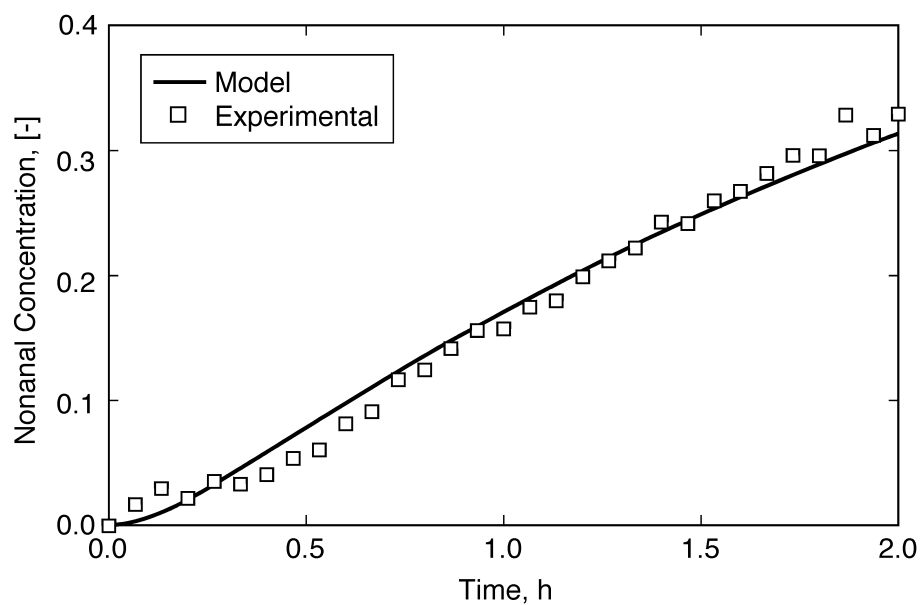
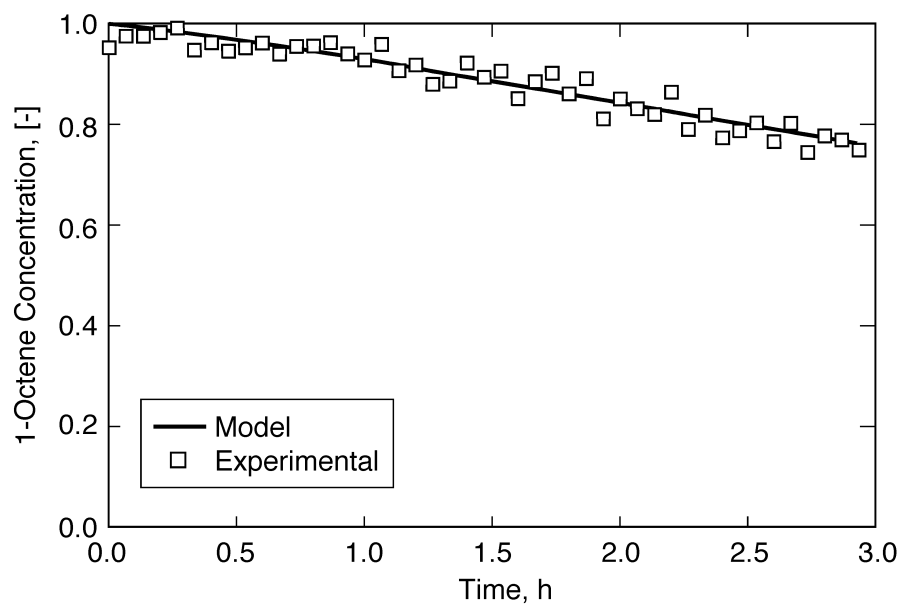


Figure 3.4 Comparison of experimental and predicted normalized concentration profiles of 1-octene and nonanal in neat 1-octene hydroformylation at low conversion using preliminary kinetic scheme in Table 3.1

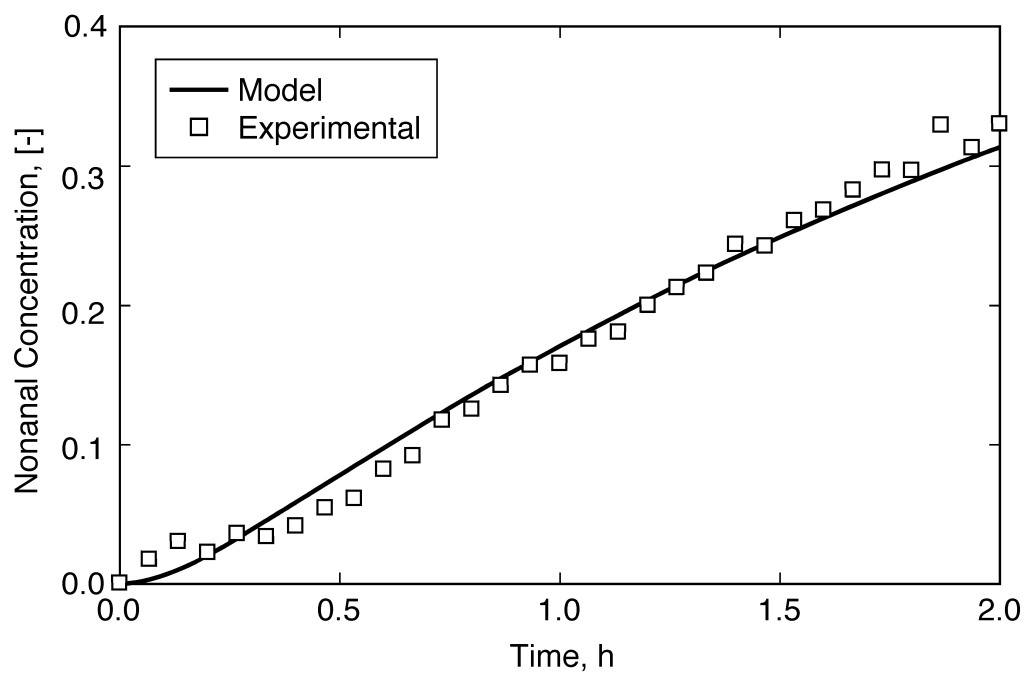
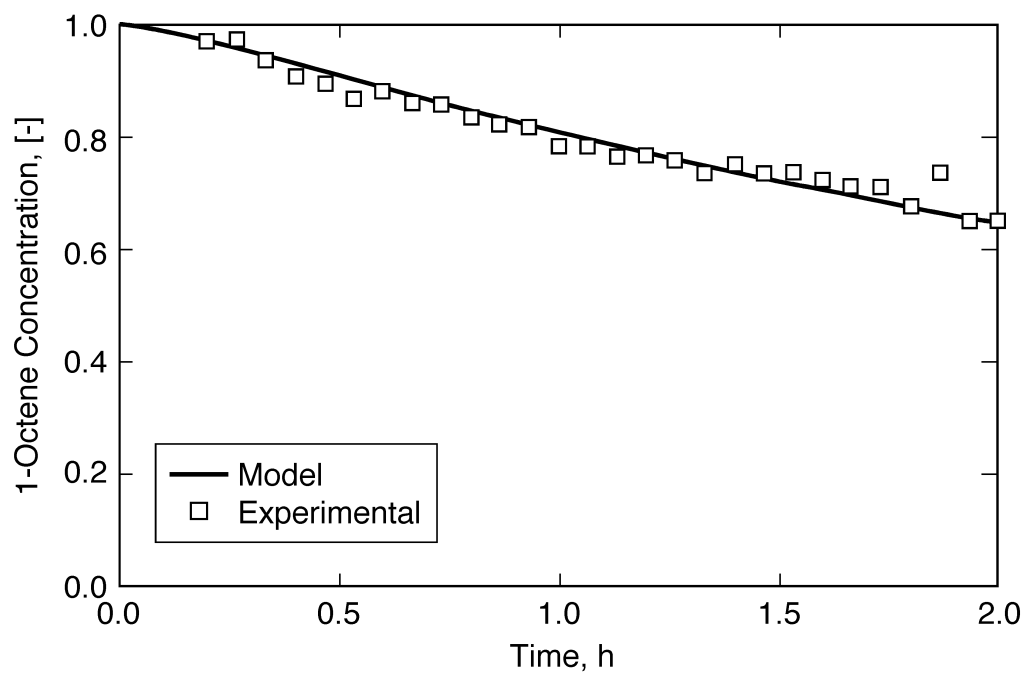
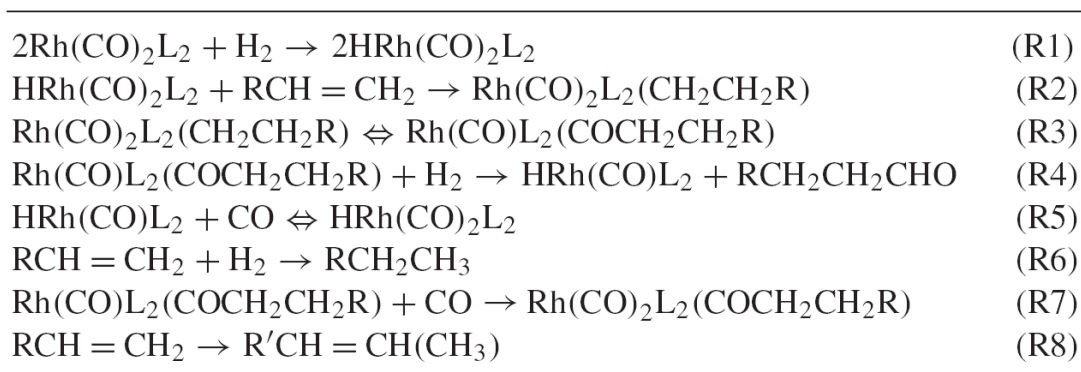


Figure 3.5 Comparison of experimental and predicted dimensionless concentration profiles of 1-octene and nonanal in CO₂-expanded 1-octene hydroformylation at low conversion using preliminary kinetic scheme in Table 3.1

Table 3.4 Modified kinetic scheme for rhodium catalyzed hydroformylation reaction



It has been reported that the olefin coordination step (step 2) can become rate limiting at low 1-octene concentrations.³⁶ A strong inhibition effect of CO on turnover frequency (TOF) has also been reported,³⁹ attributed to the removal of active Rh by the deactivation step (step 7). Based on these evidences, the kinetic scheme was modified as shown in Table 3.4 considering steps 2 and 7 as irreversible and slow. In other words, the constants for these steps are estimated rather than being kept fixed. As before, the reversible steps are assumed fast with large rate constants in both forward and backward directions and kept fixed. This requires the estimation of five kinetic constants as follows: catalyst hydrogenation (k_1), olefin coordination (k_2), nonanal formation (k_4), catalyst deactivation (k_7) and isomerization (k_8). The experimental data considered earlier with lower 1-octene conversion provides unreliable prediction of the kinetic parameters when five constants are estimated, considering the fact that the 95% confidence intervals show negative values for some cases, as shown in Table 3.5.

Table 3.5 Estimated kinetic constants using modified kinetic scheme in Table 3.4 at low conversion

Parameter	Unit	Value	95% confidence intervals
Neat 1-octene hydroformylation (3 hours)			
k1	(m ³ /mol-s)	2.84E-06	-1.12E-05 to 1.69E-05
k2	(m ³ /mol-s)	1.11E-04	-2.15E-02 to 2.17E-02
k4	(m ³ /mol-s)	5.51E-04	-5.46E-03 to 6.57E-03
k7	(m ³ /mol-s)	8.55E-10	-3.80E-06 to 3.80E-06
k8	(1/s)	1.50E-05	1.39E-05 to 1.61E-05

Hence, the experimental conversion data in both neat 1-octene and CO₂-expanded 1-octene were obtained over a longer time period (about 12 h) resulting in higher 1-octene conversions in both cases. The reaction conditions and model parameters for these two cases are shown in Table 3.6.

Table 3.6 Experimental conditions and model parameters for both neat 1-octene and CO₂-expanded 1-octene hydroformylation reactions at high conversions

Systems	Neat 1-octene	CO ₂ -expanded 1-octene
Experimental conditions		
Pressure, MPa	2.0	3.8*
Time, hrs	11.5	12.0
n/i ratio	4.7	9.5
X, %	81	84
S(al), %	97.1	93.4
Model parameters		
Conc., mol·m ⁻³		
Initial 1-octene	6400	5818
CO saturation	92	25
H ₂ saturation	56	49

X: Conversion; S (al): Selectivity towards aldehydes; T=60°C; Impeller speed: 1000 rpm; P/Rh=207; CO/H₂=1:1 molar ratio; 1-octene/Rh=2168; * 3.2 MPa CO₂ plus 0.6 MPa CO/H₂

Significantly reliable predictions of the kinetic constants are obtained with the new data that cover a wider range of 1-octene and nonanal concentrations. The estimated kinetic constants are listed in Table 3.7 along with their 95% confidence interval values. Significant improvements in the confidence intervals were obtained.

Table 3.7 Estimated kinetic constants for neat and CO₂-expanded 1-octene hydroformylation using modified kinetic scheme in Table 3.4 at high conversions

Parameter	Unit	Value	95% confidence intervals
Neat 1-octene hydroformylation (12 hours)			
k1	(m ³ /mol-s)	3.34 E-06	2.70E-06 to 3.99E-06
k2	(m ³ /mol-s)	5.29E-04	2.94E-04 to 7.64E-04
k4	(m ³ /mol-s)	3.29E-03	2.99E-03 to 3.60E-03
k7	(m ³ /mol-s)	1.11E-06	9.98E-07 to 1.22E-06
k8	(1/s)	1.73E-09	-3.75E-07 to 3.78E-07
CO ₂ -expanded 1-octene hydroformylation			
k1	(m ³ /mol-s)	1.29 E-05	8.62E-06 to 1.71E-05
k2	(m ³ /mol-s)	1.16E-04	2.01E-05 to 2.12E-04
k4	(m ³ /mol-s)	4.52E-03	2.70E-03 to 6.34E-03
k7	(m ³ /mol-s)	4.38E-06	2.99E-06 to 5.77E-06
k8	(1/s)	2.07E-07	-1.01E-07 to 5.15E-07

The comparison of experimental and predicted concentration profiles for both cases is shown in Figures 3.6 and 3.7 respectively.

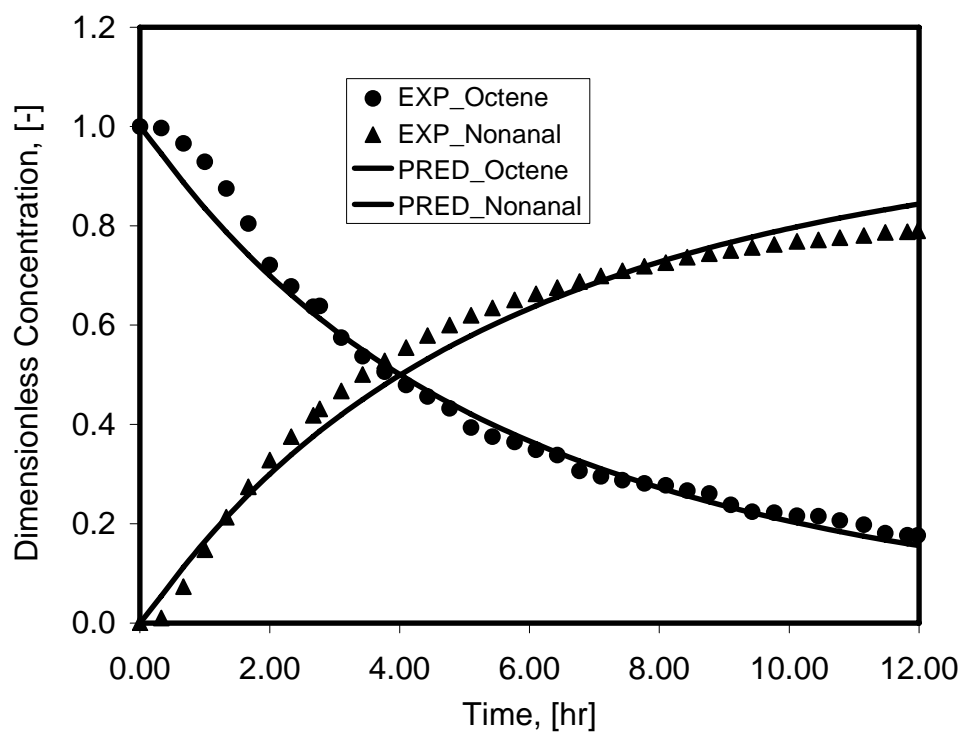


Figure 3.6 Comparison of experimental and predicted normalized concentration profiles of 1-octene and nonanal in neat 1-octene hydroformylation at high conversion using modified kinetic scheme in Table 3.4

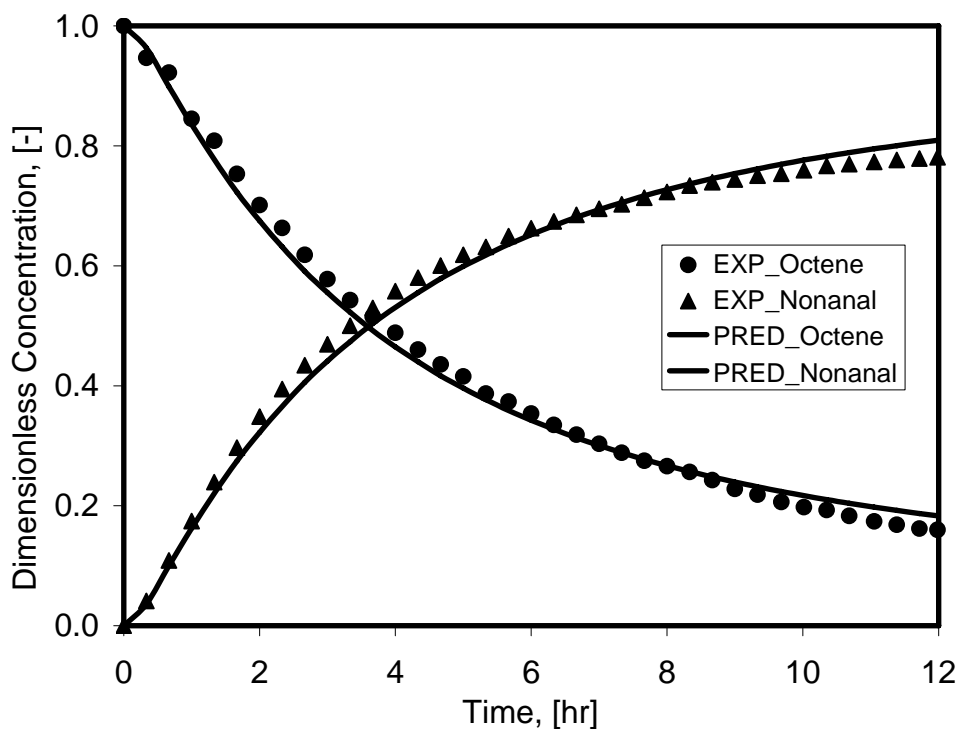


Figure 3.7 Comparison of experimental and predicted normalized concentration profiles of 1-octene and nonanal in CO₂-expanded 1-octene hydroformylation at high conversion using modified kinetic scheme in Table 3.4

Table 3.8 Comparison of estimated kinetic constants for neat and CO₂-expanded 1-octene hydroformylation using modified kinetic scheme in Table 3.4 at high conversions

Kinetic Step	Kinetic Constants	Pure 1-Octene	CO ₂ -Expanded 1-Octene
Catalyst hydrogenation	$k_1 \times 10^6, \text{ m}^3/\text{mol}\cdot\text{s}$	3.34 ± 0.64	12.87 ± 4.26
Olefin insertion	$k_2 \times 10^4, \text{ m}^3/\text{mol}\cdot\text{s}$	5.29 ± 2.35	1.16 ± 0.96
Aldehyde formation	$k_4 \times 10^3, \text{ m}^3/\text{mol}\cdot\text{s}$	3.29 ± 0.30	4.52 ± 1.82
Catalyst deactivation	$k_7 \times 10^6, \text{ m}^3/\text{mol}\cdot\text{s}$	1.11 ± 0.11	4.38 ± 1.39

As shown in Table 3.8, the four intrinsic kinetic constants are more or less of the same order of magnitude in both cases, and unaffected by addition of CO₂. This suggests that the higher reaction rate observed in CXLs might be attributed to the

enhanced H₂ concentration in the liquid phase rather than any intrinsic solvent effects. In the future, more experiments need to be conducted at varying CO/H₂ ratio, catalyst concentrations, reaction temperatures and volume expansions to thoroughly understand the CO₂ effects on the reaction rate. Besides CO₂, different organic solvents, such as toluene, hexane, and methanol, will be intentionally chosen according to their dielectric constants and investigated to explore solvent effects as well. Additionally, the reactor model and ReactIR setup established in this work are also applicable for explorations of kinetics of different catalyst systems, such as the newly developed polymer bound phosphite ligands.^{8,40}

It must be noted that aldehydes are “lumped” together in this model since ReactIR data do not distinguish between branched and linear aldehydes. This makes it impossible to predict solvent effects on the *n/i* ratio so that separate mechanistic steps for the formation of linear and branched aldehydes are essential to develop proper kinetic models. In addition, the assumed kinetic mechanism could not be rigorously tested. These drawbacks are addressed as follows. First, in addition to *in situ* aldehydes/time profiles obtained from ReactIR, a duplicate reaction will be carried out to measure *n/i* ratio by GC analysis at different reaction times. Secondly, separate reaction steps for branched aldehyde formation will be added to the reaction mechanism. By quantifying the *n*- and *i*-aldehydes and the revised reaction mechanism, new kinetic parameters will be obtained to better understand the underlying reason for enhanced regioselectivity of 1-octene hydroformylation in CXL media.

Further modifications to the kinetic scheme should be considered based on the experimental observations reported in the literature²⁸ including first order assumption for the initial catalyst hydrogenation step and dissociative mechanism with $\text{HRh}(\text{CO})\text{L}_2$ as the active catalyst species.

3.6 Concluding Remarks and Future Work

A semi-batch reactor model was developed and efficiently applied to estimate kinetic parameters for rhodium catalyzed higher olefin hydroformylation from *in situ* ReactIR data. Most of the estimated kinetic constants with narrow confidence intervals are on the same order of magnitude for neat and CO_2 -expanded 1-octene, which implies that the addition of CO_2 doesn't significantly affect the intrinsic reaction rate for most of the elementary steps. The estimated kinetic parameters will be useful to update the CXL process simulated in the previous economic and environmental impact analyses. A routine tool and procedure for kinetic studies of homogeneous reaction was developed for wider dissemination and use for different operating conditions and catalyst systems.

In the future, experimental and modeling studied in this work will continue in support of newly developed polymer bound phosphite ligand⁸ and more information about this type of ligands is provided in the next two chapters.

3.7 References

1. Bektesevic, S.; Kleman, A. M.; Marteel-Parrish, A. E.; Abraham, M. A., Hydroformylation in supercritical carbon dioxide: catalysis and benign solvents. *Journal of Supercritical Fluids* **2006**, 38, (2), 232-241.
2. Cole-Hamilton, D. J., Homogeneous catalysis - new approaches to catalyst separation, recovery, and recycling. *Science* **2003**, 299, (5613), 1702-1706.
3. Frisch, A. C.; Webb, P. B.; Zhao, G.; Muldoon, M. J.; Pogorzelec, P. J.; Cole-Hamilton, D. J., "Solventless" continuous flow homogeneous hydroformylation of 1-octene. *Dalton Transactions* **2007**, (47), 5531-5538.
4. Webb, P. B.; Kunene, T. E.; Cole-Hamilton, D. J., Continuous flow homogeneous hydroformylation of alkenes using supercritical fluids. *Green Chemistry* **2005**, 7, (5), 373-379.
5. Fang, J.; Jin, H.; Ruddy, T.; Pennybaker, K.; Fahey, D.; Subramaniam, B., Economic and environmental impact analyses of catalytic olefin hydroformylation in CO₂-expanded liquid (CXL) media. *Industrial & Engineering Chemistry Research* **2007**, 46, (25), 8687-8692.
6. Jin, H.; Subramaniam, B., Homogeneous catalytic hydroformylation of 1-octene in CO₂-expanded solvent media. *Chemical Engineering Science* **2004**, 59, (22-23), 4887-4893.
7. Jin, H.; Subramaniam, B.; Ghosh, A.; Tunge, J., Intensification of catalytic olefin hydroformylation in CO₂-expanded media. *AIChE Journal* **2006**, 52, (7), 2575-2581.
8. Wang, R.; Cai, F.; Jin, H.; Xie, Z.; Subramaniam, B.; Tunge, J. A., Hydroformylation in CO₂-expanded media. In *Gas-Expanded Liquids and Near-Critical Media: Green Chemistry and Engineering*, Hutchenson, K. W.; Scurto, A. M.; Subramaniam, B., Eds. American Chemical Society: Washington, D.C., **2009**; pp 202-217
9. Tunge, J. A.; Subramaniam, B.; Fang, J.; Jana, R. Continuous reaction and product separation using a nanofiltration membrane employing soluble polymer-supported catalyst complexes dissolved in liquids including gas-expanded liquids. Patent Application submitted.
10. Guha, D.; Jin, H.; Dudukovic, M. P.; Ramachandran, P. A.; Subramaniam, B., Mass transfer effects during homogeneous 1-octene hydroformylation in CO₂-expanded solvent: modeling and experiments. *Chemical Engineering Science* **2007**, 62, (18-20), 4967-4975.
11. Deshpande, R. M.; Bhanage, B. M.; Divekar, S. S.; Kanagasabapathy, S.; Chaudhari, R. V., Kinetics of hydroformylation of ethylene in a homogeneous medium: comparison in organic and aqueous systems. *Industrial & Engineering Chemistry Research* **1998**, 37, (6), 2391-2396.
12. Bernas, A.; Maki-Arvela, P.; Lehtonen, J.; Salmi, T.; Murzin, D. Y., Kinetic modeling of propene hydroformylation with Rh/TPP and Rh/CHDPP catalysts. *Industrial & Engineering Chemistry Research* **2008**, 47, (13), 4317-4324.

13. Salmi, T.; Ahlkvist, J.; Bernas, A.; Warna, J.; Maki-Arvela, P.; Still, C.; Lehtonen, J.; Murzin, D. Y., Hydroformylation of 1-butene on Rh catalyst. *Industrial & Engineering Chemistry Research* **2009**, 48, (3), 1325-1331.
14. Rosales, M.; Chacon, G.; Gonzalez, A.; Pacheco, I.; Baricelli, P. J.; Melean, L. G., Kinetics and mechanisms of homogeneous catalytic reactions: Part 9. Hydroformylation of 1-hexene catalyzed by a rhodium system containing a tridentated phosphine. *Journal of Molecular Catalysis A: Chemical* **2008**, 287, (1-2), 110-114.
15. Deshpande, R. M.; Chaudhari, R. V., Kinetics of hydroformylation of 1-hexene using homogeneous HRh(CO)(PPh₃)₃ complex catalyst. *Industrial & Engineering Chemistry Research* **1988**, 27, (11), 1996-2002.
16. Rosales, M.; Duran, J. A.; Gonzalez, A.; Pacheco, I.; Sanchez-Delgado, R. A., Kinetics and mechanisms of homogeneous catalytic reactions Part 7. Hydroformylation of 1-hexene catalyzed by cationic complexes of rhodium and iridium containing PPh₃. *Journal of Molecular Catalysis A-Chemical* **2007**, 270, (1-2), 250-256.
17. Rosales, M.; Gonzalez, A.; Guerrero, Y.; Pacheco, I.; Sanchez-Delgado, R. A., Kinetics and mechanisms of homogeneous catalytic reactions Part 6. Hydroformylation of 1-hexene by use of Rh(acac)(CO)₂/dppe [dppe=1,2-bis(diphenylphosphino)ethane] as the precatalyst. *Journal of Molecular Catalysis A-Chemical* **2007**, 270, (1-2), 241-249.
18. van Rooy, A.; Orij, E. N.; Kamer, P. C. J.; van Leeuwen, P. W. N. M., Hydroformylation with a rhodium/bulky phosphite modified catalyst. A comparison of the catalyst behavior for oct-1-ene, cyclohexene, and styrene. *Organometallics* **1995**, 14, (1), 34-43.
19. Bhanage, B.; Divekar, S.; Deshpande, R.; Chaudhari, R., Kinetics of hydroformylation of 1-dodecene using homogeneous HRh(CO)(PPh₃)₃ catalyst. *Journal of Molecular Catalysis A-Chemical* **1997**, 115, (2), 247-257.
20. Bergounhou, C.; Neibecker, D.; Mathieu, R., Kinetics and mechanism of the hydroformylation of styrene catalysed by the rhodium/TPP system (TPP = 1,2,5-triphenyl-1H-phosphole). *Journal of Molecular Catalysis A: Chemical* **2004**, 220, (2), 167-182.
21. Nair, V. S.; Mathew, S. P.; Chaudhari, R. V., Kinetics of hydroformylation of styrene using homogeneous rhodium complex catalyst. *Journal of Molecular Catalysis A-Chemical* **1999**, 143, (1-3), 99-110.
22. Abatjoglou, A. G.; Bryant, D. R.; Desposito, L. C., Rhodium-catalyzed low-pressure hydroformylation of vinyl esters - solvent and phosphine effects on catalyst activity, selectivity and stability. *Journal of Molecular Catalysis* **1983**, 18, (3), 381-390.
23. Barros, H. J. V.; da Silva, J. G.; Guimaraes, C. C.; dos Santos, E. N.; Gusevskaya, E. V., Hydroformylation of monoterpenic polyenes: effect of the conjugation of double bonds on reactivity. *Organometallics* **2008**, 27, (17), 4523-4531.

24. Scott, P. J.; Rempel, G. L., Homogeneous catalytic hydroformylation of styrene-butadiene copolymers in the presence of $\text{HRh}(\text{CO})(\text{PRh}_3)_3$. *Macromolecules* **1992**, 25, (11), 2811-2819.
25. Im-Erbsin, S.; Prasassarakich, P.; Rempel, G. L., Hydroformylation of high-molecular-weight cis-1,4-polybutadiene catalyzed by $\text{HRh}(\text{CO})(\text{PPh}_3)_3$. *Journal of Applied Polymer Science* **2004**, 93, (2), 854-869.
26. Evans, D.; Osborn, J. A.; Wilkinso, G., Hydroformylation of alkenes by use of rhodium complex catalysts. *Journal of the Chemical Society A-Inorganic Physical Theoretical* **1968**, (12), 3133-3142.
27. van der Slot, S. C.; Kamer, P. C. J.; van Leeuwen, P. W. N. M.; Iggo, J. A.; Heaton, B. T., Mechanistic studies of the hydroformylation of 1-alkenes using a monodentate phosphorus diamide ligand. *Organometallics* **2001**, 20, (3), 430-441.
28. Leeuwen, P. W. N. M. v.; Claver, C., Rhodium catalyzed hydroformylation. Kluwer Academic Publishers: Dordrecht [Netherlands]; Boston, **2000**; Vol. 22, p 284.
29. Chaudhari, R. V.; Seayad, A.; Jayasree, S., Kinetic modeling of homogeneous catalytic processes. *Catalysis Today* **2001**, 66, (2-4), 371-380.
30. Palo, D. R.; Erkey, C., Kinetics of the homogeneous catalytic hydroformylation of 1-octene in supercritical carbon dioxide with $\text{HRh}(\text{CO})[\text{P}(\text{p-CF}_3\text{C}_6\text{H}_4)_3]_3$. *Industrial & Engineering Chemistry Research* **1999**, 38, (10), 3786-3792.
31. Guo, Y.; Akgerman, A., Hydroformylation of propylene in supercritical carbon dioxide. *Industrial & Engineering Chemistry Research* **1997**, 36, (11), 4581-4585.
32. Lopez-Castillo, Z. K.; Flores, R.; Kani, I.; Fackler, J. P.; Akgerman, A., Evaluation of polymer-supported rhodium catalysts in 1-octene hydroformylation in supercritical carbon dioxide. *Industrial & Engineering Chemistry Research* **2003**, 42, (17), 3893-3899.
33. Davis, T.; Erkey, C., Hydroformylation of higher olefins in supercritical carbon dioxide with $\text{HRh}(\text{CO})[\text{P}(3,5\text{-(CF}_3)_2\text{-C}_6\text{H}_3)_3]_3$. *Industrial & Engineering Chemistry Research* **2000**, 39, (10), 3671-3678.
34. Bach, I., Hydroformylation of hex-1-ene in supercritical carbon dioxide catalyzed by rhodium trialkylphosphine complexes. *Chemical Communications* **1998**, 14, 1463-1464.
35. Koeken, A. C. J.; de Bakker, S. J. M.; Costerus, H. M.; van den Broeke, L. J. P.; Deelman, B. J.; Keurentjes, J. T. F., Evaluation of pressure and correlation to reaction rates during homogeneously catalyzed hydroformylation in supercritical carbon dioxide. *Journal of Supercritical Fluids* **2008**, 46, (1), 47-56.
36. Kamer, P. C. J.; van Rooy, A.; Schoemaker, G. C.; van Leeuwen, P. W. N. M., In situ mechanistic studies in rhodium catalyzed hydroformylation of alkenes. *Coordination Chemistry Reviews* **2004**, 248, (21-24), 2409-2424.
37. Palo, D. R.; Erkey, C., Homogeneous hydroformylation of 1-octene in supercritical carbon dioxide with $[\text{RhH}(\text{CO})(\text{P}(\text{p-CF}_3\text{C}_6\text{H}_4)_3)_3]$. *Industrial & Engineering Chemistry Research* **1999**, 38, (5), 2163-2165.
38. <http://www.netlib.org>

39. Jin, H., Exploiting CO₂-expanded liquids as reaction media for catalytic hydroformylation of higher olefins. *Ph.D Dissertation* **2006**.
40. Jana, R.; Tunge, J. A., A homogeneous, recyclable rhodium(I) catalyst for the hydroarylation of Michael acceptors. *Organic Letters* **2009**, 11, (4), 971-974.

Chapter 4. Batch Membrane Nano/Ultra-Filtration of Rhodium Complexes from Homogeneous Organic Solutions

In this chapter, membrane nano/ultra-filtration of designed polymer-bound Rh complex catalyts is demonstrated as an effective *in situ* catalyst recovery method for homogeneous hydroformylation reaction systems. Quantitative extents of recovery of the rhodium metal and phosphorus-based ligands were investigated in batch membrane filtration experiments with various soluble polymer bound rhodium complexes dissolved in toluene. Inductively coupled plasma (ICP) technique was explored for analyses of Rh and P in organic matrix.

Section 4.1 briefly introduces the research goals and the potential of membrane nano/ultra-filtration as a promising technology to recover rhodium catalyst in its active form from homogenous post-reaction mixtures. Section 4.2 reviews the recent literature on catalyst separation, recovery and recycling with emphasis on membrane filtration of the organometallic catalyst compounds, its industrial practice and commercially available membrane and filter. The experimental apparatus is presented in Section 4.3, including the specifications and capabilities of STARMEM[®] membrane and MET cell along with the modifications that were made for air-free and continuous operation. Section 4.4 details the catalytic systems tested in batch mode and their preparation procedure. Analytical methodology and calibrations for both rhodium and phosphorus in organic matrix are also presented in this section, supplemented with ICP method development in Appendix III and uncertainty analysis in Appendix IV. Section 4.5 describes all the experimental procedures related to membrane preconditioning and equilibration, membrane flux measurements, and

batch membrane filtration. Among all the tested ligands, polymer bound phosphite ligands exhibit excellent Rh recoverability.

4.1 Introduction and Background

As explained in Chapter 2, preliminary quantitative economic analyses indicate that the CXL process has clear potential to be economically feasible if the recovery of the rhodium is at least 99.8% per pass.¹

One of the strategies for Rh recovery in CXL media is to precipitate Rh catalyst complexes by adding antisolvent CO₂ after reaction completion to initiate phase splitting by tuning the polarity and dielectric constant of the reaction mixture. However, this requires high CO₂ pressures and filtration under pressure to avoid redissolution of the catalyst. Another approach is to utilize a bulky phosphite ligand to form a soluble rhodium complex that is amenable to filtration by size exclusion and can be recovered in its active form by membrane filtration. This type of rhodium complex may also be recycled by precipitation as solid particles (by adding methanol) followed by filtration and redissolution as a homogeneous catalyst. The integration of CXL media for reaction followed by catalyst separation using membrane filtration technique is illustrated in Figure 4.1:

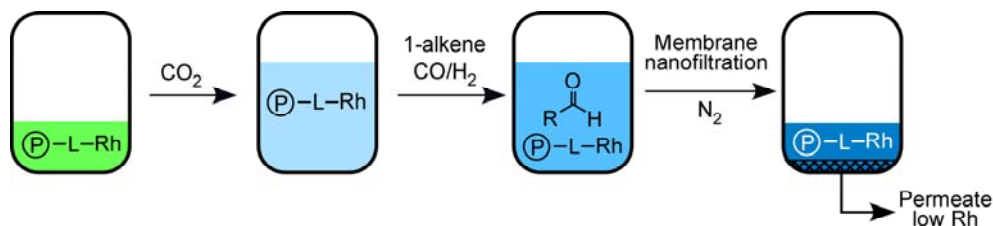


Figure 4.1 The schematic of reaction coupled with membrane filtration

In this scheme, the polymer bound rhodium complex is dissolved in the hydroformylation reaction mixture to form a homogenous mixture. By pressurizing this mixture with carbon dioxide, a single phase CXL is generated while maintaining the catalyst complex in solution. Synthesis gas is then introduced into the reactor to form the desired aldehyde in the CXL-based reactor followed by membrane filtration such that the aldehyde products pass through the membrane, leaving the bulky polymer bound rhodium complex in the retentate for recycle. By retaining a substantial amount of the catalyst complex in the reactor itself, the membrane separation process obviates post-reactor catalyst precipitation and regeneration steps and also avoids the rhodium complex from being subjected to thermally induced decomposition that occurs under high temperature distillation of the reaction mixture.

This chapter details the development of the methods for near-quantitative recovery and recycle of rhodium complex catalysts. To achieve the targeted Rh recovery rate (99.8% per pass based on economic analysis at an aldehyde production rate of 19,900 kg/(kg Rh · h)), polymer bound bulky phosphorus ligands were synthesized by collaborators from the Department of Chemistry (by Dr. Ranjan Jana under the direction of Professor Jon Tunge) to form a Rh complex in homogeneous solution. The goals are to establish a standard methodology to evaluate the quantitative recoverability of various rhodium catalysts and to demonstrate the application of membrane nanofiltration in homogeneous catalytic systems. The specific objectives are:

- To design and construct a membrane-based nano/ultra- filtration system for separation of catalyst from reaction mixture
- To develop analytical methods for elemental analysis of rhodium metal and phosphorus ligands using inductively coupled plasma analysis
- To quantify the extent of rhodium recovery using the polymer bound phosphite ligands provided by Professor Tunge's group

The results will provide guidance to researchers in designing catalyst and solvents to maximize rhodium recovery for economic viability.

4.2 Literature Review

Homogenous catalysis with organometallic compounds is widely applied in chemical synthesis, such as hydroformylation, hydrogenation, olefin polymerization, olefin oxidation and asymmetric synthesis.² Despite the attractive features of homogeneous catalysis in terms of activity and selectivity under mild reaction conditions, homogeneous catalysis has only been commercialized when there is no heterogeneous catalyst that is capable of promoting the desired reaction, or when selectivity to a higher added value product is possible using a homogeneous catalyst. Homogeneous catalyst separation and recovery can be extremely energy intensive and time consuming, and still remains as a formidable challenge in many industrial applications.³ Considerable research efforts have been ongoing in both academia and industry to address this challenge. The various methods for homogenous catalyst separation and recovery are briefly reviewed here.

One of the most elegant solutions to combine the advantages of homogenous and heterogeneous catalysis is the anchoring of homogeneous catalysts to solid particle supports to form a heterogenized catalyst that can be easily applied in fixed bed or slurry type reactors. However, this approach still suffers from several drawbacks as follows that prevent it from being commercially viable: a) metal leaching from the support; b) reduced activity and selectivity compared to the homogeneous counterpart; c) nonuniform structures of the resulting heterogeneous catalysts;⁴ and d) mass transfer limitations due to hindered diffusion.

Biphasic catalysis employs various solvent combinations such as aqueous/organic⁵ and fluoruous/organic⁶ to form two immiscible liquid phases that can facilitate elegant separation and recycle of catalysts. Typically, the catalyst and the substrate are dissolved in one phase while the insoluble product is transferred to the second immiscible phase upon reaction and is thus easily separated. In the Ruhrchemie/Rhône-Poulenc (RCH/RP) process involving the hydroformylation of propene to butyraldehydes, rhodium catalysts modified by water-soluble ligand such as TPPTS (triphenylphosphine *m*-trisulfonate) is used. The oxo product is immiscible in the aqueous phase. Phase splitting to separate catalyst from product might also be induced by temperature tuning.⁷

Other methods using different agents such as ionic liquids⁸ or scCO_2 ⁹ to form or induce a second phase are also of great interest and under investigation. All the abovementioned methods are related to non-destructive reuse and separation involving phase transferring of catalysts or substrate and product. Another possible

route to recover catalysts in their catalytically active form without destruction is membrane separation such that the catalysts can be recycled without any further treatment.

4.2.1 Membrane filtration

Membrane technology works without the addition of chemicals and is a well known technique with relatively low energy consumption. Based on the size of the solute to be filtered, the membrane filtration is divided into four categories: reverse osmosis, nanofiltration, ultrafiltration and microfiltration. Figure 4.2 shows the filtration and separation spectrum measured in micrometers, Ångströms and molecular weight units, along with relative size of common materials. The separation for organometallic catalyst complexes from organic phase falls in the nanofiltration range (solute molecular weight from 200 Daltons to 15,000 Daltons) for unmodified or small-sized ligand modified ones and in the ultrafiltration range (solute molecular weight from 5,000 Daltons to 200,000 Daltons) for bulky or polymerized ligand modified ones.

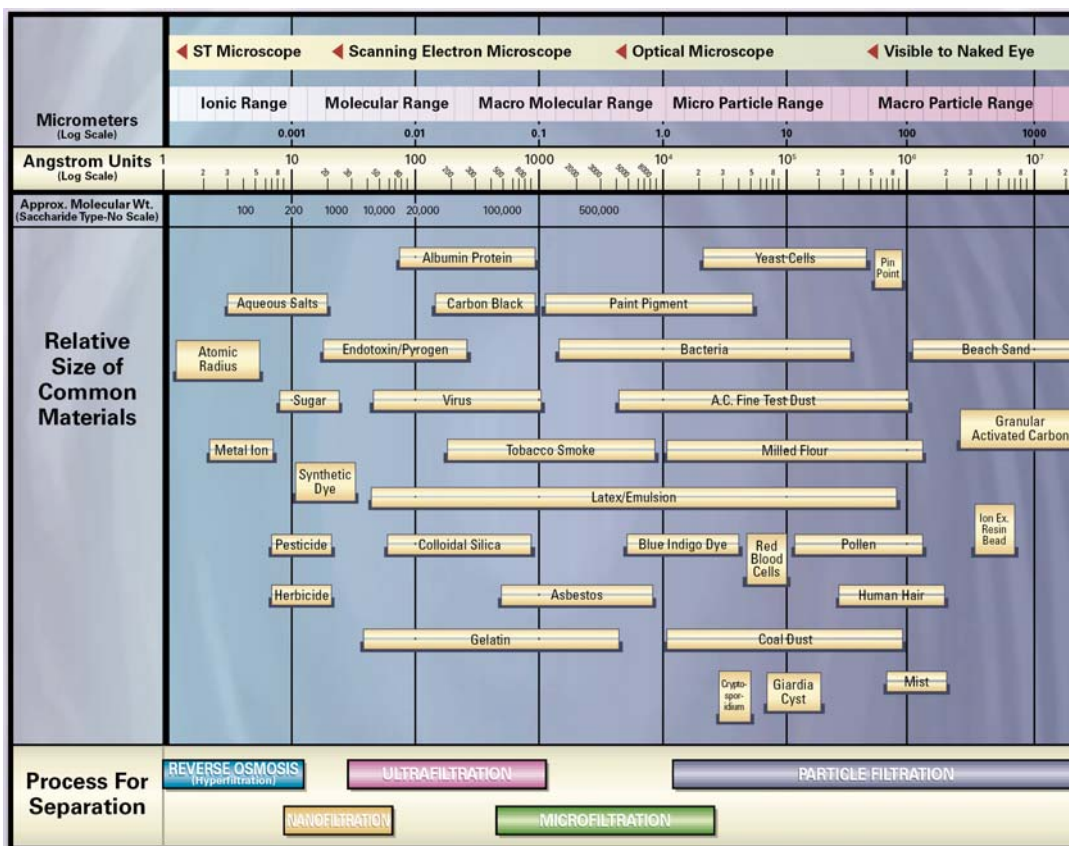


Figure 4.2 Filtration and separation spectrum taken from www.osmolabstore.com

Membrane filtration has been applied in a variety of industrial processes such as food processing, water purification, catalytic processes, petrochemical industry and pharmaceutical manufacturing. Its application and progress mainly depend on the availability of highly solvent-resistant membranes. Vandezande *et al.*¹⁰ provide a review of journal papers and patents in the areas of membrane preparation, transport mechanisms, and the practical applications of membrane filtration for the aforementioned industries. Additionally, Ronde and Vogt¹¹ published a book chapter in regard to the membrane filtration for separation of various types of homogenous

catalysts. To improve the efficiency of metal recovery and maintain the homogenous feature of the catalyst complex in organic solvents, ligand design is the main challenge to achieve the optimum size of the catalyst solute for quantitative retention. The literature relative to ligand design is classified into the following three groups according to the type of ligands used in size control.

4.2.1.1 *Dendrimer supported catalysts*

The dendrimers have attracted tremendous attention after being pioneered by Vögtle *et al.*¹² They were first applied as homogeneous catalyst nickel carrying an agent showing regiospecific catalytic activity for the Kharasch addition of polyhalogenoalkanes to C=C double bounds.¹³ The combination of membrane filtration with the relatively arbitrary enlargement of dendrimers laced with precious metal catalyst is a burgeoning subject, as indicated by the increasing number of publications in the past two decades. It has been attempted in the Kharasch addition, hydrovinylation, Michael addition, hydroformylation, hydrogenation, Heck and allylic substitution reactions.^{11,14, 15} The invention disclosed by Union Carbide Chemicals & Plastics Technology Corporation (UCC) in U.S. patents 6,350,819¹⁶ and 6,525,143¹⁷ relates to dendritic macromolecules and their use in metal-dendritic macroligand complex-catalyzed hydroformylation, facilitating the separation of desired product from catalyst by membrane filtration. Three types of membranes including MPF-50, GKSS (1 μm active layer thickness) and GKSS (10 μm) were tested and in most runs the Rh retention is greater than 99.9%. The amounts of macroligands were undetectable in the permeate solutions.

4.2.1.2 Soluble polymer supported catalysts

The soluble transition metal-containing polymers include crosslinked or non-crosslinked polystyrene, polymethacrylate, methyl hydrosiloxane-dimethylsiloxane copolymer, polysiloxane and hyperbranched poly(triallylsilane). A new class of catalysts, soluble polymer-attached homogeneous catalysts, was first reported by Bayer and Schurig¹⁸, prepared by reacting soluble polystyrene with appropriate Rh metal precursor, e.g. $\text{RhH}(\text{CO})(\text{PPh}_3)_3$, and separated from the 1-pentene hydrogenation reaction mixture by either precipitation or by filtration through a semipermeable membrane following reaction.

Datta *et al.*¹⁹ presented nanofiltration for separating homogeneous catalysts for Heck, Sonogashira, and Suzuki coupling reactions of aryl halides and bromides using soluble phosphinated polymersupported palladium catalysts. The catalyst complex is obtained by reacting brominated linear poly(4-methylstyrene) with (1-Ad)₂PH (bis(adamant-1-yl)phosphine or di-1-adamantylphosphine) to synthesize a polymer loaded with sterically demanding and electron-rich $-\text{CH}_2\text{P}(\text{1-Ad})_2$ groups as the respective air-stable phosphonium salt. The separation was done over a solvent-resistant nanofiltration membrane composed of a dense poly(dimethylsiloxane) (PDMS) layer cast on a porous sublayer of poly(acrylonitrile) (PAN). The membrane displays virtually quantitative retention of the polymeric catalyst; furthermore, palladium was not detected in the permeate. TXRF and spectrophotometric determinations indicated > 99.95% retention of the catalyst. The activity of the catalyst in the retentate is almost unchanged, as shown by the high (typically > 90%)

and nearly constant yields of the coupling reactions, as well as by the constant turnover frequencies of the catalysts following membrane separation for up to nine cycles of Sonogashira and Suzuki reactions.

Kragl and Dreisbach²⁰ demonstrated continuous asymmetric synthesis using soluble homogenous catalyst prepared by coupling the enantioselective chiral ligand α,α -diphenyl-L-prolinol with copolymerized 2-hydroxyethyl methacrylate and octadecyl methacrylate with a molecular weight of $96,000 \text{ g mol}^{-1}$. More than 99.8% of the polymer supported ligand was retained using polyaramide ultrafiltration membrane (Hoechst Nadir UF PA20) during continuous operation. Another soluble polymer-enlarged catalyst was prepared by Wandrey *et al.* by attaching an oxazaborolidine *via* a hydrosilylation reaction to a methyl hydrosiloxane-dimethylsiloxane copolymer and tested in the enantioselective reduction of acetophenone giving 86% yield with an ee of 97%, similar to the ones obtained with unbound analogs.²¹ With this catalyst system, Kragl *et al.* demonstrated dead-end continuous operation and obtained higher ee's than batch experiments in which the ketone was added at one time initially. The comparison between oxazaborolidine and alcohol dehydrogenase for the asymmetric reduction of acetophenone was presented by Risson *et al.* and both systems were run in a continuous membrane reactor for several residence times.²² The catalyst deactivation was blamed for short half-life times (1.2 and 31.1 days, respectively) in both chemical and enzymatic systems rather than due to leaching.

Schwab and Mecking²³ reported an approach for immobilization of a catalytically active rhodium complex bound by electrostatic interactions of multiply sulfonated phosphine ligands with a soluble polyelectrolyte. The polyelectrolyte-bound rhodium catalyst was used to catalyze hexene hydroformylation and could be recovered and recycled by ultrafiltration with retention of up to 99.8% per cell volume on an asymmetric polyethersulfone membrane (nominal MWCO 50 kDa). By comparison, the non-immobilized complex passed the membrane under the same conditions and > 90% was found in the filtrate. The catalytic activities and rhodium losses upon recycling were found to be repeatable.

Gold nanosols stabilized with poly(vinylalcohol) were used as homogeneous oxidation catalysts for 1,2- diols with varying chain length, both in water and in a variety of alcoholic solvents. They were efficiently recycled by means of nanofiltration using cellulose acetate membranes for the aqueous filtration and poly(dimethylsiloxane) (PDMS) membranes for the solvent resistant filtration. The stabilized sols retained their activity over extended periods and the activity of the sol was of the same order as previously reported for stabilized nanoparticles deposited on carbon supports. Recycling tests after nanofiltration showed that catalytic activity was largely preserved in consecutive runs.²⁴

4.2.1.3 *Unmodified or non-macromolecular ligand modified catalysts*

U.S. Patent 5,681,473²⁵ by Union Carbide Corporation discloses the membrane separation of organic solubilized rhodium-organophosphite complex catalyst and free organophosphites from a homogenous, non-aqueous

hydroformylation mixture using a setup with three filters in parallel. The difference in solubility parameters between polymer membranes and hydroformylation reaction compounds, and the ratio of the molar volume of phosphite ligands to aldehyde product, were used as criteria to choose a solvent compatible membrane and appropriate ligands in terms of size. The highest rhodium retention was obtained with a polydimethylsiloxane composite membrane (99.2%, equivalent to 4.2 ppm in the permeate), with no detectable amounts of bidentate phosphite ligand with a molecular weight of approximately 840 g/mol.

U.S. Patent 5,174,899²⁶ by Hoechst reports a process for separating organometallic compounds and/or metal carbonyls from organic media by a semi-permeable membrane made of an aromatic polyamide (polyaramide). In the first example of dicyclopentadiene (DCP) hydroformylation, the separation of rhodium modified by the triisooctylammonium salt of tris(*m*-sulfophenyl)phosphane from the raw product was demonstrated in a two-stage membrane filtration. The results show that the first stage retained 95% rhodium and 78% of phosphorus (based on feed) and the overall Rh and P(III) retentions were greater than 99.5% and 94.4%, respectively.

Solvent resistant nanofiltration was applied to Co-Jacobsen catalyst in the hydrolytic kinetic resolution (HKR) of epoxides, 1,2-epoxyhexane and styrene oxide as test substrates.²⁷ Several commercially available membranes and laboratory prepared membranes were subjected to separation tests of Co-Jacobsen catalyst in diethylether (Et₂O), isopropyl alcohol and solvent-free conditions. The lab-made nanofiltration membrane COK M2 gave the best catalyst retention of 98% in Et₂O in

a cross-flow filtration cell. Catalyst recycling for up to four times was demonstrated in a batch membrane reactor with slightly decreasing conversion, due to the incomplete retention and gradual catalyst deactivation.

Livingston's group applied nanofiltration in separating mixtures of various solute-solvent combinations, such as transition metal catalyst and ionic liquids in Suzuki reaction mixture²⁸ and in asymmetric hydrogenation reaction mixture,²⁹ the Jacobsen, Wilkinson and Pd-BINAP catalysts in organic solvents (ethyl acetate, tetrahydrofuran and dichloromethane),³⁰ aromatic acids and bases in wastewater,³¹ separating dyes in aqueous and organic solvents³² as well as phase-transfer catalyst in organic solvents.³³ Livingston's group also demonstrated solvent-specific membrane performance, such as the flux, retention and stability, compatibility of the solvent-membrane combinations,³⁰ nanofiltration membrane cascade for continuous solvent exchange,³⁴ temperature, concentration and pressure effects on solvent flux and solute rejection,^{30, 35, 36} and solvent transport.³⁷

Cornils³⁸ group separated rhodium complex modified by water-insoluble quaternary ammonium salts of functionalized ligand (trisulfonated triphenylphosphine TPPTS) from hydroformylation mixture using polyamide membrane (UF-PA-5, Hoechst AG). Following dicyclopentadiene hydroformylation with amines of molecular weight increasing from 350 to 3000 g/mol, separate membrane filtrations showed that the retention of Rh and ligands could be up to 99.7% and 98.7%. Further optimization was done by hydroformylation of propylene with the Rh-distearyl amine/TPPTS catalyst system. With high P/Rh ratio of 100, the

subsequent quantitative separation enabled the catalyst recycling for up to 10 times with no observable deactivation.

4.2.2 Commercially available membranes and filtration setups

Several membranes have been claimed to be capable of nanofiltration in organic solvent, known as solvent resistant nanofiltration (SRNF) membranes. Koch SelRO[®] membrane systems³⁹ (USA) are solvent-stable, commercially available and supplied in a wet form. Among of the most popularly examined membranes (MPF-60, MPF-44 and MPF-50), MPF-50 has been the most studied commercial SRNF membrane in many applications^{10, 30, 40} and the other two membranes have been discontinued. STARMEM[®] from Membrane Extraction Technology (UK)⁴¹ and Solsep membranes from SolSep BV-Robust Membrane Technologies (The Netherlands)⁴²⁻⁴⁴ appeared in the market recently and have been successfully demonstrated in the literature for organic solvent nanofiltration. Another series of membranes, Desal-5 and Desal-5-DK^{30, 43} from GE Osmonics (USA) are designed for aqueous applications, but are also selective in SRNF. Vandezande *et al.*¹⁰ summarized more membrane information in the most recently published paper.

The membrane nanofiltration setups described in the literature can be categorized into two groups according to the flow direction relative to the membrane surface: dead-end filter (perpendicular) and cross-flow filter (parallel).¹¹ Table 4.1 provides the specifications of the commercially available dead-end filtration cells: solvent-resistant stirred cell from Millipore⁴⁵ (USA), MET cell from Membrane

Extraction Technology Ltd.⁴¹ (UK) and HP4750 stirred cell from Sterlitech Corporation⁴⁶ (USA).

Table 4.1 Commercial dead-end membrane filters

Filtration	Millipore		MET	HP4750
	ultrafiltration		nano/ultra-filtration	nano/ultra-filtration
Cell Diameter, mm	80	110	60 flared to 120	51
Cell Height, mm	122	165	171	199
Membrane Diameter, mm	47	76	90	49
Filtration Area, cm ²	15	40	54	14.6
Max. Working Volume, mL	75	300	270	300
Hold-up Volume, mL	0.3	1	5	1
Max. Working Pressure, bars	6.2	6.2	69	69
Max. Temperature, °C	Autoclavable [#]		60	121 at 55 bars
Stirrer	PTFE*		PTFE*	Teflon*

* PTFE, i.e. poly(tetrafluoroethylene) is most well known by the DuPont brand name Teflon. [#] No specific operating temperature was provided. The cell can be autoclaved at 120 °C for 30 minutes during sterilization.

A Septa ST pressure cell from Osmonics⁴⁷ (USA) described by Livingston *et al.*³⁰ is not marketed anymore. However, an alternative setup GE Sepa™ CF II Med/High foulant system shown in Figure 4.3, allows for cross-flow filtration with any membrane.



Figure 4.3 GE Sepa™ CF II Med/High foulant system from Osmonics (USA)

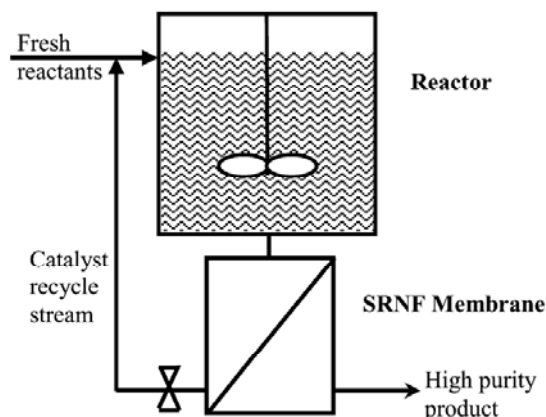


Figure 4.4 Cross-flow filtration scheme^{48, 49}

Other cross-flow filtration reactors were described by Nair *et al.*,⁵⁰ Patterson *et al.*,⁵¹ Roengpithya *et al.*,⁵² Peeva, *et al.*,⁵³ and Vogt *et al.*^{48, 49} Figure 4.4 shows a typical operation of cross-flow type of filtration coupled with an external reactor. To avoid concentration polarization, a high-speed HPLC pump is usually employed in the recycle stream for rapid retentate circulation.

4.3 Experimental Apparatus

4.3.1 STARMEM[®] membrane

The STARMEM[®] nano/ultra-filtration membrane is distributed by Membrane Extraction Technology, UK and manufactured by W.R. Grace-Davison (USA).⁵⁴ The membrane is made of highly cross-linked asymmetric polyimide. The thickness of the active layer is less than 0.2 mm with a pore size of < 50 Ångström.³⁰ This membrane has a diameter of 90 mm and an active surface area of 54 cm². The

molecular weight cut-off (MWCO) of the membrane ranges from 200 to 400 Daltons, based on 90% retention of the solute. This membrane is compatible with most of the conventional organic solvents, such as alkanes, aldehydes, alcohols and aromatics. Its durability is for up to one year with a maximum operating temperature of 60 °C.¹¹

4.3.2 MET cell

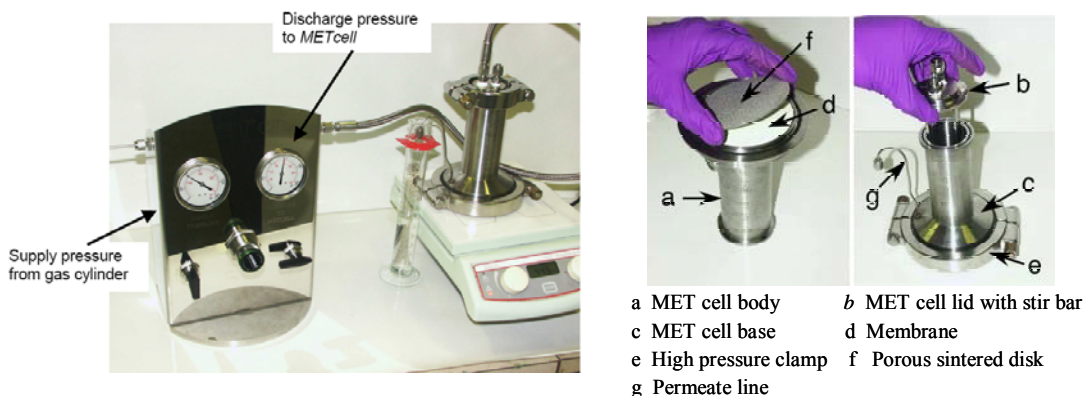


Figure 4.5 Configuration of MET cell assembly

The MET cell shown in Figure 4.5 was purchased from a British company Membrane Extraction Technology (MET) Ltd. in London, UK and made of 316 stainless steel. The flat paper-like membrane is placed at the bottom of the MET cell and supported by a porous sintered stainless steel disk, which provides mechanical strength to the membrane. Thus the membrane functions as a dead-end filter. The maximum working volume of the MET cell is 270 mL with a hold-up volume of 5 mL. The two inlets (one for feed and the other for pressurizing gas) enable continuous and air-free operation. The cell is equipped with a Teflon-coated magnetic stirrer bar fixed on a metal bracket soldered to the top lid. The maximum

operating pressure is 1000 psi (69 bars). This is a dead-end mode filter with a flat membrane sheet.

4.3.3 Setup

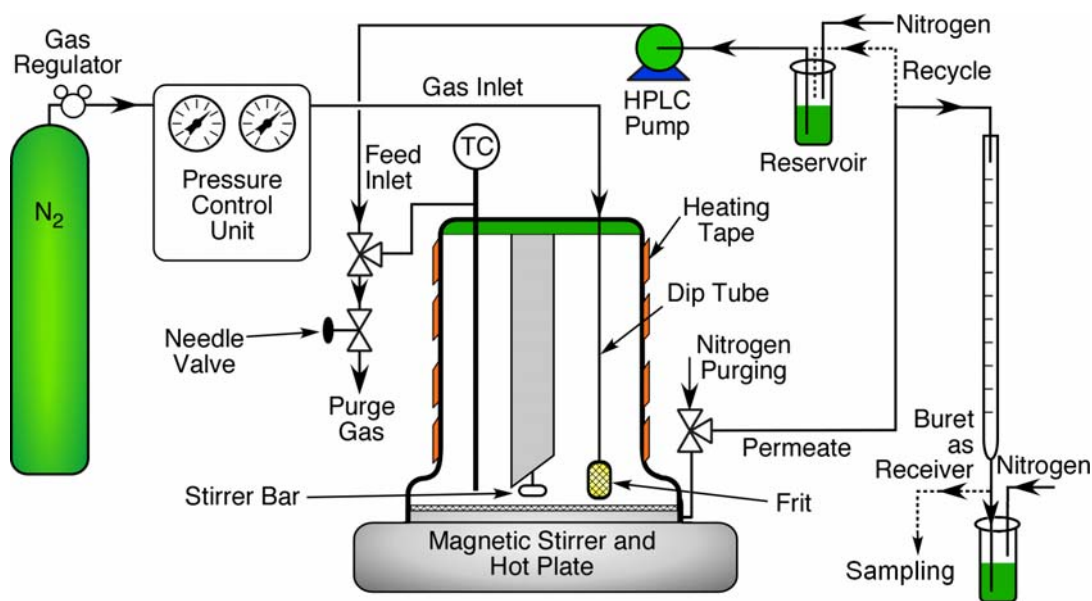


Figure 4.6 Membrane filtration setup configuration

Figure 4.6 shows the schematic of the membrane filtration setup. The cell body is wrapped with a heating tape and insulation and placed on a magnetic stirrer and hot plate (Barnstead Cimarec Stirrer with stirrer setting of 1-12 and stirrer speed range of 60-1200 rpm) for mixing and heating. A thermocouple, interfaced with LabView® data acquisition, measures the solution temperature. The solvent or the substrate is pumped into the cell at a constant flowrate ranging from 0.01 to 20 mL/min. Both the feed reservoir and permeate receiver are blanketed with inert nitrogen gas. This setup is capable of either batchwise or continuous filtration under

air-free condition. There are a variety of inert gases that can serve as pressurizing gases. Nitrogen was used in the current studies. CO₂ will also be used in future studies to create CO₂-expanded solvent media with lower viscosity. For performing homogeneous hydroformylation reactions with simultaneous filtration of the catalyst complex, either synthesis gas (CO/H₂ = 1:1 molar) or its mixture with CO₂ will be employed as the pressurizing gas. Following filtration, the cell pressure is released gradually via a regulating valve to avoid membrane doming caused by sudden pressure change. The permeate may be recycled back to the cell, with provisions for sample withdrawal for analysis purposes.

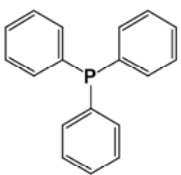
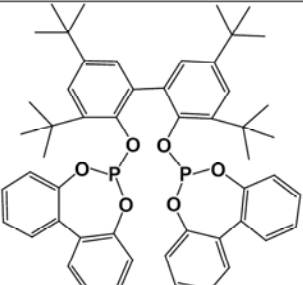
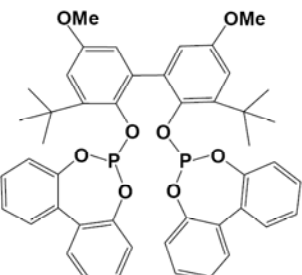
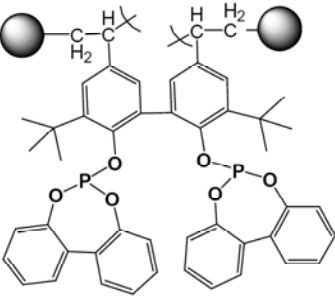
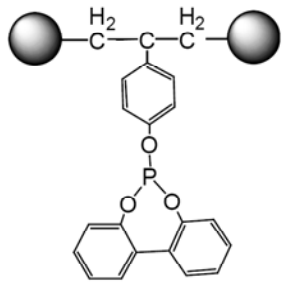
4.4 Catalytic Systems and Analytical Methodology

4.4.1 Catalytic systems

The homogeneous catalytic systems tested for filtration consist of the catalyst precursor Rh(acac)(CO)₂ (Rh-50) and various phosphorus ligands dissolved in toluene. Triphenylphosphine (TPPine) was used as the benchmark ligand with the lowest molecular weight. Biphephos and BiPhPhM bulky bidentate phosphite ligands were synthesized and supplied by Professor Tunge's group at the KU Department of Chemistry. Another group of ligands is bulky bidentate or mono- phosphite ligands bound to a polymer backbone, with styrene to crosslinker ratio of 10 or 20.⁵⁵ These types of ligands have molecular weights around 10,000 Daltons, with a fairly narrow distribution. A lettering protocol (a, b, and c) after the polymer bound ligands is used to designate different batches of polymer following the same synthesis procedure.

Table 4.2 provides the structures of all the phosphorus ligands and their molecular weights. The shaded circles represent the polymer backbone. Appendix V provides phosphorus loading information for the synthesized polymer bound ligands.

Table 4.2 Phosphorus ligands and their molecular weights

		
<p>TPPine, MW=262.29 g/mol</p>	<p>BiPhePhos, MW=838.94 g/mol</p>  <p>PBB10a, b, c $M_N=10,000$ g/mol</p>	<p>BiPhPhM, MW=786.78 g/mol</p>  <p>PBP10a, $M_N=10,000$ g/mol</p>

Catalyst solutions were prepared by dissolving known amounts of Rh(acac)(CO)₂ (Rh-50) and other ligands in toluene and leaving the stirred solutions in a glove box overnight to allow Rh binding. The solutions were blanketed by an inert gas during mixing, binding and transferring. The starting or feed solutions containing the catalyst complex or ligands are designated as F. The solution passing through the membrane is called the permeate (designated as P) and the solution rejected by the membrane is called the retentate (designated as R). The adduct of Rh(acac)(CO)₂ and ligands (L) under inert gas is Rh(acac)L₂. Under

hydroformylation reaction conditions (CO/H₂ pressure), the most possible adducts of Rh(acac)(CO)₂ and ligands (L) include HRh(CO)L₃ and HRh(CO)₂L₂ for monodentate ligands and HRh(CO)₂L₂ only for bidentate ligands. The amount of each species depends on the ligand concentrations and the CO partial pressure. These adducts might coexist with the free Rh(acac)(CO)₂ and the free ligand (L) due to the reversible nature of the complex formation.

The unmodified rhodium catalyst, Rh(acac)(CO)₂, designated as Rh-50, with a purity of 99% and the ligand, triphenylphosphine (PPh₃) with purity of 99%, were obtained from Alfa Aesar. Anhydrous toluene in Sure/Seal™ at purity of 99.8% was purchased from Sigma-Aldrich, Inc.

4.4.2 Analytical techniques

Inductively coupled plasma optical emission spectroscopy (ICP-OES) was employed to quantify the rhodium and phosphorus concentrations in the starting catalyst solution, the retentate and the permeate. The ICP is an emission spectroscopic technique based on the principle that the intensity of the light emitted by excited ions is proportional to the respective elemental concentration in the analytical solution. The excitation energy is supplied by an electrical current produced by electromagnetic induction. The ICP is widely applied for elemental analyses in metallurgy, agriculture, biology, environment and geological materials.⁵⁶ In most cases, aqueous analysis is preferred after acid digesting the heterogeneous sample. In contrast, organic matrix analysis is rarely used due to the paucity of standards for organic matrix and their short shelf life. In our case, we chose toluene

as solvent to accommodate phosphorus bound rhodium complexes, due to its strong solvation power for the catalyst complex and the hydroformylation reaction mixture. Table III.3 in Appendix III gives the applications of ICP in organic matrixes reported by Jobin Yvon.

4.4.2.1 *The ICP configuration and specifications*

The ICP instrument used in this work was purchased from HORIBA Jobin Yvon⁵⁷ with radial plasma view and monochromator optical system. Figure 4.7 gives the schematic of the ICP sample introduction system. The liquid sample solution is introduced by peristaltic pump and then sprayed and converted to aerosols by Meinhard concentric nebulizer. The aerosols are sorted by the cyclonic spray chamber and only droplets smaller than 10 μm reach the torch and plasma. It should be noted that only a small quantity of sample aerosols is allowed so as to keep the plasma from being extinguished.

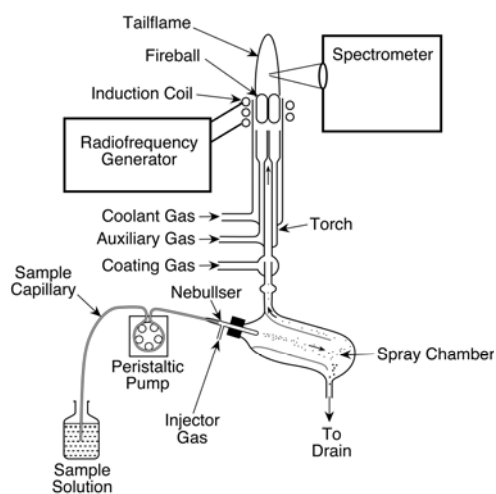


Figure 4.7 Schematic of the ICP sample introduction

The radio frequency generator supplies energy for sustaining the plasma and produces a high-frequency electromagnetic field in the induction coil with output power of between 800 to 1500 W at a frequency of 40.68 MHz. Inside the high temperature plasma, the aerosols carried by argon gas are preheated to dryness and then excited by the ionized gas to high-energy atoms and ions. After passing the radiation zone, these particles release the energy in the form of photons at certain frequencies or wavelengths. Each element has its own characteristic emission lines. The principles of atomic emission, operating safety, matrix selection and maintenance are detailed in the manufacturer-supplied manuals “User Manual Jobin-Yvon ICP Spectrometers” and “User Manual ICP V5 Software”. Figure 4.8 shows the configuration of the JY ICP in our lab and the instrument specifications are listed in the Table 4.3.

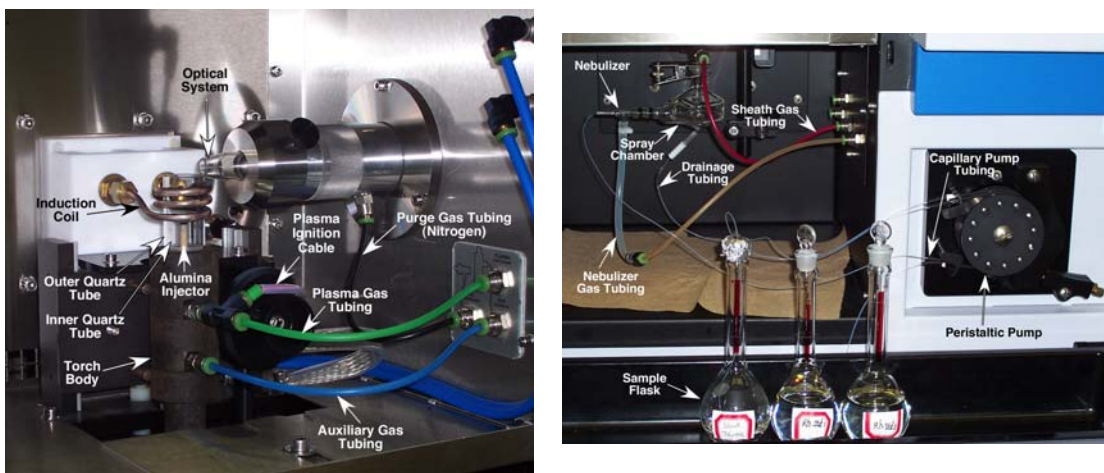


Figure 4.8 The configuration of Jobin Yvon 2000 2 ICP

Table 4.3 The Jobin Yvon 2000 2 ICP specifications

Parameters	Specifications
Model	Jobin Yvon 2000 2
Radio frequency generator	40.68 MHz
Cooling	Deionized water
Mounting (monochromator)	Czerny Turner
Focal Length	0.64 m
Grating number of grooves	4320 gr/mm
Order	II
Spectral range	180-400 nm (near UV)
Resolution	10 pm FWHH
Operating gas	Argon (Ar)
Purging gas	Nitrogen (N ₂)
Torch design	Vertical demountable
Plasma View	Radial
Nebulizer	Concentric, Meinhard TR-30-C0.5
Spray chamber	Cyclonic
Detector	Photomultiplier tube (PMT)

4.4.2.2 Calibration

Calibration standards were made by dissolving Rh(acac)(CO)₂ and triphenylphosphine (TPPine) in toluene. Toluene was also used to dilute the samples and calibration solutions to lower the viscosity of the sample solutions and reduce its influence on the results. The calibration graphs in Figures 4.9 and 4.10 show excellent linearity for both Rh and P spanning several orders of magnitude down to ppb level. For example, dissolved Rh can be detected quantitatively at concentrations as low as 20 ppb. Appendix III provides relevant details for ICP method development, calibration procedure, analysis protocols and operation.

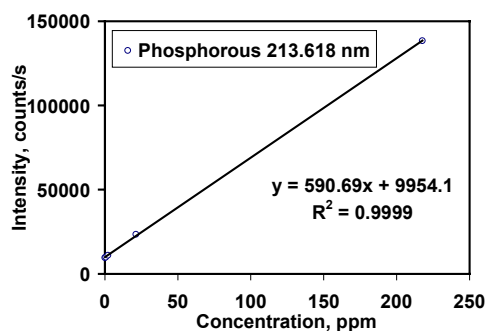


Figure 4.9 Calibration curves for P

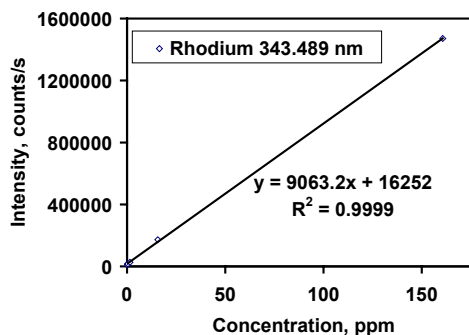


Figure 4.10 Calibration curves for Rh

4.5 Experimental Procedure

4.5.1 Membrane preconditioning and equilibration

Prior to filtration, the membrane was conditioned by flushing pure toluene through it under nitrogen pressure of 3.0 MPa for one hour. The permeate from this conditioning run was disposed of due to contamination of the solvent with membrane by lubricating oil (used as membrane preservative). Following the preconditioning step, the flushing was continued with fresh toluene that was continuously circulated back to the cell. This step was continued till the flux (mL toluene per min) through the membrane leveled out, signaling membrane equilibration. The equilibration step normally takes about 3 days to get a stable solvent flux.³⁷ After these pretreatment steps, the membrane was ready for the nanofiltration studies of the solution containing dissolved catalyst complexes. Between each filtration run, the membrane was washed three times and soaked overnight in toluene.

4.5.2 Flux measurements

During each filtration run, the permeate fluxes were periodically recorded to ensure constant rate thereby eliminating any variations due to physical damage to the membrane (i.e. cracking, clogging and other defects on the membrane surface). Furthermore, a blank filtration run with pure toluene was carried out before and after each filtration with the solution containing dissolved catalyst complex. Under identical gas pressures, lower fluxes were typically observed for the runs with dissolved catalyst compared to pure toluene. This is attributed to the increased viscosity of the catalyst solution containing dissolved polymer supports.

The permeate volume was measured in a 100 mL burette of which the ungraduated bottom part was calibrated as 5.5 mL. The accuracy of the burette is ± 0.2 mL. A stopwatch with an accuracy of ± 1 s was used to record the time for collecting certain volumes of permeate. The transient permeate flux is represented by the average flux in a small period of time, in a form of $J = \frac{\Delta V}{A\Delta t}$, where J is the membrane flux ($\text{L} \cdot \text{m}^{-2} \cdot \text{hr}^{-1}$), ΔV is the permeate volume (L) during the period of time Δt (hours) and A is active membrane surface area (m^2), equal to 54 cm^2 specified by the manufacturer. Another parameter characterizing the membrane flux is the membrane permeability, a normalized transient permeate flux to pressure ratio with a unit of $\text{L} \cdot \text{m}^{-2} \cdot \text{hr}^{-1} \cdot \text{bar}^{-1}$.²⁷

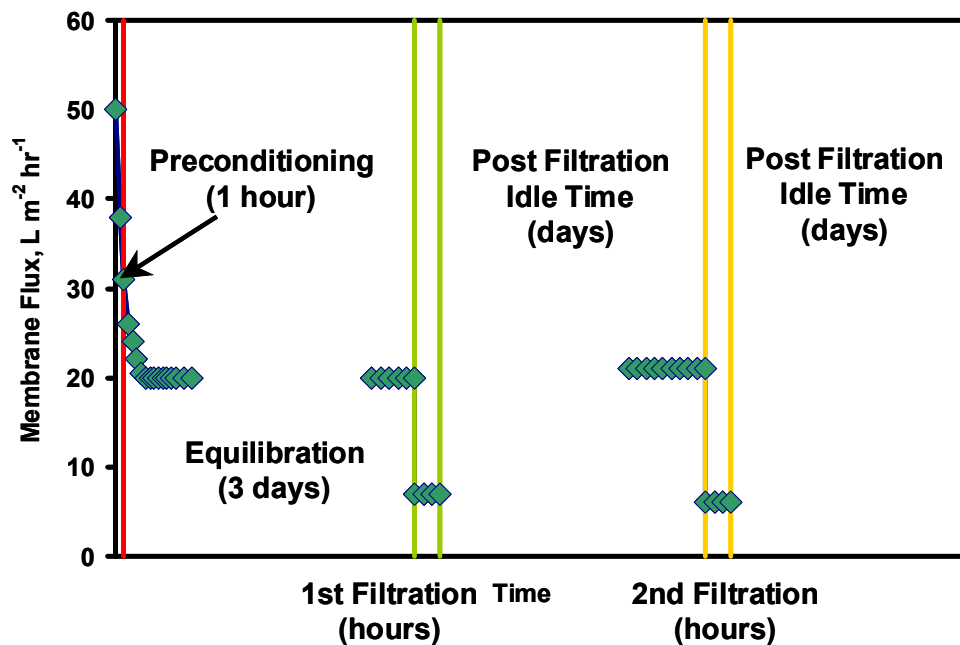


Figure 4.11 A typical flux measurement protocol

Figure 4.11 shows flux measurements during all the experiments performed with a membrane during its lifetime. The flux decline during preconditioning of a fresh membrane was found to be a common phenomenon during the preconditioning and equilibration stages, and at the beginning of each filtration run due to the membrane compaction under pressure.^{32, 58} The initial compaction is a long process and irreversible, reaching a steady state after several days. The flux value specified by the manufacturer is the flux obtained under nitrogen pressure of 5.5 MPa after 24 hours of filtration using pure toluene. Our flux measurement results show good repeatability of the steady state flux using the same solvent, indicating that the membrane has no defect or cracking on the surface and is ready to use.

For the filtration (either batch or continuous) of toluene with dissolved solute, *i.e.* organometallic rhodium complexes, the permeate flux is lower than that of the pure solvent toluene. Further, this permeate flux gradually decreases with time even though the pressure is maintained constant. This is attributed to the increase in the viscosity of the retentate as it becomes concentrated in the solute with filtration. This flux decrease is however insignificant and is not shown in Figure 4.11. This could also be caused by reversible compaction, concentration polarization, adsorption, fouling, pore blocking and hindered diffusion within the pores.³² It has been reported that in some cases, the membrane flux could be totally hindered either due to high viscosity of the solution²⁷ or membrane incompatibility with solvent used. The idle time between each filtration ranged from one to several days and the filtration time varied from minutes to hours to days.

4.5.3 Batch filtration experiment procedure

To begin the batch filtration, the catalyst solution is transferred *via* air-tight syringe into the MET cell through the feed inlet with concurrent nitrogen purging at low pressure of a few psi. The typical volume of the initial solution is 60 mL. Then the cell is pressurized with nitrogen to the desired pressure (1.0 MPa). The cell pressure is maintained constant by replenishing the dissolved gas that escapes through the membrane with fresh nitrogen from a source gas cylinder. The magnetic stirring rate is set at 4 out of 1-12 settings and the 100 mL burette permeate receiver is purged with nitrogen. The filtration is commenced by opening the permeate valve and allowing the cell contents to be filtered through the membrane until half of the initial

volume is collected as permeate. The permeate flux is calculated by timing the volumetric flow with the 100 mL burette placed in the effluent. After the desired amount of permeate is collected, the permeate check valve is shut off to stop filtration. The retentate and permeate streams are then sampled for Rh and P elemental analysis by ICP. The foregoing procedural steps were all done at room temperature (about 21°C). Then the MET cell is transferred into a glove box and the retentate is collected after washing three times and overnight soaking in pure toluene. Before reusing the membrane, a visual check and flux measurement are made to ensure the membrane is in good condition.

The Rh metal or P pass-through was calculated as follows:

$$\text{Pass-through} = \frac{\text{total Rh or P in permeate}}{\text{total Rh or P in starting solution}}$$

4.6 Results and Discussions

4.6.1 Triphenylphosphine (TPPine), BiPhePhos and PBB20 ligands

TPPine (a monodentate ligand), BiPhePhos (a bidentate ligand) and PBB20 (a soluble polymer bound ligand) were first tested in batch filtration mode using fresh membranes after pretreatment at room temperature (21°C) under constant nitrogen pressure of 4.0 MPa with stirring.

20.1 mg Rh(acac)(CO)₂ and 401.5 mg TPPine (molar P/Rh = 20) were dissolved in 100 mL toluene. The absolute amounts of rhodium and phosphorus are 8.0 mg and 47.4 mg, respectively. The 100 mL catalyst solution was filtered through the membrane (MWCO = 200 Daltons) at room temperature (21 °C) and under

nitrogen pressure of 1.0 MPa with stirring until approximately half of the initial volume was collected as permeate. From Table 4.4, it can be inferred that the Rh and P were preferentially filtered. The higher pass-through of P (13.6%) relative to that of Rh (6.3%) is due to the smaller size of free TPPine ligand compared to the TPPinebound Rh complex. The distinct excess of free TPPine suggests that most Rh metal centers remain bound to the TPPine in the solution being filtered. A small mass balance deficit, ranging from 6-9 wt.%, was observed as shown in Table 4.4.

Table 4.4 Batch filtration results for TPPine ligand

	Feed (F)	Retentate (R)	Permeate (P)	Total (T)	MB	PT
Volume, mL	100.0	51.0	49.0	100.0		
Rh, mg	8.0	6.81	0.46	7.27	91%	6%
P, mg	47.4	38.32	6.02	44.34	94%	13%

Total (T) = R+P; MB = Mass Balance = (R+P)/F; PT = Pass-through = P/F

In another test, 7.2 mg Rh(acac)(CO)₂ and 431.2 mg PBB20 (molar P/Rh = 3.7) were dissolved in 100 mL toluene. Of this solution, 80 mL were injected into the MET cell and the remaining 20 ml was used for feed analysis. A fresh membrane (MWCO = 200 Daltons) was used and the filtration was performed at room temperature (21 °C) under nitrogen pressure of 4.0 MPa with stirring. Approximately, 40 mL permeate was collected. The Rh and P contents in the feed solution, permeate and retentate were determined by ICP. As shown in Table 4.5, the mass balance closure for Rh and P are 94% ± 4% and 97% ± 3%, respectively.

Table 4.5 Batch filtration results for PBB20 ligand

	Feed (F)	Retentate (R)	Permeate (P)	Total (T)	MB	PT
Volume (V), mL	80.0	40.0	40.0			
Rh, mg	2.45	2.27	0.03	2.30	94%	1%
P, mg	4.17	4.05	0.00	4.05	97%	0%

Total (T) = R+P; MB = Mass Balance = (R+P)/F; PT = Pass-through = P/F

The uncertainties in the mass balance closure for the runs summarized in Tables 4.4 and 4.5 stem mainly from the ± 1 mL accuracy of the volumetric cylinder and the relative standard deviation (RSD) of the repeated measurements. To reduce the overall uncertainty, the volume measurements were replaced with more accurate mass measurements (± 0.1 mg) for both the samples and standards in all subsequent filtration tests. Detailed error analysis is provided in Appendix IV.

The bidentate BiPhePhos ligand and Rh-50 (molar P/Rh = 4.0) were weighed in a glove box and dissolved in anhydrous toluene to a total volume of 100 mL. To facilitated complete ligand binding, the solution was left in the glove box for about 2 days with stirring. It was observed that there were some black particles on the bottom of the flask and the color of the mixture turned yellowish green. The black particles might be Rh metal and could be from degraded Rh-50, which was stored for over a year. Only the upper clear portion (60 mL) of the mixture was used in the filtration studies with a fresh, preconditioned membrane (MWCO = 220 Daltons). Following filtration, the reactor was moved to a glove box to recover the retentate. The membrane was washed three times with pure toluene and then soaked twice in pure toluene for at least one hour for each time.

As seen from Table 4.6, the lower pass-throughs for Rh (5%) and for P (0%) than those observed with the Rh-50 + TPPine complexes (Table 4.4) are attributed to the bulkier nature of the BiPhePhose ligand as well as the stronger binding between the Rh and the bidentate ligand. However, compared to the Rh-50 + PBB20 system (Table 4.5), the much higher Rh and P pass-throughs are attributed to the smaller size (> 10-fold) of the BiPhePhos ligand and the larger pore size of the membrane used with the BiPhePhos ligand (MWCO = 220 Daltons).

Table 4.6 Batch filtration results for BiPhePhos ligand

	Feed (F)	Permeate (P)	Retentate (R)	Total (T)	MB	PT
Rh, mg	3.72	0.18	3.55	3.72	100%	5%
P, mg	2.06	0.00	1.92	1.92	93%	0%

Total (T) = R+P; MB = Mass Balance = (R+P)/F; PT = Pass Through = P/F

These foregoing three experiments were carried out during the early stages of method development and the experience gained from them helped to standardize the operation procedures as follows:

- Air-free operation for all steps starting from solution preparation, ligand binding, sample transfer to filtration and cleaning
- Overnight ligand binding under inert gas protection before filtration tests
- Expressing the Rh and P concentrations in the samples and standards as $\mu\text{g/g}$ (ppm) rather than as mg/L, taking advantage of the more sensitive mass measurement compared to volume measurements.

4.6.2 BiPhPhM and PBB10 ligands

The three soluble polymer bound ligands (PBB10a, PBB10b and PBB10c) as well as one bidentate ligand (BiPhPhM) were tested. The catalyst solution contained Rh and P at concentrations ranging from 70-110 ppm and 90-300 ppm, respectively, and a molar P/Rh ratio of 4-8, as given in Table 4.7.

Table 4.7 Catalyst and ligand compositions in the initial catalyst solutions in each run

Ligands	Runs	[Rh]	[P]	P/Rh
		$\mu\text{g/g (ppm)}$	$\mu\text{g/g (ppm)}$	molar
PBB10a	1st Run	109.20	266.23	8.1
PBB10a	2nd Run	87.18	211.46	8.1
PBB10b	1st Run	101.76	218.24	7.2
PBB10b	2nd Run	97.07	208.18	6.9
PBP10a	1st Run	83.11	98.37	4.0
PBP10a	2nd Run	80.38	95.15	4.0
BiPhPhM	Run1	68.80	181.20	8.8
BiPhPhM	Run2	79.69	189.99	8.0

All filtrations and flux measurements were run at room temperature (21 °C). The permeate flux was measured before and after each filtration with pure toluene as blank run to check repeatability of the membrane flux so as to ensure that the membrane is in good condition. Table 4.8 provides membranes and nitrogen pressure used for each run. Figure 4.12 shows the permeate flux attained in various filtration runs performed with different solutions and different membranes:

Table 4.8 Membrane, permeate flux and nitrogen pressure used in each run

Ligands	Membrane MWCO Daltons	Flux, L/(m ² hr) (nitrogen pressure, MPa)			
		Before (pure toluene)	1 st filtration	After (pure toluene)	2 nd filtration
PBB10a	400	70 (2.0)	23 (1.0)	55 (2.0)	24 (1.0)
PBB10b	200	32 (3.0)	12 (1.0)	34 (3.0)	13 (1.0)
PBP10a	200	19 (3.0)	7 (1.0)	20 (3.0)	6 (1.0)
BiPhPhM	200	17 (3.0)	7 (1.0)	23 (3.0)	-
BiPhPhM	200	19 (3.0)	6 (1.0)	22 (3.0)	-

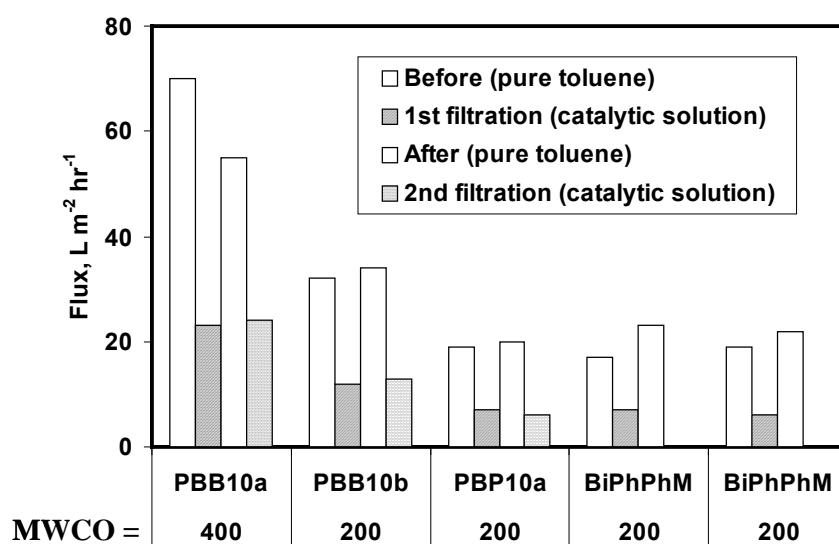


Figure 4.12 Permeate fluxes before, during and after filtration of catalytic solutions containing each ligand

Filtration conditions: T = 21 °C and under constant nitrogen pressure of 1.0 MPa; About half of the initial catalyst solution was filtered in each case.

In Figure 4.12, the white bars represent the blank filtration runs with pure toluene only, while the hatched and dotted bars represent the first and second filtration runs, respectively, performed with solutions containing dissolved catalyst complexes. For each of the three polymer bound ligands PBB10a, PBB10b and PBB10c, two consecutive runs performed with the same membrane yielded nearly

identical permeate fluxes, confirming the stability of the membrane. For the bidentate ligand (BiPhPhM), two repeated runs each were performed on two different membranes. These fluxes were reproducible as well.

Figure 4.13 gives the ICP-measured Rh concentration in the permeate stream for each batch run.

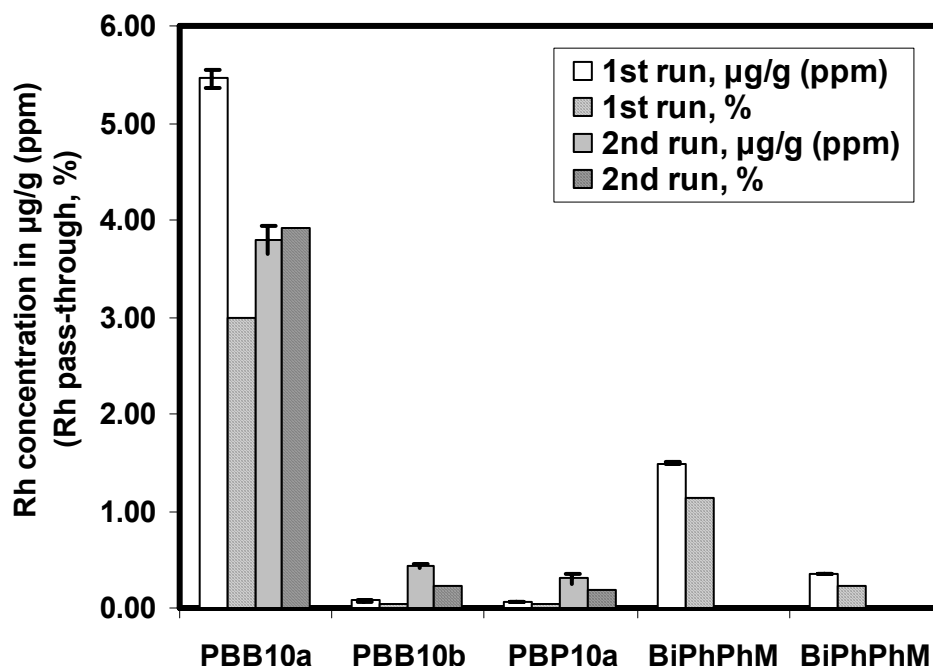


Figure 4.13 Rhodium concentrations in permeate and the Rh pass-through for batch filtrations of solutions containing various dissolved catalyst + ligands combinations. Filtration conditions: $T = 21\text{ }^{\circ}\text{C}$ and under constant nitrogen pressure of 1.0 MPa; About half of the initial catalyst solution was filtered in each case. Initial catalyst solution: volume = 40-60 mL, $[\text{Rh}] = 70\text{-}110\text{ ppm}$, $[\text{P}] = 90\text{-}300\text{ ppm}$, molar P/Rh ratio = 4-8.

For the PBB10a ligand, the Rh concentrations in the permeate are approximately $5.5\text{ }\mu\text{g/g (ppm)}$ and $3.8\text{ }\mu\text{g/g (ppm)}$ in the first and second runs, respectively. The Rh pass-through estimates are approximately 3% and 4%, based on filtration of half of the initial solution volume. The rather high pass-through values

are attributed to larger pores in the higher MWCO membrane. They could also be due to either incomplete membrane equilibration and/or impurities in the polymer that degrade the membrane surface.

For the PBB10b and PBP10a ligands, the two first runs at constant membrane flux rates yield significantly low Rh pass-through values, on the order of a few tens of ppb. The second run yielded a somewhat higher rhodium concentrations in the permeate, albeit still at ppb levels.

For the bidentate ligand (BiPhPhM), Rh concentrations in the permeate are higher as expected compared to those for the polymer bound ligands (PBB10b and PBP10a), which is attributed to the almost 10 fold smaller size of the non-polymer bound ligand and complex.

Figure 4.14 shows the same trends of P concentrations in permeate as Rh. Polymer bound ligands (PBB10b and PBP10a) yield the lowest P concentrations, and correspondingly lowest pass-through values, in the permeate. For both polymer bound ligands (PBB10b and PBP10a), the two consecutive runs on the same membrane give good repeatability in the concentrations and pass-throughs for both Rh and P.

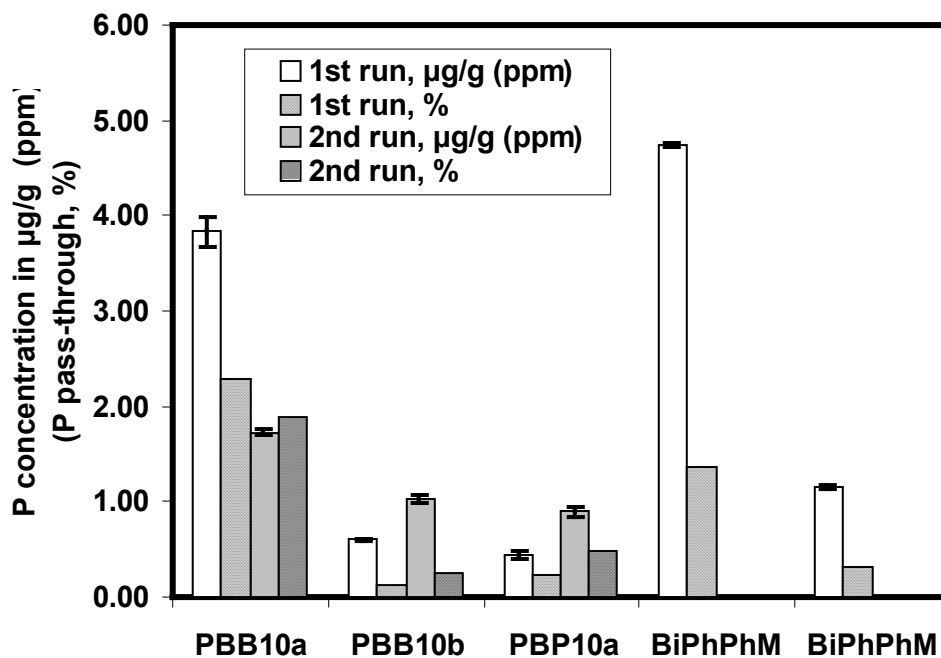


Figure 4.14 Phosphorus concentrations and pass-through values in permeate for batch filtrations of solutions containing various dissolved catalyst + ligands combinations. Filtration conditions: $T = 21\text{ }^{\circ}\text{C}$ and under constant nitrogen pressure of 1.0 MPa; About half of the initial catalyst solution was filtered in each case. Initial catalyst solution: volume = 40-60 mL, $[\text{Rh}] = 70\text{-}110\text{ ppm}$, $[\text{P}] = 90\text{-}300\text{ ppm}$, molar P/Rh ratio = 4-8.

4.7 Summary and Future Work

In conclusion, by employing polymer bound bulky phosphite ligands, specially synthesized by Professor Tunge's group, a membrane-based nanofiltration technique was successfully demonstrated to reduce Rh leakage to economically acceptable levels in the effluent. A selectively separating device, membrane nanofilter, was constructed and modified for air-free operation either batchwise or in continuous mode. The operating procedures for the setup and membrane were

standardized. The ICP analysis protocol was developed for sensitive elemental analyses of trace amount of Rh and P (down to ppb levels) in an organic matrix.

The batch filtration with various phosphorus ligands indicates that the size of the ligand used significantly affects the rhodium retention rate, which is in accordance with the membrane separation principle, size exclusion. In the batch filtration with polymer bound phosphite ligand PBB10, P was observed in the permeate, suggesting the removal of perhaps unbound Rh and P from the initial mixture and also from the fraction of the polymers that are lighter than or close to the MWCO of the membrane. Our chemistry synthesis team will provide the evidence of imperfect molecular weight distribution of polymer bound ligand by analyzing the polymer with gel permeation chromatography (GPC). In addition, the permeate will be collected under inert gas protection and examined by NMR. The results can be used to gain insight into catalyst leaching, deactivation, and polymer molecular weight distribution based on Rh-P binding form.

In the future, the organometallic rhodium complex recovery rate from homogeneous toluene solution obtained in this research can be used as data input to update the economic and environmental analysis in Chapter 1. Development of a continuous reactor model with integrated membrane separation will help to predict the membrane performance and understand the relation of solvent flux and solute rejection with the physical properties of the solution.

Membrane filtration coupled with hydroformylation reaction in continuous operation mode with and without CO₂, aimed at demonstrating nearly stable

hydroformylation activity, will be presented in the next chapter. The modeling of membrane fluxes based on viscosity measurements with and without CO₂ will be discussed in Chapter 6.

4.8 References

1. Fang, J.; Jin, H.; Ruddy, T.; Pennybaker, K.; Fahey, D.; Subramaniam, B., Economic and environmental impact analyses of catalytic olefin hydroformylation in CO₂-expanded liquid (CXL) media. *Industrial & Engineering Chemistry Research* **2007**, 46, (25), 8687-8692.
2. Cornils, B.; Herrmann, W. A., *Applied homogeneous catalysis with organometallic compounds*. Wiley-VCH: Weinheim, **2002**; Vol. 1.
3. Cole-Hamilton, D. J.; Tooze, R. P., Homogenous catalysis: advantages and problems. In *Catalyst separation, recovery and recycling: chemistry and process design*, Cole-Hamilton, D. J.; Tooze, R. P., Eds. Springer: Dordrecht, The Netherlands, **2006**; Vol. 30.
4. Reek, J. N. H.; van Leeuwen, P. W. N. M.; van Der Ham, A. G. J.; De Haan, A. B., Immobilisation of tailor-made homogeneous catalysts. In *Catalyst separation, recovery and recycling: chemistry and process design*, Cole-Hamilton, D. J.; Tooze, R. P., Eds. Springer: Dordrecht, The Netherlands, **2006**; Vol. 30, p 73.
5. Wiebus, E.; Cornils, B., Biphasic systems: water-organic. In *Catalyst separation, recovery and recycling: chemistry and process design*, Cole-Hamilton, D. J.; Tooze, R. P., Eds. Springer: Dordrecht, The Netherlands, **2006**; Vol. 30, p 73.
6. Mathison, C. R.; Cole-Hamilton, D. J., Fluorous biphasic catalysis. In *Catalyst separation, recovery and recycling: chemistry and process design*, Cole-Hamilton, D. J.; Tooze, R. P., Eds. Springer: Dordrecht, The Netherlands, **2006**; Vol. 30, p 73.
7. Behr, A.; Henze, G.; Schomacker, R., Thermoregulated liquid/liquid catalyst separation and recycling. *Advanced Synthesis & Catalysis* **2006**, 348, (12-13), 1485-1495.
8. Wasserscheid, P.; Haumann, M., Catalyst recycling using ionic liquids. In *Catalyst separation, recovery and recycling: chemistry and process design*, Cole-Hamilton, D. J.; Tooze, R. P., Eds. Springer: Dordrecht, The Netherlands, **2006**; Vol. 30, p 73.
9. Gordon, C. M.; Leitner, W., Supercritical fluids: compressed gases as mobile phase and catalyst support. In *Catalyst separation, recovery and recycling: chemistry and process design*, Cole-Hamilton, D. J.; Tooze, R. P., Eds. Springer: Dordrecht, The Netherlands, **2006**; Vol. 30, p 73.
10. Vandezande, P.; Gevers, L. E. M.; Vankelecom, I. F. J., Solvent resistant nanofiltration: separating on a molecular level. *Chemical Society Reviews* **2008**, 37, (2), 365-405.
11. Ronde, N. J.; Vogt, D., Separation by size-exclusion filtration: homogeneous catalysts applied in membrane reactors. In *Catalyst separation, recovery and recycling: chemistry and process design*, Cole-Hamilton, D. J.; Tooze, R. P., Eds. Springer: Dordrecht, The Netherlands, **2006**; Vol. 30, p 73.
12. Buhleier, E.; Wehner, W.; Vogtle, F., Cascade-chain-like and nonskid-chain-like syntheses of molecular cavity topologies. *Synthesis-Stuttgart* **1978**, (2), 155-158.

13. Knapen, J. W. J.; Vandermade, A. W.; Dewilde, J. C.; Vanleeuwen, P. W. N. M.; Wijkens, P.; Grove, D. M.; Vankoten, G., Homogeneous catalysts based on silane dendrimers functionalized with arylnickel (II) complexes. *Nature* **1994**, 372, (6507), 659-663.
14. van Heerbeek, R.; Kamer, P. C. J.; van Leeuwen, P. W. N. M.; Reek, J. N. H., Dendrimers as support for recoverable catalysts and reagents. *Chemical Reviews* **2002**, 102, (10), 3717-3756.
15. Berger, A.; Klein Gebbink, R.; van Koten, G., Transition metal dendrimer catalysts. In *Dendrimer Catalysis*, Springer Berlin / Heidelberg: **2006**; Vol. 20, pp 1-38.
16. Tulchinsky, M. L.; Miller, D. J. Dendritic macromolecules for metal-ligand catalyzed processes U.S. Patent 6,350,819 **2002**.
17. Tulchinsky, M. L.; Miller, D. J. Dendritic macromolecules for metal-ligand catalyzed processes U.S. Patent 6,525,143 **2003**.
18. Bayer, E.; Schurig, V., New Class of Catalysts. *Chemtech* **1976**, 6, (3), 212-214.
19. Datta, A.; Ebert, K.; Plenio, H., Nanofiltration for homogeneous catalysis separation: Soluble polymer-supported palladium catalysts for Heck, Sonogashira, and Suzuki coupling of aryl halides. *Organometallics* **2003**, 22, (23), 4685-4691.
20. Kragl, U.; Dreisbach, C., Continuous asymmetric synthesis in a membrane reactor. *Angewandte Chemie-International Edition in English* **1996**, 35, (6), 642-644.
21. Felder, M.; Giffels, G.; Wandrey, C., A polymer-enlarged homogeneously soluble oxazaborolidine catalyst for the asymmetric reduction of ketones by borane. *Tetrahedron-Asymmetry* **1997**, 8, (12), 1975-1977.
22. Rissom, S.; Beliczey, J.; Giffels, G.; Kragl, U.; Wandrey, C., Asymmetric reduction of acetophenone in membrane reactors: comparison of oxazaborolidine and alcohol dehydrogenase catalysed processes. *Tetrahedron: Asymmetry* **1999**, 10, (5), 923-928.
23. Schwab, E.; Mecking, S., Immobilization of a catalytically active rhodium complex by electrostatic interactions of multiply charged phosphine ligands with a soluble polyelectrolyte and recovery by ultrafiltration. *Organometallics* **2001**, 20, (26), 5504-5506.
24. Mertens, P. G. N.; Bulut, M.; Gevers, L. E. M.; Vankelecom, I. F. J.; Jacobs, P. A.; De Vos, D. E., Catalytic oxidation of 1,2-diols to alpha-hydroxy-carboxylates with stabilized gold nanocolloids combined with a membrane-based catalyst separation. *Catalysis Letters* **2005**, 102, (1-2), 57-61.
25. Miller, J. F.; Bryant, D. R.; Hoy, K. L.; Kinkade, N. E.; Zanolaidou, R. H. Membrane separation process U.S. Patent 5,681,473 **1997**.
26. Bahrmann, H.; Haubs, M.; Kreuder, W.; Muller, T. Process for separating organometallic compounds and/or metal carbonyls from their solutions in organic media. U.S. Patent 5,174,899 **1992**.
27. Aerts, S.; Buekenhoudt, A.; Weyten, H.; Gevers, L. E. M.; Vankelecom, I. F. G.; Jacobs, P. A., The use of solvent resistant nanofiltration in the recycling of the

- Co-Jacobsen catalyst in the hydrolytic kinetic resolution (HKR) of epoxides. *Journal of Membrane Science* **2006**, 280, (1-2), 245-252.
28. Wong, H. T.; Pink, C. J.; Ferreira, F. C.; Livingston, A. G., Recovery and reuse of ionic liquids and palladium catalyst for Suzuki reactions using organic solvent nanofiltration. *Green Chemistry* **2006**, 8, (4), 373-379.
 29. Wong, H. T.; See-Toh, Y. H.; Ferreira, F. C.; Crook, R.; Livingston, A. G., Organic solvent nanofiltration in asymmetric hydrogenation: enhancement of enantioselectivity and catalyst stability by ionic liquids. *Chemical Communications* **2006**, (19), 2063-2065.
 30. Scarpello, J. T.; Nair, D.; dos Santos, L. M. F.; White, L. S.; Livingston, A. G., The separation of homogeneous organometallic catalysts using solvent resistant nanofiltration. *Journal of Membrane Science* **2002**, 203, (1-2), 71-85.
 31. Daisley, G. R.; Dastgir, M. G.; Ferreira, F. C.; Peeva, L. G.; Livingston, A. G., Application of thin film composite membranes to the membrane aromatic recovery system. *Journal of Membrane Science* **2006**, 268, (1), 20-36.
 32. Yang, X. J.; Livingston, A. G.; dos Santos, L. F., Experimental observations of nanofiltration with organic solvents. *Journal of Membrane Science* **2001**, 190, (1), 45-55.
 33. Nair, D.; Luthra, S. S.; Scarpello, J. T.; White, L. S.; Freitas dos Santos, L. M.; Livingston, A. G., Homogeneous catalyst separation and re-use through nanofiltration of organic solvents. *Desalination* **2002**, 147, (1-3), 301-306.
 34. Lin, J. C. T.; Livingston, A. G., Nanofiltration membrane cascade for continuous solvent exchange. *Chemical Engineering Science* **2007**, 62, (10), 2728-2736.
 35. Silva, P.; Livingston, A. G., Effect of concentration polarisation in organic solvent nanofiltration - flat sheet and spiral wound systems. *Desalination* **2006**, 199, (1-3), 248-250.
 36. Silva, P.; Livingston, A. G., Effect of solute concentration and mass transfer limitations on transport in organic solvent nanofiltration - partially rejected solute. *Journal of Membrane Science* **2006**, 280, (1-2), 889-898.
 37. Silva, P.; Han, S. J.; Livingston, A. G., Solvent transport in organic solvent nanofiltration membranes. *Journal of Membrane Science* **2005**, 262, (1-2), 49-59.
 38. Bahrmann, H.; Haubs, M.; Muller, T.; Schopper, N.; Cornils, B., Quaternary ammonium salts of phosphines as ligands and their recycling by membrane techniques or phase separation. Part I: monophasic systems. *Journal of Organometallic Chemistry* **1997**, 545-546, 139-149.
 39. <http://www.kochmembrane.com>
 40. Luthra, S. S.; Yang, X. J.; dos Santos, L. M. F.; White, L. S.; Livingston, A. G., Homogeneous phase transfer catalyst recovery and re-use using solvent resistant membranes. *Journal of Membrane Science* **2002**, 201, (1-2), 65-75.
 41. <http://www.membrane-extraction-technology.com>
 42. <http://www.solsep.com>
 43. Geens, J.; Van der Bruggen, B.; Vandecasteele, C., Transport model for solvent permeation through nanofiltration membranes. *Separation and Purification Technology* **2006**, 48, (3), 255-263.

44. Van der Bruggen, B.; Jansen, J. C.; Figoli, A.; Geens, J.; Boussu, K.; Drioli, E., Characteristics and performance of a "universal" membrane suitable for gas separation, pervaporation, and nanofiltration applications. *The Journal of Physical Chemistry B* **2006**, 110, (28), 13799-13803.
45. <http://www.millipore.com>
46. <http://www.sterlitech.com>
47. <http://www.osmolabstore.com>
48. Eggeling, E. B.; Hovestad, N. J.; Jastrzebski, J. T. B. H.; Vogt, D.; van Koten, G., Phosphino carboxylic acid ester functionalized carbosilane dendrimers: Nanoscale ligands for the Pd-catalyzed hydrovinylation reaction in a membrane reactor. *Journal of Organic Chemistry* **2000**, 65, (26), 8857-8865.
49. Hovestad, N. J.; Eggeling, E. B.; Heidebuchel, H. J.; Jastrzebski, J. T. B. H.; Kragl, U.; Keim, W.; Vogt, D.; van Koten, G., Selective hydrovinylation of styrene in a membrane reactor: Use of carbosilane dendrimers with hemilabile P,O ligands. *Angewandte Chemie-International Edition* **1999**, 38, (11), 1655-1658.
50. Nair, D.; Scarpello, J. T.; Vankelecom, I. F. J.; Dos Santos, L. M. F.; White, L. S.; Kloetzing, R. J.; Welton, T.; Livingston, A. G., Increased catalytic productivity for nanofiltration-coupled Heck reactions using highly stable catalyst systems. *Green Chemistry* **2002**, 4, (4), 319-324.
51. Patterson, D. A.; Yen Lau, L.; Roengpithya, C.; Gibbins, E. J.; Livingston, A. G., Membrane selectivity in the organic solvent nanofiltration of trialkylamine bases. *Desalination* **2008**, 218, (1-3), 248-256.
52. Roengpithya, C.; Patterson, D. A.; Livingston, A. G.; Taylor, P. C.; Irwin, J. L.; Parrett, M. R., Towards a continuous dynamic kinetic resolution of 1-phenylethylamine using a membrane assisted, two vessel process. *Chemical Communications* **2007**, (33), 3462-3463.
53. Peeva, L. G.; Gibbins, E.; Luthra, S. S.; White, L. S.; Stateva, R. P.; Livingston, A. G., Effect of concentration polarisation and osmotic pressure on flux in organic solvent nanofiltration. *Journal of Membrane Science* **2004**, 236, (1-2), 121-136.
54. <http://www.grace.com>
55. Jana, R.; Tunge, J. A., A homogeneous, recyclable rhodium(I) catalyst for the hydroarylation of Michael acceptors. *Organic Letters* **2009**, 11, (4), 971-974.
56. Nölte, J., *ICP emission spectrometry: a practical guide*. Wiley-VCH: Weinheim [Germany], **2003**; p xiv, 267 p.
57. <http://www.jobinyvon.com>
58. White, L. S.; Nitsch, A. R., Solvent recovery from lube oil filtrates with a polyimide membrane. *Journal of Membrane Science* **2000**, 179, (1-2), 267-274.

Chapter 5. Continuous Homogeneous Hydroformylation of 1-Octene in a Stirred Reactor Equipped with *in situ* Membrane Filtration

This chapter deals with continuous membrane filtration coupled with hydroformylation reaction at elevated temperature and pressure to determine whether steady operation characterized by constant flux, stable substrate conversion and selectivity can be demonstrated for extended periods. The soluble polymer ligands that displayed the best retention properties during the batch and continuous filtration runs described in the previous chapter were employed in the investigations under the conditions of hydroformylation.

The experimental setup is identical to the unit described in Chapter 4, except that syngas, instead of nitrogen, is used as the pressurizing gas. Section 5.1 discusses the concept of hydroformylation in CXL media combined with membrane filtration for catalyst recycle and reuse. Section 5.2 reviews the literature on continuous membrane filtration for homogeneous organometallic catalyst recovery, as well as the important findings in the membrane performance and catalyst deactivation. Section 5.3 briefly describes chemicals, experimental apparatus and procedure for continuous and air-free operation. Section 5.4 discusses the results obtained from continuous homogeneous filtration in a stirred reactor equipped with a membrane filter at the bottom through which the reaction mixture flows out while the catalyst complex is substantially retained in the reactor vessel. Section 5.5 summarizes the conclusions.

5.1 Introduction and Background

Membrane technology offers the possibility of continuously separating catalysts from the product in a nondestructive way and re-feeding the catalyst into the process. The aim of a continuous process in a membrane reactor is to decouple the residence times of the catalyst and reactants in order to achieve high total turnover numbers (TTONs) for the catalyst.¹ The objective of this chapter is to demonstrate catalyst performance and membrane performance in a continuously operated MET membrane reactor (Figure 5.1). There are many potential advantages of continuous filtration, such as high throughput and better control and optimization of reaction conditions to optimize conversion and selectivity. Steady continuous operation also permits a simpler measurement of reaction rates at uniform concentrations and temperatures. From such data, reliable rate expressions can be obtained.

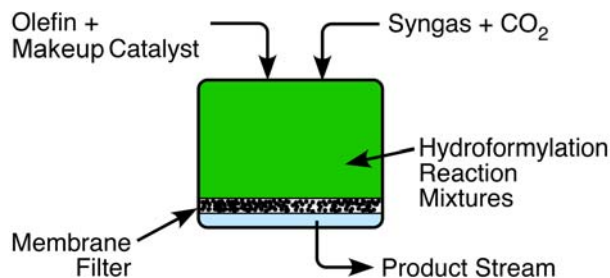


Figure 5.1 Schematic representation of a nano/ultra-filtration membrane unit

5.2 Literature Review

There are a number of publications on continuous filtration either with or without reaction. Kragl and Dreisbach² demonstrated enantioselective addition of diethyl zinc to benzaldehyde in a continuous, stirred, dead-end, polyamide

ultrafiltration membrane reactor for up to 150 hours, using different residence times and starting material ratios. More than 99.8% of the soluble and highly recyclable polymer support, a chiral ligand, was retained providing stable conversion for up to a week. The enantiomeric excess values attained in the continuous reactor were similar to those obtained in a batch reactor operated with similar feed concentrations and temperature. While the substrate conversion increased from 7 to 30% with increasing reactor residence time, the enantiomeric excess was uninfluenced by conversion in the 7-30% range. In contrast, the enantiomeric excess varied continuously with conversion in a batch reactor.

An identical experimental setup was used by Giffels *et al.*³ to conduct the enantioselective reduction of several ketones in a continuous mode, employing two types of polymer enlarged oxazaborolidines, with the operating time ranges from 25 - 65 hours. The continuous experiments exhibited higher enantioselectivities than batch experiments, by continuous removal of the product whose accumulation inhibits the uncatalyzed reduction step that yields the racemate. The catalyst showed a slight deactivation under reaction conditions, and this subsequently led to an observable decrease of conversion as well as enantiomeric excess (ee) for tetralone during a 17 hour run. The total turnover number (TTON, defined as the amount of product produced per amount of the oxazaborolidines) was enhanced up to a value of 560 during the 17 hr continuous operation. For acetophenone as substrate, this TTON value would be equivalent to an initial catalyst concentration of only 0.18 mol% in a batch experiment of similar duration and product yield. Additionally, the chiral

alcohols were obtained in good to excellent ee (up to 99% for tetralone) and space-time yield (STY up to 1.4 kg per liter reactor volume per day for acetophenone). The extent of catalyst retention was not quantified.

With the same polystyrene-bound oxazaborolidine catalyst system, Rissom *et al.*⁴ demonstrated the asymmetric reduction of acetophenone in THF medium and compared the performance with an alcohol dehydrogenase-catalyzed reaction in water medium. Both systems were run in a continuous membrane reactor for a number of residence times. The chemocatalytic reaction has a 16 fold greater space-time yield than the maximum value attained in the enzymatic reaction. This is attributed to the lower solubility of the substrate and product in water compared to THF. In contrast, the catalyst half-life time was shorter (1.2 days) for the polystyrene-bound oxazaborolidine catalyst system compared to that for the enzymatic system (31.1 days), which led to a TTON of 560 vs. 2.4×10^8 respectively. For the chemocatalytic system, the ee (90-94%) decreased with time due to catalyst deactivation and favored byproducts, while the enzymatic reaction showed almost complete stereoselectivity, giving an ee of > 99% throughout the reaction time. The quantitative measurement of the extent of catalyst retention was not mentioned in this work.

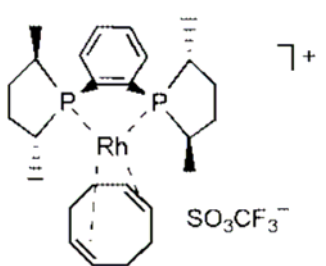


Figure 5.2 Rh-EtDUPHOS (MW=723 Da)

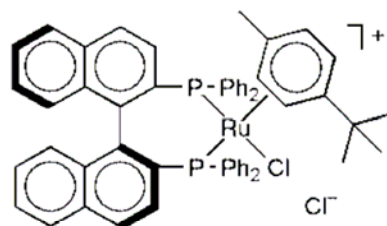


Figure 5.3 Ru-BINAP (MW=929 Da)

De Smet *et al.*⁵ studied the continuous enantioselective hydrogenation of dimethylitaconate (DMI) with Ru–BINAP and of methyl 2-acetamidoacrylate (MAA) with Rh–EtDUPHOS. The ligand structures and molecular weights are given in Figures 5.2 and 5.3. The continuous reactions were performed in a stirred 100 mL autoclave containing an MPF-60 membrane at the bottom. The hydrogenation of DMI showed a constant enantiomeric excess with time. The very small decrease in conversion after several hours was observed and the retention of Ru–BINAP is ~ 98%. Nevertheless, after ten residence times (over 40 hours), an enantiomeric excess of 93% equaling the value reached in batch-wise reference reaction under homogeneous conditions was observed. For the hydrogenation of MAA with Rh–EtDUPHOS, the approximately 97% retention of the complex and a slow deactivation of the catalyst, possibly due to oxidation of the phosphine ligand, were both implicated for the more significant decrease in enantiomeric excess and conversion in the long term. The TTON values for the hydrogenation with Ru–BINAP and Rh–EtDUPHOS were 1950 and 930 during 40 and 22 hr continuous runs, respectively.

Goetheer *et al.*⁶ presented the hydrogenation of 1-butene using a fluororous derivative of Wilkinson's catalyst $[\text{RhCl}\{\text{P}-(\text{C}_6\text{H}_4\text{-}i{p}\text{-SiMe}_2\text{CH}_2\text{CH}_2\text{C}_8\text{F}_{17})_3\}_3]$ in supercritical carbon dioxide with *in situ* catalyst separation. Continuous separation of the homogeneous catalyst from the products and continuous production of *n*-butane was achieved at a temperature of 353 K and a pressure of 20 MPa in an inorganic microporous membrane reactor. Following each of three consecutive runs, the catalyst was precipitated by depressurization (which also stops the reaction) and then

dissolved again for reuse by adding high-density carbon dioxide. At the end of the third run, the conversion (or TOF) dropped from 40% down to about 33% with a TOF of $3 \times 10^3 \text{ h}^{-1}$ (corresponding to a turnover number of 1.2×10^5 in 32 h), about 60% lower than the corresponding value from a batch experiment (TOF = $9.4 \times 10^3 \text{ h}^{-1}$). UV-Vis spectroscopy and ICP-AAS analyses confirmed near-complete (> 99.9%) retention of the catalyst and possibly the free ligand. The decrease in conversion was therefore attributed to deactivation of the catalyst by oxidation, caused by possible traces of oxygen present in the carbon dioxide or the feed.

Brinkmann *et al.*⁷ first successfully demonstrated homogeneous transition metal catalyst retention with dendritic ligands in a continuous membrane reactor. Two diaminopropyl-type dendrimers were tested, for the synthesis of N-[3-phenyl-2-propenyl]-morpholin through allylic substitution. Better retention results were obtained using a catalyst based on the higher molecular weight ligand.

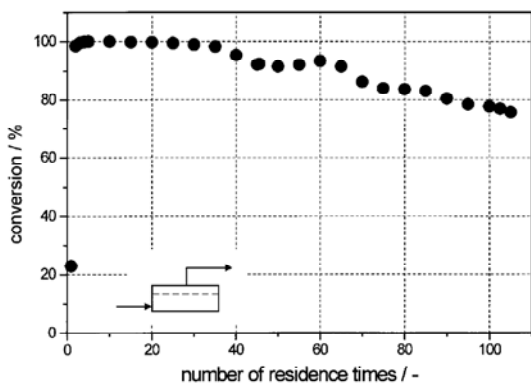


Figure 5.4 Allylic substitution in a continuous membrane reactor with the catalyst based on dendritic ligand

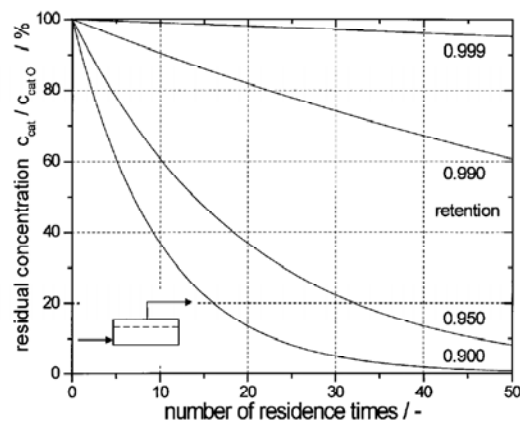


Figure 5.5 Residual concentration as function of the number of residence times

From a typical run shown in Figure 5.4, the substrate conversion gradually decreased to 80% beginning with complete conversion due to a leaching of palladium (0.07 to 0.14% per residence time). The retention rates of the palladium phosphine complexes tethered to the dendrimer backbone were greater than 99.9% resulting in a six-fold increase of the total turnover number for the Pd catalyst compared to optimized conditions in a batch reaction with the nonbound ligand. The influence of the Pd retention fraction on the catalyst leaching is shown in Figure 5.5 for a continuous reactor. As expected, the catalyst leaching increases with less retention/pass and for this system, the catalyst is washed out in 50 residence times. This Pd leaching and the formation of inactive palladium species were assumed to be responsible for a loss of the palladium bound in the catalytically active complex.

De Groot *et al.* reported continuous processes in a membrane reactor using novel phosphine functionalized carbosilane dendrimers-based palladium complexes in the allylic alkylation^{8,9} and allylic amination with piperidine as the nucleophile⁹. Urea adamantyl functionalized poly(propylene imine) dendrimer-based Pd complexes were also tested in the allylic amination of crotyl acetate.¹⁰ The observed decrease in catalyst activity was attributed to the decomposition of the palladium complex rather than to the loss of the dendrimeric catalyst.

Oosterom¹¹ *et al.* studied the hydrogenation of dimethyl itaconate in a continuous membrane reactor using the rhodium complexes of the dppf-based core-functionalized dendrimeric diphosphine ligand. They compared the performance of the rhodium complex of dendrimer (Figure 5.6) with that of dppf (1,1-

bis(diphenylphosphino)ferrocene) under identical conditions (5 bars of hydrogen and 40 °C, Koch/SeIRO MPF-60 NF membrane with molecular weight cut-off 400 Da). Figure 5.7 shows the temporal conversion of dimethyl itaconate using dppf (a) and dendrimeric ligand (b). The lower maximum using dppf was attributed to the lower rate of hydrogenation and leaching of active complex during the first 10 residence times.

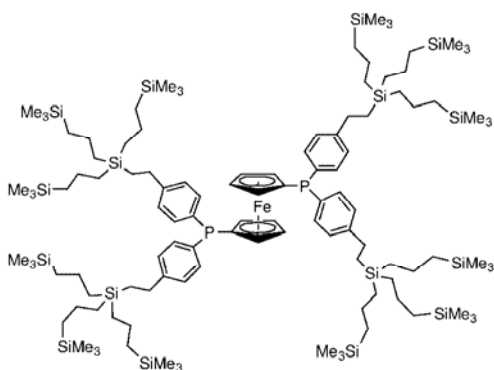


Figure 5.6 dppf-based dendrimer

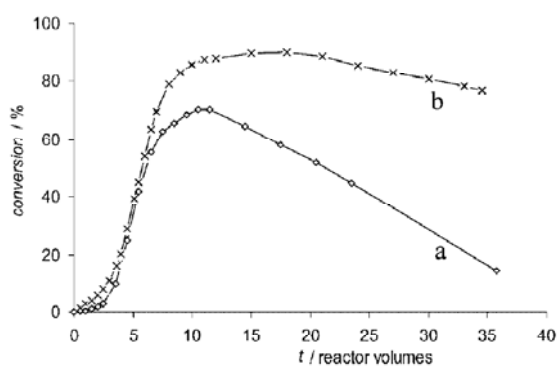


Figure 5.7 Continuous hydrogenation using dppf (a) and dendrimeric ligand (b)

The retention for the large-sized dendrimeric catalyst (99.8%) under continuous operation was fairly stable under the conditions applied, and is much higher than that for dppf-rhodium complex (97%). The small decrease in conversion found using the dendrimer catalyst was a result of dendrimer leaching.

In summary, quite a few studies have been reported on the homogeneous transition metal complex retention by membrane filtration. The method of ligand enlargement is widely applied to improve catalyst complex retention and the size of the enlarged ligand has to be controlled to ensure the complex soluble. In most cases, the continuous runs were operated in laboratory-scale reactors for hours to days and

the common observation was that conversion decreased. Both catalyst deactivation and the leaching of metal remain as major problems. Overall, membrane filtration is a promising approach for substantial retention of homogeneous catalyst complexes in reactors, thereby facilitating continuous reactor operation while obviating the need for post-reactor catalyst separation and recycle. In this chapter, such a technique will be tested for the continuous retention and use of rhodium catalyst complex modified by polystyrene-based bidentate phosphite for 1-octene hydroformylation.

5.3 Experimental Procedure

5.3.1 Materials

The chemicals, including organic liquids, catalysts, ligands and gases, as well as the pretreatment and storage methods are identical to those mentioned in Section 3.3.2 and Section 4.4.1.

5.3.2 Filtration apparatus

Based on the degree of integration between reaction and filtration, there are two combinations of reactor and membrane filter that will achieve catalyst separation after reaction completion: reactor-and-filter-in-one (called membrane reactor) and reactor-then-filter-in-series.

In the case of hydroformylation catalysis, the system has to be kept under strictly airtight conditions due to the propensity for catalyst deactivation in the presence of moisture and oxygen. The combination used for continuous filtration coupled with reaction in this work is the first type, the same as the one described in

Section 4.3.3. In the reported set-up, the syngas pressure needed for the hydroformylation of the substrate provides the driving force for the membrane permeation.

5.3.3 Continuous experiment procedure without reaction

For the continuous filtration without reaction, all the membrane and sample preparation procedures are the same as the batch runs described above. The main difference is that pure toluene is pumped continuously into the cell by means of an HPLC pump at a predetermined flow rate such that the liquid volume in the cell is maintained constant during filtration. A metering valve in the effluent stream is used to ensure that the feed and permeate flow rates are maintained constant. Permeate samples are withdrawn periodically for analysis. When running at elevated temperatures, the cell is preheated and the temperature of the cell contents is stabilized before filtration is commenced.

5.3.4 Continuous experimental procedure with reaction

A substrate solution of toluene and 1-octene ($v/v = 70:30$) was prepared. After installing the membrane in the reactor, it was conditioned and equilibrated with anhydrous toluene under a nitrogen pressure of 3.0 MPa, as explained in Section 4.5.1.

A 60 mL solution of $\text{Rh}(\text{acac})(\text{CO})_2$ and polymer bound ligand in toluene was injected *via* syringe into the MET cell under a nitrogen atmosphere. The mixture was stirred while repressurizing the system with syngas and raising the temperature to 60 °C. The feedstock pump was started at a flowrate of 0.1-0.5 mL/min, while

simultaneously opening the permeate valve slowly and adjusting the permeate flow rate to the same value as that of the feed. The flowrate in this range ensures that the substrate has adequate residence time (at least 120 minutes) in the catalytic reactor. Every hour, a sample was taken from the permeate stream. One small portion of this sample was diluted with dichloromethane, and analyzed by gas chromatography Varian GC 5800 (CP-Si15CB Chromapack[®] capillary column). The other portion of this sample was analyzed by ICP JY 2000 2 for Rh and P analyses.

Each run was terminated by shutting down the syngas supply and closing the feed and permeate valves. However, reaction would still continue inside the membrane reactor until it reached equilibrium. This is signified by a drop in syngas pressure, sometimes down to zero when the substrate 1-octene was in excess. Continuous operation is resumed by re-establishing syngas and feedstock flows, and by opening the permeate valve. The conversion *versus* time profile exhibited a rising profile during the start-up stage and then reached a steady state.

5.4 Results and Discussion

5.4.1 Continuous filtration runs without reaction

5.4.1.1 Polymer bound ligand (PBB10)

Two repeated filtration runs were performed using toluene-based solutions containing dissolved polymer bound ligand (PBB10c) with two fresh membranes (MWCO of 200 Daltons). The catalyst solutions contain Rh and P at concentrations ranging from 100-150 ppm with a molar P/Rh ratio of 4.

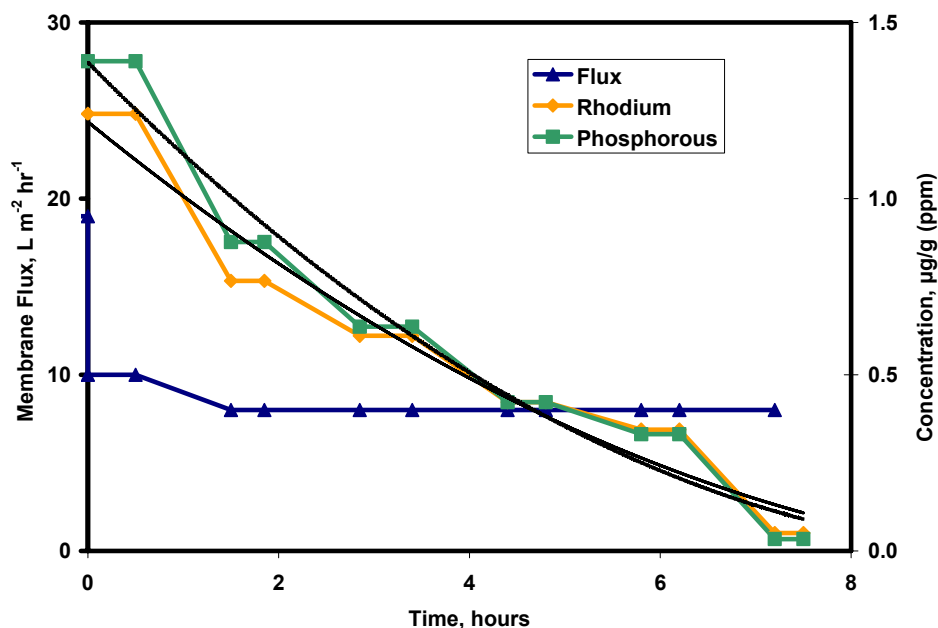


Figure 5.8 Membrane flux, rhodium and phosphorous concentrations in permeate for the first continuous filtration run
 Filtration conditions: T = 21 °C, under nitrogen pressure of 1.0 MPa. Initial catalyst solution: [Rh] = 121 ppm, [P] = 144 ppm, molar P/Rh ratio = 4

The first continuous filtration run shown in Figure 5.8 lasted for 7.5 hours. The permeate flux during the entire run remained constant at 8 L m⁻² hr⁻¹, which is approximately 40% of the flux attained with pure toluene at identical cell pressures. The Rh and P concentrations in the effluent were high initially and decreased with time, suggesting the removal of perhaps unbound Rh and P from the initial mixture and also from the fraction of the polymers that are lighter than or close to the MWCO of the membrane. The Rh and P concentrations lined out at ppb levels (~ 50 ppb) after several hours. Total losses of Rh and P during the line-out duration are 2.1% and 1.9%, respectively, obtained by integrating the area under the empirically fitted concentration vs. time curves. This means that about 98% of the Rh and P was

retained in the cell. Assuming that the Rh and P leaching is substantially complete during the line-out period and remained at these values (~ 50 ppb), the resulting rhodium retention would easily meet the economic viability criterion at a aldehyde production rate of 19,900 kg aldehyde/(kg Rh · h).

Figure 5.9 shows the permeate flux along with the Rh and P concentrations in the permeate *versus* time for the second continuous filtration run. This filtration run lasted for 17 hours in total, and was performed in three stages as follows. The first stage (the first 8 hours) represents a repeat of the first continuous run. After two weeks, during which the cell contents were maintained in nitrogen atmosphere at a constant pressure, the filtration was resumed and continued for another 6 hours. Similar to the first run, the permeate flux remains constant. The rhodium and phosphorous concentrations in permeate decreased down to 20 ppb and 90 ppb, respectively, after 14 hours of filtration. Total losses of Rh and P during the line-out period are 1.9% and 2.6%, respectively, obtained by integrating the area under the empirically fitted concentration versus time curves. The Rh and P losses are similar to those obtained during the line out phase of the first run.

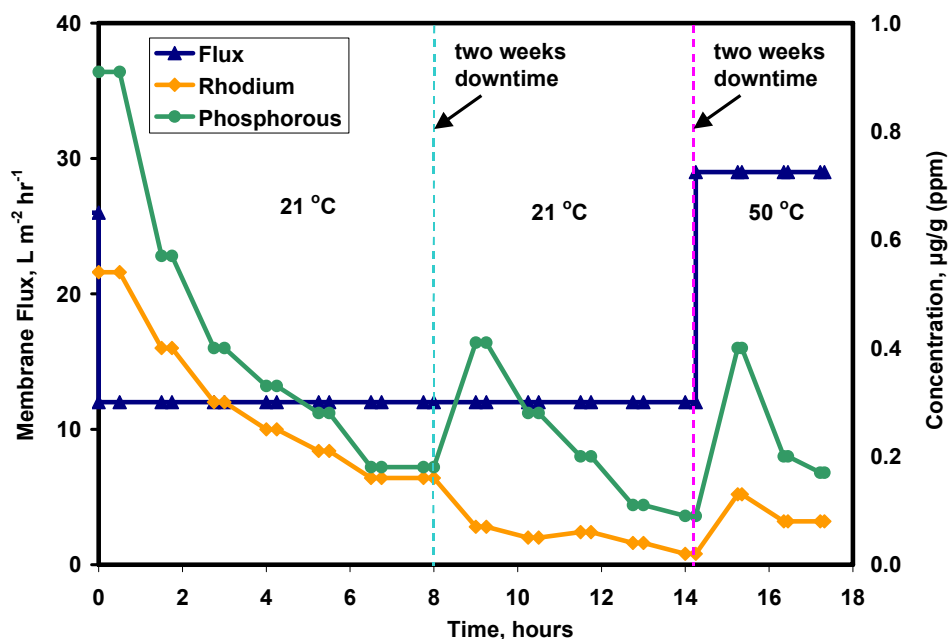


Figure 5.9 Membrane flux, rhodium and phosphorous concentrations in permeate for the second continuous filtration run
 Filtration conditions: $T = 21\text{ }^{\circ}\text{C}$, under nitrogen pressure of 1.0 MPa. Initial catalyst solution: $[\text{Rh}] = 117\text{ ppm}$, $[\text{P}] = 142\text{ ppm}$, molar P/Rh ratio of 4. During the downtimes, the catalyst solution was sealed in the MET cell under nitrogen pressure of 1.0 MPa.

In order to test the temperature effects, the filtration of the previous cell mixture (filtered for 14 hours at room temperature) was continued after two weeks, heating the cell to $50\text{ }^{\circ}\text{C}$. The membrane flux was approximately 2.5 times greater than that at $21\text{ }^{\circ}\text{C}$, due partly to the lower mixture viscosity at higher temperature. However, the Rh concentration is still at tens of ppb levels.

The P concentration curve exhibits a spike at the beginning of each continued run. This is attributed to the flushing of the Rh and P that may have accumulated in the hold-up volume (under the membrane assembly) by slow diffusion across the

membrane during the two weeks. When the filtration resumes, the accumulated Rh and P are first washed out before the profiles line out again at previously attained values (tens of ppb levels), as shown in Figure 5.9.

5.4.2 Continuous filtration runs with reaction

5.4.2.1 Run with PBB10d under 0.6 MPa syngas

The continuous experiment for 1-octene hydroformylation catalyzed by PBB10d modified rhodium complex was carried out at temperature of 60 °C and under syngas pressure of 0.6 MPa. The solution was kept stirred at a setting that is equivalent to 1000 rpm. The Rh and P concentrations in the initial solution are 139 ppm and 184 ppm, respectively. The molar P/Rh ratio is 4.4.

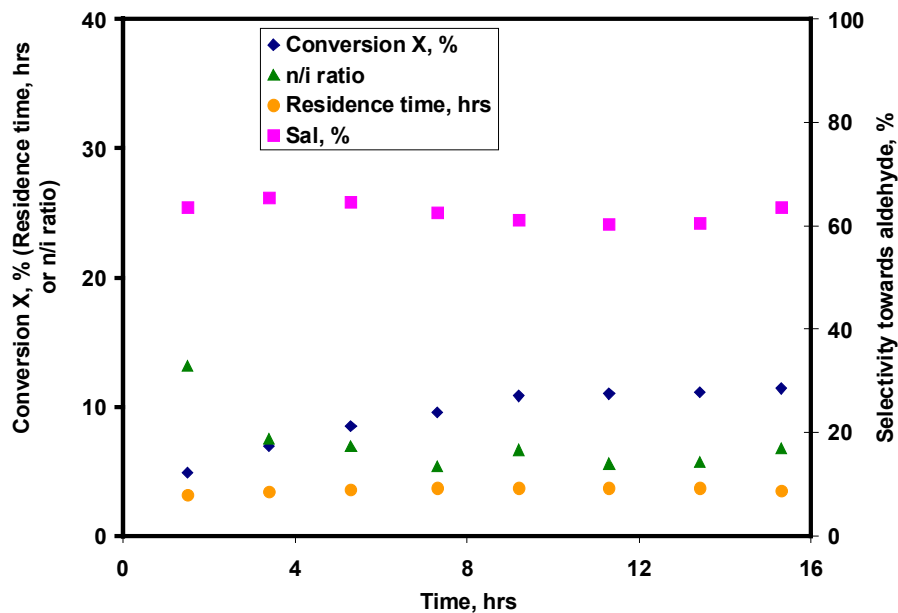


Figure 5.10 Experimental results for continuous 1-octene hydroformylation with *in situ* membrane

Experimental conditions: T = 60 °C, constant syngas pressure P = 0.6 MPa, ligand: PBB10d; Initial catalyst solution: [Rh] = 139 ppm, [P] = 184 ppm, molar P/Rh ratio = 4.4.

As shown in Figure 5.10, the conversion slowly increases during the first 8 hours of the initial run and then remains at 11% for the following 8 hours while the residence time is kept constant at 3.5 hours. The regioselectivity *n/i* ratio decreases from 13 for the first sample down to 6 at the end of the 15-hour run. The selectivity towards aldehyde product reaches a steady value in the range of 60-65 %, with relatively less variation.

After sealing the reaction mixture for 8 days in the reactor at the same stirrer speed as the previous reaction, the continuous run was resumed at a higher syngas pressure (2.0 MPa) for another 15 hours, with an average residence time of approximately 3 hours. The purpose of this run was to investigate the effect of syngas partial pressure on conversion and selectivity.

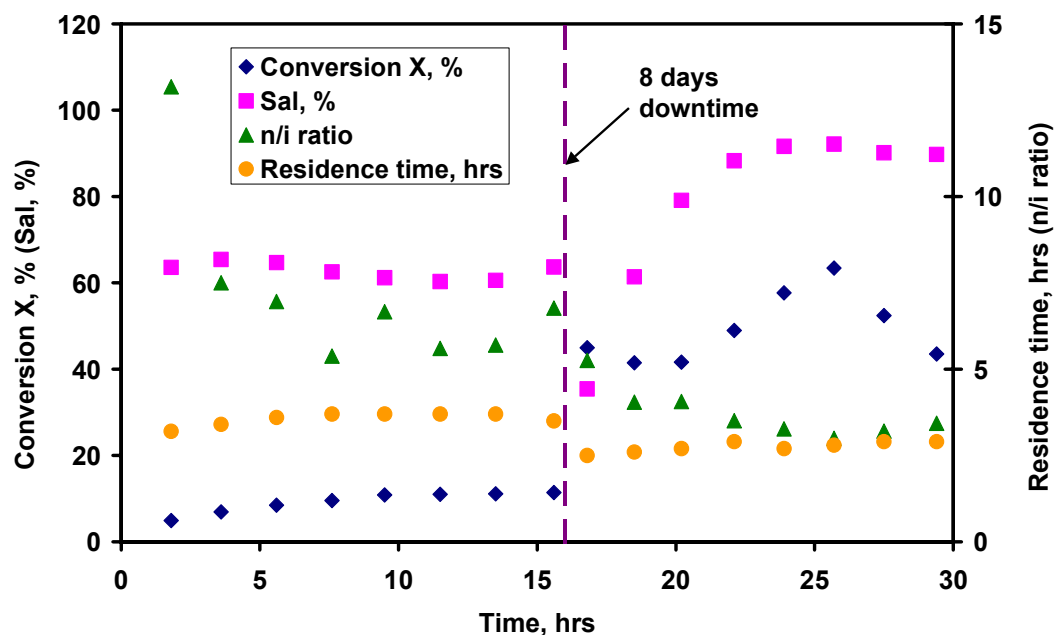


Figure 5.11 Experimental results for continuous 1-octene hydroformylation with *in situ* membrane at different syngas pressures

Experimental conditions: $T = 60\text{ }^{\circ}\text{C}$, constant syngas pressures, $P = 0.6\text{ MPa}$ for the first 15 hours and $P = 2.0\text{ MPa}$ for the second 15 hours, ligand: PBB10d; Initial catalyst solution: $[\text{Rh}] = 139\text{ ppm}$, $[\text{P}] = 184\text{ ppm}$, molar P/Rh ratio = 4.4.

At the end of the first 15-hour run, the catalyst solution was sealed in the MET cell. The reaction continued and the catalyst solution containing excess 1-octene would eventually be in a syngas starved environment.

As inferred from Figure 5.11, the reaction under 2.0 Mpa syngas gives higher conversion ($> 40\%$) and higher selectivity to aldehydes ($> 90\%$), compared to the run under 0.6 MPa syngas. In contrast, the *n/i* ratio gradually decreases from 6 down to 3.5.

5.4.2.2 Batch runs in ReactIR

The conversion and selectivity results from the first continuous runs (Row#2, Table 5.1) including are not consistent with those obtained from the batch data

(Row#1, Table 5.1). To better understand this discrepancy, an 11-hour batch reaction (Row#3, Table 5.1) was performed in a ReactIR using 25 mL of a feed mixture identical to that used in the first continuous run. The results are shown in Table 5.1.

Table 5.1 Batch and continuous data comparisons

Run	Polymer**	Stirrer rpm	Time hrs	Vol mL	P/Rh -	Oct/Rh -	Conv. X %	TOF hr ⁻¹	Sal %	Soctane %	n/l
Batch #1*	PBB10b	1000	2	4	3.0	1000	93.4	467	85.7	1.1	2.1
Cont #11	PBB10d	1000**	2	60	4.4	2203	~ 11.0	-	60.4	18.6	~ 6.0
Batch #11	PBB10d	1000	11.5	20	4.4	2203	90.5	-	93.7	2.8	4.8

* Dr. Ranjan Jana's data in a 10 mL autoclave reactor with magnetic stirrer

** Magnetic stirrer was set at 10 out of 1-12 settings (60-1200 rpm)

All reactions were run at 60 °C and 0.6 MPa syngas

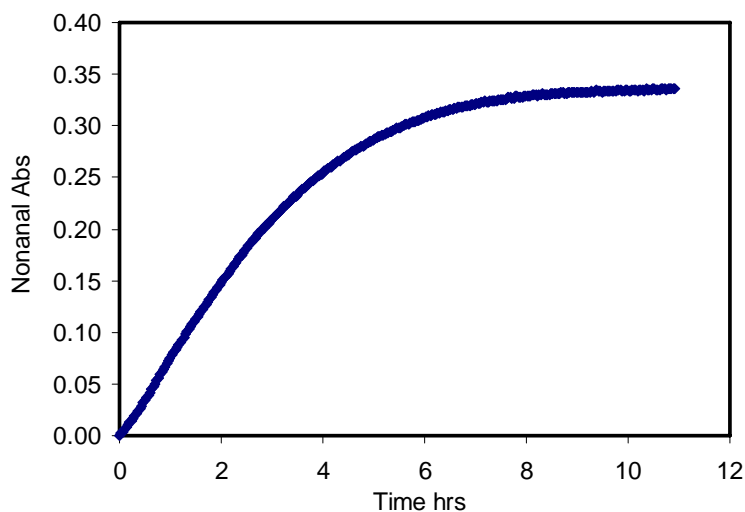


Figure 5.12 The nonanal absorbance *vs* time profile for batch reaction #11 in Table 5.1

Experimental conditions: T = 60 °C, constant syngas pressure P = 0.6 MPa, ligand: PBB10d, [Rh] = 139 ppm, [P] = 184 ppm, Octene/Rh = 2203, molar P/Rh ratio = 4.4.

The final 1-octene conversion is 90% with 93.7% selectivity to aldehydes. From the nonanal absorbance *versus* time profile obtained from ReactIR in Figure 5.12, it takes approximately 35 minutes to achieve 11% conversion and 3.5 hours to

achieve 63% conversion. Both conversion and selectivity (63% and 93.7%) of this batch run are higher than those of the continuous run (11% and 60-65%), while the n/i ratio (4.8) is lower than that of the continuous run (6 at stable state). It is speculated that syngas starvation is the reason for the lower conversion and aldehydes selectivity but higher n/i ratio in the continuous run. The syngas starvation might be caused by inadequate mixing provided by the magnetic stirrer bar in the membrane reactor.

It should be noted that there is a discrepancy in the results between batch #1 and batch #11. This may be explained by the difference between these two cases: 1) different batches of polymers used (PBB10d for batch #11, PBB10b for batch #1); 2) different Rh and ligand loadings (amount used in batch#1 are approximately half of those used in batch #11); 3) scale of the reactor (Batch #1 was run in a 10 mL autoclave reactor with 5 mL reaction solution and batch #11 in 50 mL ReactIR with 20 mL reaction solution).

The discrepancy between the Batch #11 and Cont #11 runs indicates that the MET cell has to be modified in order to improve gas-liquid mixing so that the continuous reaction data can match with the batch reaction data.

5.4.2.3 Rh and P concentrations in the permeate

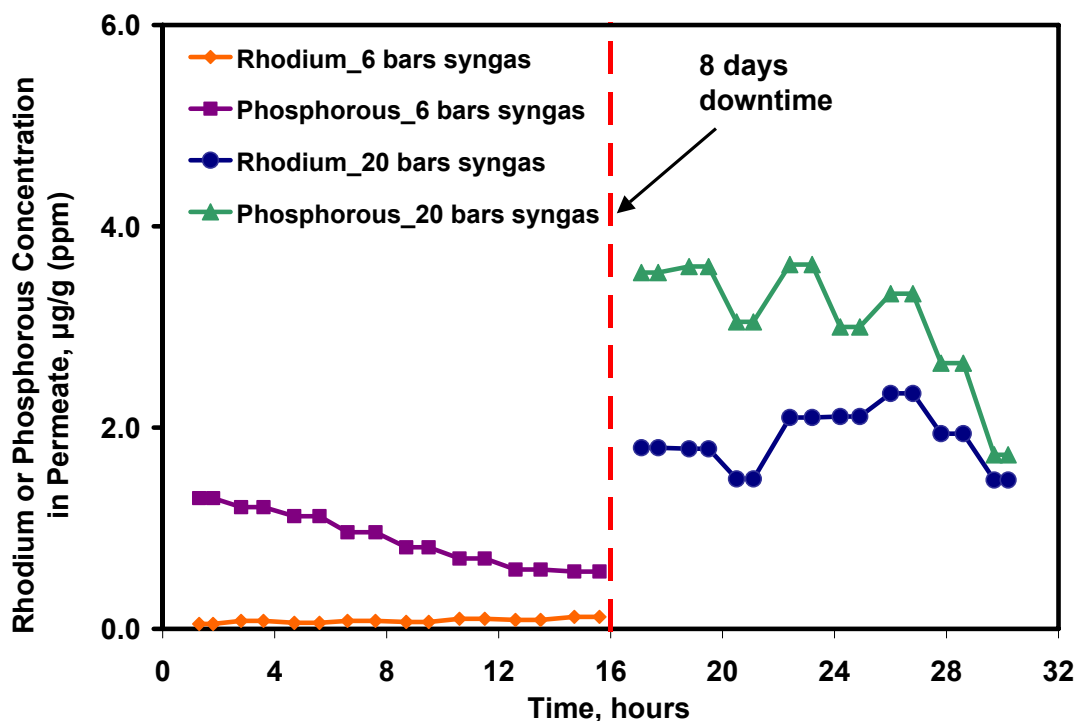


Figure 5.13 Rh and P concentrations in permeate for the two consecutive continuous 1-octene hydroformylation runs at different syngas pressures
Experimental conditions: $T = 60\text{ }^{\circ}\text{C}$, constant syngas pressures, $P = 0.6\text{ MPa}$ for the first 15 hours and $P = 2.0\text{ MPa}$ for the second 15 hours, ligand: PBB10d; Initial catalyst solution: $[\text{Rh}] = 139\text{ ppm}$, $[\text{P}] = 184\text{ ppm}$, molar P/Rh ratio = 4.4.
At the end of the first 15-hour run, the catalyst solution was sealed in the MET cell. The reaction continued and the catalyst solution containing excess 1-octene would eventually be in a syngas starved environment.

The ICP analysis for the Rh and P concentrations in the permeate in the two consecutive continuous runs at different operating conditions is shown in Figure 5.13. The first continuous run at 0.6 MPa syngas gives Rh contents in permeate lower than 120 ppb during the 15-hour run and P contents decreasing from 1.3 ppm to 570 ppb due to the pass-through of smaller size of polymer bound ligand. The molecular weight distribution of the polymer bound ligand was determined by gel permeation

chromatography (GPC) analysis and a lower molecular weight fraction was found to be present, as shown in Figure 5.14.

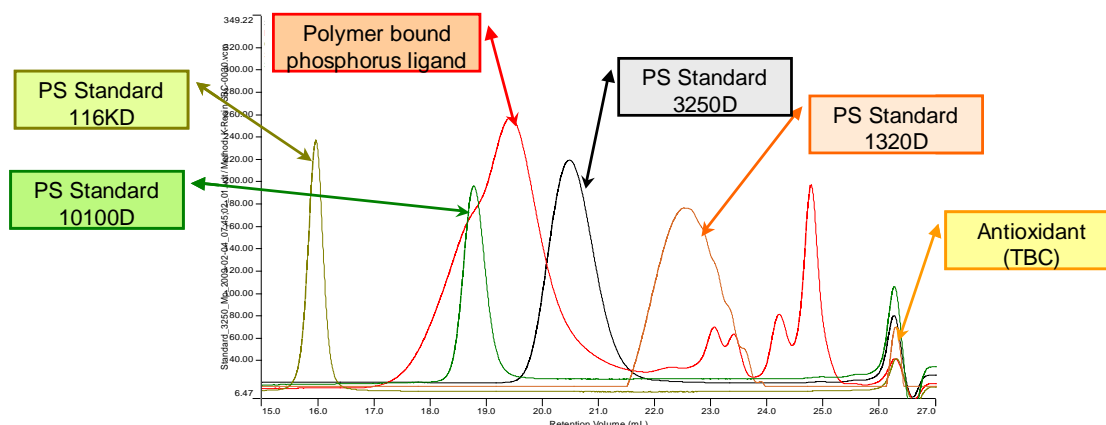
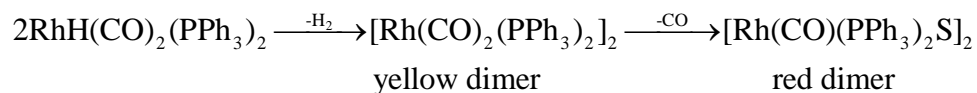


Figure 5.14 GPC analysis of polymer bound phosphorous ligand (red line)¹²

The Rh and P levels from the second continuous run at 2.0 MPa syngas pressure are at low ppm levels. The reason for the increased pass-through is not clear at this time but it was observed that following the second continuous run, the retentate color (dark red) was completely different from that of the retentate for the batch runs (yellow). It is speculated that rhodium dimer was formed during the idle time between the two consecutive runs in the syngas starved environment and at the elevated temperature 60 °C. The rhodium dimer formation reported in the literature¹³⁻¹⁷ often occurs at low pressures of hydrogen and high rhodium concentrations. The color changes can be associated with the reactions as follows where the ligand is triphenylphosphine (PPh₃):



The same type of reactions might also occur when polymer bound ligand is used. The binding between the resulting rhodium dimer and the polymer bound ligand PBB10 might be weak, thus causing high Rh leaching through the membrane due to the smaller size of the dimer than the PBB10 rhodium complex.

5.5 Summary

To sum up, in the continuous filtration with polymer bound phosphite ligand PBB10 without reaction, a decreasing trend was observed for Rh and P concentrations in the permeate after several hours, suggesting the removal of perhaps unbound Rh and P from the initial mixture and also from the fraction of the polymers that are lighter than or close to the MWCO of the membrane. During those continuous filtration, the Rh leaching in permeate stabilizes at tens of ppb level (< 100 ppb) after a line-out period, suggesting that the CXL process has the potential to be economically viable if the aldehyde production rate of 15,700 kg/(kg Rh · h) is also achieved.

The results at 60 °C and under 0.6 MPa syngas show that the conversion, selectivity and *n/i* ratio stabilized after the first 8 hours, with stable and low Rh (< 120 ppb) and P (< 570 ppb) leaching. However, the steady state conversion and selectivity values were low due likely to syngas starvations caused by inadequate mixing. It is recommended that the continuous membrane reactor experiments be repeated for extended time domains (for a few days) with better mixer design in the

MET cell and with soluble polymer catalyst complexes that show less intra-batch variability in properties. Once, such conversion and selectivity data are demonstrated, experiments must be performed with CO₂-expanded reaction media to alleviate syngas starvation and also improve the membrane flux.

5.6 References

1. Felder, M.; Giffels, G.; Wandrey, C., A polymer-enlarged homogeneously soluble oxazaborolidine catalyst for the asymmetric reduction of ketones by borane. *Tetrahedron-Asymmetry* **1997**, 8, (12), 1975-1977.
2. Kragl, U.; Dreisbach, C., Continuous asymmetric synthesis in a membrane reactor. *Angewandte Chemie-International Edition in English* **1996**, 35, (6), 642-644.
3. Giffels, G.; Beliczey, J.; Felder, M.; Kragl, U., Polymer enlarged oxazaborolidines in a membrane reactor: enhancing effectivity by retention of the homogeneous catalyst. *Tetrahedron: Asymmetry* **1998**, 9, (4), 691-696.
4. Rissom, S.; Beliczey, J.; Giffels, G.; Kragl, U.; Wandrey, C., Asymmetric reduction of acetophenone in membrane reactors: comparison of oxazaborolidine and alcohol dehydrogenase catalysed processes. *Tetrahedron: Asymmetry* **1999**, 10, (5), 923-928.
5. De Smet, K.; Aerts, S.; Ceulemans, E.; Vankelecom, I. F. J.; Jacobs, P. A., Nanofiltration-coupled catalysis to combine the advantages of homogeneous and heterogeneous catalysis. *Chemical Communications* **2001**, (7), 597-598.
6. Goetheer, E. L. V.; Verkerk, A. W.; van den Broeke, L. J. P.; de Wolf, E.; Deelman, B. J.; van Koten, G.; Keurentjes, J. T. F., Membrane reactor for homogeneous catalysis in supercritical carbon dioxide. *Journal of Catalysis* **2003**, 219, (1), 126-133.
7. Brinkmann, N.; Giebel, D.; Lohmer, G.; Reetz, M. T.; Kragl, U., Allylic substitution with dendritic palladium catalysts in a continuously operating membrane reactor. *Journal of Catalysis* **1999**, 183, (2), 163-168.
8. de Groot, D.; Eggeling, E. B.; de Wilde, J. C.; Kooijman, H.; van Haaren, R. J.; van der Made, A. W.; Spek, A. L.; Vogt, D.; Reek, J. N. H.; Kamer, P. C. J.; van Leeuwen, P. W. N. M., Palladium complexes of phosphine functionalised carbosilane dendrimers as catalysts in a continuous flow membrane reactor. *Chemical Communications* **1999**, (17), 1623-1624.
9. de Groot, D.; Reek, J. N. H.; Kamer, P. C. J.; van Leeuwen, P. W. N. M., Palladium complexes of phosphane-functionalised carbosilane dendrimers as catalysts in a continuous-flow membrane reactor. *European Journal of Organic Chemistry* **2002**, (6), 1085-1095.
10. de Groot, D.; de Waal, B. F. M.; Reek, J. N. H.; Schenning, A. P. H. J.; Kramer, P. C. J.; Meijer, E. W.; van Leeuwen, P. W. N. M., Noncovalently functionalized dendrimers as recyclable catalysts. *Journal of the American Chemical Society* **2001**, 123, (35), 8453-8458.
11. Oosterom, G. E.; Steffens, S.; Reek, J. N. H.; Kamer, P. C. J.; van Leeuwen, P. W. N. M., Core-functionalized dendrimeric mono- and diphosphine rhodium complexes; application in hydroformylation and hydrogenation. *Topics in Catalysis* **2002**, 19, (1), 61-73.
12. Personal communications with Dr. Ranjan Jana at Department of Chemistry in the University of Kansas.

13. Brown, C. K.; Wilkinso. G, Homogeneous hydroformylation of alkenes with hydridocarbonyltris-(triphenylphosphine)rhodium(I) as catalyst. *Journal of the Chemical Society A -Inorganic Physical Theoretical* **1970**, (17), 2753-&.
14. Evans, D.; Yagupsky, G.; Wilkinso.G, Reaction of hydrodicarbonyltris(triphenylphosphine)rhodium with carbon monoxide and of reaction products hydridodicarbonylbis(triphenylphosphine)rhodium and dimeric species with hydrogen. *Journal of the Chemical Society A -Inorganic Physical Theoretical* **1968**, (11), 2660.
15. van Leeuwen, P. W. N. M., Decomposition pathways of homogeneous catalysts. *Applied Catalysis A-General* **2001**, 212, (1-2), 61-81.
16. Yagupsky, M.; Brown, C. K.; Yagupsky, G.; Wilkinso.G, Further studies on hydridocarbonyltris(triphenylphosphine)rhodium(I). 1. Nature of inactivation of catalytic reactions. *Journal of the Chemical Society A-Inorganic Physical Theoretical* **1970**, (6), 937.
17. Kamer, P. C. J.; Reek, J. N. H.; van Leeuwen, P. W. N. M., Rhodium phosphite catalysts. In *Rhodium catalyzed hydroformylation*, Leeuwen, P. W. N. M. v.; Claver, C., Eds. Kluwer Academic Publishers: Dordrecht [Netherlands] ; Boston, 2000; Vol. 22, p 284.

Chapter 6. Viscosity Measurements of CO₂-Expanded Hydroformylation Systems

In this chapter, we describe the experimental systems used to determine the phase equilibrium, volume expansion and viscosities of fluid mixtures containing organic solvent, carbon dioxide, polymer bound phosphorus ligands as well as catalytic hydroformylation reaction systems. Phase equilibrium and expansion were determined primarily using a high-pressure Jerguson[®] view cell. Viscosities were determined using a moving piston type viscometer. Section 6.1 introduces the objectives of this work followed by the literature review on the related area in Section 6.2. Section 6.3 presents the apparatus used in this measurement and experimental procedures for expansion studies, cloud point and viscosity measurements. Section 6.4 discusses the results and conclusions. Section 6.5 summarizes the findings and offers a few recommendations for future work.

6.1 Introduction and Background

The dissolved polymer bound phosphite ligands, used to facilitate better catalyst retention, could significantly increase the viscosities of hydroformylation reaction mixtures, especially at high concentration. When CO₂ is added into the organic solvent (toluene in this case), the organic solvent expands and the physical properties of the CO₂-expanded solvent are altered with CO₂ pressure.^{1,2}

The transport properties of the CO₂-expanded organic media (CXLs) are between those of supercritical CO₂ and neat organic solvents, as shown in Figure 6.1. Upon expansion by CO₂, the viscosity typically decreases and the diffusivity

increases. Decreased viscosity favors enhanced permeate fluxes through the membrane and therefore increase throughput through the membrane reactor.

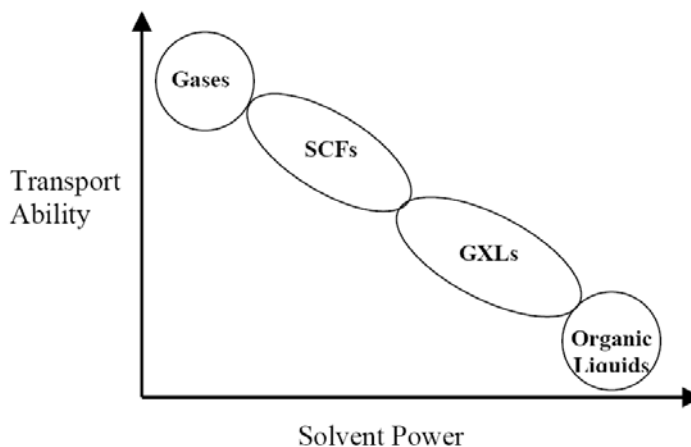


Figure 6.1 Relative solvent power and transport ability of different solvent types³

The ligands used in the membrane filtration were specially designed and synthesized by the Tunge's group. Expansion, cloud point and viscosity data are not available for these ligands. To correlate permeate flux with viscosity, it is imperative to obtain accurate viscosity measurements. Such data are also essential for developing accurate mathematical models representing membrane-based CXL reactor systems. The viscosities of the polymer bound phosphorus ligands dissolved in 1-octene + toluene and toluene solvents at various concentrations were determined experimentally. The proposed measurements are particularly crucial since CO₂ addition to the hydroformylation reaction mixture not only improves the linear aldehyde selectivity (demonstrated in previous work¹) but also decreases viscosity, thus providing an ability to tune the membrane flux.

6.2 Literature Review

6.2.1 Viscosity

6.2.1.1 *Viscosity measurement methods*

Viscosity is one of the most important physical properties of a compound or mixture, and it is an indispensable parameter in fluid transport (heat and mass transfer) engineering calculations and in process design and optimization. There are many methods used to determine the gas and liquid viscosities at high pressures. According to the different measuring principles, traditional viscometers can be categorized as follows: capillary flow viscometry,^{4, 5} oscillating body viscometry (disk, cup or sphere),⁶⁻⁹ vibrating-wire viscometry,^{10, 11} vibrating-quartz viscometry,¹² falling ball viscometry,^{13, 14} light scattering spectroscopy^{15, 16}, and other emerging techniques.

The information about the viscosity measurement methods and instruments is commonly scattered among the introduction sections of most data-intensive literature. Fortunately, a few excellent references summarized and evaluated the prevailing techniques in a systematic manner. Nieto de Castro *et al.*¹⁷ extensively discussed the best measurement methods, accuracy, reference, and traceability of the measurements to the International System of Units. Brooks *et al.*¹⁸ reviewed a number of methods used to measure the viscosity of liquid metals and model equations for viscosity estimation. Other papers by Liu *et al.*¹⁹ and Yokoyama²⁰ provided reviews on specific topics like viscosity measurement for a crystallization process and for

supercritical fluid mixtures. Other techniques were described such as inclined-tube viscometry²¹ and dual vibrating-wire techniques.²²

6.2.1.2 Toluene viscosity with or without CO₂

Toluene is a common organic solvent and its physical properties have been well studied.²³ Numerous published works report toluene viscosity at broad temperature and pressure ranges either with or without CO₂.²⁴ Toluene is also popularly proposed as a calibration solution for viscosity measurement instruments, a second choice next to water.

Assael *et al.*²⁵ proposed a correlation in terms of temperature and molar volume for the viscosity of pure liquid toluene as a reference for high-pressure viscosity measurements based on the literature data. The temperature range covered was from 213 to 373 K (-60 to 100 °C), and the pressure range from atmospheric pressure up to 250 MPa. The standard deviation of the proposed correlation was 1.36% and the error was 2.7% within a 95% confidence limit. Santos *et al.*²⁶ recommended the standard reference data of pure liquid toluene with uncertainties of 0.5% (95% confidence level) for $260\text{ K} \leq T \leq 370\text{ K}$ ($-13\text{ °C} \leq T \leq 97\text{ °C}$) and 2% for $210\text{ K} \leq T \leq 260\text{ K}$ ($-63\text{ °C} \leq T \leq -13\text{ °C}$) and $370\text{ K} \leq T \leq 400\text{ K}$ ($97\text{ °C} \leq T \leq 127\text{ °C}$). The proposed value for the viscosity of liquid toluene at 298.15 K (25 °C) and 0.1 MPa was $554.2 \pm 3.3\ \mu\text{Pa s}$. Other researchers^{22, 27-29} also reported viscosities of pure liquid toluene in a wide range of temperature and pressure.

A number of researchers put tremendous efforts in measuring the viscosities of organic solvent under CO₂ pressure. Sih *et al.* exploited the viscosities for a series of organic and carbon dioxide systems including methanol with CO₂³⁰, acetone with CO₂^{31,32} and ethanol with CO₂.³³ In all these mixtures, it was observed that viscosity reduction was a function of increasing carbon dioxide concentration in the liquid phase, liquid volume expansion, liquid density and system pressure.

6.2.1.3 Viscosities of toluene and polymer mixture with or without CO₂

Terao *et al.*³⁴ reported viscosity measurements on two series of poly(macromonomer) samples consisting only of polystyrene (PS) having different fixed side chain lengths in toluene at 15 °C. The intrinsic viscosities obtained as functions of (total) weight-average molecular weight (M_w) in the ranges of 10^3 to 10^7 were nearly constant up to a molecular weight of 6×10^4 and rose linearly with increasing M_w above 4×10^5 .

Poh and Ong³⁵ measured the viscosities of solutions of polystyrene in toluene for concentrations up to 400 kg m^{-3} at 298 K (25 °C) with polymers of molecular weights ranging from 8.7×10^3 to 2.4×10^6 . It was observed that viscosity of the polymer solutions depended on molecular weight and concentration. With increasing concentration and polymer molecular weight, the viscosities increased and the rate of increase was greater at higher values of the these two parameters.

Polystyrene/toluene was one of the binary mixtures studied by Modarress *et al.*³⁶ and its viscosities *versus* polymer concentration were measured by a Haake

viscometer at different temperatures. As expected, the viscosity decreased with increasing temperature and increased with increasing polymer concentration.

Yeo^{37, 38} measured the viscosities of toluene or toluene + carbon dioxide solutions with dissolved polystyrene (PS) in a falling cylinder-type viscometer at pressures up to 35 MPa and temperatures 320-360 K (47-87 °C). PS concentrations were up to 7 wt% with a molecular weight M_w of 50,000 and with a polydispersity $M_w/M_n < 1.06$. Here, the polydispersity is calculated as the ratio of the weight average molecular weight (M_w) to the number average molecular weight (M_n). It was found that viscosity of the polymer solutions decreased as the concentration of carbon dioxide in the mixture increased and the largest viscosity reduction was observed at the lowest temperature and at the highest concentration of polymer.

Li *et al.*³⁹ investigated the effect of dissolved CO₂ in toluene on the conformation of PS in solution and found that the viscosity of PS solution decreased faster with increasing antisolvent CO₂ pressure than that of the solvent in the absence of the polymer. This study also determined the cloud point pressure and volume expansion of the solutions at different antisolvent pressures. The cloud point pressure is the CO₂ pressure at which the dissolved solute PS is no longer completely soluble, precipitating as a second phase giving the fluid a cloudy appearance. Solutions of various concentration of PS were prepared. Upon addition of CO₂, the cloud point pressures of these solutions were found to decrease with increasing PS concentration for a given temperature, and to increase with temperature for a given initial PS concentration. The effect of PS concentration on the volume expansion was not very

remarkable because the initial PS concentrations were very low, ranging from 4.6×10^{-4} to 9.2×10^{-3} g/cm³. The authors attributed all these phenomena to the shrinking of the PS chain during the course of adding the gas antisolvent, as the interaction between the polymer and solvent becomes weaker.

In summary, the viscosity of polymer organic solvent solution is altered by the polymer concentration, polymer molecular weight and temperature. The viscosity of polymer solution can be substantially reduced by the addition of CO₂ and polymer demixing occurs when the CO₂ pressure reaches the cloud point pressure of the mixture.

6.2.2 Membrane flux and solute rejection prediction

Permeate flux is a key parameter for membrane filter throughput prediction, sizing and capital cost estimation. There are three mathematical models to describe the transport mechanisms through solvent resistant membranes, for predicting solvent flux and solute rejection.⁵⁵ The first type of model stems from irreversible thermodynamics, regarding the membrane as a black box through which the free energy is dissipated and entropy is produced. The only unknown variables for the dissipation function are the driving forces acting on the system for each species. The other two models take into account membrane properties. These are the pore-flow model and the solution-diffusion model.

The pore-flow model is applicable to filtration processes starting at the microfiltration-end of the filtration spectrum, and considers feed viscosity and membrane pore size. In the case when no significant concentration gradient is present

in the porous membrane, the Hagen-Poiseuille equation is used to correlate solvent flux and viscosity for polyimide membranes.⁵⁶

$$J = \frac{\varepsilon r_p^2}{8\eta\tau} \cdot \frac{\Delta P}{l} = \frac{\varepsilon r_p^2}{8\tau l} \cdot \frac{\Delta P}{\eta}$$

where J is volume flux for solvent [$\text{m}^3 \text{m}^{-2} \text{s}^{-1}$], ΔP is the pressure drop across the membrane [Pa], η is solution viscosity [$\text{kg} (\text{m s})^{-1}$], ε is membrane porosity, r_p is membrane pore radius [m], τ is tortuosity, and l is membrane thickness [m]. Solvent flux J increases with increasing pressure drop across the membrane and with decreasing viscosity. Obviously, viscosity is the only solution parameter that affects the solvent flux. All other parameters are related to membrane properties.

For membranes with a dense top-layer, where only the free volume elements between the polymer chains allow transport, the solution-diffusion model is generally applied to simulate the transport mechanism. In this model, unlike the pore-flow model, the free-volume elements are assumed to statistically fluctuate in about the same time scale as the permeate passing through the membrane. The polyimide membranes used in our work fall in this category.

Silva *et al.*⁵⁷ predict solvent fluxes for methanol/toluene and ethyl acetate/toluene mixtures in STARMEMTM 122 and conclude that the solution-diffusion model gives more accurate predictions than the Hagen-Poiseuille model. Considering concentration polarization and non-ideality of solution at the membrane surface, predictions by the same model using the same STARMEMTM 122 were

improved for tetraoctylammonium bromide (TOABr) separation from concentrated toluene.⁵⁸

White⁵⁹ reported the separation of mixtures of alkanes and aromatic compounds from toluene with polyimide membranes and preferential rejection was observed for aromatic solutes. Aerts *et al.*⁶⁰ show that the decreased viscosity is an important factor influencing the membrane permeability, which is linearly proportional to the reciprocal of the retentate viscosity.

6.2.3 Cloud point measurements

Cloudiness is a common phenomenon observed when excessive antisolvent carbon dioxide is added into the solution of organic solvent and polymer. Cloud point measurements for polymer-organic-CO₂ systems can be easily found in the literature, such as dichloromethane + poly(vinyl pyrrolidone) + CO₂,⁴⁰ poly(methyl methacrylate) + methyl methacrylate + CO₂ ternary system,⁴¹ poly(methyl methacrylate) + ethanol + CO₂ ternary system,⁴² poly(ethylene glycol) + ethanol + CO₂ mixture,⁴³ poly(heptadecafluorodecyl acrylate) + heptadecafluorodecyl acrylate + CO₂ system,⁴⁴ poly(L-lactic acid) + dichloromethane + CO₂,⁴⁵ poly(L-lactide) + chlorodifluoromethane + CO₂,⁴⁶ polyethylene in carbon-dioxide toluene⁴⁷ etc. The cloud points vary with solvent composition, polymer molecular weight as well as temperature. The cloud point measurements of hydroformylation reaction mixtures containing polymer ligands are clearly needed to delineate homogeneous mixture regions for the reaction studies.

6.2.4 Volume expansion measuring techniques

Several different methods were employed for the volume expansion measurements, as follows: 1) visual observation through the glass of a transparent volume-calibrated container such as a Jerguson[®] view cell, as described elsewhere;⁴⁸⁻⁵⁰ 2) acoustic technique for phase boundary detection by delay time (speed of sound) and sound amplitude (sound attenuation);⁵¹ 3) high-pressure densitometer method;⁵² 4) photofibric probe using the difference in the refractive index of liquid, gas, and optical fiber to distinguish between the vapor and the expanded liquid phase;⁵³ 5) UV-Vis spectroscopy through measuring the absorbance of the internal reference standard.⁵⁴ In this study, we use the high-pressure fixed volume view cell to conduct the volume expansion measurements.

6.3 Experimental Details

6.3.1 Chemicals

Materials used in this work included industrial grade CO₂ obtained from Airgas Inc., and anhydrous toluene of 99.8% purity and 1-octene of 98 % purity from Sigma-Aldrich Co. The phosphorus ligands including bulky bidentate and polymer bound mono- or bidentate phosphite ligands were synthesized in-house and supplied by Professor Tunge's group in the Department of Chemistry at KU.⁶¹ The materials involved in the ligand synthesis route were purchased from Sigma-Aldrich Inc. and purified by column chromatography. All of the other materials obtained were used as received without further purification.

6.3.2 Apparatus

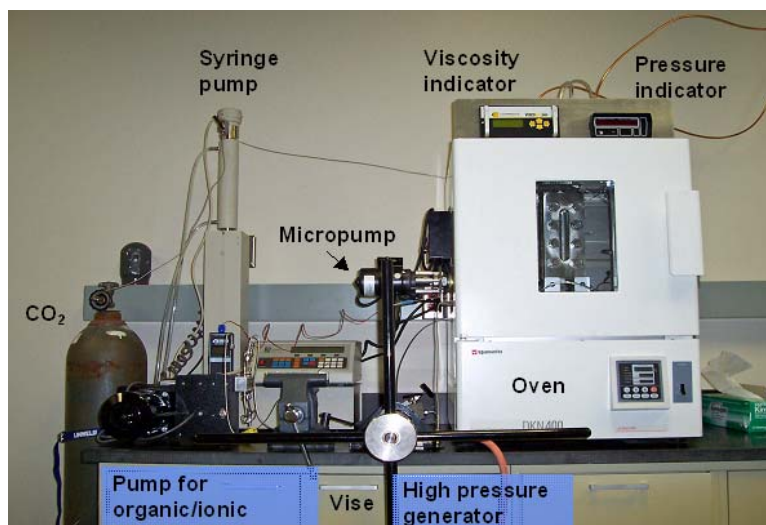


Figure 6.2 Experimental setup for volume expansion, cloud point pressure and viscosity measurements

Figure 6.2 shows the whole experimental setup used for volume expansion, cloud point pressure and viscosity measurements, consisting of an air bath oven, feed and CO₂ supply, and viscosity and pressure measurement devices. The oven and viscometer contained within the oven were originally purchased as the ViscoPro 2000 System 4 from Cambridge Viscosity. The oven was later modified to include the Jerguson[®] view cell and circulation micropump head in addition to the viscometer, shown in Figure 6.3.

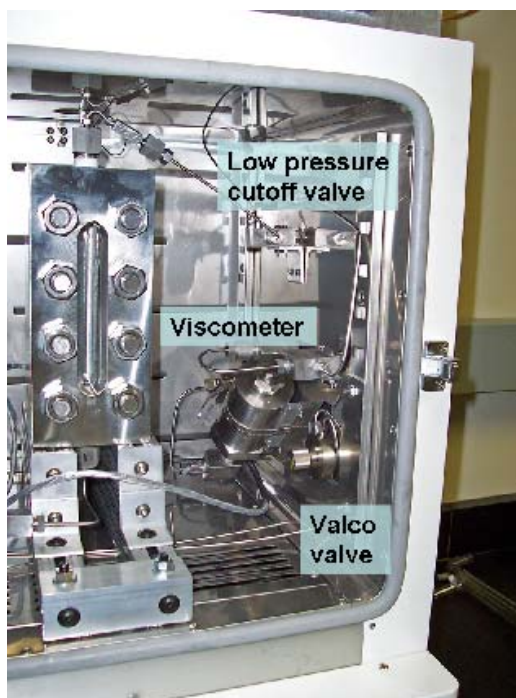


Figure 6.3 Configuration of the air bath including Jerguson viewcell, viscometer and micropump (on the left wall of the oven, not shown in the picture)

The Yamato constant temperature air bath oven (Model DKN400) provides a uniform temperature environment for the view cell, micropump head and viscometer. The temperature of the air bath is controlled by a digital controller. The Jerguson[®] view cell (Model 13-R-40) from Clark-Reliance is made of stainless steel and rated to 5000 psi (34.5 MPa). It has a total volume of about 30 mL. Cloud point and volume expansion phenomena were observed visually at the side glass of the equipped Jerguson[®] view cell, by looking through a window in the door of the oven. Volume is read from a calibrated scale located on the gage adjacent to the view glass of the gage. The circulation micropump (Micropump[®] Model 1805 °C) is rated to 340 bars

(34.0 MPa), with a maximum pressure head of 75 psi (0.52 MPa) and maximum temperature of 250 °C.

The feed pump (Eldex Laboratories Inc. Model 1020 BBB-4) outside the oven is used to pump the organic solvent into the system. CO₂ is pressurized by a syringe pump (ISCO Model 260D) and the pump cylinder has a water jacket plumbed to a circulating water bath (Isotemp 30165 Fisher Scientific) to maintain the CO₂ at the desired temperature. The system pressure is recorded by a pressure transducer with a maximum pressure limit of 30,000 psi (206.8 MPa), located in a Heise digital pressure indicator on the top of the oven.

The viscosity measurements were performed using ViscoPro 2000 System 4 with SPL-440 high-pressure viscometer and Viscolab software, supplied by Cambridge Applied Systems (currently Cambridge Viscosity). The viscometer is a cylindrical cell with a movable piston inside it. A cross-section of the SPL-440 sensor is shown in Figure 6.4.

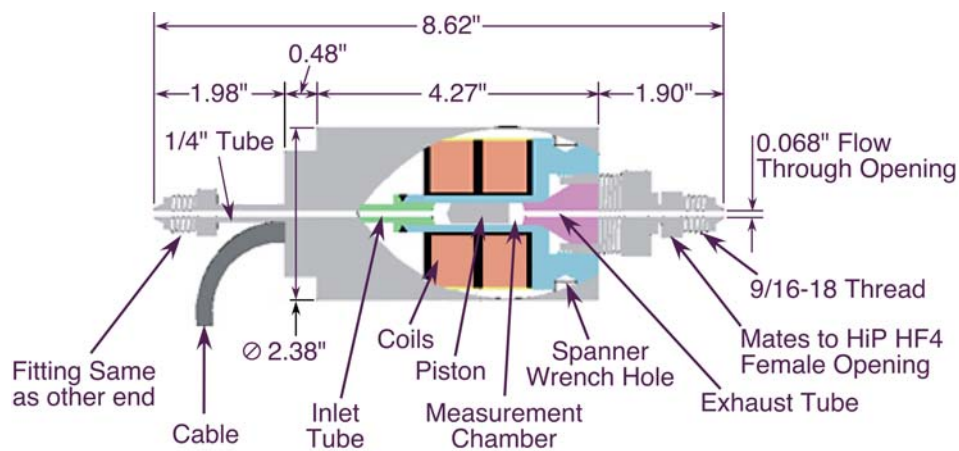


Figure 6.4 Cross section of SPL-440 viscometer sensor

Two magnetic coils inside the sensor body vibrate the piston over a fixed distance, forcing the fluid in the measurement chamber to flow through the annular space between piston and chamber. The time required for the piston to complete a two-way cycle is directly related to the viscosity of the fluid. Fluid may be measured under low flow or static conditions. The system measures viscosity, temperature and temperature compensated viscosity. The built-in temperature detector (RTD) senses the actual temperature in the sampling chamber. The viscometer sensor is capable of measuring viscosities from 0.02 to 10000 cP with maximum operating pressure of 20,000 psi (1379 bar, 137.9 MPa) and an operating temperature range of -40 to +190 °C. The viscometer has a total system volume of 5 mL and maximum particle size tolerance of 25-800 microns, depending on the range of viscosities being measured. For example, for a piston that measures 0.2-2 cP, the tolerable size range is 25-35 microns. According to Cambridge Viscosity personnel, the particle size tolerance for measuring viscosity of 10,000 cP is 800 microns. A micro-filter of 10 microns was installed on the line between the circulating pump and the viscometer. The viscometer is oriented at a 45° angle so that any gas bubble trapped inside can be purged easily. According to manufacture's specifications, the accuracy of the viscosity measurement is ± 1.0 % of the full scale and the repeatability is $\pm 0.8\%$ of reading. The viscometer temperature is measured by a temperature sensor located at the bottom of the viscometer, with an accuracy of ± 0.01 °C. The raw viscosity data from the instrument reading were adjusted by temperature and pressure with a

program provided by manufacturer. The experimental setup is similar to one used by Kho et al.⁶²

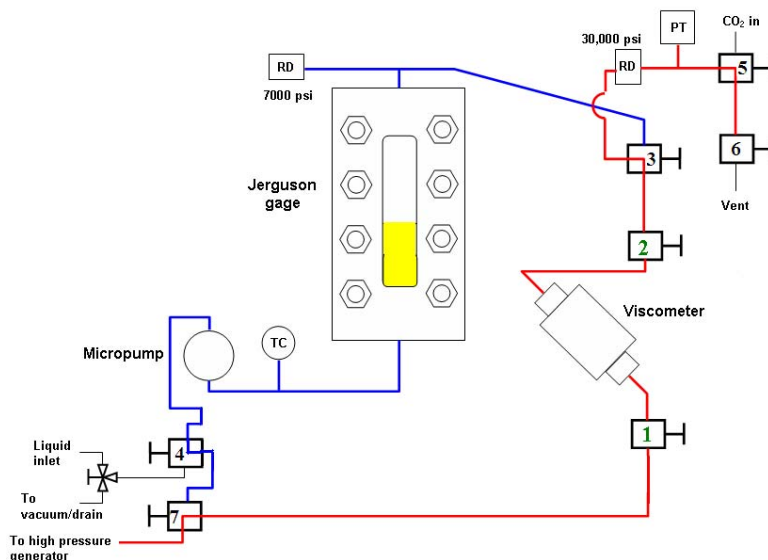


Figure 6.5 Schematic of the experiment setup

In the schematic of the experimental setup shown in Figure 6.5, the blue lines indicate tubing that withstand pressures below 5000 psi (34.5 MPa) (limit of the Jerguson[®] gage and micropump) while red lines denote tubing capable of withstanding up to 30,000 psi (206.8 MPa) (typically used when measuring the viscosity of ionic liquids).

6.3.3 Expansion and cloud point measurement procedure

The phase behavior of ternary systems consisting of toluene, polymer bound ligands and CO₂, with or without the presence of trace amounts of Rh precursor is determined. Prior to viscosity measurements, the volume expansion of organic

mixtures with various phosphorus ligands dissolved in toluene was performed in the Jerguson[®] view cell. A standard procedure for expansion studies is as follows. A known amount of solution (a mixture containing toluene and polymer bound phosphite ligand) is admitted into the view cell after the whole setup has been vacuumed, and the mixture is heated to the desired temperature. Dense CO₂ is gradually added from the top of the view cell and allowed to equilibrate with the mixture while circulating the fluid with the micropump. After the temperature and pressure stabilize, the volume of the mixture is recorded. This step of CO₂ addition, mixing, and volume measurement is repeated until the CO₂ pressure is such that mixture becomes cloudy or a phase separation is observed. The maximum CO₂ pressure that the organic mixture can tolerate while remaining homogeneous is called the cloud point pressure. The volume expansion is recorded in terms of the relative increase in the liquid volume from the initial state (CO₂-free, atmospheric pressure) to the final state (CO₂-expanded, equilibrated pressure) at the same temperature. The cloud points are different for each specific mixture with different concentrations of phosphorus ligands.

During the expansion and cloud point measurements, the viscometer was bypassed to prevent the piston from being scratched by any particles formed when the cloud point is approached.

6.3.4 Viscosity measurement procedure

During the viscosity measurements, the temperature and pressure stabilization follows the same procedure as stated in the volume expansion section. Following

that, viscometer sensor is purged three times to drive the trapped gas bubbles out of the chamber and the viscometer is isolated by turning off the inlet and outlet valves. Then a viscosity measurement is taken. The same procedure is repeated to record at least three measurements.

Before any measurements were taken, the viscometer was calibrated with manufacturer supplied calibration solution corresponding to the viscosity range, following the validated procedure. To validate the experimental procedure and test the setup, viscosities of pure toluene at three temperatures (25 °C, 40 °C and 60 °C) under atmospheric pressure were measured and compared with literature data. As shown in Figure 6.6, our data are in excellent agreement with the literature data.

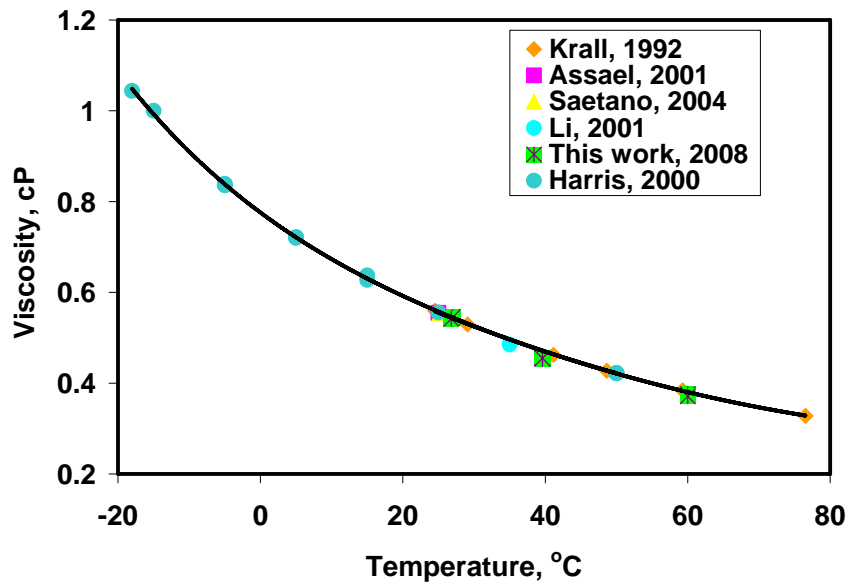


Figure 6.6 Pure toluene viscosities in this work compared to the reported data in literature

6.4 Results and Discussion

6.4.1 Volume expansion studies and cloud point data measurements

Figure 6.7 shows the expansion data for various systems with and without phosphorus ligands dissolved in toluene at different temperatures (30 °C, 40 °C and 60 °C). The larger sized data points at the end of volume expansion curves represent the cloud points for the mixtures where the dissolved ligands precipitate at the specified CO₂ pressures.

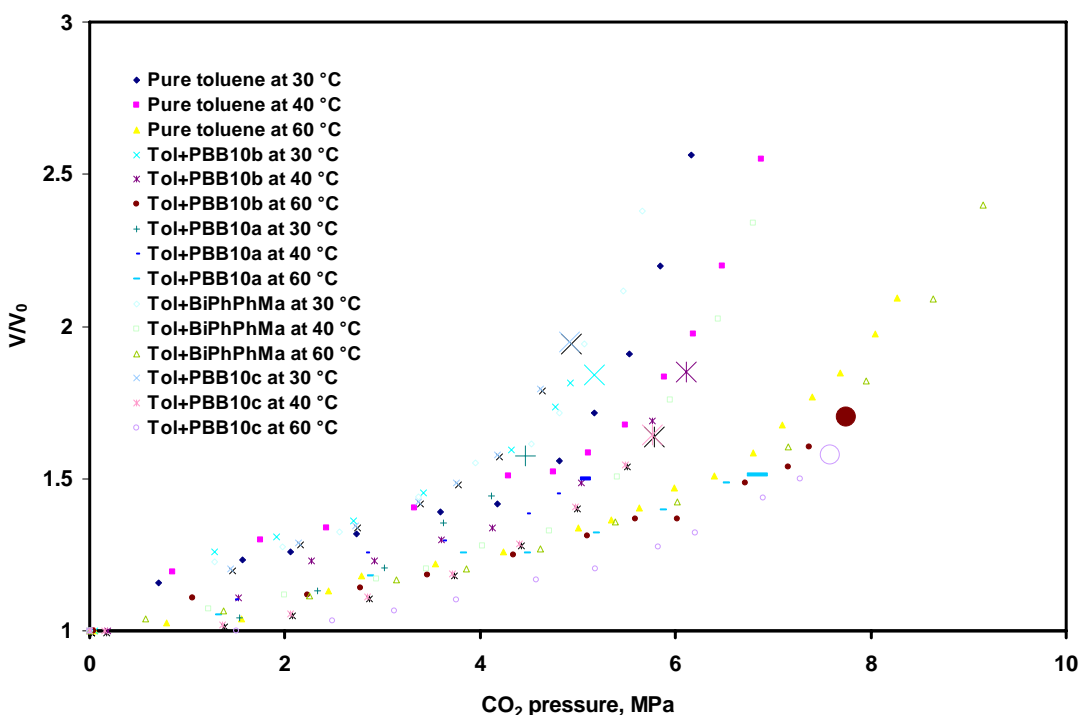


Figure 6.7 Expansion data for various systems at three temperatures

Of the systems tested in this study (shown in Figure 6.7), pure toluene and the mixture of toluene and BiPhPhM ligand are miscible with CO₂ and do not display cloud points in the pressure and temperature ranges tested. Polymer bound ligands

PBB10b, PBP10a and PBB10c precipitate out at the CO₂ pressures shown in Figure

6.8. The cloud point pressure increases with increasing temperature.

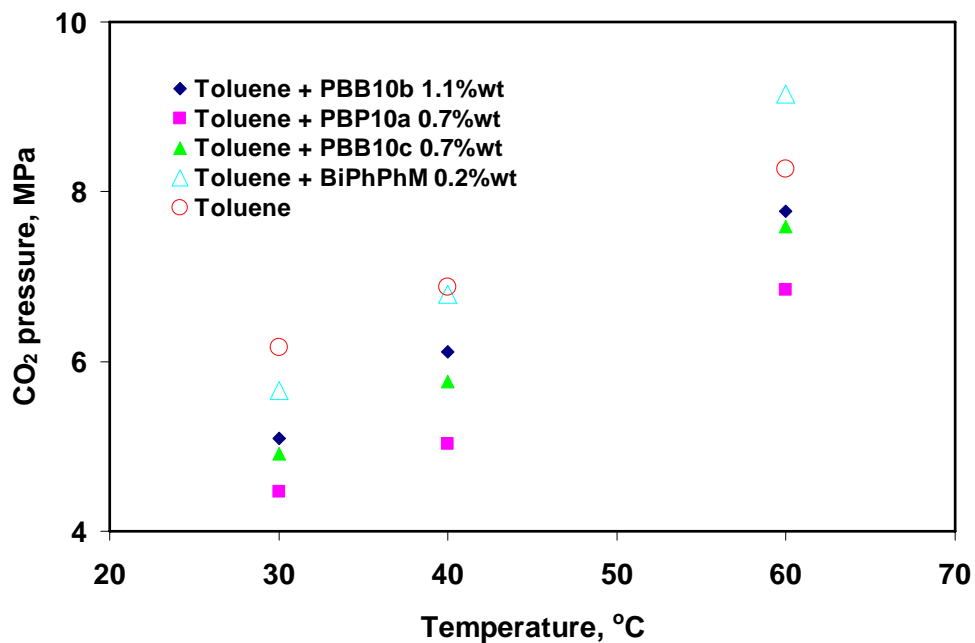


Figure 6.8 Cloud point measurements of different (toluene + soluble polymer bound ligand + CO₂) mixtures at different temperatures

6.4.2 Viscosity measurements

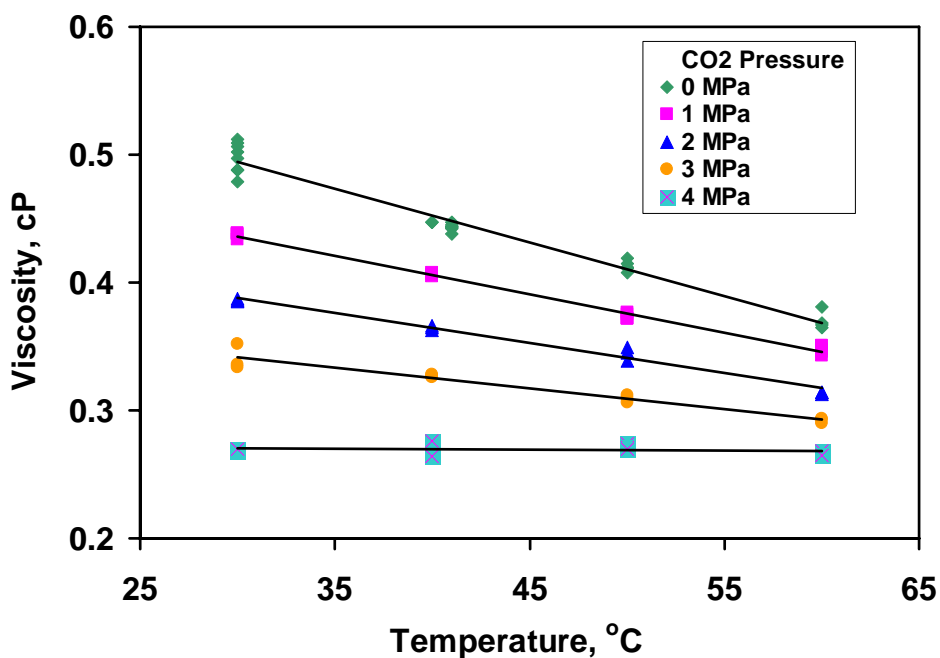


Figure 6.9 Variation of viscosities with temperature for toluene + 0.7 wt% PBB10c mixtures at different CO₂ pressures

Figure 6.9 shows the viscosities measured for the mixture of toluene and PBB10c at a concentration of 0.7% by weight, at four temperatures and five CO₂ pressures below the cloud point pressure. The viscosities decrease with increasing temperature at the same CO₂ pressure and with increasing CO₂ pressure at the same temperature. When adding CO₂ up to 4.0 MPa at temperatures of 30 °C and 60 °C, viscosities decrease 50% and 30%, respectively. However, negligible change in viscosity with temperature was observed at CO₂ pressure of 4.0 MPa.

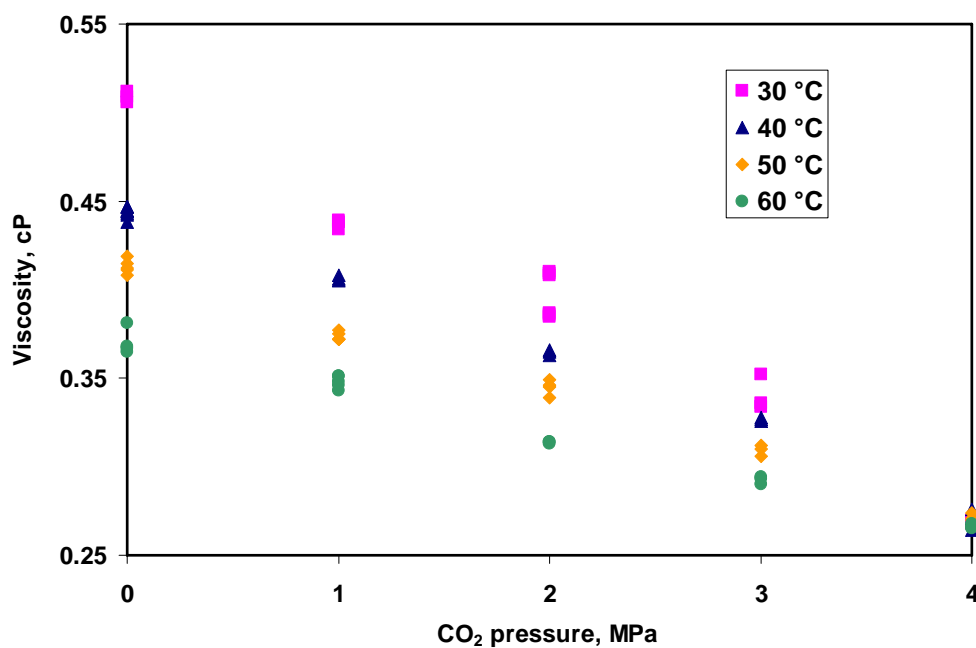


Figure 6.10 Variation of viscosities of toluene + 0.7 wt% PBB10c mixtures with CO₂ pressures at different temperatures

The relation of viscosity and CO₂ pressure at different temperature for the mixture toluene + PBB10c at a concentration of 0.7% by weight is plotted in Figure 6.10. Clearly, the viscosity drops when increasing CO₂ pressure at all temperatures. At lower temperature, the viscosity decreases more rapidly than that at higher temperature. This observation is consistent with the fact that at low temperature the mixture has higher volume expansion (higher CO₂ solubility) than at high temperature under the same CO₂ pressure.

The same trends were observed for the change in viscosities with temperature and CO₂ pressure in Figure 6.11 and Figure 6.12, respectively, for a system containing higher concentrations of polymer bound ligands (1.8% by weight).

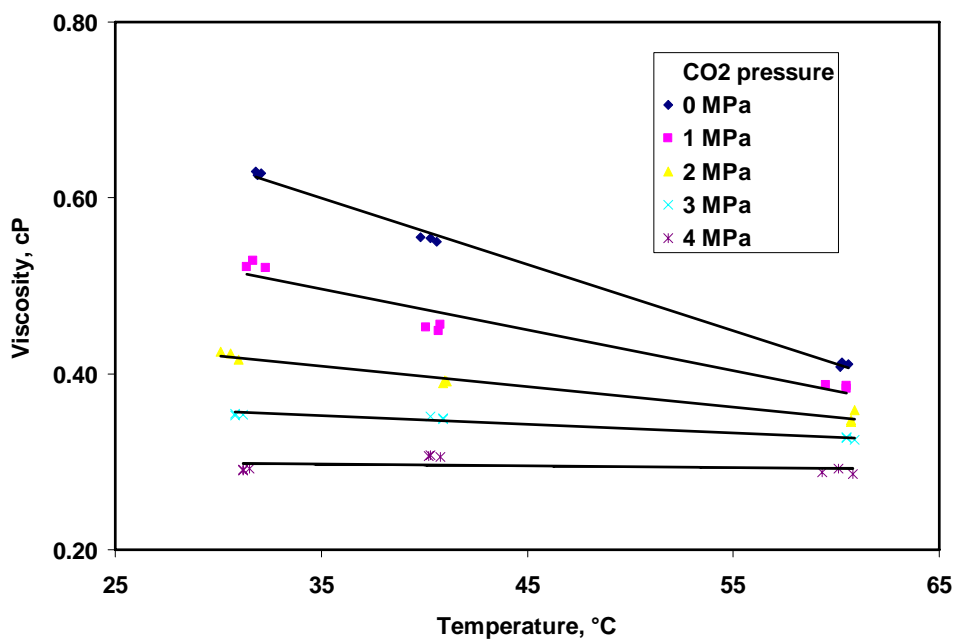


Figure 6.11 Variation of viscosities with temperature for toluene + 1.8 wt% PBB10c mixtures at different CO₂ pressures

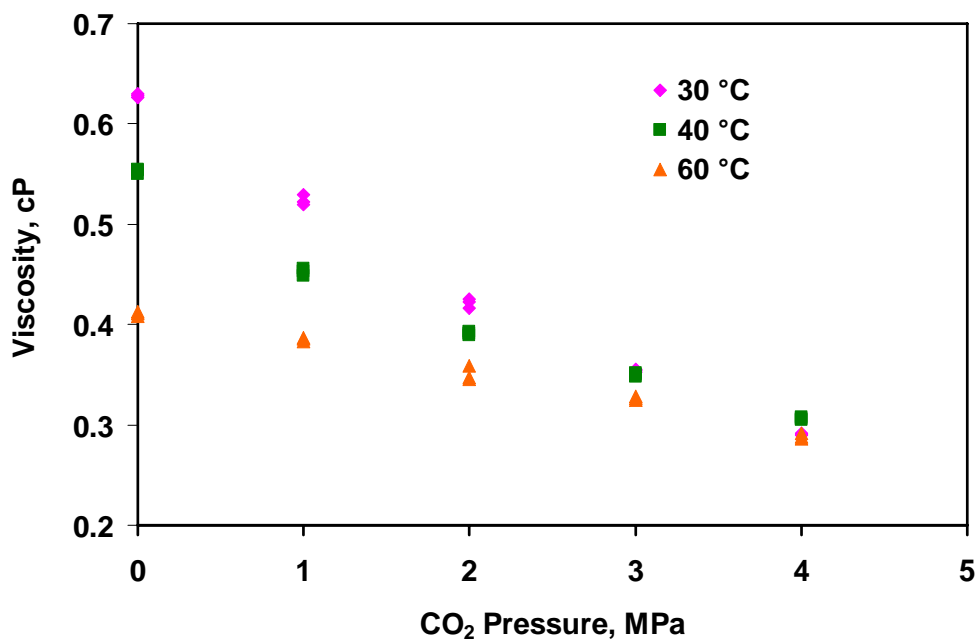


Figure 6.12 Variation of viscosities of toluene + 1.8 wt% PBB10c mixtures with CO₂ pressures at different temperatures

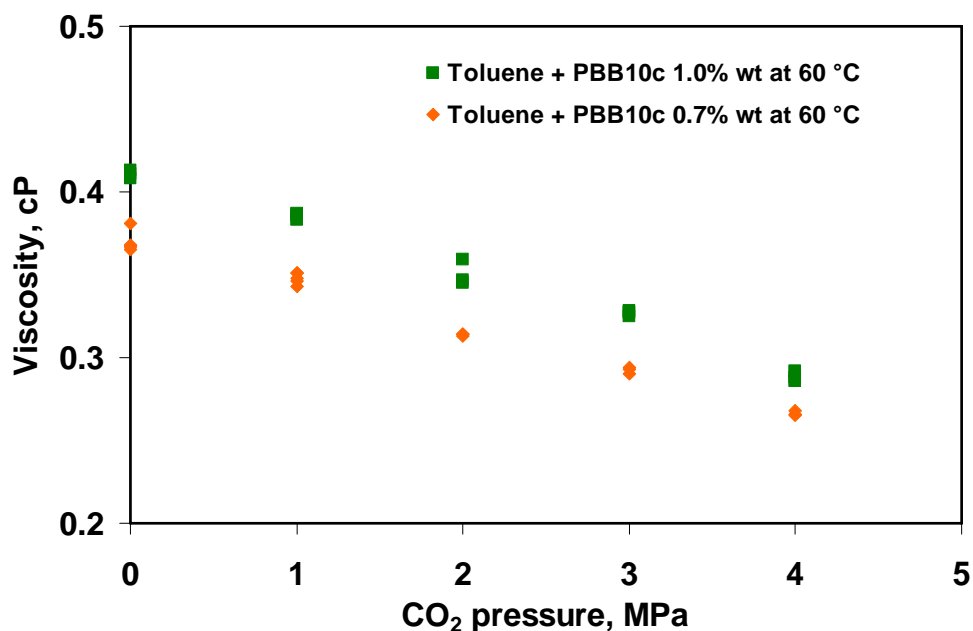


Figure 6.13 Viscosities versus CO₂ pressures of toluene + 1.8 wt% PBB10c mixture at 60 °C

Figure 6.13 shows the change in viscosity change with CO₂ pressure at 60 °C for different polymer concentrations. At the same temperature and CO₂ pressure, the viscosity increases with increasing polymer concentration. The degree of reduction in viscosity upon CO₂ addition is similar for both low and high polymer concentration mixtures.

6.5 Summary

Volume expansion, cloud point and viscosity of mixtures of toluene containing various phosphorus ligands were measured in an air heated batch oven containing a Jerguson[®] view cell and high pressure viscometer. Except for the BiPhPhM ligand, the polymer bound PBB10b, PBP10a and PBB10c ligands

dissolved in toluene precipitate when the CO₂ pressure reached the cloud point. It is also observed that the cloud point pressure increases with increasing temperature.

The viscosities of two toluene and PBB10c mixtures at different polymer concentrations (0.7% wt and 1.8% wt) were measured at four temperatures (30 °C, 40 °C, 50 °C and 60 °C) and varying CO₂ pressures up to 4.0 MPa. The decreasing trend of viscosity with CO₂ addition hints that the CXL media offers an opportunity to operate membrane filtration reactor at higher flux thereby increasing reactor throughput.

The dissolution of CO₂ in organic solvents reduces the viscosities and increases the diffusivities of the organic solvents. Compared with other inert gas such as nitrogen, CO₂ could not only serve as a pressurizing gas, but also as a reagent to tune the viscosities of the organic mixtures. Viscosity measurements of organic mixtures with various phosphorus ligands dissolved in toluene at different CO₂ pressures and temperatures provide the evidence for the CO₂ tuning ability.

To obtain the physical properties of catalyst solutions representing the actual reaction mixtures, measurements with 1-octene and nonanal addition must also be considered in future studies. The viscosity measurements must be exploited in designing experiments aimed at developing reliable membrane flux equations.

6.6 References

1. Jin, H.; Subramaniam, B.; Ghosh, A.; Tunge, J., Intensification of catalytic olefin hydroformylation in CO₂-expanded media. *AIChE Journal* **2006**, 52, (7), 2575-2581.
2. Yin, J. Z.; Tan, C. S., Solubility of hydrogen in toluene for the ternary system H₂ + CO₂ + toluene from 305 to 343 K and 1.2 to 10.5 MPa. *Fluid Phase Equilibria* **2006**, 242, (2), 111-117.
3. Maxey, N. B., Transport and phase transfer catalysis in gas-expanded liquids. *Ph.D. Dissertation* **2006**.
4. Rubero, P. A., Effect of hydrogen sulfide on the viscosity of sulfur. *Journal of Chemical & Engineering Data* **1964**, 9, (4), 481-484.
5. Cook, L. P.; Nwankwo, E.; Schleiniger, G.; Wood, B., Rapid, unambiguous polymer characterization by flow-referenced capillary viscometry. *Siam Journal on Applied Mathematics* **2002**, 62, (5), 1657-1676.
6. Teske, V.; Vogel, E., Viscosity measurements on methanol vapor and their evaluation. *Journal of Chemical & Engineering Data* **2006**, 51, (2), 628-635.
7. Brillo, J.; Chathoth, S. M.; Koza, M. M.; Meyer, A., Liquid Al₈₀Cu₂₀: atomic diffusion and viscosity. *Applied Physics Letters* **2008**, 93, (12), 121905/1-121905/3.
8. Mark, M.; Hausler, K.; Dual, J.; Reinhart, W. H., Oscillating viscometer - evaluation of a new bedside test. *Biorheology* **2006**, 43, (2), 133-146.
9. Wischmann, B.; Norsker, M.; Adler-Nissen, J., Food product models developed to evaluate starch as a food ingredient. *Nahrung-Food* **2002**, 46, (3), 167-173.
10. Assael, M. J.; Papadaki, M.; Wakeham, W. A., Measurements of the viscosity of benzene, toluene, and meta-xylene at pressure up to 80 MPa. *International Journal of Thermophysics* **1991**, 12, (3), 449-457.
11. Padua, A. A. H.; Fareleira, J. M. N. A.; Calado, J. C. G.; Wakeham, W. A., A vibrating-wire densimeter for liquids at high-pressures - the density of 2,2,4-trimethylpentane from 298.15 to 348.15 K and up to 100 MPa. *International Journal of Thermophysics* **1994**, 15, (2), 229-243.
12. Debock, A.; Grevendo, W.; Awouters, H., Pressure dependence of viscosity of liquid argon and liquid oxygen measured by means of a torsionally vibrating quartz crystal. *Physica* **1967**, 34, (1), 49-52.
13. Estrada-Baltazar, A.; Alvarado, J. F. J.; Iglesias-Silva, G. A.; Barrufet, M. A., Experimental liquid viscosities of decane and octane + decane from 298.15 K to 373.15 K and up to 25 MPa. *Journal of Chemical & Engineering Data* **1998**, 43, (3), 441-446.
14. Pensado, A. S.; Comunas, M. J. P.; Lugo, L.; Fernandez, J., Experimental dynamic viscosities of 2,3-dimethylpentane up to 60 MPa and from (303.15 to 353.15) K using a rolling-ball viscometer. *Journal of Chemical & Engineering Data* **2005**, 50, (3), 849-855.

15. Froba, A. P.; Leipertz, A., Viscosity of diisodecyl phthalate by surface light scattering (SLS). *Journal of Chemical and Engineering Data* **2007**, *52*, (5), 1803-1810.
16. Froba, A. P.; Leipertz, A., Accurate determination of liquid viscosity and surface tension using surface light scattering (SLS): Toluene under saturation conditions between 260 and 380 K. *International Journal of Thermophysics* **2003**, *24*, (4), 895-921.
17. Nieto de Castro, C. A.; Santos, F. J. V.; Fareleira, J. M. N. A.; Wakeham, W. A., Metrology of viscosity: have we learned enough? *Journal of Chemical & Engineering Data* **2009**, *54*, (2), 171-178.
18. Brooks, R. F.; Dinsdale, A. T.; Queded, P. N., The measurement of viscosity of alloys - a review of methods, data and models. *Measurement Science & Technology* **2005**, *16*, (2), 354-362.
19. Liu, W.-p. Z., Qing-li; Yin, Shao-tang; Sun, Dun-lu; Shao, Shu-fang; Zhang, Xia; Gu, Chang-jiang., Progress of the viscosity measurement methods. *Rengong Jingti Xuebao* **2007**, *36*, (2), 381-384.
20. Yokoyama, C., Measurement of viscosity of supercritical fluid mixtures. *Koatsuryoku no Kagaku to Gijutsu* **2001**, *11*, (2), 121-128.
21. Zhang, Y.; He, M. G.; Xue, R.; Wang, X. F.; Zhong, Q.; Zhang, X. X., A new method for liquid viscosity measurements: inclined-tube viscometry. *International Journal of Thermophysics* **2008**, *29*, (2), 483-504.
22. Caetano, F. J. P.; da Mata, J. L. C.; Fareleira, J. M. N. A.; Oliveira, C. M. B. P.; Wakeham, W. A., Viscosity measurements of liquid toluene at low temperatures using a dual vibrating-wire technique. *International Journal of Thermophysics* **2004**, *25*, (1), 1-11.
23. Ozokwelu, E. D., Toluene. *Kirk-Othmer Encyclopedia of Chemical Technology (5th Edition)* **2007**, *25*, 158-188.
24. Lay, E. N.; Taghikhani, V.; Ghotbi, C., Measurement and correlation of CO₂ solubility in the systems of CO₂ plus toluene, CO₂ plus benzene, and CO₂ plus n-hexane at near-critical and supercritical conditions. *Journal of Chemical and Engineering Data* **2006**, *51*, (6), 2197-2200.
25. Assael, M. J.; Avelino, H. M. T.; Dalaouti, N. K.; Fareleira, J. M. N. A.; Harris, K. R., Reference correlation for the viscosity of liquid toluene from 213 to 373 K at pressures to 250 MPa. *International Journal of Thermophysics* **2001**, *22*, (3), 789-799.
26. Santos, F. J. V.; de Castro, C. A. N.; Dymond, J. H.; Dalaouti, N. K.; Assael, M. J.; Nagashima, A., Standard reference data for the viscosity of toluene. *Journal of Physical and Chemical Reference Data* **2006**, *35*, (1), 1-8.
27. Krall, A. H.; Sengers, J. V.; Kestin, J., Viscosity of liquid toluene at temperatures from 25 to 150-degrees-C and at pressures up to 30 MPa. *Journal of Chemical and Engineering Data* **1992**, *37*, (3), 349-355.
28. Harris, K. R., Temperature and density dependence of the viscosity of toluene. *Journal of Chemical and Engineering Data* **2000**, *45*, (5), 893-897.

29. Harris, K. R.; Malhotra, R.; Woolf, L. A., Temperature and density dependence of the viscosity of octane and toluene. *Journal of Chemical and Engineering Data* **1997**, 42, (6), 1254-1260.
30. Sih, R.; Dehghani, F.; Foster, N. R., Viscosity measurements on gas expanded liquid systems - methanol and carbon dioxide. *Journal of Supercritical Fluids* **2007**, 41, (1), 148-157.
31. Sih, R.; Foster, N. R., Viscosity measurements on saturated gas expanded liquid systems - acetone and carbon dioxide. *The Journal of Supercritical Fluids* **2008**, 47, (2), 233-239.
32. Liu, K.; Kiran, E., Viscosity, density and excess volume of acetone plus carbon dioxide mixtures at high pressures. *Industrial & Engineering Chemistry Research* **2007**, 46, (16), 5453-5462.
33. Sih, R.; Armenti, M.; Mammucari, R.; Dehghani, F.; Foster, N. R., Viscosity measurements on saturated gas-expanded liquid systems - ethanol and carbon dioxide. *The Journal of Supercritical Fluids* **2008**, 43, (3), 460-468.
34. Terao, K.; Hokajo, T.; Nakamura, Y.; Norisuye, T., Solution properties of polymacromonomers consisting of polystyrene. 3. Viscosity behavior in cyclohexane and toluene. *Macromolecules* **1999**, 32, (11), 3690-3694.
35. Poh, B. T.; Ong, B. T., Dependence of viscosity of polystyrene solutions on molecular weight and concentration. *European Polymer Journal* **1984**, 20, (10), 975-978.
36. Modarress, H.; Mohsen-Nia, M.; Mahdavi, M. A., Experimental and theoretical studies of polymer/solvent viscosity mixtures. *Journal of Applied Polymer Science* **2004**, 91, (3), 1724-1729.
37. Yeo, S. D.; Kiran, E., High-pressure viscosity of polystyrene solutions in toluene plus carbon dioxide binary mixtures. *Journal of Applied Polymer Science* **2000**, 75, (2), 306-315.
38. Yeo, S. D.; Kiran, E., Viscosity reduction of polystyrene solutions in toluene with supercritical carbon dioxide. *Macromolecules* **1999**, 32, (21), 7325-7328.
39. Li, D.; Han, B. X.; Liu, Z. M.; Liu, J.; Zhang, X. G.; Wang, S. G.; Zhang, X. F.; Wang, J.; Dong, B. Z., Effect of gas antisolvent on conformation of polystyrene in toluene: viscosity and small-angle X-ray scattering study. *Macromolecules* **2001**, 34, (7), 2195-2201.
40. Shin, M. S.; Lee, J. H.; Kim, H., Phase behavior of the poly(vinyl pyrrolidone) plus dichloromethane plus supercritical carbon dioxide system. *Fluid Phase Equilibria* **2008**, 272, (1-2), 42-46.
41. Gornert, M.; Sadowski, G., Phase-equilibrium measurement and modeling of the PMMA/MMA/carbon dioxide ternary system. *Journal of Supercritical Fluids* **2008**, 46, (3), 218-225.
42. Matsuyama, K.; Mishima, K., Phase behavior of the mixtures of CO₂ plus poly(methyl methacrylate) plus ethanol at high pressure. *Journal of Chemical and Engineering Data* **2008**, 53, (5), 1151-1154.

43. Matsuyama, K.; Mishima, K., Phase behavior of CO₂ plus polyethylene glycol plus ethanol at pressures up to 20 MPa. *Fluid Phase Equilibria* **2006**, 249, (1-2), 173-178.
44. Shin, J.; Lee, Y. W.; Kim, H.; Bae, W., High-pressure phase behavior of carbon dioxide plus heptadecafluorodecyl acrylate plus poly(heptadecafluorodecyl acrylate) system. *Journal of Chemical and Engineering Data* **2006**, 51, (5), 1571-1575.
45. Kalogiannis, C. G.; Panayiotou, C. G., Bubble and cloud points of the system poly(L-lactic acid) plus carbon dioxide plus dichloromethane. *Journal of Chemical and Engineering Data* **2005**, 50, (4), 1442-1447.
46. Lee, B. C.; Lim, J. S.; Lee, Y. W., Effect of solvent composition and polymer molecular weight on cloud points of poly(L-lactide) in chlorodifluoromethane plus carbon dioxide. *Journal of Chemical and Engineering Data* **2003**, 48, (4), 774-777.
47. Kiran, E.; Zhuang, W. H.; Sen, Y. L., Solubility and demixing of polyethylene in supercritical binary fluid mixtures - carbon-dioxide cyclohexane, carbon-dioxide toluene, carbon-dioxide pentane. *Journal of Applied Polymer Science* **1993**, 47, (5), 895-909.
48. Houndonougbo, Y.; Jin, H.; Rajagopalan, B.; Wong, K.; Kuczera, K.; Subramaniam, B.; Laird, B., Phase equilibria in carbon dioxide expanded solvents: experiments and molecular simulations. *Journal of Physical Chemistry B* **2006**, 110, (26), 13195-13202.
49. Houndonougbo, Y.; Kuczera, K.; Subramaniam, B.; Laird, B. B., Prediction of phase equilibria and transport properties in carbon-dioxide expanded solvents by molecular simulation. *Molecular Simulation* **2007**, 33, (9-10), 861-869.
50. Jessop, P. G.; Subramaniam, B., Gas-expanded liquids. *Chemical Reviews* **2007**, 107, (6), 2666-2694.
51. Zevnik, L.; Levec, J., Gas-expanded liquids: determination of the expansion coefficient by an acoustic technique. *Journal of Supercritical Fluids* **2007**, 41, (1), 158-163.
52. Chang, C. M. J., Volume expansion coefficients and activity-coefficients of high-pressure carbon-dioxide dissolution in organic liquids at 298 K. *Journal of Chemical Engineering of Japan* **1992**, 25, (2), 164-170.
53. Mueller, S. G.; Werber, J. R.; Al-Dahhan, M. H.; Dudukovic, M. P., Using a fiber-optic probe for the measurement of volumetric expansion of liquids. *Industrial & Engineering Chemistry Research* **2007**, 46, (12), 4330-4334.
54. Elvassore, N.; Bertucco, A.; Di Noto, V., On-line monitoring of volume expansion in gas-antisolvent processes by UV-vis spectroscopy. *Journal of Chemical and Engineering Data* **2002**, 47, (2), 223-227.
55. Vandezande, P.; Gevers, L. E. M.; Vankelecom, I. F. J., Solvent resistant nanofiltration: separating on a molecular level. *Chemical Society Reviews* **2008**, 37, (2), 365-405.
56. Iwama, A.; Kazuse, Y., New polyimide ultrafiltration membranes for organic use. *Journal of Membrane Science* **1982**, 11, (3), 297-309.

57. Silva, P.; Han, S. J.; Livingston, A. G., Solvent transport in organic solvent nanofiltration membranes. *Journal of Membrane Science* **2005**, 262, (1-2), 49-59.
58. Silva, P.; Livingston, A. G., Effect of concentration polarisation in organic solvent nanofiltration - flat sheet and spiral wound systems. *Desalination* **2006**, 199, (1-3), 248-250.
59. White, L. S., Transport properties of a polyimide solvent resistant nanofiltration membrane. *Journal of Membrane Science* **2002**, 205, (1-2), 191-202.
60. Aerts, S.; Buekenhoudt, A.; Weyten, H.; Gevers, L. E. M.; Vankelecom, I. F. G.; Jacobs, P. A., The use of solvent resistant nanofiltration in the recycling of the Co-Jacobsen catalyst in the hydrolytic kinetic resolution (HKR) of epoxides. *Journal of Membrane Science* **2006**, 280, (1-2), 245-252.
61. Jana, R.; Tunge, J. A., A homogeneous, recyclable rhodium(I) catalyst for the hydroarylation of Michael acceptors. *Organic Letters* **2009**, 11, (4), 971-974.
62. Kho, Y. W.; Conrad, D. C.; Knutson, B. L., Phase equilibria and thermophysical properties of carbon dioxide-expanded fluorinated solvents. *Fluid Phase Equilibria* **2003**, 206, (1-2), 179-193.

Chapter 7. Conclusions and Recommendations

7.1 Conclusions

Researchers at the Center for Environmentally Beneficial Catalysis (CEBC) had previously reported a novel rhodium-based hydroformylation process concept based on the use of CO₂-expanded liquids (CXLs) to intensify rates and obtain higher linear/branch aldehydes selectivity at relatively mild temperatures (30-60°C) and pressures (~4 MPa). This dissertation has contributed to significant advances in both fundamental and practical issues associated with this concept.

ReactIR studies of Rh/triphenylphosphine catalyzed 1-octene hydroformylation, complemented by microkinetic and reactor modeling investigations, revealed that the intrinsic kinetic rate constants are of similar magnitude with or without CO₂ addition to the reaction mixture. The Rh catalytic mechanism is derived from the literature and includes elementary steps including catalyst activation, olefin coordination, CO insertion, hydrogen oxidative addition, reductive elimination, and byproducts formation. The estimated intrinsic kinetic rate constants are on the same order of magnitude (within the confidence intervals) with or without CO₂ addition to the reaction mixture. This implies that CO₂ doesn't significantly affect the intrinsic reaction rate for most of the elementary steps and the enhanced reaction rate observed in CXL is due to the increased hydrogen solubility in that medium.

Plant-scale simulations of the CXL and Exxon processes were generated using Aspen HYSYS[®] software assuming higher olefin C₈ as substrate with a capacity of

200 kton/yr. Environmental impact analysis revealed that the overall toxicity index for the CEBC process is approximately 40 times less than the Exxon process against which the CEBC process was benchmarked. The acetic acid emissions during the catalyst recovery step are identified as the main environmental impact source for the simulated conventional process. The CXL process also has a roughly 50% lower E-factor (ratio of waste/desired products) value than the simulated conventional process.

Preliminary economic analysis shows that the CXL process has the potential to be economically competitive than the simulated conventional process. The CXL reactor costs are significantly lower than the conventional process, due to the attainment of higher TOF and to comparable or better product selectivity at relatively mild operating conditions. For identical plant production capacities, the estimated capital cost is 50% lower and the production cost is 15% lower in CXL process compared to the conventional process. This result was obtained even though catalyst recovery costs were not included in the simulated conventional process but were included in the CXL process. The comparative economic analysis of the CXL concept revealed that at an aldehyde production rate of 19,900 kg/(kg Rh · h), > 99.8% Rh has to be recovered per pass for the CEBC process to be competitive with the simulated conventional process.

To achieve the targeted Rh recovery rate, CEBC researchers from the Tunge group in the Department of Chemistry synthesized and supplied a series of bulky, soluble and recyclable polymer bound phosphorus ligands to facilitate quantitative Rh retention in homogeneous hydroformylation reaction mixtures nano/ultra-filtration

membrane techniques. Rh recovery levels that exceed the criterion ($> 99.8\%$ per pass assuming the same hydroformylation activity) for economic viability were successfully demonstrated in a membrane-based nano/ultra-filtration reactor system using polymer bound phosphorus ligands. Both batch and continuous filtrations were conducted in a commercially available high-pressure MET cell under air-free operation equipped with a solvent-resistant, polyimide STARMEM[®] membrane. The retention of the catalyst precursor Rh(acac)(CO)₂ bound to various ligands, including TPPine, BiPhePhos, BiPhPhM and polymer bound ligands, were investigated. Concentrations of Rh and P in the range of 100-400 ppm, typical of hydroformylation reaction mixtures, were tested. As expected, the size of the ligands significantly affects the Rh retention. During continuous filtration of a toluene-based solution containing bidentate polymer bound Rh complexes, the Rh and P concentrations in the permeate, quantified using ICP analysis, were on the order of a few tens of ppb. During continuous 1-octene hydroformylation studies with such catalyst complexes in a membrane reactor at a syngas pressure of 0.6 MPa and 60 °C, the 1-octene conversion and product (mostly aldehydes) concentrations reached a steady state with the Rh concentrations in the permeate stream being lower than 120 ppb, well below the economically acceptable limit (equivalent to 278 ppb when the Rh concentration in the reactor is 139 ppm assuming the same hydroformylation activity). However, the conversions and product concentrations during the continuous run are lower than those obtained in a batch ReactIR under identical operating conditions. This is attributed to syngas starvation in the membrane reactor that might be caused by

inadequate mixing afforded by the magnetic stirrer bar at the bottom of the membrane reactor.

In complementary investigations, volume expansion, cloud points and viscosities of mixtures of toluene with various phosphorus ligands were measured in an air bath oven equipped with a Jerguson[®] view cell and a moving piston viscometer system. It was found that the dissolution of CO₂ in the organic phase (to create CO₂-expanded liquids) decreases the viscosities of the mixtures with increasing CO₂ pressure. Cloud point measurements were also performed to determine the maximum CO₂ pressure below which homogeneous catalysis is possible. With the exception of BiPhPhM ligand, the other soluble polymer bound ligands (PBB10b, PBP10a and PBB10c) in toluene solution exhibited cloud points at certain CO₂ pressures. It is also observed that the cloud point pressure increases with increasing temperature. The viscosities of two mixtures of toluene and PBB10c at different polymer concentrations (0.7% wt and 1.8% wt) were measured at four temperatures (30 °C, 40 °C, 50 °C and 60 °C) and varying CO₂ pressures up to 4.0 MPa. The decreasing trend of viscosity with CO₂ addition implies that the use of CO₂ offers an opportunity to enhance mixing and also tune the membrane flux so as to increase the throughput of the membrane filter. These physical property data are also essential to rationally design, model and optimize such systems.

7.2 Recommendations

The key findings in this dissertation lead to the following research for future consideration:

- In the preliminary economic and environmental analyses for the simulated conventional process, cobalt catalyst recovery and heavy product hydrogenation steps were not included due to the lack of available data. The capital investment costs and operating costs involved in these steps will be taken into account according to information in the SRI report for the Exxon oxo process. Considering the hidden costs makes unbiased comparison even though it won't significantly change the current conclusion. Updating the CXL process is also necessary when laboratory kinetic, mass transport and gas solubility data are available for better understanding of the kinetic scheme in CO₂-expanded media. Undoubtedly, such improved estimations will aid in making better informed judgment.
- Based on the demonstrated *in situ* catalyst retention concept, the Rh retention rate in the CXL process will be updated. The use of a membrane reactor, an integrated combination of reactor with membrane filter, should bring down both capital and operating costs in the CXL process. However, the cost of solvent-resistant membrane is currently unknown. Despite the solvent-resistant membrane for large-scale operation being not available, membrane filtration with polyamide membrane in pilot plant¹ scale was reported by Hoechst AG for the separation of homogeneous rhodium complexes from hydroformylation mixture of dicyclopentadiene to tricyclodecanaldehyde in toluene. In addition, the Rh catalyst cost is a key factor on the CXL process economy. The price of Rh fluctuates to a great extent recently as evidenced

by the price drop from \$11,000/troy ounce (Jun 2008) to \$1,000/troy ounce (Mar 2009). Regardless, Rh is still almost 1000 times more expensive than cobalt.

- In quantitative environmental analysis, it is important to update the physical, chemical and toxic properties and emission factors for each chemical involved in both processes for more accurate prediction of environmental impacts. It is recommended to regularly check the updated data and evaluation tools provided by US Environmental Protection Agency (EPA). The major change in the simulated conventional process is to replace acetic acid with formic acid for the cobalt catalyst recovery. Formic acid decomposes primarily to water and CO in the gas phase or to CO₂ and H₂ in the aqueous phase. Either decomposition pathway generates less toxic emission than acetic acid, the dominant environmental impact contributor to the simulated conventional process. Furthermore, the removal of antisolvent methanol from the Rh recovery step in CXL process will also significantly reduce the total waste generation.
- For a thorough understanding the effect of CO₂ on the hydroformylation reaction rate, other methods should be considered to obtain empirical rate expressions according to the assumption of different rate-limiting steps. Rival kinetic models are discriminated based on quality of fit between experimental and predicted concentration versus time data. Systematic experiments are needed at various CO/H₂ ratios, catalyst concentrations, temperatures, and

volume expansions for a short period of time to obtain the initial reaction rates.

- CO₂ effects on the regioselectivity of Rh/triphenylphosphine catalyzed 1-octene hydroformylation could not be predicted due to the inability of ReactIR to differentiate between the linear and branched aldehyde products. Modification of the ReactIR and new sampling techniques are required to allow periodic sample withdrawing for GC analysis of aldehyde isomers. Additional reaction steps for branched aldehyde formation will be added to the kinetic mechanism. In addition to CO₂, different organic solvents, such as toluene, hexane, and methanol, should be intentionally chosen according to their dielectric constants and investigated to explore solvent effects as well. Corresponding phase behavior studies, including solubility and volume expansion measurements as well as mass transfer studies, would be needed for all the investigated solvents.
- The mechanism in the microkinetic modeling needs to be modified and the considerations include first order assumption for the initial catalyst hydrogenation step and dissociative mechanism with HRh(CO)L₂ as the active catalyst species.
- Ligand synthesis should continue to be examined aimed at screening various polymer bound ligand candidates in ReactIR for better catalyst performance and for optimizing the reaction conditions in CXL media. The kinetic data for these systems are valuable input for kinetic modeling. Design of polymers

that are soluble in reaction mixtures containing 1-octene and nonanal (to avoid the usage of an additional solvent) and quantification of how polymer characteristics affect retention are underway.

- The results of continuous membrane filtration with simultaneous hydroformylation revealed lower conversion and aldehyde selectivity compared to batch runs. These results are attributed to inefficient mixing provided by the magnetic stirrer. Replacement of the magnetic stirrer with a magnetically driven mechanical stirrer should improve syngas transfer into the liquid phase in the membrane filter, thereby enhancing conversion and selectivities. Automation of the membrane filtration apparatus is essential to enable unattended operation during extended periods of time. Establishment of long-term operation helps gain insights into Rh leaching, deactivation and catalyst durability. Both Rh and phosphorus were observed in the permeate stream and it is uncertain whether the Rh is in unbound or bound form. NMR analysis of the permeate samples would help shed insights into the bound form of the Rh and if the leached Rh could be catalytically active.
- Measurements of volume expansion, cloud points and viscosities for actual hydroformylation reaction mixtures including 1-octene, nonanal and polymer bound Rh complex (as well as any additional solvent such as toluene) are useful for the determination of optimal reaction conditions and correlation of the membrane flux with the physical properties of the neat and CO₂-expanded

1-octene hydroformylation mixtures. A mathematical model of the membrane reactor should be developed for rational design and scale-up.

- Rh cost per pound of aldehyde produced (based on the optimal aldehyde yield and actual Rh loss in continuous runs) should be employed as the key indicator to evaluate the quantitative recoverability of various Rh catalysts and the application of membrane nanofiltration in homogeneous catalytic systems for industry consideration.

The methods and protocols developed in this dissertation are also helpful in other research areas:

- Economic and environmental analysis tools are helpful for life-cycle costs and environmental impact analyses in any process at any stage of development.
- ReactIR and kinetic model may be adapted for kinetic studies of other homogeneous reaction systems.
- The demonstrated technology concept involving the retention of soluble polymer bound catalysts by membrane filtration, should find applications in a variety of other applications in homogeneous catalysis, including hydrogenation and carbonylation.
- ICP for organic analysis protocol may be adopted for elemental analysis of other homogeneous organic mixtures.

7.3 Reference

1. Muller, T.; Bahrmann, H., Separation of catalyst compounds in two-phase and uni-phase systems by membranes. *Journal of Molecular Catalysis A-Chemical* **1997**, 116, (1-2), 39-42.

Appendix I. Economic and Environmental Analysis

I.1 Tables

Table I.1 Total Capital Investment (TCI) calculation

Units	Remark	Percentage	Operation Units
Purchased Cost, \$ PC			input
<u>Purchased-Equipment Delivery</u>	Per. Of PC	10.0%	=PC*0.1
<u>Concrete Foundations</u>	Per. Of PC	6.6%	=PC*0.066
<u>Piping</u>	Per. Of PC	61.4%	=PC*0.614
<u>Steel Support</u>	Per. Of PC	5.0%	=PC*0.05
<u>Instrumentation</u>	Per. Of PC	13.5%	=PC*0.135
<u>Insulation</u>	Per. Of PC	8.9%	=PC*0.089
<u>Electrical</u>	Per. Of PC	14.5%	=PC*0.145
<u>Painting</u>	Per. Of PC	1.3%	=PC*0.013
<u>Equipment Setting</u>	Per. Of PC	5.0%	=PC*0.05
Instal. Equip. Costs, \$ IEC	PC+above	226.2%	=PC*2.262
<u>Freight</u>	Per. Of PC	3.0%	=PC*0.03
<u>Yard Improvements</u>	Per. Of PC	11.0%	=PC*0.11
<u>Environmental Control</u>	Per. Of PC	0.0%	=PC*0
<u>Buildings</u>	Per. Of PC	43.0%	=PC*0.43
Direct Costs, \$ DC	IEC+above	283.2%	=PC*2.832
<u>Engineering Costs</u>	Per. Of DC	16.0%	=DC*0.16
<u>Construction Overhead</u>	Per. Of DC	26.0%	=DC*0.26
<u>Contingency</u>	Per. Of DC	23.0%	=DC*0.23
<u>Contractor's Fee</u>	Per. Of DC	17.0%	=DC*0.17
Indirect Costs, \$ IDC	above	72.0%	=DC*0.72
Auxiliaries/Off-site, \$ AO	Per. Of DC	31.5%	=DC*0.315
Fixed Cap. Invest., \$ FCI	DC+IDC+AO		=DC+IDC+AO
Working Cap. \$ WC	Per. Of TCI	20.0%	=TCI-FCI
Total Cap. Invest. \$ TCI	Per. Of TCI	100.0%	=FCI/0.8

Reference:

Max S. Peters and Klaus D. Timmerhaus, Ronald E. West
Plant design and economics for chemical engineers, 5th edition, 2003

Table I.2 Total Production Cost (TPC) calculation

	Remarks	Percentage	Calculation
Variable Production Costs, \$ VPC			
Raw Materials			input
Direct Operating Labor, DOL			input
Supervisory and Clerical Labor, SCL	of Operat. Labor	15%	=DOL*0.15
Utilities			
	<u>Electricity</u>		input
	<u>Steam</u>		input
	<u>Water, cooling</u>		input
Plant Maintenance and Repairs, PMR	of FCI	7%	=FCL*0.07
Operating Supplies	of Maint.&Repairs	15%	=PMR*0.15
Laboratory Charges	of Operat. Labor	15%	=DOL*0.15
Patents and Royalties	of TPC	4%	=TPC*0.04
Catalysts			input
Solvents			input
Subtotal: Variable Production Costs, VPC			=sum of above
Fixed Charges, \$ FCh			
Depreciation	w/o		
Taxes (property)	of FCI	2%	=FCI*0.02
Financing (interest)	of FCI	1%	=FCI*0.01
Insurance	of FCI	8%	=FCI*0.08
Rent	of FCI	5%	=FCI*0.05
Subtotal: Fixed Charges, FCh			=sum of above
Plant Overhead Costs, \$ POC			
Safety and Protection			
General Plant Overhead			
Payroll Overhead, and so on			
Subtotal: Plant Overhead Costs, POC of TPC			10%
Total Operating Costs, \$ OC			=VPC+FCh+POC
General Expenses, GE			
Administrative costs	of TPC	4%	=TPC*0.04
Distribution and marketing costs	of TPC	10%	=TPC*0.10
Research and development costs	of TPC	5%	=TPC*0.05
Total General Expenses, \$ GE			= sum of above
Total Production Cost, \$ TPC*			=OC+GE

Reference:

Max S. Peters and Klaus D. Timmerhaus, Ronald E. West

Plant design and economics for chemical engineers, 5th edition, 2003

* Without depreciation

Table I.3 The chemicals and utilities inventory and prices

Chemical	Prices, \$/kg	
Olefins	0.34	Chevron Phillips
Syngas	0.09	National Renewable Energy Laboratory
CO ₂	0.05	TORP Group, University of Kansas
Methanol	0.32	Chemical Market Reporter, August, 2005
Rhodium catalyst	30000	http://www.kitco.com/charts/rhodium.html
Ligand TPP	10.00	Assumed value
n-Nonanal	2.20	Suggested by Dr. Darryl Fahey
Cobalt acetate	22	Sigmaaldrich
Acetic acid	0.3	http://www.the-innovation-group.com/
Utilities	Prices	
Electricity	0.0825	\$/kW hr, from SCENE database
Steam	0.01	\$/lb, from SCENE database
Cooling water	0.0343	\$/m ³ , from SCENE database

Table I.4 The equipment purchased costs for CXL and the simulated conventional processes

	CXL Process \$	the Simulated Conventional Process, \$
Reactor	5.5E+05	4.1E+06
Heat Exchangers	3.8E+05	3.4E+05
DisColumns	2.8E+05	1.2E+05
Separators	1.3E+05	2.4E+05
Pumps	5.3E+04	1.2E+05
Compressors	1.2E+06	7.5E+05
Filters	1.7E+05	0.0E+00
Total	2.8E+06	5.6E+06

The purchased costs (PC) for each operation unit was calculated following the method in the literature based on the sizing and material costs. The purchased costs also were adjusted to the costs in 2005 according to the cost index.

Table I.5 Summary of material, labor and utilities costs

	CXL Process \$	the Simulated Conventional Process, \$
Raw materials	6.0E+07	7.4E+07
Direct Operating Labor	3.7E+06	3.3E+06
Utilities	3.4E+06	2.4E+06
Catalysts	3.5E+06	8.8E+05
Solvents	5.0E+05	0.0E+00

Table I.6 The emission of each chemical from each process per year

CXL Process kg/yr	the Simulated Conventional Process kg/yr
Aldehyde	0.0E+00
Octene	2.3E+05
Carbon monoxide	1.0E+05
Carbon dioxide	6.7E+07
Nitrogen dioxide	1.5E+05
Sulfur dioxide	9.3E+02
TOC	1.6E+03
Acetal	7.6E+03
Methanol	2.8E+04
Aldehyde	0.0E+00
Octene	7.2E+05
Carbon monoxide	2.5E+05
Carbon dioxide	1.4E+08
Nitrogen dioxide	1.2E+05
Sulfur dioxide	3.5E+03
TOC	1.2E+03
Acetal	1.4E+05
Acetic acid	3.8E+03

Table I.7 The chemical partition summary

Chemical	Percent in:			
	Air	Sediment	Soil	Water
Aldehyde	78.9	0.3	13.0	7.8
Octene	99.0	0.0	0.9	0.1
Carbon monoxide	100.0	0.0	0.0	0.0
Carbon dioxide	99.8	0.0	0.0	0.2
Nitrogen dioxide	99.9	0.0	0.0	0.1
Sulfur dioxide	93.1	0.0	0.0	6.9
TOC	99.9	0.0	0.1	0.0
Methanol	0.0	0.9	40.4	58.6
Acetal	99.2	0.0	0.0	0.8
Acetic acid	2.4	0.0	0.1	97.5

II.2 Aldehyde Production Rate Calculation

Liquid feed composition: 1-Octene : CO₂ = 1 : 0.1 (v/v) at 10 % volume expansion, Liquid hourly space velocity (LHSV) = 5 h⁻¹ (m³ liquid/ m³ reactor/ h), Liquid level in the reactor = 80%, Reactor volume: V m³, [Rh] = 280 ppmw, based on olefins, Olefin density = 715 kg/m³, Conversion = 90%,; Aldehyde selectivity = 97.5%, Aldehyde yield = 88%, 1-octene molecular weight = 112.2 g/mol, nonanal molecular weight = 142.2 g/mol

Total mass of rhodium in the reactor (kg):

$$m_{Rh} = V \text{ m}^3 \text{ reactor} \times 80\% \text{ liquid level} \times \frac{1 \text{ m}^3 \text{ liquid 1-octene}}{(1 + 0.1) \text{ m}^3 \text{ liquid 1-octene and CO}_2} \\ \times 715 \text{ kg 1-octene/m}^3 \times 280 \text{ ppmw} \times 10^{-6} \text{ kg Rh/kg 1-octene}$$

Total aldehyde produced per hour (kg/h):

$$m_{al} = 5 \text{ m}^3 \text{ liquid/m}^3 \text{ reactor/h} \times V \text{ m}^3 \text{ reactor} \times 80\% \text{ liquid level} \\ \times \frac{1 \text{ m}^3 \text{ liquid 1-octene}}{(1 + 0.1) \text{ m}^3 \text{ liquid 1-octene and CO}_2} \times 715 \text{ kg 1-octene/m}^3 \\ \times \frac{1}{112.2 \text{ g/mol}} \times 0.88 \text{ aldehyde yield} \times 142.2 \text{ g/mol}$$

Aldehyde production rate: $m_{al}/m_{Rh} = 19,916 \text{ kg aldehyde} / (\text{kg Rh} \cdot \text{h})$

The aldehyde turnover rate is in the range reported in the literature¹ and varies with different assumed LHSV (for example, LHSV = 0.5 h⁻¹, aldehyde production rate is 1,992 kg aldehyde / (kg Rh · h)).

¹ Breit, B.; Winde, R.; Mackewitz, T.; Paciello, R.; Harms, K., Phosphabenzene as monodentate pi-acceptor ligands for rhodium-catalyzed hydroformylation. *Chemistry-A European Journal* 2001, 7, (14), 3106-3121.

Appendix II. Experimental Kinetic Studies

II.1 Calibration of Pressure Transducer

This exemplary calibration procedure is described for the pressure transducer mounted on the top of the syngas reservoir and also applicable for calibration of any pressure transducer under the rated pressure.

1. First install a digital pressure gauge DTG-6000 from 3D Instruments, LLC (maximum pressure of 3000 psi (20.7 MPa)) with accuracy of 0.25% full scale to the syngas reservoir, which is then isolated for pressure testing and ensured to be leak free
2. Select the output signal range of from -0.325 to 0.325 volts in the Measurements and Automation Explorer (National Instruments, Corp.) for Channel 6, with which the pressure transducer (output range of 0-20 mV) is connected
3. Pressurize the reservoir with the inert gas nitrogen at a pressure of a fixed and constant value, read from the digital pressure gauge. Record the transducer response after it reaches stabilized. The response of the transducer was measured in terms of the voltage output, directly read from the Measurements and Automation Explorer as the transducer's output.
4. Repeat the above procedure step 3 for various pressures spanning from zero to the pressure at the desired operating conditions, which has to be lower than the lowest upper limit pressure of the vessel, the transducer and the gauge. The data are tabulated in Table II.1.

5. Correlate the response of the transducer in voltage with the actual pressure and obtain a linear relationship as Figure II.1. Input the new values of the slope and intercept in the data acquisition software Labview® (National Instruments, Corp.). The non-zero voltage is recorded for zero gauge pressures and hence the line does not pass through the origin although the linearity still holds good. The relative error grows as the gauge pressure approaches zero, shown in Table II.1.

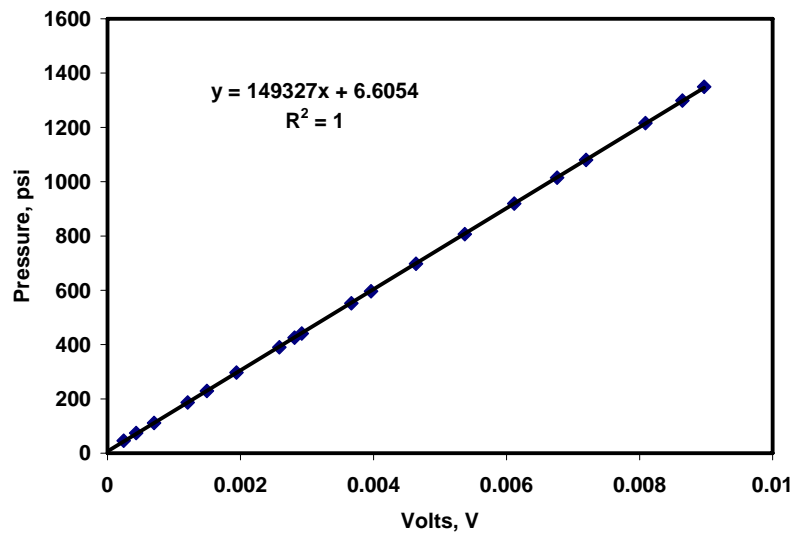


Figure II.1 Calibration of pressure transducer

Table II.1 Pressure transducer calibration data

Signal Values, V	Gauge Pressure, psi	by equation	Relative error, %
0.008971	1349.4	1346.22	-0.24
0.008644	1298.9	1297.39	-0.12
0.008088	1215.5	1214.36	-0.09
0.007196	1080.5	1081.16	0.06
0.006759	1015.1	1015.91	0.08
0.006115	919.5	919.74	0.03
0.005371	807	808.64	0.20
0.004637	697.8	699.03	0.18
0.003962	596.5	598.24	0.29
0.003665	552.3	553.89	0.29
0.002921	440.6	442.79	0.50
0.002812	425.6	426.51	0.21
0.002584	389.9	392.47	0.66
0.001939	296.9	296.15	-0.25
0.001493	229	229.55	0.24
0.001205	187	186.54	-0.25
0.000699	111.3	110.98	-0.29
0.000431	74.3	70.97	-4.48
0.000243	46	42.89	-6.76
-0.000045	0.2	-0.11	-155.00

II.2 ReactIR Purge Gas Generator Operation and Diagnosis

The ReactIR light path is purged by dry and hydrocarbon-free air supplied by a heatless self-generated compressed air dryer (Model No. PCDA1112B122; maximum pressure of 150 psi (1.03 MPa); Puregas LLC).

When the gas generator couldn't provide dry, CO₂-free (< 1 ppm CO₂, < 1 ppm H₂O vapor at -73.3 °C dewpoint) and stable purge gas for ReactIR unit, poor quality background and fluctuation in the sample spectra for a dry and clean probe were observed. From the ReactIR backgrounds as shown in Figure II.3, the background in (a) gives intensive water vapor absorption in the wavenumber range from 1300-1800 cm⁻¹ and 3500-4000 cm⁻¹, while in contrast the good-quality purge in (a) shows significantly reduced water absorption at the acceptable level in the same wavenumber range and more smooth background. Our main hydroformylation product, aldehydes absorbing light at wavenumber of 1729 cm⁻¹ falls amid this range.

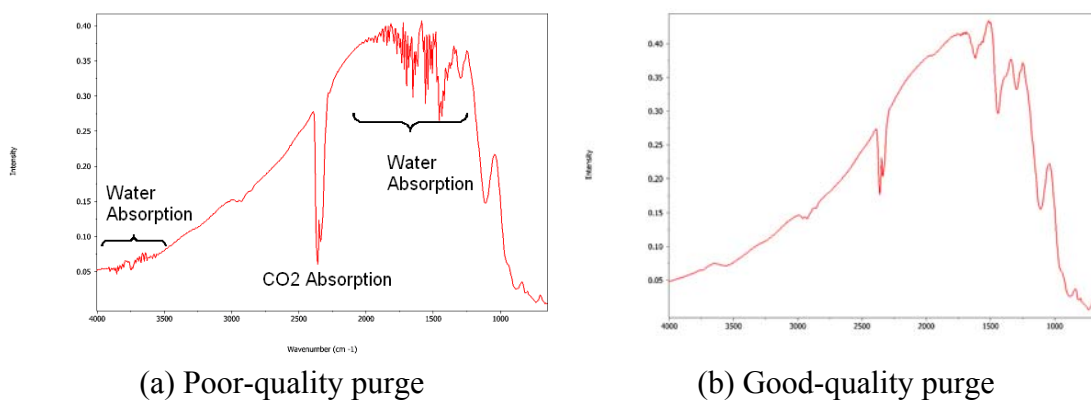


Figure II.3 ReactIR background comparison for different purge gas qualities

The instability of purge gas is demonstrated by collecting 3-D reaction spectra for three hours using a dry and clean IR probe without any sample loading. The periodical (every 8 minutes) fluctuation and non-zero absorption at the wavenumbers characteristic of water (the absorbance of up to 0.05 is 10 times the value of ReactIR probe cleaning goal), shown in Figure II.4, indicates the poor performance and malfunction of the purge gas generator.

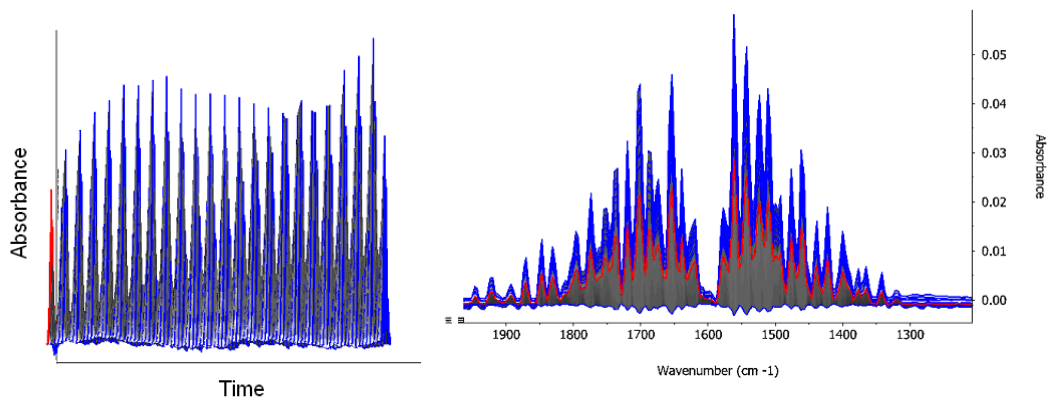


Figure II.4 IR spectra for a dry and clean IR probe with poor-quality purge

The low-quality air results from the high flowrate demand through the generator by the three parallel ReactIR units and low inlet air pressure provided by the air compressor in the facility. In any drying operation, it is important that nominal operating pressure be maintained at the dryer inlet in order to insure efficient drying service. In addition, the gas generator only can self-regenerate at high enough pressure of gas supply and at fixed inlet and outlet flowrates. To eliminate the problem and comply with the operating requirement, the following procedure has been taken:

- Acquire air source from building facility as stable as possible and increase generator inlet air pressure to 100 psig (0.69 MPa) minimum; improve upstream compressed air treatment if possible
- Reduce outlet flowrate to 14 Lpm maximum for each ReactIR and ensure outlet tubing lengths to ReactIR are less than 1 meter OR use copper/PEEK tubing, which is not hygroscopic.
- Install an air regulator at the inlet of the gas generator and a flowmeter at the outlet of gas generator where dry gas is ready for end users to control gas flowrate.

II.3 Purification and Storage of Solvents and Substrate

Purification of solvents and substrate follows the method illustrated in literature “The Manipulation of Air-sensitive Compounds”² and “Purification of laboratory chemicals”³.

Solvents such as toluene and hexane are purchased from Sigmaaldrich in the grade of “anhydrous in Sure/Seal™”, which is ready to be stored in glove box for use or in the grad “ACS reagent” which needs distillation or molecular sieves (effective pore size 3A) absorbents to remove water and solvent purging using a septum and a double needle arrangement to remove oxygen. Removing oxygen from ethers and olefins needs chemical means or adsorbents to purify them prior to distillation since purging methods are not effective where peroxide formation occurs through chemical interactions.

The impurities in olefins such as oxygen and water may oxidize alkyl phosphines ligands to the corresponding oxides and the peroxides and dienes may deactivate the rhodium catalyst. Therefore, moisture, oxygen, dienes and peroxides have to be thoroughly removed from our reagents and solvents before starting catalytic hydroformylation reaction.⁴ In the present work, freshly purchased substrate 1-octene are stored under sliced sodium metal to eliminate water and the peroxides as well as dienes and alkynes. Then 1-octene will be distilled under inert gas nitrogen

² Shriver, D. F.; Drezdson, M. A. *The Manipulation of Air-sensitive Compounds*. Second edition, John Wiley & Sons, Inc., New York, **1986**

³ Amarego, W. L. F.; Chai, C. L. L., *Purification of laboratory chemicals*. 5th ed. Oxford : Butterworth-Heinemann ; Burlington, Mass. : Elsevier Science, **2003**.

⁴ van Leewen, P. W. N. M. Decomposition Pathways of Homogeneous Catalysts. *Applied Catalysis A: General*, **2001**, 212, 61-81

over calcium dihydride CaH_2 ^{5,6} to remove water. The distilled 1-octene was degassed by the method called freeze-pump-thaw cycling or by inert gas bubbling using Schlenk line technique. The degassed 1-octene is stored in glove box for further usage.

Peroxides are strong oxidizing agents which may react explosively with strong reducing agents such as LiAlH_4 or alkali metals. Large amounts of peroxides may be removed by storing the liquids over activated alumina. Van der Slot⁷ reported that the alkene was filtered over neutral alumina to remove peroxides. Van Leeuwen: percolation over neutral alumina is usually sufficient for a hydroformylation reaction (peroxides). Treatment over sodium or sodium-potassium on a support will also remove alkynes and dienes that may influence the catalyst performance. Distillation from sodium may give isomerization of alkenes as an undesirable side reaction.⁸ Peroxides can also be removed by percolation through dried, acid washed alumina. And then stored under nitrogen in the dark.⁹

Rigorous drying and deoxygenating agents which have been used include LiAlH_4 , sodium wire or shot, sodium-benzophenone, Na-K alloy, and CaH_2 . Solid Na and CaH_2 often have unfavorable rates of reaction with impurities and therefore are not highly effective even at the reflux temperature of the solvent. Liquid Na-K alloy and soluble LiAlH_4 are discouraged to use for the purification of solvents

⁵ Feng, J.; Garland, M. *Organometallics* **1999**, 18, 417-427

⁶ Bergounhou, C.; Neibecker, D.; Mathieu, R. *J. Mol. Cat. A: Chemical*, **2004**, 220, 167-182.

⁷ *Organometallics* 2001, 20, 430-441

⁸ Decomposition pathways of homogeneous catalysts, *Applied Catalysis A: General* **2001**, 212, 61-81.

⁹ Armarego, Wilfred L.F.; Chai, Christina L. L. Purification of laboratory chemicals, fifth edition, **2003**, MPG Books Ltd., Bodmin, Cornwall, Great Britain.

because there is significant risk of explosion if these materials are not handled carefully. Sodium-benzophenone represents a good compromise between ease of use and safety for obtaining very low levels of water and oxygen.

II.4 Gas Chromatography Methods for Analysis of Typical Hydroformylation Reaction Mixtures

(a) GC method

Table II.2 GC method for hydroformylation reaction mixture analysis

Model	Varian CP-3800 GC
Column	CP-Si15CB Chromapack® capillary column (25m × 0.32 mm × 1.2 µm); Part# CP7760
Autosampler	Varian CP-8400 autosampler
Injection volume	1 µL
Solvent	Dichloromethane (DCM)
Column temperature programming	30 °C for 5 min; ramp @ 10 °C/min to 180 °C hold 0 min; ramp @ 20 °C/ min to 220 °C hold 2 min
Middle injector	250 °C
Middle FID	300 °C
Split injection	Split ratio= 100/1

(b) For the internal standard analysis, 2-propanol is used as the internal standard. The response factors for the chemicals involved are calculated by the formula as follows:

$$\text{Response Factor} = \frac{(\text{Area/Molar Amount})_{\text{Unknown}}}{(\text{Area/Molar Amount})_{\text{InternalStandard}}}$$

Table II.3 Response factors for the chemical with 2-propanol as internal standards

Chemicals	Response factor
1-Octene	1.03
n-Octane	0.97
Other C ₈ olefins isomers	1.00
C ₉ aldehydes	0.79
C ₉ alcohols	0.85

(c) For the external standard analysis, there is the internal standard. The concentration of component *i* is calculated by the formula as follows:

$$C_i(s) = \frac{A_i(s)}{A_i(st)} C_i(st)$$

where $A_i(s)$ is the area of the peak for solute (i) in the sample chromatogram, $A_i(st)$ is the area of the peak for solute (i) in the reference chromatogram, and $C_i(st)$ is the concentration of the standard in the reference solution.

II.5 ReactIR Peak Calibration

The QuantIR software (Version 2.21) combined with ReactIR™ 3.0 has been used for component calibrations. The IR probe is not able to discriminate isomers of C₉ aldehydes and three isomers of 1-octene so that at present we only consider two main representative components, product 1-nonanal and substrate 1-octene. The standard solutions was made by adding 1-nonanal of 0, 5, 10, 30, 50, 70, 80, 95, 100 mL in 100 mL volumetric flask and the rest of the volume is balanced by adding 1-octene. The densities of pure 1-nonanal and 1-octene are 5.81 mol/L and 6.37 mol/L. The densities or concentrations of each component in the standard mixtures are calculated based on the accurate amount of each component added in the fixed volume.

The calibration procedure is described as follows:

1. Dry and clean the IR probe and align the conduit and mirror angle to a position where the system has optimum peak height and contrast. It is necessary to keep the light path and signal intensity constant for quantitative analysis since the variations in the mirror angle and the contrast level that occurred during the set-up disassembling can cause unrepeatable signal.
2. Load one standard solution into the reactor and heat up the system to the desired temperature under the desired pressure (atmospheric pressure in this case) while stirring until the condition is stable.
3. Collect sample spectrum for the standard solution of known concentration or extract individual spectrum from a reaction using ReactIR 3.0 software. Then

save as the sample spectrum in SPA type. Repeat steps 1-3 for each standard solution of different concentration.

4. Start the QuantIR software and load the sample spectra collected in step 3. Design a quantitative method such as partial least squares (PLS) by using the normal menu commands in the QuantIR software. Then convert a series of sample spectra to a quant file for a correspondent individual chemical at the characteristic peak location at known concentrations (for example, nine spectra were collected for 1-octene at concentrations of from 0 mol/L to 6.37 mol/L at peak wavenumber of 1640 cm^{-1} , refer to Figure II.5)
5. Go back to ReactIR 3.0 software and use command “Convert Quant v2 Files” to convert the quant files (with extension of .QNT). Now, the quant file is ready to use to calculate component concentrations quantitatively.
6. Apply the quantitative analysis file for the chemical component of interest to the reaction spectra or a single spectrum by running the built-in QuantIR in the ReactIR software and obtain the absolute concentration or temporal profile for each component

The charts below show the calibration curves for 1-octene in Figure II.5 and 1-nonanal in Figure II.6 obtained by QuantIR at $60\text{ }^{\circ}\text{C}$ under atmospheric pressure.

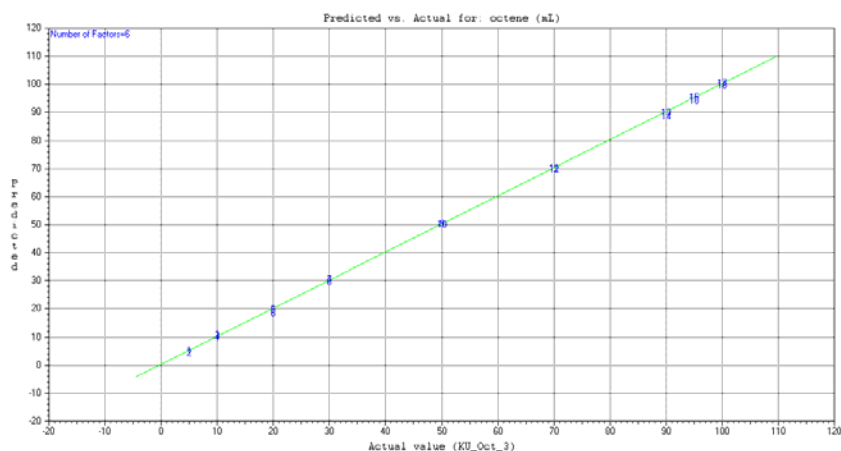


Figure II.5 The predicted vs. actual concentration for 1-octene

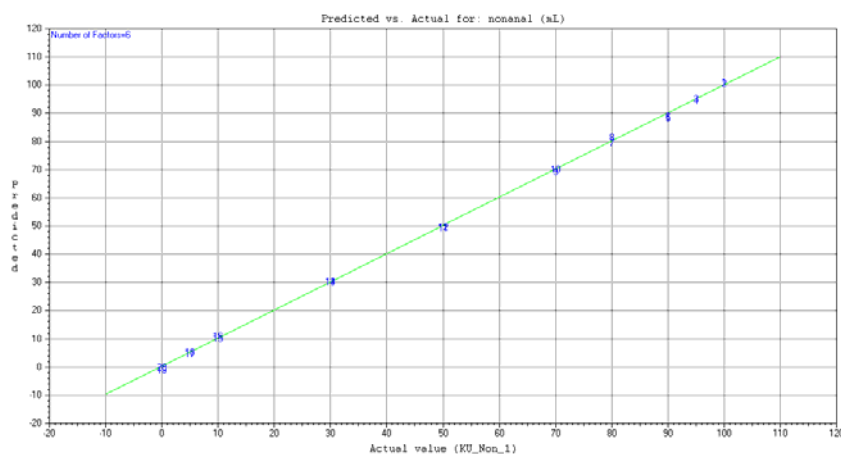


Figure II.6 The predicted vs. actual concentration for nonanal

As shown in the figures, linear correlations between the predicted and the actual concentrations for both components are observed in the concentration ranges correspond to 0 to 100% 1-octene conversions and 0 to 100% 1-nonanal yield. However, this linearity does not always mean linear relationship between the peak absorbance and the compound concentration. Unsurprisingly, the plotting of

absorbance with concentrations of 1-octene and 1-nonanal, respectively, give straight lines with high correlation coefficient of greater than 0.99.

It should be noted that the temperature and pressure have significant effects on the peak height. At lower temperatures and higher pressures, stronger absorbance is observed. Therefore, the calibration conditions have to match the reaction conditions in terms of temperature and pressure. Moreover, during the calibration, the applied high-pressure gas should not have high solubility in the organic liquid phase, otherwise, the compositions of the liquid phase will be altered and does not reflect the actual component concentrations. After reaction, apply ConcIRT™ to the 3-D reaction data exemplified in Figure II.7 to extract 2-D absorbance profiles against reaction time. Then, apply the calibration curve to convert absorbance to absolute concentration.

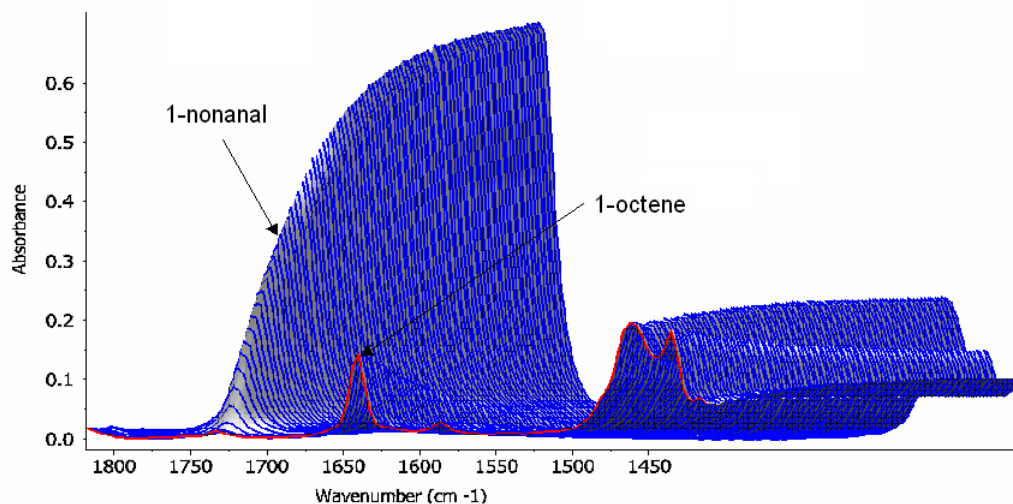


Figure II.7 An example of 3-D hydroformylation reaction data profile (Neat 1-octene, 2.0 MPa syngas, 60 °C, 12hrs)

In the present work, we used normalized absorbance (A/A_0) to represent the value for concentration (C/C_0), where A_0 is the absorbance at the initial concentration C_0 . Or we used the two GC data for the starting solution and exhaust mixture at the end of the reaction to calibrate the absorbance vs. time profile since the calibration is overly time-consuming and varying with experimental condition and can't be acquired in a once-for-all manner.

II. 6 Reproducibility of the Experiments

The CO₂-expanded 1-octene hydroformylation using triphenylphosphine modified rhodium as catalyst were repeated for three times at the following conditions: Temperature: 60 °C; Pressure: 3.8 MPa (3.2 MPa CO₂ and 0.6 MPa syngas); Syngas: H₂/CO = 1; Solvent(CO₂) = 2 mL (10% volume expansion); Substrate: 1-octene, 20 mL; Catalyst: Rh(acac)(CO)₂, 15.20 mg; Ligand: triphenylphosphine, 3.2 g; TPP/Rh = 207 molar ratio; 1-octene/Rh = 2168 molar ratio

Figure II.8 shows the temporal profiles of temperature, pressure and the stirring speed for a typical run.

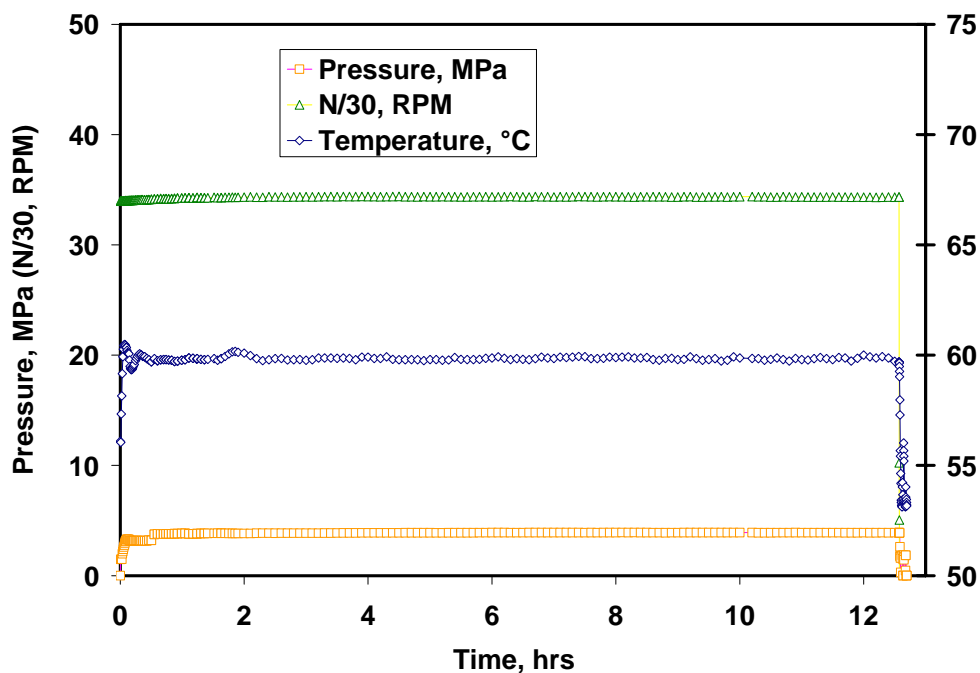


Figure II.8 Temperature, pressure and impeller speed profiles for a typical reaction

The conversion, selectivity and *n/i* ratio for these three runs a, b and c are given in Table II.4 and the AARD (average absolute relative deviation) for each are lower than 7% except selectivity to *n*-octane.

Table II.4 Experimental results for three repeated runs

#	Conv, %	S(n)	S(iso)	S(n+iso)	S(octane)	S(trans)	S(heavy products)	n/iso
a	88.3	83.3	10.3	93.6	0.1	6.2	0.1	8.1
b	83.3	84.6	8.9	93.5	0.4	6.0	0.2	9.5
c	84.2	84.5	8.9	93.4	0.4	6.0	0.2	9.5
AARD, %	2.36	0.65	6.75	0.09	53.92	1.09	6.34	7.04

The AARD (average absolute relative deviation) is calculated based on the equation below:

$$\alpha\% = \frac{1}{N} \sum_{i=1}^N \frac{|x_i - \bar{x}|}{x} \times 100$$

Appendix III. ICP-OES Elemental Analysis

III.1 ICP Method Optimization

III.1.1 Spectral interference and analytical lines

Analytical lines selection is based on the comprehensive consideration of spectral interference, sensitivity, robustness and limit of detection (LOD). The profiles were scanned for four solutions including blank toluene, rhodium complex only in toluene and phosphorus only in toluene at concentration of a few ppm, and TPPine modified rhodium in toluene at concentrations of a few ppm. Spectral interference was examined by overlapping the profiles for the above-mentioned four solutions at the chosen lines, shown in Table III.1.

Table III.1 Analytical lines for Rh and P and their state of ionization

Line number	Wavelength	State of Ionization
1	P=185.880 nm	Atomic line (I)
2	P=213.618 nm	Atomic line (I)
3	P=253.565 nm	Atomic line (I)
4	P=255.328 nm	Atomic line (I)
5	Rh=233.477 nm	Ionic line (II)
6	Rh=249.077 nm	Ionic line (II)
7	Rh=343.489 nm	Atomic line (I)
8	Rh=369.236 nm	Atomic line (I)

For example, there is no spectral interference between P and Rh at line Rh = 343.489 nm.

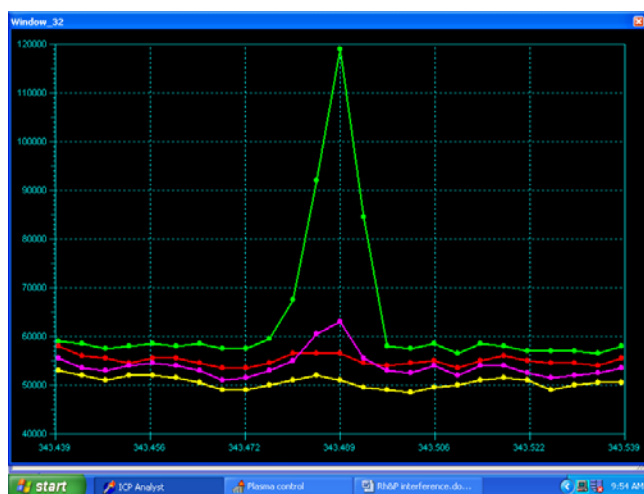


Figure III. 1 Spectra at line Rh = 343.489 nm for blank toluene (red line), P only in toluene (yellow line) at concentration of a few ppm, Rh only in toluene (green line) at concentration of a few ppm as well as Rh and P in toluene at concentrations of a few ppm (purple line)

III.1.2 Power optimization

According to the ICP operating manual, for volatile solvent the generator power is set above 1200W. To optimize the generator power, a series of calibration standards was measured at three different powers 1300 W, 1350 W and 1400 W. The power at which gives the lowest limit of detection (LOD) will be chosen for the later analyses. From the Figure III.2, the LODs for rhodium at 1300 W is the lowest (best) one. However, there are not much difference at these three powers for both rhodium and phosphorus at different lines. Considering the matrices difference in the analysis of polymer ligands and TPPine ligand, higher power (1400 W) was selected to minimize the matrix effects.

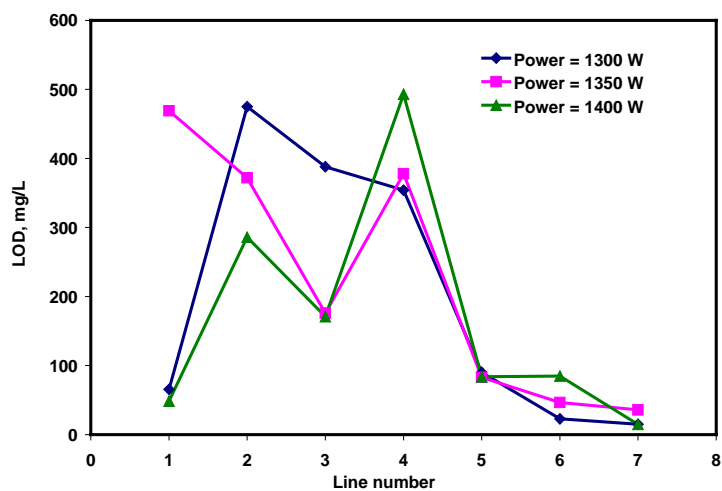


Figure III.2 Power effects on the limit of detection

III.1.3 Nebulizer pressure and flowrate as well as gainage optimization

The intensities for four Rh lines and four P lines are measured at three different nebulizer pressures P_{neb} (bars) and gainage flowrates G₂ (L/min). The nebulizer flowrate F_{neb} (L/min) depends on the nebulizer pressure due to the inherent nature of the nebulizer.

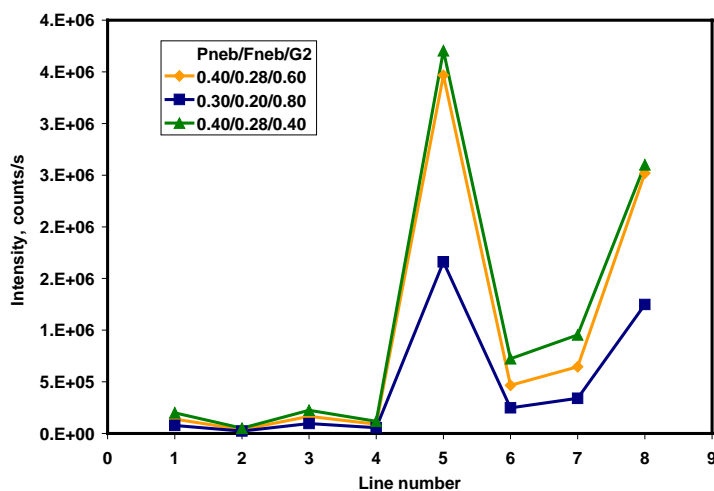


Figure III.3 Nebulizer flowrate (pressure) and the gainage effects on the intensity

From Figure III.3, the nebulizer pressure and gainage flowrate have negligible effects on the intensities for four P lines while higher intensities for four Rh lines are observed at higher nebulizer pressure and lower gainage flowrate. For more sensitive Rh analysis, we choose the optimum conditions ($P_{\text{neb}}/F_{\text{neb}}/G_2=0.40/0.28/0.40$) for most analysis.

III.1.4 Uptake and rinse-out profiles

The uptake and rinse-out profiles is shown in Figure III.4 using a toluene solution with Rh = 100 mg/L. The uptake time is about 180 seconds and the corresponding sample size for rinsing is 1.2 mL at sample uptake of 0.4 mL/min. It takes 50 seconds for 1% rinse-out and 120 for 0.5% rinse-out.

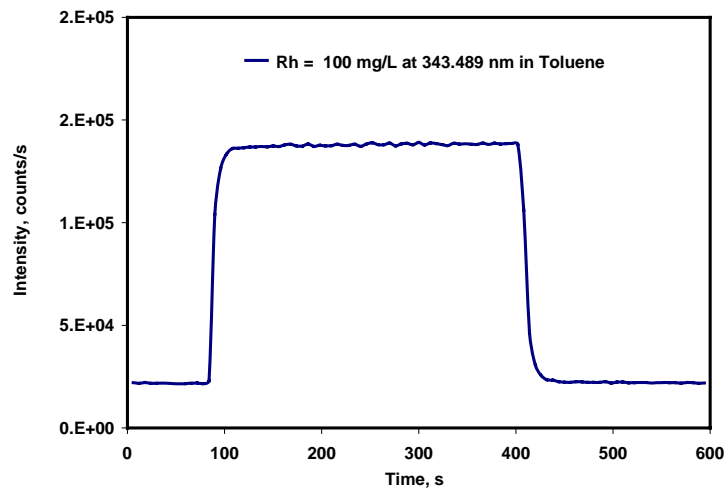


Figure III.4 Uptake and rinse-out profile for rhodium at concentration of 100 mg/L

III.2 Calibration Procedure

III.2.1 Standards availability and chemical reagents

The chemicals used for calibration are Rh(acac)(CO)₂: 99% purity from Alfa Aesar and triphenylphosphine (TPPine) 99% purity from Alfa Aesar. Toluene 99.8% purity, anhydrous from Sigma Aldrich. Chemicals were used as received without any further purification. The lab synthesized phosphorus ligands are assumed having a purity of 100% and the phosphorus content from NMR analysis was used as reference while filtration solution preparation. Toluene chosen as solvent based on solubilizing rhodium complex and ligands as well as compatibility with polyimide membrane

III.2.2 Excitation conditions

Operating conditions as shown in Table III.2 were chosen for most of the organic phase analyses based on the optimization results stated in the previous section. Excitation conditions for analysis in different organic matrixes in literature are summarized in Table III.3.

Table III.2 ICP excitation condition for analysis in organic matrix (toluene)

Parameters	Excitation Conditions
RF generator power	1400 W
Plasma gas flowrate (PL2)	18 L/min
Auxiliary gas flowrate (Aux)	1.0 L/min
Sheath gas flowrate (G2)	0.40 L/min
Nebulizer flowrate	0.30 L/min
Nebulizer pressure	0.40 bar (0.04 MPa)
Use argon humidificator	No
Pump speed	10 rpm
Sample uptake	0.43 ml/min
Pump tubing	viton, black-sampling/white-drainage
Type of nebulizer	Meinhard TR-30-C0.5
Type of spray chamber	Cyclonic
Injector tube diameter	3.0 mm

Table III.3 Excitation conditions for analysis in different organic matrixes in literature

Parameters	Unit	Sample Matrix											
		Toluene	Xylene	Bio-Ethanol	water	Gasoline	butylolactone	Mix. Ispr-,	Lubricating	Naphtha	95%		
Generator power	W	1400	1200	1200	1000	1500	1450	1400	1200	1450	1400	1400	
Plasma gas	L/min	18	18	16	12	18	16	18	14	16	18	18	
Auxiliary gas	L/min	1	1.2	0.8	0	1	0.6	1	0.8	0.6	0.8	0.8	
Sheath gas	L/min	0.6	0.2	0.35	0.2	0.4	0.2	0.65	0.3	0.2	0.15	0.15	
Nebulizer gas	L/min	0.3	0.5	0.35	1.2	0.6	0.61	0.2	-	0.61	0.35	0.35	
Nebulizer pressure	bars	0.4	-	1.7	3	-	2.1	0.42	2.51	2.1	1.2	1.2	
Sample uptake	mL/min	0.43	-	0.8	1	0.4	0.5	-	0.8	0.5	0.3	0.3	
Pump speed	rpm	10	-	15	-	10	-	13	-	-	-	-	
Argon humidifier		no	no	no	-	no	no	no	no	no	yes	yes	
Pump tubing		viton	Solvex	viton	-	-	-	solvflex	-	-	-	-	
Nebulizer		TR-30-C0.5*	JY org. Net	paralell flow	concentricC-30-0.5*	Meinhard	Meinhard	K3 type*	JY0.7	Meinhard	concentric	concentric	
Spray chamber		cyclonic	Scott	cyclonic/scott^	cylconic	-	Scott	cyclonic	Scott	Scott	cylconic	cylconic	
Injector diameter	mm	3.0 mm	0.7	3	3	3	3	3	3	3	3	3	
JY Appl. Note No		this work	Petro 03	Petro 02	10	ICP-xx/E	33	43	29	7	4	4	

Note: * Meinhard, ^ Cooled

JY application notes are available at Jobin Yvon website <http://www.jobinyvon.com/>.

III.2.3 Operating procedure

- Check argon gas supply with purity of > 99.999% and pressure setting at 90 psi (0.62 MPa) and check nitrogen purging gas supply with purity of > 99.999% and pressure setting at 6 psi (0.041 MPa) all the time
- Start plasma while nebulizer flowrate set to zero, zero pump flow rate to keep the organic sample loading minimum at RF generator power =1400 W, plasma flowrate (PL2) = 12 L/min, plasma is on and sustains itself, increase it to 18 L/min
- Gradually increase the pump flowrate to the set value of 10 rpm and wait for 30 minutes to warm up the instrument stable
- Peak searching and auto-attenuated using the highest concentrated standards
- Collect spectra for spectral interference and line selection, background correction
- Calibrate with the instruments with freshly made standards and measure intensity for peaks of interest for unknown samples

III.2.4 Calibration curves

The calibration curves show excellent linearity for both Rh and P spanning several orders of magnitude down to ppb level, as shown in Figures III.5 and III.6. The calibration curve does not necessarily have to pass through the origin since the non-zero intensity at zero concentration represents the intensity obtained for blank toluene, which is related to the background equivalent concentration (BEC) and limit of detection (LOD). For phosphorus line $\lambda = 213.618$ nm, the calibration curve has

BEC = 14.2 mg/L and LOD = 369 ug/L. For rhodium line $\lambda = 343.489$ nm, the calibration curve has BEC = 1.26 mg/L and LOD = 15.7 ug/L.

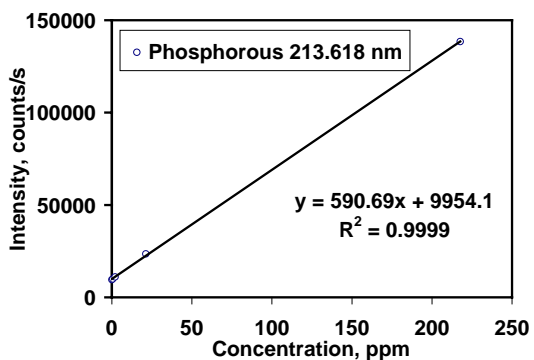


Figure III.5 Calibration curves for P

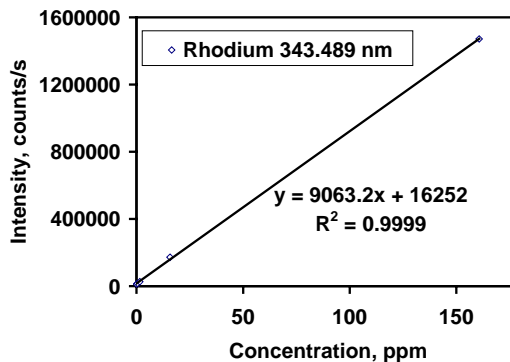


Figure III.6 Calibration curves for Rh

III.2.5 Shelf life of standards

The organometallic standards are usually unstable and not suitable for long time storage. Two series of organometallic standards containing different concentrations of Rh and P were made on two different days three months apart and the intensities of peak Rh=343.489 nm were measured, as given in Table III.3, using the same excitation method. Standard series 1 with both rhodium and phosphorus were kept in volumetric flask for over 90 days. Standard series 2 with only Rhodium were freshly made. Both standard series are exposed to air. The plot of intensity at Rh = 343.489 nm vs. concentration shows excellent linearity, as shown in Figure III.7. This indicates that the shelf life of standards can be up to 90 days. However, in all measurements in this work, standards were freshly made and never used after over one-week storage.

Table III.3 Peak intensity at Rh = 343.489 nm vs. standard concentrations for two series of standards

Rh Concentration, mg/L	Intensity, Rh=343.489 nm
0	48686
2.52	120463
5.04	192287
7.98	263608
12.62	407548
15.95	518116
47.86	1477057

Series1 (unhighlighted) were made on July 10, 2007 containing Rh & P in toluene.
 Series2 (highlighted) were made on March 26, 2007 containing Rh only in toluene.

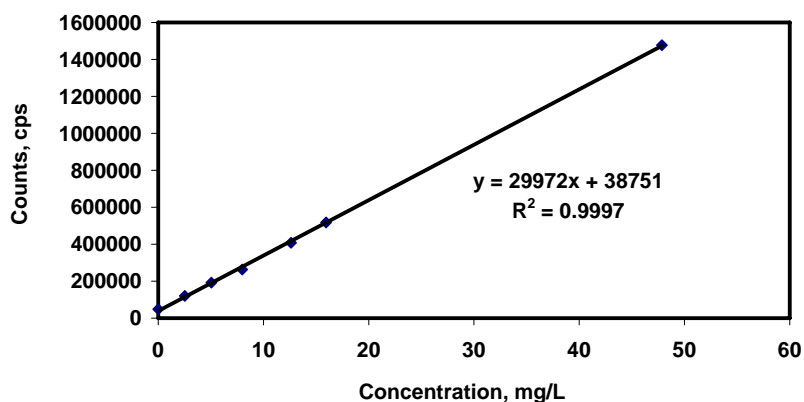


Figure III.7 Peak intensity at Rh = 343.489 nm vs. concentration for standard

III.3 Study Materials

The ICP principles and application could be found in the ICP application manual and software manual as well as on Jobin Yvon website <http://www.jobinyvon.com/>. Other reading materials are recommended:

- CRC Handbook of Inductively Coupled Plasma Atomic Emission Spectroscopy. Asha, Varma, 1991

- Dean, John R., Practical inductively coupled plasma spectroscopy, Hoboken, NJ : John Wiley, 2005.
- Nölte, Joachim, ICP emission spectrometry: a practical guide, Weinheim: Wiley-VCH, 2003.
- ICP Operations on website <http://www.ivstandards.com/>

Appendix IV. Mass Balance and Uncertainty Analysis

IV.1 Mass Balance and Uncertainty Analysis Calculation Formulae

The mass of the sample is measured by 4-place balance with accuracy of $\Delta m = s_m = 0.0001g$. The nomenclature and formula for mass and concentration of each sample are summarized in Table IV.1.

Table IV.1 Nomenclature and formula used for uncertainty analysis

Sample	Original (O)	Permeate (P)	Retentate (R)
Mass, g	m_O	m_p	m_R
Uncertainty, \pm	$\Delta m = s_m$	$\Delta m = s_m$	$\Delta m = s_m$
Conc., ug/g	C_O	C_p	C_R
Uncertainty, \pm	$\Delta C_O = C_O \times RSD_{C_O}$	$\Delta C_p = C_p \times RSD_{C_p}$	$\Delta C_R = C_R \times RSD_{C_R}$

The original solution (O) represents the mixture that was charged into the MET cell and subjected to membrane filtration. The permeate solution (P) is the portion collected from the permeate line with solutes at low concentration. The retentate solution (R) is the portion retained above the membrane with rejected solutes.

The mass of Rh in the permeate solution is equal to the mass of the solution times the Rh concentration.

$$m_{p,Rh} = m_p \times C_{p,Rh} \text{ or } \ln(m_{p,Rh}) = \ln(m_p) + \ln(C_{p,Rh})$$

The uncertainty in the Rh mass in the permeate solution is calculated by:

$$\frac{\Delta m_{p,Rh}}{m_{p,Rh}} = \sqrt{\left(\frac{\Delta m_p}{m_p}\right)^2 + \left(\frac{\Delta C_{p,Rh}}{C_{p,Rh}}\right)^2 + 2 \times \left(\frac{\Delta m_p}{m_p}\right) \times \left(\frac{\Delta C_{p,Rh}}{C_{p,Rh}}\right)} = \sqrt{\left(\frac{\Delta m_p}{m_p}\right)^2 + \left(\frac{\Delta C_{p,Rh}}{C_{p,Rh}}\right)^2}$$

The calculation of the uncertainty in the Rh mass in the retentate or original solutions follows the same rule. The total Rh mass in the permeate and retentate is equal to:

$$m_T = m_{p,Rh} + m_{r,Rh}$$

The uncertainty in the total Rh mass is calculated as follows:

$$\Delta m_T = \sqrt{(\Delta m_{p,Rh})^2 + (\Delta m_{r,Rh})^2 + 2 \times (\Delta m_{p,Rh}) \times (\Delta m_{r,Rh})} = \sqrt{(\Delta m_{p,Rh})^2 + (\Delta m_{r,Rh})^2}$$

$$\text{Total Mass} = m_T \pm \Delta m_T$$

The mass balance (MB) compares the measured Rh amount in the original solution and the sum of those in permeate and retentate solutions. The calculation is as follows:

$$\text{MB} = \frac{m_T}{m_O} \text{ and } \frac{\Delta \text{MB}}{\text{MB}} = \sqrt{\left(\frac{\Delta m_T}{m_T}\right)^2 + \left(\frac{\Delta m_O}{m_O}\right)^2}$$

$$\text{Mass Balance} = \text{MB} \pm \Delta \text{MB}$$

The pass through (PT) quantify how many percent of Rh is leached through the membrane into the permeate based on the measured Rh amount in the original solution. The calculation follows:

$$\text{PT} = \frac{m_p}{m_O} \text{ and } \frac{\Delta \text{PT}}{\text{PT}} = \sqrt{\left(\frac{\Delta m_p}{m_p}\right)^2 + \left(\frac{\Delta m_O}{m_O}\right)^2}$$

$$\text{Pass Through} = \text{PT} \pm \Delta \text{PT}$$

IV.2 Example

For example, the mass balance and uncertainty analysis for Rh is calculated for a typical filtration experiment and the mass and concentration for each sample are given in Table IV.2.

Table IV.2 Mass and concentration for each sample in a typical filtration run

Sample	Original (O)	Permeate (P)	Retentate (R)
Mass, g	51.8211	33.6014	86.1586
Uncertainty, g	0.0001	0.0001	0.0001
Rh concentration, ug/g	71.72	5.26	41.15
RSD, %	1.9	1.01	0.036

Rhodium mass in Original (O) solution and the uncertainty:

$$m_{O,Rh} = m_O \times C_{O,Rh} = 51.8211\text{g} \times 71.72\text{ug/g} = 3.717\text{mg}$$

$$\begin{aligned} \frac{\Delta m_{O,Rh}}{m_{O,Rh}} &= \sqrt{\left(\frac{\Delta m_O}{m_O}\right)^2 + \left(\frac{\Delta C_{O,Rh}}{C_{O,Rh}}\right)^2} = \sqrt{\left(\frac{\Delta m_O}{m_O}\right)^2 + (RSD_{C_{O,Rh}})^2} \\ &= \sqrt{\left(\frac{0.0001\text{g}}{51.8211\text{g}}\right)^2 + (1.9\%)^2} = 1.9\% \end{aligned}$$

$$\Delta m_{O,Rh} = m_{O,Rh} \times 1.91\% = 3.717\text{mg} \times 1.91\% = 0.071\text{mg}$$

$$\therefore m_{O,Rh} \pm \Delta m_{O,Rh} = 3.717\text{mg} \pm 0.071\text{mg}$$

Rhodium mass in Permeate (P) solution and the uncertainty:

$$m_{P,Rh} = m_P \times C_{P,Rh} = 33.6014\text{g} \times 5.26\text{ug/g} = 0.177\text{mg}$$

$$\begin{aligned} \frac{\Delta m_{P,Rh}}{m_{P,Rh}} &= \sqrt{\left(\frac{\Delta m_P}{m_P}\right)^2 + \left(\frac{\Delta C_{P,Rh}}{C_{P,Rh}}\right)^2} = \sqrt{\left(\frac{\Delta m_P}{m_P}\right)^2 + (RSD_{C_{P,Rh}})^2} \\ &= \sqrt{\left(\frac{0.0001\text{g}}{33.6014\text{g}}\right)^2 + (1.01\%)^2} = 1.01\% \end{aligned}$$

The absolute uncertainty in the Rh mass in permeate is:

$$\Delta m_{p,Rh} = m_p \times 1.01\% = 0.177\text{mg} \times 1.01\% = 0.002\text{mg}$$

$$\therefore m_{p,Rh} \pm \Delta m_{p,Rh} = 0.177\text{mg} \pm 0.002\text{mg}$$

Rhodium in Retentate (R) solution and the uncertainty:

$$m_{p,Rh} = m_p \times C_{p,Rh} = 86.1586\text{g} \times 41.15\text{ug/g} = 3.545\text{mg}$$

$$\begin{aligned} \frac{\Delta m_{R,Rh}}{m_{R,Rh}} &= \sqrt{\left(\frac{\Delta m_R}{m_R}\right)^2 + \left(\frac{\Delta C_{R,Rh}}{C_{R,Rh}}\right)^2} = \sqrt{\left(\frac{\Delta m_R}{m_R}\right)^2 + (RSD_{C_{R,Rh}})^2} \\ &= \sqrt{\left(\frac{0.0001\text{g}}{86.1586\text{g}}\right)^2 + (0.036\%)^2} = 0.04\% \end{aligned}$$

$$\Delta m_{R,Rh} = m_R \times 0.04\% = 3.545\text{mg} \times 0.04\% = 0.001\text{mg}$$

$$\therefore m_{R,Rh} \pm \Delta m_{R,Rh} = 3.545\text{mg} \pm 0.001\text{mg}$$

Rhodium total in both Permeate (P) and Retentate (R):

$$m_T = m_{O,Rh} + m_{R,Rh} = 0.177\text{mg} + 3.545\text{mg} = 3.722\text{mg}$$

$$\Delta m_T = \sqrt{(\Delta m_{p,Rh})^2 + (\Delta m_{R,Rh})^2} = \sqrt{(0.002\text{mg})^2 + (0.001\text{mg})^2} = 0.002\text{mg}$$

$$\frac{\Delta m_T}{m_T} = \frac{0.002\text{mg}}{3.722\text{mg}} = 0.059\%$$

Mass balance calculation:

$$MB = \frac{m_T}{m_O} = \frac{3.722\text{mg}}{3.717\text{mg}} = 100.1\%$$

$$\frac{\Delta MB}{MB} = \sqrt{\left(\frac{\Delta m_T}{m_T}\right)^2 + \left(\frac{\Delta m_O}{m_O}\right)^2} = \sqrt{(0.059\%)^2 + (1.90\%)^2} = 1.9\%$$

$$MB = 100.1\% \pm 1.9\%$$

Pass Through calculation:

$$PT = \frac{m_p}{m_o} = \frac{0.177\text{mg}}{3.717\text{mg}} = 4.76\%$$

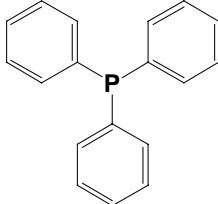
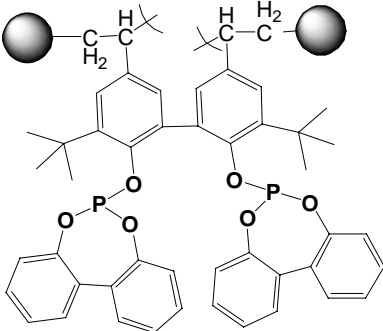
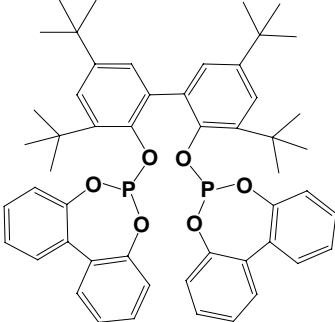
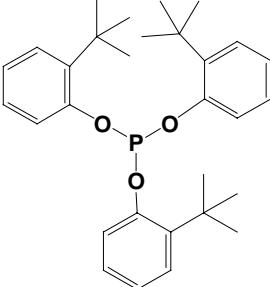
$$\frac{\Delta PT}{PT} = \sqrt{\left(\frac{\Delta m_p}{m_p}\right)^2 + \left(\frac{\Delta m_o}{m_o}\right)^2} = \sqrt{(1.01\%)^2 + (1.90\%)^2} = 2.15\%$$

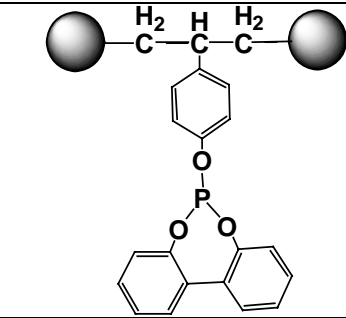
$$\Delta PT = PT \times 2.15\% = 4.8\% \times 2.15\% = 0.10\%$$

$$PT = 4.76\% \pm 0.10\%$$

For phosphorus, the calculation of uncertainties in the mass balance and pass through follows the same procedure.

Appendix V. Phosphorus Ligands

Ligands	Chemical Structure
Triphenylphosphine (TPPine), $P(C_6H_5)_3$ MW = 262.29 g/mol CAS Number: 603-35-0	
Polymer-bound Biphephos (PBB20) $M_N = 20,000$ g/mol cross-linking 4.8% L incorporation = 0.12 mmol/g Theoretical loading = 0.17 mmol/g	
BiPhePhos MW=838.94 g/mol	
BiPhPhM $P(OC_{10}H_{13})_3$ MW=478.60 g/mol	

<p>Polymer-bound phosphite (PBP10) $M_N = 10,000$ g/mol P loading for each batch: PBB10a: 0.436 mmol/g</p>	
<p>Polymer-bound Biphephos (PBB10) $M_N = 10,000$ g/mol P loading for each batch: PBB10a: 0.949 mmol/g PBB10b: 0.634 mmol/g PBB10c: 0.645 mmol/g PBB10d: 0.640 mmol/g PBB10e: 0.600 mmol/g</p>	